ADSORPTION OF PHARMACEUTICAL COMPOUNDS IN WASTEWATER USING ASH DERIVED FROM AGRI-RESIDUE AND IT'S SOLIDIFICATION

A THESIS

Submitted in partial fulfilment of the
requirements for the award of the degree

of

DOCTOR OF PHILOSOPHY

in

ENVIRONMENTAL SCIENCE & TECHNOLOGY

by

GURLEENJOT KAUR
(Regd. No. 901614002)

SCHOOL OF ENERGY AND ENVIRONMENT
THAPAR INSTITUTE OF ENGINEERING AND TECHNOLOGY
(Deemed to be University)
Patiala - 147004, Punjab (India)

August, 2021

CANDIDATE'S DECLARATION

This is to declare that the research work which is being presented in this thesis entitled "**Adsorption of Pharmaceutical Compounds in Wastewater using Ash Derived from Agri-residue and it's Solidification**" in fulfilment of the requirement of the degree of 'Doctor of Philosophy in School of Energy and Environment, Thapar Institute of Engineering and Technology, Patiala, India, is an authentic record of my research work carried out under the supervision of Dr. Neetu Singh (Associate Professor, Department of Chemical Engineering, TIET, Patiala, India) and Dr. Anita Rajor (Associate Professor, School of Energy and Environment, TIET, Patiala, India). The matter presented in this thesis has not been submitted, in part or full, to any other institute in India or Abroad for the award of any degree. Works of other authors cited in this thesis have been duly acknowledged under the reference section of this thesis.

Gurleenjot Kaur

Gurleenjot Kaur
(Regd. No. 901614002)

CERTIFICATE

This is to certify that the thesis entitled "**Adsorption of Pharmaceutical Compounds in Wastewater using Ash Derived from Agri-residue and it's Solidification**" which has been submitted by Ms. Gurleenjot Kaur in the fulfillment of the requirements for the award of the degree of 'Doctor of Philosophy' in School of Energy and Environment, Thapar Institute of Engineering and Technology, Patiala, India, is a record of the candidate's own independent and original research work carried out by her under our supervision and guidance. The matter embodied in this thesis has not been submitted, in part or full, to any other institute for the award of any degree in other universities or institutes.

Supervisors

Dr. NEETU SINGH
Associate Professor
Department of Chemical Engineering
TIET, Patiala, India

Dr. ANITA RAJOR
Associate Professor
School of Energy & Environment
TIET, Patiala, India

ABSTRACT

The improper discharge of drugs from hospitals and pharmaceutical industries is the leading cause of negative impacts on the natural environment's physical, chemical and biotic features, especially water. In addition, the production of several categories of pharmaceutical compounds due to the rise in geometric population and falling health status of the general public has enhanced the problem. These contaminants, usually stated as “emerging pollutants” are the real threat to human health. Various types of pharmaceutical compounds have been extensively examined in aqueous environments in concentration ranges of μg/L to mg/L. The high rate of bioaccumulation, persistence and non-biodegradability causes great resistance in eliminating these contaminants by conventional treatment processes. Among the different categories of pharmaceutical compounds, antibiotics are an important class of pharmaceuticals that have their unique properties because they kill pathogens without disturbing the metabolic system of human beings.

The term “antibiotic” is typically used to characterize several classes of organic molecules which could successfully prevent bacterial growth. Based on chemical structures, antibiotics have been classified as fluoroquinolones, tetracyclines, sulfonamides and chloramphenicol. The estimated worldwide average consumption of antibiotics is more than 100 x 10^6 kg per year. Such great consumption of antibiotics for agriculture and veterinary purposes results to its excessive emission, which may lead to several environmental issues. Recently, the residues of the antibiotic pollutants have been detected in various aqueous systems, particularly in industrial effluent, domestic influent and effluent, drinking water, groundwater and surface water. According to the present status of COVID-19 coronavirus, Various antibiotics have sparked interest as potential COVID-19 treatment options in the year 2020. The huge demand and consumption of OFL and DOX, its incomplete metabolism and complex behavior in the atmosphere are causing a great ecological issue, which needs to be solved. Antibiotic-resistant bacteria (ARB) and antibiotic-resistant genes (ARG) in aquatic systems are a critical concern due to their ecotoxicity.

In this regard, researchers have widely preferred the adsorption process in the past two decades due to its various advantages like simple operation, cost-effective, no by-products, no sludge generation and environmental friendliness. Therefore, tremendous endeavors have been done for exploring the different types of adsorbents with excellent performance. As a result, numerous natural, modified and functionalized materials have been evolved to adsorb

pharmaceuticals from aqueous systems. However, the molecular structure, specific surface area, surface charge and affinity towards adsorbate are the most important features for the effective performance of a particular adsorbent. Thus, Adsorption is a significantly important process from a technological point of view due to the micro and macroporous nature of the materials. In the present study, Doxycycline hydrochloride (DOX) and Ofloxacin (OFL), which belongs to the tetracyclines and fluoroquinolones category, respectively were chosen as model pollutants. Moreover, for appropriate management of exhausted adsorbents, its disposability studies were carried out by stabilization technique, using Portland cement as a solidifying agent. Further, the toxicity study of leachate from solidified adsorbents using different microbes confirmed almost complete encapsulation of OFL and DOX and ensured that concentration of antibiotics in leachates were insufficient to affect the microbial growth. Thus, Cytotoxicity assessment indicated that the solidified matrix of OFL and DOX did not exhibit any toxic effect after adsorption and stabilisation processes.

Adsorptive removal of antibiotics such as OFL and DOX using several types of natural and modified adsorbents has been reported by various authors. In the present study, RHA, PJAC and PSSAC adsorbents were prepared using rice husk ash, Prosopis juliflora and pumpkin seed shell respectively. Further, RHA and PSSAC were modified using deep eutectic solvent (DES) as functionalization agent to give DES-RHA and DES-PSSAC adsorbents. The studied adsorbents were characterized to determine their chemical and morphological characteristics employing FTIR, XRD, ^{1}HNMR, TGA, SEM-EDX, FESEM, HR-TEM and zeta potential. Surface area and pore size distribution were evaluated with the help of BET and BJH characterization techniques, respectively.

Batch adsorption experiments were performed for OFL and DOX removal. The influence of various adsorption parameters suggested by the central composite design (CCD) model was evaluated by Response surface methodology (RSM). A set of 30 experiments with 6 replicates were performed for each antibiotic. The interactive effects of initial adsorbate concentration (C_0), adsorbent amount (m), pH and removal time (t) were optimized. The 3D response surface graphs were also obtained for capacity (mg/g) and removal (%) of both responses. Furthermore, as suggested by ANOVA, the polynomial quadric model was significant for both antibiotics with higher coefficient values of R^2.

At optimized experimental conditions, thermodynamic and kinetic studies were also performed. The experimental data were examined by applying various kinetic and isotherm models. Pseudo-first order and pseudo-second order kinetic models were used to study the

adsorption kinetics. Further, the adsorption rate controlling mechanism was investigated using an intra-particle diffusion model. Interactions of OFL and DOX molecules with the surfaces of RHA, PJAC, PSSAC, DES-RHA and DES-PSSAC adsorbents were examined and the adsorption process controlling mechanism was explored.

The effect of temperature on the adsorption of OFL and DOX was studied at the different ranges of temperature from 288 to 318 K. The well-suited isotherms for fitting experimental data were Langmuir, Freundlich, Redlich-Peterson (R-P) and Temkin equilibrium models. The thermodynamics parameters were obtained from the linear plot of ln K_D versus 1/T. The negative value of $\Delta G°$ at each reaction temperature directed that the adsorption of antibiotics on the adsorbents was instantaneous and thermodynamically favorable. Moreover, the positive value of parameter $\triangle H°$ established the endothermic nature of antibiotics onto adsorbents. Furthermore, the increase in the randomness of the adsorbates molecules at the liquid-solid interface was approved by the positive $\Delta S°$ values. Thus, from the thermodynamic study, the adsorption of antibiotics on adsorbents was spontaneous and endothermic. Finally, adsorbents' good regeneration capability and high adsorption capacity represent their excellent potential to alleviate pharmaceutical wastes from industrial effluents.

ACKNOWLEDGMENTS

First and foremost, I would like to express my sincere gratitude to my supervisors ***Dr. Neetu Singh*** and ***Dr. Anita Rajor*** *for their continuous support in my Ph.D. study and related research. I appreciate their contribution of time, ideas, motivation, knowledge and funding to make my Ph.D. experience productive and stimulating.*

I express my heartfelt gratitude to ***Dr. Prakash Gopalan****, Director, TIET, Patiala, for providing the opportunity to work in this esteemed organization. Without their precious support, it would not be possible to conduct this research. I feel special gratitude towards* ***Dr. Rafat Siddique****, Dean, Research and Sponsored Projects, TIET, Patiala for his valuable guidance and support during my research work. I am very thankful to* ***Dr. Anoop Verma****, the former Head of School of Energy and Environment, Thapar University for providing me access to the laboratory and research facilities.*

Besides my advisors, I would like to thank the rest of my doctoral committee: ***Dr. N.Tejo Prakash****,* ***Dr. J.P. Kushwaha*** *and* ***Dr. Amit Dhir*** *for their insightful comments and encouragement, but also their keen interest in me at every stage of my research work from various perspectives.*

I am thankful to ***Mr. Suhail****,* ***Mr. Gurpreet Singh*** *and* ***Mr. Bharat*** *for their constant support and kind help throughout my research work. This research work would have not come to successful completion without the help I received from SAI Labs, TIET, Patiala, SAIF, PU, Chandigarh and MRC, MNIT, Jaipur.*

I take this opportunity to thank my special lab-mates ***Ms. Harsimranpreet Kaur, Dr. Himadri Rajput*** *and* ***Dr. Rahil Changotr*** *for the stimulating discussions, cheerful support, cooperation and for all the fun that we have had together. The group has been a source of friendships as well as good advice and collaboration.*

I am very much indebted to dear parents who have raised me with love and encouragement and always showering blessings on me. I am also grateful to my other family members and friends who have supported me along the way. Last but not least, I would like to mention the love, support and encouragement I got from ***Mr. Ranvir Singh Somal*** *whose faithful support during every stage of this Ph.D. is much appreciated.*

Above all, I owe it all to the Almighty God for granting me the wisdom, health and strength to undertake this research task and enabling me to its completion.

Gurleenjot Kaur

CONTENTS

LIST OF TABLES

LIST OF FIGURES

NOMENCLATURE

ABBREVIATIONS

^{1}HNMR	Proton nuclear magnetic resonance
AC	Activated carbon
ACFs	Activated carbon fibers
AC-GS	Activated carbon guava seeds
AMX	Amoxicillin
ANOVA	Analysis of variance
ARB	Antibiotic-resistant bacteria
ARG	Antibiotic-resistant genes
ATL	Atenolol
BAS	Biological activated sludge
BBD	Box–Behnken Designs
BC	Raw biochar
BC	*Bacillus subtilis*
BC-PM	Pig manure biochar
BC-PW	Pine wood biochar
BDAT	Best demonstrated available technology
BET	Brunauere Emmette Teller
BJH	Barrett–Joyner–Halenda
BPA	Bisphenol A
BPF	Bisphenol F
CBZ	Carbamazepine

CCD	Central composite Design
CEX	Cephalexin
CF	Cellulose fibre
CFN	Cellulose from Flax Noil
CFN	Caffeine
CFX	Cephalexin
ChC	Choline Chloride
CIP	Ciprofloxacin
CKD	Cement-kiln dust
CNTs	Carbon Nanotubes
CSH	Calcium silicate hydrate
Cu-BC	Copper nitrate modified biochar
DC	Doxycycline
DCF	Diclofenac
DCV	Dichlorvos
DES-PSSAC	Deep eutectic solvent pumpkin seed shell activated carbon
DES-RHA	Deep eutectic solvent rice husk ash
DESs	Deep eutectic solvents
DFC	Sodium Diclofenac
DI	Deionized water
DM	Doehlert Matrix
DMSO	Dimethyl sulfoxide
DOX	Doxycycline hydrochloride
DRH	Desilicated Rice Husk

E1	17α – estradiol
E2	17α – ethynylestradiol
EC	*Escherichia coli*
ECs	Emerging contaminants
EPA	Environmental Protection Agency
FESEM	Field emission scanning electron microscope
FTIR	Fourier-transform infrared spectroscopy
GAC	Granular Activated Carbon
GhO	Graphene oxide
GNS	Graphene nanosheet
GS	Grape stalk
GSAC	Grape stalk activated carbon
HBA	Hydrogen bond acceptor
HBD	Hydrogen bond donor
HQ	Hazard quotient
HR-TEM	High-resolution transmission electron microscopy
ILs	Ionic liquids
IPD	Intra-particle diffusion
LKD	Lime kiln dust
LTB	Larger the best
MAC	Magnetic activated carbon
MCFA	Modified Coal Fly Ash
MGS	Modified Grape stalk
MHA	Mueller and Hinton agar

MLD	Million liters per day
MNZ	Metronidazole
MOP	*Moringaoleifera* pod husk
MPSD	Marquardt's percent standard deviation
MSWI	Municipal solid waste inceration
MWCNTs	Multi-walled carbon nanotubes
NM	Nimesulide
NOR	Norfloxacin
NSAID	Non-steroidal anti-inflammatory drug
NTB	Nominal the best
NZ	Natural Zeolite
OFL	Ofloxacin
PAC	Commercial Powdered Activated Carbon
PACs	Pharmaceutically active compounds
PAH	Polyaromatic hydrocarbon
PCPs	Personal care products
PCT	Paracetamol
PD	Potassium diclofenac
Ph-MSs	Phenyl-functionalized mesoporous silicas
PhTES	Phenyltriethoxysilane
PJAC	Prosopis juliflora activated carbon
PP	Pomegranate Peel
PPCPs	Pharmaceutical compounds and personal care products
PPy	Polypyrrole cellulose fibre

PRO	Propranol
PSS	Pumpkin seed shell
PSSAC	Pumpkin seed shell activated carbon
QCFN	Quaternized Cellulose from Flax Noil
RCRA	Resource Conservation and Recovery Act
RHA	Rice husk ash
R-P	Redlich-Peterson
RSM	Response surface methodology
S/S	Solidification and Stabilisation
SAs	Sulfonamide
SBTL	Spent black tea leaves
SD	Sawdust
SD	HCl-treated sawdust
SEM -EDX	Scanning electron Microscopy- Energy dispersive X-Ray analysis
SERMs	Selective estrogen receptor modulators
SMX	Sulfamethoxazole
STB	Smaller the best
TC	Tetracycline
TGA	Thermal gravimetric analysis
WWTPs	Wastewater treatment plants
XRD	X-ray diffraction

NOTATIONS

B_T	Variation of adsorption energy (KJ/mol)
C_a	Adsorbate concentrations in adsorbent (mg/L)
C_l	Adsorbate concentrations in leachate (mg/L)
K_d	Equilibrium constant
q_e	Specific equilibrium amount of adsorbate (mg/g)
q_m	Maximal adsorption capacity of adsorbent (mg/g)
$\Delta G°$	Changes in Gibb's free energy (kJ/mol)
$\Delta H°$	Changes of enthalpy (kJ/mol)
$\Delta S°$	Changes in the entropy (KJ/mol/K)
C_e	Adsorbate equilibrium concentration (mg/L)
C_e	Equilibrium adsorbate concentrations (mg/L)
C_f	Final adsorbate concentrations (mg/L)
C_o	Initial adsorbate concentrations (mg/L)
h	Initial adsorption rate (g/mg/min)
K_F	Freundlich constant (L/mg)
k_f	Pseuso first order rate constant (min^{-1})
K_L	Langmuir constant (L/mg)
k_s	Pseuso second order rate constant (g/mg/min)
k_T	Equilibrium binding constant (L/g)
m	Adsorbent amount (g/L)
MPSD	Marquardt's percent standard deviation
n	Empirical constant (g/L)
pH_{pzc}	Point of zero charge
R	Universal gas constant (8.314 J/mol/K).
R^2	Correlation coefficients

t	Removal time (min)
V	Volume of the adsorbate solution (L)
X_1	Antibiotic removal (%)
X_2	Adsorption

Chapter – 1

INTRODUCTION

1.1. GENERAL

Water is the basis of life on earth and is considered one of the essential resources existing on our planet. Water accounts for almost 70 % of the earth's portion and all the life forms that exist need water for their survival. Apart from the fact that water is a necessity for life, anthropogenic activities are the main reason for water pollution. Lakes, streams, rivers, oceans, as well as groundwater are contaminated by point and non-point sources. The global trend of industrialization, urbanization and release of numerous toxic compounds have become the main cause of water pollution (Yang et al., 201; Imteaz et al., 2013). Due to the consumption of contaminated drinking water, many fatal diseases are born every year. The contaminated water is not only harming the living species but also affects the entire environment. By 2050, the expected global population growth will reach up to 9.3 billion and the world may face scarcity of freshwater (Deng et al., 2016; Huang et al., 2010). Therefore, it is a major concern and priority to act upon eliminating the ecologically harmful pollutants from the water bodies.

Among the several noxious chemicals, pharmaceutically active compounds (PACs) are of great concern (Gupta and Nayak, 2012; Gupta et al., 2015a). PACs are accredited as arising pollutants because of their bioactivity, broad application and probable health & environmental hazards (Gupta et al., 2015b; Virkutyte et al., 2006). Antibiotics are a main class of PACs which are very frequently recommended to save the human beings from diseases caused due to bacterial infections and animal growth improvement (Qi and Liu, 2014). The existence of these drugs in the H_2O cycle of the ecosystem is widely recognized throughout the world. While examining, these contaminants were also visible in the ground and drinking water samples at low concentrations (ng/L to mg/L).

According to the studies conducted in many countries, the pollution caused by pharmaceuticals or drugs in the ground and surface water resources has been recognized as an environmental problem that led to the establishment of a well-known research field such as pharmaceuticals in the environment. Pharmaceutical drugs are defined as therapeutic compounds that are mainly used to treat or prevent human and animal disorders, while the consumption of personal care products (PCPs) leads to the betterment of life (Deng et al., 2016). But,

when these drugs and their by-products are continuously released into the aquatic biota, they may induce a serious health hazard for all living organisms. Pharmaceutical compounds are consumed in large numbers globally (Kaur et al., 2021b; Iveti et al., 2014; Puga et al., 2020). Likely, the presence of many synthetic pharmaceutical compounds in the environment such as antibiotics, analgesics, anti-inflammatory, beta-blockers, blood lipid regulators and selective estrogen receptor modulators (SERMs), etc. have been identified at the global level (Kummerer, 2009; Guinea et al., 2009). These compounds are considered as emerging contaminants (ECs) and can be commonly found in hospital effluents, drug manufacturers, and landfill sites (Lu et al., 2016; Nazari et al., 2016). They have no existing threshold values and thus they remain unregulated in the effluents due to their properties such as high stability, resistance to degradation, high persistence in the aqueous system and their accumulating potential as shown in fig. 1.1.

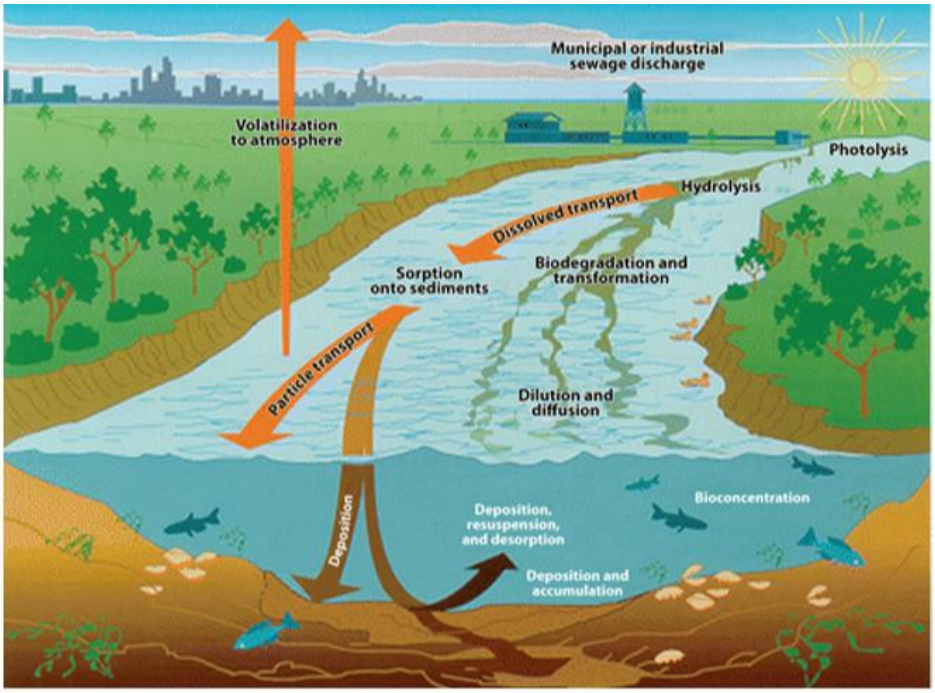

Fig. 1.1. Pathways of pharmaceuticals in water (Kummerer, 2009).

Pharmaceutical compounds at ng/L levels have major adverse effects on human beings and wildlife. In Asia, 97 % of the vulture's species were declined due to exposure of diclofenac which is a non-steroidal anti-inflammatory drug (NSAID) that caused the failure of their kidney followed by death in few days. Diclofenac also has the potential to cause an undesirable

impact on human health. In India, as per the latest estimation, out of 22,900 million liters per day (MLD) of wastewater generated in the country, about 5900 MLD (26 %) is treated, and the rest 17000 MLD is disposed-off untreated (Nabi et al., 2006; Pavithra et al., 2017). Moreover, in Europe and the USA, the existence of pharmaceutical compounds and personal care products (PPCPs) were examined in the 1960s and then in 1999. The potential risk was enhanced due to decreased fertilization rate of fishes downstream of wastewater treatment plants (WWTPs) as a side effect of the existence of pharmaceutical pollutants in river waters (Kaur et al., 2021c; Kyzas et al., 2015a; Fernandez-Sanroman et al., 2020). Amongst the various pharmaceuticals from all of the different categories, antibiotics are the most widely used class of drug around the world.

1.2. Antibiotics as emerging contaminants

Antibiotics have been extensively used for the prevention and cure of human and animal diseases that originated due to different pathogenic bacteria. Because the body cannot metabolize these antibiotics, therefore direct discharge of these antibiotics take place into the environment. Presently, pollution with antibiotics has created pandemonium in the aquatic environment, due to its large consumption and discharge (Kaur et al., 2021d; Hapeshi et al., 2013). The antibiotics or xenobiotic compounds come under the emerging contaminants category due to their wide reactivity, consumption on a larger scale that can cause chronic health hazards and ecological risks (Tajernia et al., 2014; Rehman et al., 2015). Moreover, contaminants along with their concentration range from ng/L to mg/L of metabolites eventually outcome in the enlargement of drug-resistant genes generated by micro-organisms that have the great potential to develop as a serious universal problem (Kristiansson et al., 2011; Munir and Xagoraraki, 2011). Common drugs like erythromycin, chlortetracycline, norfloxacin, ofloxacin, doxycycline hydrochloride, atenolol and sulfadimethoxine are found in surface and groundwater samples in the concentration of 381.5, 122.3, 134.2, 135.1, 77.3, 52.9, and 164 ng/L, respectively (Qi and Liu, 2014). The high production and usage rate of antibiotics has led to their water reservoirs and accumulation in the aquatic environment. Consequently, it has become an emerging issue in environmental science to achieve effective antibiotic removal from the wastewaters before discharge into the environment. Thus, major efforts to examine this problem and palliate its effects are a priority.

1.2.1. The sources and occurrence of antibiotics in the environment

The worldwide marketing of antibiotics has been estimated to be in the range of 100,000 to 200,000 tons/year (Zucatto et al., 2016). The sources causing pharmaceutical contamination include production sites, pharmaceutical industries, hospital effluents, excretion of drugs after consumption by humans and animals, direct disposal of drugs from households, etc. (Guinea at al., 2009; El-Ghenymy et al., 2013). Afterward, the drugs enter into the aquatic environment and eventually reach drinking water reservoirs after being discharge from conventional wastewater treatment plants (WWTPs) as these plants are not designed for the treatment and removal of highly polar micro-pollutants (Xu et al., 2007). A wide range of pharmaceuticals and personal care products has been detected in bio-solids. Several antibiotic compounds such as ofloxacin, galactoside, 17β-estradiol, 17α-ethinylestradiol, ciprofloxacin, doxycycline hydrochloride, norfloxacin, triclosan and triclocarban show a high hazard quotient (HQ) that is greater than one which proves their potential risk to the environment (Langdon et al., 2010). The high consumption of antibiotics by human beings would lead to their excessive concentrations in the ecosystem as their accumulation rate is quite higher than their rate of elimination (Pinheiro et al., 2013; Lombardo et al., 2014). It has been estimated that approximately 20–90 % of the metabolized forms of ingested antibiotics are released into the environment in their active forms, leading to considerable loads being discharged into domestic wastewater (Kummerer, 2009). The concentration of pharmaceutical compounds detected in WWTPs before and after treatment has been represented in table 1.1.

Table 1.1: Pharmaceutical concentrations detected in various WWTPs before and after treatment (Petrovik et al., 2005).

Type of pharmaceuticals	Substance detected	WWTP inlet (ng/L)	WWTP outlet (ng/L)
Analgesics and anti-inflammatories	Ketoprofen	451	318
	Naproxen	99	108
	Ibuprofen	516	266
	Diclofenac	250	215
	Acetaminophen	10194	2102
Lipid-lowering drugs	Bezafibrate	23	10
	Clofibrate	72	28

	Gemfibrozil	155	120
Antiepileptics	Carbamazepine	420	410
Antacids	Ranitidine	188	135
Antibiotics	Azithromycin	152	96
	Metronidazole	80	43
	Ofloxacin	590	390
	Trimethoprim	1172	290
β-Blockers	Atenolol	400	395
	Sotalol	185	167
	Propanolol	290	168

The supply of clean water fit for drinking purposes in India is only 36 % of the whole population. This population rate is significantly lesser than that of Brazil (81.3 %), Indonesia (58.8 %) as well as China (65.3 %). Amongst all these countries, India experiences a series of infectious diseases such as dengue, swine flu, malaria, urinary tract infections, respiratory tract infection, tendon rupture, insomnia and lowering of seizure threshold and peripheral nervous system, etc. In the year 2010, the major consumption of antibiotics or drugs in India was 12.9 $\times 10^9$ units (Boeckel et al., 2014). Therefore, every year a huge amount of antibiotics are introduced into the biosphere (Sharma et al., 2019; Chuudhary and Chaudhari, 2017; Patel et al., 2020).

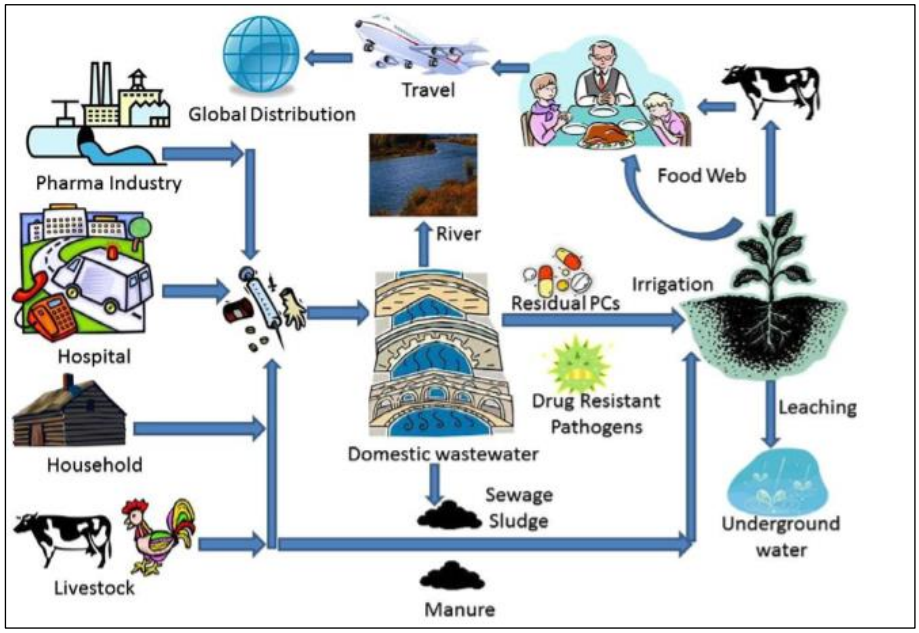

Fig. 1.2. Antibiotics in the environment (Rehman et al., 2015).

1.2.2. Transformation of antibiotics in the environment

The different routes of antibiotic compounds follow the interconnected network towards the aquatic atmosphere as shown in Fig. 1.2. The presence of antibiotics and their complex metabolite forms in the H_2O cycle of the ecosystem are widely recognized throughout the world and their concentrations have been examined in the ground as well as drinking water samples (Choudhary et al., 2021; Yadav et al., 2015; Kumar et al., 2010).

One case study examined from the Patancheru industrial area (Hyderabad, India) with the quality of wastewater containing more than 90 pharmaceutical manufacturing units has been described by a few researchers. They observed that antibiotics concentrations were up to 31 mg/L even after passing through wastewater treatment plants (WWTPs) (Fick et al., 2009; Larsson et al., 2007). It can be postulated that WWTPs are not reliable for the complete removal of contaminants from effluents because it may results in the formation of more complex metabolite forms as shown in Fig. 1.3. The concentrations of ofloxacin, ciprofloxacin, metoprolol, amoxicillin, and sulfamethoxazole antibiotics were 40 times higher in the treated discharges of Indian WWTPs as compared to the treated effluents of WWTPs in Australia, North America, Europe, and Japan (Bansal et al., 2016).

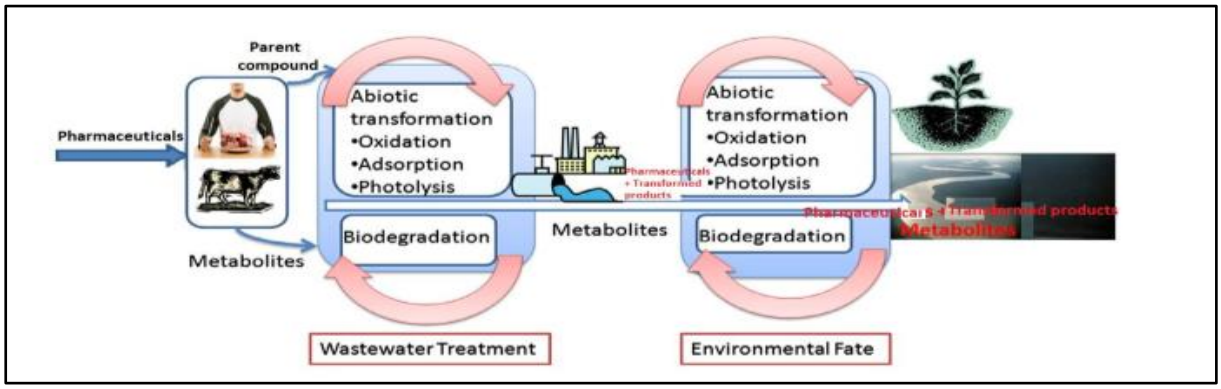

Fig. 1.3. Transformation of antibiotics in the environment (Sobsey and Bartram, 2002).

1.3. Overview of several processes of wastewater treatment

In the United States, it is estimated that approximately 25 % to 33 % of pharmaceuticals are not accurately disposed off by WWTPs and landfill sites. Therefore, these contaminants ultimately come in contact with drinking water sources that can cause a serious risk to the

ecosystem, as shown in Fig. 1.1. Most of the researchers have reported the degradation or removal of antibiotics by using different techniques such as different chemical oxidation methods, biological methods, ion-exchange methods, different filtration methods and adsorption (Arsla-Alaton and Dogruel, 2004; Kosutic et al., 2007; Gobel et al., 2007; Putra et al., 2009; Navalon et al., 2008; Rozas et al., 2010; Kushwaha et al., 2010a; Amorim et al., 2014). The several types of methods can be used either on a smaller and larger scale (Table 1.2).

Table 1.2. Merits and demerits of different methods (Crini and Lichtfouse, 2019).

Techniques	Main Characteristics	Merits	Demerits
Chemical oxidation Simple oxidation process Ozonation Hypochlorite treatment Hydrogen peroxide	Use of different types of oxidants likely O_3, ClO_2, Cl_2, $KMnO_4$, H_2O_2, etc.	• An efficient process for the good elimination of organic and inorganic compounds. • No sludge generation problems. • Water recycling possibility through bacterial strains.	• Variety of chemical Requirements • The necessity for Pre-treatment • Formation of toxic intermediates. • Release of volatile and aromatic compounds.
Biological methods Bioreactors Biological activated sludge (BAS) Microbiological treatments Enzymatic decomposition lagoon	Use of biological (pure or mixed) cultures	• Well accepted method due to simplicity and economically attractive for degradation of organic matter. • The high removal rate of BOD and suspended solids (BAS) • Also used in future technologies for elimination of emerging contaminants.	• Favorable under optimum environmental conditions. • Higher pretreatment and maintenance cost. • Poor rate of the kinetics of certain molecules. • Biological sludge formation and undesired products. • The complexity of the process. • The necessity of knowledge for the complete decomposition of pollutants.
Ion exchange method Chelating resins, selective resins, Macroporous resins,	Nondestructive process	• Technically tested procedures, easy to control and	• High cost of selective resins, maintenance and re-

polymer-based hybrid adsorbents		well-established method. • Rapid and efficient regeneration capacity of resins. • The valuable removal rate of lower concentration contaminants (nm or µm)	generation. • For larger columns large volume requirements and also pre-treatment required to remove organic matters. • pH sensitivity of the effluents and not effective for certain types of pollutants (metals, dyes and drugs).
Membrane filteration Nanofilteration (NF), Microfilteration (MF), Ultrafilteration (UF), Electrodialysis (ED), Emulsion liquid membranes (ELM)	Nondestructive semi-permeable barrier	• Production of high-quality treated effluents. • No requirement of chemicals, not solid waste generation, the efficient removal rate of a variety of organic and inorganic compounds. • Well-known separation mechanisms: size-exclusion (NF, UF, MF), solubility/diffusivity, charge separation technique electrodialysis.	• High energy requirements and investment costs at smaller or medium industries. • Membrane clogging problems and low flow rates. • Membrane filteration is specified by specific applications likely potable water production, particulate, hardness reduction, etc.

Out of these available methods discussed in table 1.2. Adsorption is considered as one of the most assured physical techniques due to the merits of being convenient, nonexpensive, efficient and effective for the adsorption of organic pollutants with no unwanted by-products (Mohamed et al., 2015). Tremendous endeavors have been done for exploring the different types of adsorbents with excellent performance. As a result, numerous natural and engineered materials have been evolved to adsorb pharmaceuticals from aqueous systems.

Worldwide, a huge amount of agricultural solid waste generates every year. This waste piles up in the agro-industrial yards and has no important industrial application and commercial value (Gupta et al., 2020; Mishra et al., 2014). Consequently, it becomes a matter of concern and contributes to severe environmental problems. Thus, the utilization of such low-cost and abun-

dantly available agricultural waste is most judicious for wastewater treatment (Soltani et al., 2017). The potential of several affluently available adsorbents such as rice husk, barley straw, almond shell, poplar, walnut sawdust, orange peel, sugarcane bagasse and coconut burch waste have been studied previously (Hameed et al., 2008). However, the use of agricultural waste as adsorbent is associated with few drawbacks like, low sorption capacity, poor physical stability (partial solubility), need for modification (by physical or chemical methods) and variation in adsorption capacities by the structure of the components inherent in it (Omo-Okoro et al., 2018). In this regard, the use of agri-residues as an adsorbent has gained great attention due to its abundance of availability and very low price. Each agri-residue material has its unique cell wall properties. Thus, these are demonstrated to be effective adsorbent materials for dealing with wastewater systems (Kaur et al., 2021).

For the last two decades, ionic liquids (ILs) have been widely used as an organic modifier for adsorbents due to their special features such as minimal vapour pressure. Mainly it has been used for clay, biomasses, nanoparticles, activated carbon, carbon nanotubes and then used for the adsorption of dyes, pharmaceuticals and phenanthrene (Sun et al., 2017, Lawal et al., 2018). Despite many outstanding physicochemical properties of ILs, its non-biodegradable, toxic nature and high cost of synthesis and purification became the main hurdle in its application in the adsorption process. Deep eutectic solvents (DESs) are promising green solvents and are considered as superior to ILs because it offers several additional advantages over ILs while retaining the required physicochemical properties. Commonly DESs are formed from two (or even more) natural, non-toxic and biodegradable sources, mainly a hydrogen bond donor (HBD) and a hydrogen bond acceptor (HBA). Due to the strong hydrogen bonds between these compounds, the evolved DESs represent a very low melting temperature than independent components. Most DESs exhibit no reactivity with water and the possibility of tailoring in its physical and chemical properties is an additional advantage (Kaur et al., 2018). The green nature of DESs makes it a better substitute for hazardous chemicals in the process of functionalization.

1.3.1. Adsorption

The adsorption process is a phenomenon that adsorbs liquid, vapour and gaseous molecules onto the solid-state of the adsorbent. Where the adsorbate molecules are always in the mobile state (liquid, vapour, and gaseous molecules) which are being absorbed by the solid-state material of the adsorbent that is in a stationary state. So, the adsorbent has the capability for sorption of the several types of molecules. Likewise, desorption is the phenomenon where the adsorbed

molecules are released from the surface of the adsorbent but in the adsorption process, the sorption of molecules occurs from one phase to another phase. In this way, both sorption and desorption processes are different from one another as shown in Fig. 1.4 (Dureja and Madan, 2007).

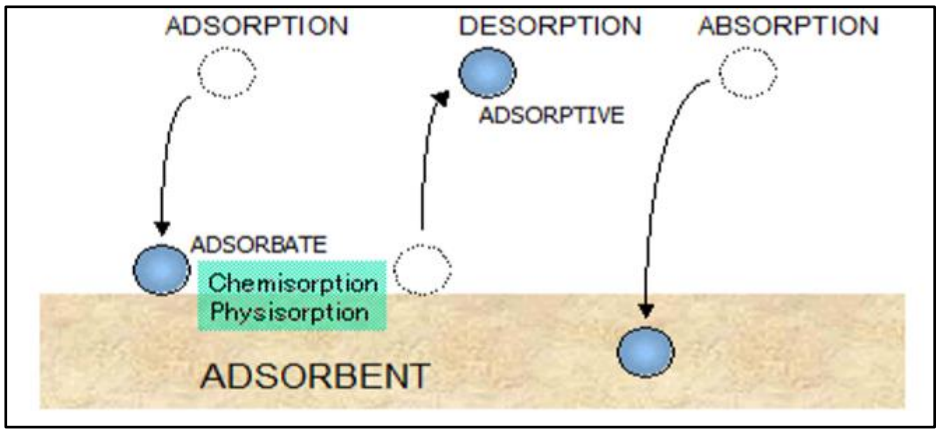

Fig. 1.4. Fundamentals of Adsorption and Desorption (Dureja and Madan, 2007).

1.3.2. Background of the adsorption process

The adsorption processes have been used since ancient times and have a long history. In 1773 and 1777, Scheele and Fontana were the first to report the adsorption behavior of various gases onto charcoal adsorbents by performing several experiments. In 1814, Saussure performed adsorption studies by systematically using adsorption apparatus and nowadays this apparatus is available in the National Historical Museum in England. In the year 1844, Chappuis calculated the adsorption results of ammonia onto charcoal at constant conditions of temperature. Then in 1881, Bois-Reymond put forward the adsorption term and also studied the concept of isotherms (Dureja and Madan, 2007).

1.3.3. Different steps of the adsorption process

Adsorption is one of the most popular technique for the adsorption of a variety of pollutants. The adsorbents are the solid and semi-solid types of material that obtain atoms and molecules from the bulk phase. The process is affected by numerous factors including the nature of the adsorbent, initial stock concentrations, pH, contact period, etc (Dureja and Madan, 2007). The adsorption process is mainly comprised of four steps as shown in Fig. 1.5. In the first step, the contaminants are transported in the solution phase. In the second step, the contaminants are transferred from the bulk phase to the outermost layer of the adsorbent surface

through a hydrodynamic boundary layer or film. In the third step, the contaminants diffuse from the outer to inner micro and mesopores of the adsorbent surface. Finally, the fourth step involves the adsorption of all the contaminants into the inner porous structure within the adsorbent (Peng and Guo, 2020).

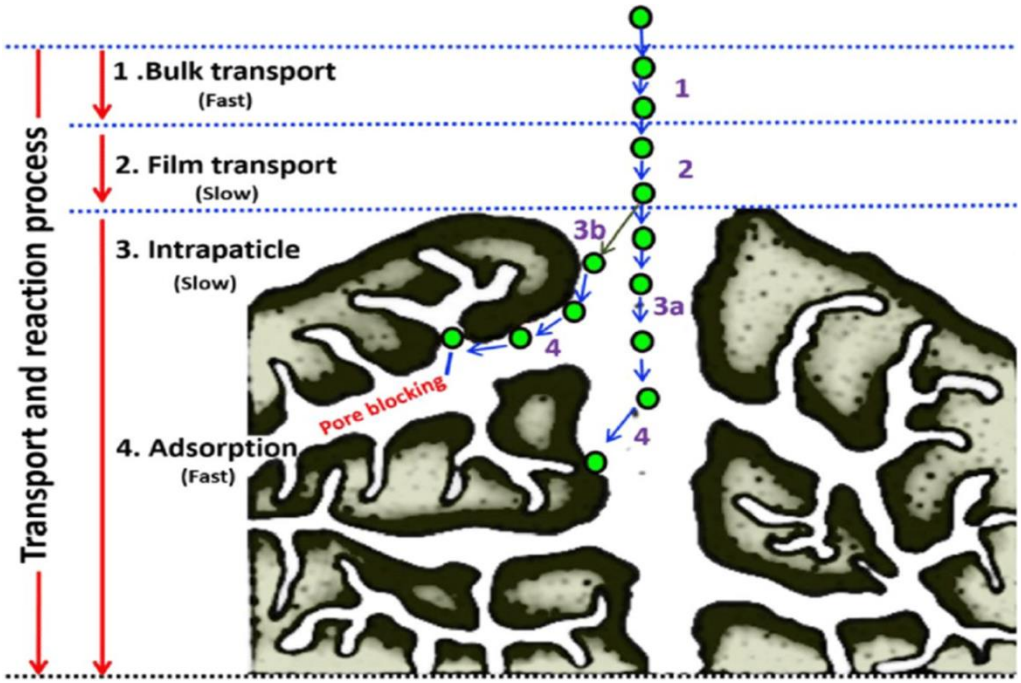

Fig. 1.5. Different Steps of Adsorption Process (Peng and Guo, 2020).

Adsorption has two main interactions one is weak interaction and the other is strong interaction. In weak interaction or Van der Waals forces, it involves the physisorption or physical adsorption having < 40 kJ/mol energy and in stronger interactions, ionic or covalent bonding is involved having > 40 kJ/mol energy that is also called chemisorption or chemical adsorption (Peng and Guo, 2020). The major difference between physisorption and chemisorption is that in physisorption all the adsorbed particles remain intact, whereas, in chemisorption, the adsorbed molecules may be fragmented into different parts upon the surface of the adsorbent. This method is called dissociative chemisorption. Moreover, the most important thing is the porous structure of the adsorbent having micropores and mesopores. The micropore has a pore size up to 2 nm and for mesopores, it is 2 to 50 nm. So that the microporous material has higher adsorption potential as compared to mesopores nature (Ania and Bandosz, 2006). For that reason, the adsorption capacities vary from adsorbent to adsorbent (Mestre, 2009). A variety of different types of adsorbents such as activated carbons, zeolites, synthetic polymers,

etc. may have variable effects on the management of different types of contaminants. So the Adsorption process has certain advantages as listed below:

- In the adsorption process, the adsorbent can be regenerated and reused in various cycles.
- No generation of sludge materials.
- Nutrients supply is not required for this process.
- The biomass used as an adsorbent can also be procured from agriculture waste residues as well as industrial wastes.
- The adsorbed contaminants can be recovered from the adsorbed adsorbents.
- No special equipment is required for the adsorption process.

On the other hand, the amount of hazardous industrial waste is increasing significantly, so its proper management can reduce harmful impacts on the ecosystem. Various technologies have been advanced to decrease the potential of toxic species into the biosphere.

1.4. Solidification/Stabilization process overview

Solidification and Stabilization is an appropriate process for the removal of toxicity from the ecosystem. It is one of the most effective technique for dealing with heavy metals, PAH, pesticides and other organic and inorganic products from contaminated sites. By applying solidification and stabilization, the mobility of hazardous substances and contaminants is significantly reduced in the environment through both physical and chemical means. Solidification is the process where it produces free-standing and monolithic masses with enhanced physical integrity. It includes an increase in compressive strength with a decrease in the permeability and encapsulation of hazardous constituents. Once the cement material comes in contact with water, tricalcium aluminate hydrates cause rapid settling which produces a rigid structure. Then the formation of secondary cementitious product calcium silicate hydrate (CSH) accounts for the strength development at the initial stages of the mixture. Whereas, stabilization is a technique that alters the chemical structure for reducing mobility and solubility of contaminants in wastewater and soils by converting the constituents into a less soluble mobile or toxic form (Agarwal, 2005; Pal et al., 2018).

1.4.1. Principle of cement-based solidification/Stabilization process

The stabilization refers to the conversion of waste contaminants to a more chemically stable form, thereby resulting in a more environmentally acceptable waste form and the used binding

agents are Portland cement, cement-kiln dust (CKD), lime, lime kiln dust (LKD), limestone, fly ash, slag, clay and phosphate mixtures, etc. (Gailius et al., 2010). Among various types of S/S binders, cement-based systems are most widely used due to their relatively low cost, wide availability and versatility (Luyao and Sisi, 2020). It involves the mixing of waste with a binder to reduce the contaminant leachability by both physical and chemical means and to convert the hazardous waste into an environmentally acceptable waste that is fit for land disposal or used for construction purposes. It has been stated that this technology has been evaluated by the United States Environmental Protection Agency as a best demonstrated available technology (BDAT) for the treatment of about 60 types of hazardous waste (Polek, 2017; Pal et al., 2018). The U.S. Environmental Protection Agency (EPA) has identified S/S as one of the best-demonstrated technology used for 57 RCRA (Resource Conservation and Recovery Act)-listed hazardous wastes, where the S/S technology was applied in 24% for the management of hazardous wastes comparatively to other remediation treatments in united states (Fig. 1.6) (Khan et al, 2004).

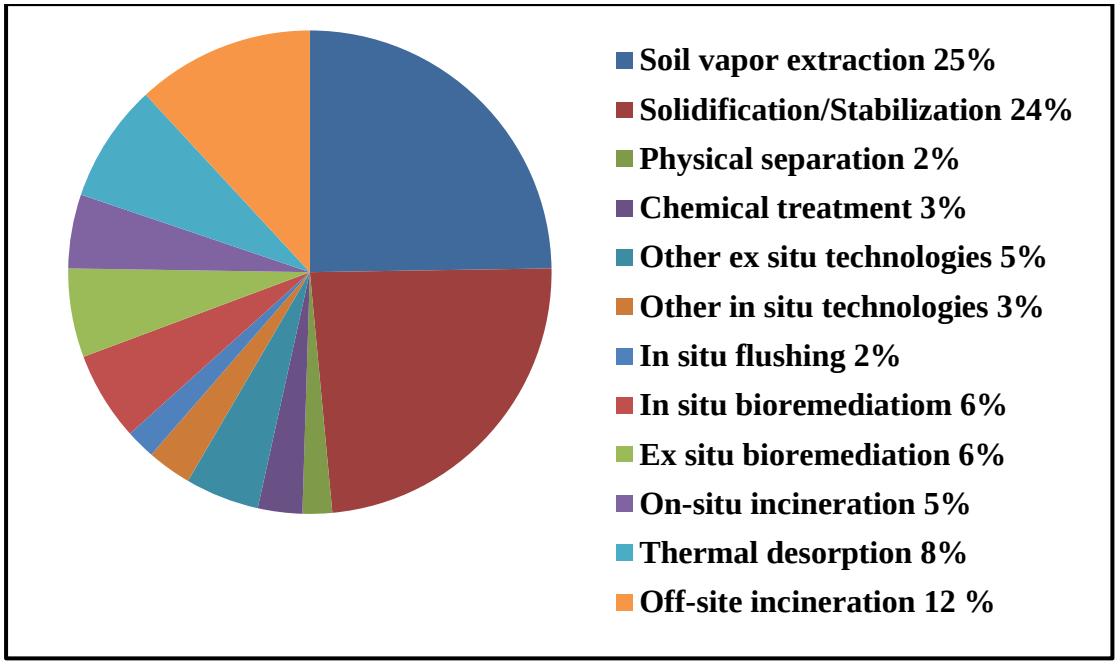

Fig. 1.6. Pie chart of different remediation technologies (Khan et al., 2004).

The cement-based S/S process has the following advantages over other remediation treatments (Luyao and Sisi, 2020):

- Relatively simple processing, low cost and easily available
- Long-term stability both physically and chemically

- No generation of toxic byproduct during processing
- Relatively higher comprehensive strength and lesser permeability in water, and
- High resistance to biodegradation process.

1.4.2. Mechanism of Cement-based solidification/stabilization treatments

The soil-based cement stabilization was firstly studied by Lea (1956) and commercialized in 1990. The components of Portland cement are tricalcium silicate (C_3S), dicalcium silicate (C_2S), tricalcium aluminates (C_3A) and tetra calcium alumina ferrite (C_3A). These components are major strength-producing ones. When water is added into the soil and cement or any toxic material, hydration reaction starts and primary cementitious product (a) hydrated calcium silicates (C_3SH_{57}, $C_3S_2H_5$), (b) hydrated calcium aluminates (C_3AH_{35}, C_3AH_8) are formed. (c) While hydrated lime ($Ca(OH)_2$), which is formed deposited as a separate crystalline solid phase. The cement particles bind with adjacent cement grain and toxicants together during the hardening and form a hard structure (Barreto et al., 2020). The following reactions were observed:

$$C_3S + H_2O \rightarrow C_3S_2H_5\ (hydrated\ gel) + Ca\ (OH)_2 \qquad \textbf{(1.1)}$$

Primary cementitious product:

$$Ca\ (OH)_2 \rightarrow Ca^{++} + 2\ (OH)^- \qquad \textbf{(1.2)}$$

$$Ca^{++} + 2(OH) + SiO_2(soil\ silica) \rightarrow CSH \qquad \textbf{(1.3)}$$

Secondary cementitious product

$$Ca^{++} + 2(OH) + Al_2O_3(soil\ alumina) \rightarrow CAH \qquad \textbf{(1.4)}$$

The hydration reaction of cement leads to raising the pH of the water which is caused by the dissociation of the hydrated lime. The hydrous alumina and silica slowly react with the calcium ions according to equation (1.3) which is formed by the hydrolysis reaction of cement to form insoluble compounds (CAH) which are shown in equation 1.4. This reaction is also called pozzolanic reaction which attests that it is the safe handling method before landfilling of the wastage at the landfill sites (Collier et al., 2006; Poon et al., 2004).

1.4.3. Fundamental tools of S/S

Fundamental tools of the Solidification and stabilization (S/S) is an attractive technique for handling harmful industrial contaminants around the sphere that reduce or entraps the leacha-

bility of contaminants by changing physical and chemical modes and convert contaminants into an ecologically adequate form for safe disposal into landfill sites. These are six physical and chemical approaches are listed as Absorption, Adsorption, Micro-encapsulation, Macro-encapsulation, De-toxification and Precipitation.

1.5. Target pharmaceutical compounds

After an intensive survey, pharmaceutical compounds like ofloxacin (OFL) and doxycycline hydrochloride (DOX) antibiotics have been examined in the present study. OFL is a member of the fluoroquinolone class of synthetic antibiotics (Francis et al., 2005). It is a broad-spectrum antibiotic used in human and veterinary medicines. OFL is frequently used for the treatment of infections caused by bacteria that are easily transported into the environment through domestic wastewaters and direct runoff (Hassan and Ali, 2014). OFL is the most frequently detected antibiotic in hospital and residential effluents. In WWTPs both raw wastewater and treated effluent have detections of fluoroquinolone like OFL at concentrations ranging from 110 to 470 ng/L (Brown et al., 2006).

Doxycycline hydrochloride (DOX) is a broad-spectrum antibiotic that comes under the tetracycline (TC) category. It has great responses against both gram-positive and negative bacterial species (Ghaemi and Absalan, 2015). Comparative to its complex structure and higher soluble nature, DOX displays high toxic effects in surface water and groundwater samples (Zhang et al., 2016). The high consumption of DOX by a human would lead to excessive concentrations in the ecosystem. Due to the continuous input of these pollutants, human health and all ecosystems would be at greater risk. Recently measured DOX and OFL concentrations in influents and effluents of wastewater streams are almost 50 – 90 % in the form of metabolites. Both antibiotics (OFL and DOX) are non-biodegradable which is revealed from their abundant existence in several aquatic environments (Ahmed et al., 2015).

1.6. OBJECTIVES

In view of the literature survey and the necessity of exploring the agriculture-based adsorbents for adsorption of PACs from wastewater, the following aims and objectives have been set for the present work:

- To investigate the adsorption of pharmaceutically active compounds (PACs) using ash derived from agri-residues.
- Optimization of parameters for removal of PACs by the selected adsorbents and to identify the kinetic and isotherm models.
- To explore the solidification and stabilization of adsorbents using cementitious material.

OVERVIEW OF THESIS

Thesis has been divided into six chapters as listed below:

CHAPTER 1 discusses the pathways of pharmaceuticals in water bodies, with particular focus on antibiotics as emerging pollutant. The sources, fate and occurrence of antibiotics in different aquatic streams and potential health threats are conferred followed by critical analysis of conventional treatment techniques, and adsorption as an efficient method.

CHAPTER 2 reviews the literature on application of adsorption process for treatment of pharmaceutical compounds using different types of adsorbents and operating conditions. Identified research gaps and objectives set for present study were mentioned thereafter.

CHAPTER 3 describes the materials and methodology followed for conducting the batch adsorption experiments.

CHAPTER 4 presents the performance of different agri-residue based adsorbents for adsorption of antibiotics (OFL and DOX). It includes the effect of relevant operating parameters on performance of different adsorbents. Kinetics, isotherms, S/S, bacterial toxicity and reusability studies of these adsorbents are also summarized in this chapter.

CHAPTER 5 covers the study of modified agri-residue adsorbents for adsorption of selected antibiotics (OFL and DOX). Modifications were done by using deep eutectic solvent as functionalization agent. Further analysis about parameters optimization, kinetics, isotherms and reusability studies of the adsorbents are also presented in same chapter.

CHAPTER 6 concludes the present study.The cited references and list of publications are added after chapter 6.

Chapter – 2

LITERATURE REVIEW

2.1. GENERAL

This chapter presents the review of literature based on the adsorption studies of antibiotics by using different types of adsorbents. On the basis of Literature review, the research gaps and objectives were set up.

2.2. Overview of pollution caused by pharmaceutical industries

In India, the improvement in the medicinal area due to rapid enhancement of population rate and industrialization has radically increased pharmaceuticals' consumption. Afterward Europe and North America, India had get 3rd position in the production of pharmaceutical compounds worldwide (Sturini et al., 2012). Pharmaceutical and industrial wastewater comes under the "red category" due to the huge volume index of hazardous waste materials generates by these sources (industrial and pharmaceutical effluents). Thus, it is necessary to require an effective process for the recyclability of wastewaters and to diminish the adversative effects on an immediate basis. Moreover, deposition of pharmaceutical contaminants as biosolids form may cause harmful effects to terrestrial and aquatic ecosystems (Michael et al., 2013; Langdon et al., 2010).

2.3. Adsorption studies of antibiotics by using different types of adsorbents

Adsorption processes have been the best one than other techniques for wastewater treatment due to their simplicity, operation, less sensitivity of toxic substances (Tong et al., 2010). Worldwide, a huge amount of agricultural solid waste generates every year. This waste piles up in the agro-industrial yards and has no important industrial application and commercial value. Consequently, it becomes a matter of concern and contributes to severe environmental problems. Thus, the utilization of such low-cost and abundantly available agricultural waste is most judicious for wastewater treatment (Soltani et al., 2017). However, the use of agricultural waste as an adsorbent is associated with few drawbacks like low sorption capacity, poor physical stability (partial solubility), need for modification (by physical or chemical methods) and variation in adsorption capacities by the structure of the components inherent in it (Omo-Okoro et al., 2018). The different categories of the adsorbents are explained in fig. 2.1.

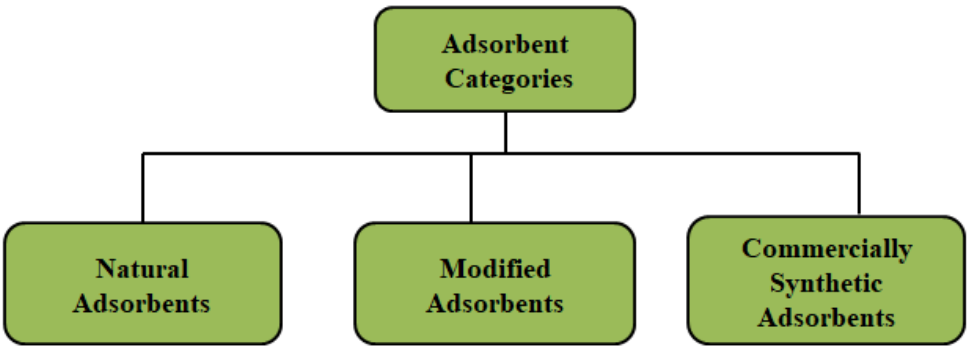

Fig. 2.1. Different categories of the adsorbents.

2.3. 1. Natural agricultural wastes as adsorbents

Natural agricultural wastes are widespread that is used for the removal of antibiotics. Different authors have reviewed the elimination of various types of contaminants from wastewater using natural agricultural wastes as adsorbents (Mo et al., 2018). Only a few works have been reported for the removal of antibiotics by using natural adsorbents. Some of the natural agricultural wastes studies have been examined for the removal of contaminants include tea waste (Zhou et al., 2015), bagasse (Rattanachueskul et al., 2016), straw (Salem and Yakoot, 2016), banana skin (Gupta and Gupta, 2015c), wheat straw (Shang et al., 2015), mustard (Safa, 2016), walnut shell (Tonucci et al., 2015), olive powder etc. (Gamiz et al., 2016). Villaescusa et al. (2011) observed the use of different types of bioabsorbents (cork bark, grape stalk and yohimbe bark) for the removal of paracetamol antibiotics and also investigated the effects of several parameters. Moreover, some of the other agricultural solid wastes such as almond shell, poplar, walnut sawdust (Aydin et al., 2004), orange peel (Arami et al., 2005), sugarcane bagasse (Ibrahim et al., 2006), coconut burch waste and seed of papaya (Hameed et al., 2008) were also examined for the removal of various types of pollutants from contaminated sites. Ifelebuegu et al. (2015) studied the adsorption properties of some selected contaminants (17 α-estradiol (E1), 17α – ethynylestradiol (E2) and bisphenol A (BPA) on black tea leaves waste and granular activated carbon (GAC) at pH 7 and 35^{o}C temperature. Nurchi et al. (2015) further determined the adsorption of ofloxacin and chrysoidine from wastewater by using grape stalk at different pH (4, 7 and 9) but the higher rate of adsorption at pH 4 for chrysoidine and at pH 7 for ofloxacin which was up to 50 % (Jung et al., 2013). Thus, natural agricultural waste adsorbents have several advantages such as low cost, easily available, abundant and easily regenerated.

2.3. 2. Modified agricultural wastes as adsorbents

The modification of the agricultural wastes to improve adsorption properties of agri-residues for the removal of antibiotics. Use of various methods which include mainly acid and alkali treatments. Some of the other modified agents such as H_3PO_4 (Umar et al., 2015), HNO_3 (Wang and Yan, 2011), H_2SO_4 (Baccar et al., 2012), NaOH (Martins et al., 2015), K_2CO_3 (Ahmed and Theydan, 2013b), KOH (Njoku et al., 2014) etc. were also used for the modification of the agricultural wastes. Alidadi et al. (2018) inspected the ability of modified sawdust adsorbent with HCl, $NaHCO_3$, $CaCl_2$ and $FeCl_3$ for removal of tetracycline antibiotics. Ahmed and Theydan (2013a) studied the preparation of activated carbon (AC) from siris seed pods by using microwave-assisted pyrolysis KOH activation technique for the removal of metronidazole (196.31 mg/g). Ahmed and Theydan (2014) also investigated the AC from albizia lebbeck seed pods by microwave pyrolysis for the removal of fluoroquinolones antibiotics. Some of the researchers have explored the utilization of different types of agricultural wastes such as rice husk (Chowdhury et al., 2011), foumanat tea waste (Pirbazari et al., 2014), wheat straw (Batzias et al., 2009), rejected tea (Nasuha and Hameed, 2011), etc. were modified by using modifying agents. For example, Nasuha and Hameed reported the modification of dried rejected tea by using NaOH solution. Later, wheat straw was modified by using H_2SO_4 solution. Wuana et al. (2015) studied chemically activated and carbonized adsorbents organized from Moringa oleifera pod husks (MOP). They found their ability to remove OFL from its aqueous solution. At a temperature range of 298-328 K and pH 5 they achieved 99.84 % to 90.98 % removal. Mukoko et al. (2015) prepared activated carbon from Zimbabwean rice hull and further activated it chemically by using phosphoric acid for the elimination of ibuprofen, aspirin and paracetamol from hospital effluent on optimum conditions like contact time, adsorbent dose and pH. All these pharmaceuticals gave 90 % results at pH 4. On the other hand, industrial wastes used such as fly ash, blast furnace slag, red mud, waste slurry are applied currently for the removal of antibiotics (Rodriguez-Diaz et al., 2015). Thus, modified agricultural waste adsorbents prove highly effective against antibiotics.

2.3.3. Commercially synthetic adsorbents

Moreover, the different species of commercially synthetic adsorbents were applied such as Fe_3C-multiwalled carbon nanotubes (MCNT) (Konicki et al., 2012), polyurethane foam (Vinhal et al., 2015), silica gel (Nie et al., 2015), CNT-Al_2O_3 (Ihsanullah et al., 2015), Pt/poly(2-methoxyaniline)- MCNT (Raoof et al., 2014), zeolite (Guo et al., 2015), magnetite, quartz (El-

Zahhar et al., 2014) etc. for the removal of contaminants from the aqueous systems. Zhang et al. (2013) examined the Multi-walled carbon nanotubes (MWCNTs) as an excellent adsorbent that can be recycled for bisphenol F (BPF) from contaminated water treatment Plants under pH 4–10 and temperature 286–313K. Moreover, Phenyl-functionalized mesoporous silicas (Ph-MSs) were synthesized for the removal of bisphenol A (BPA) from wastewaters. Ph-MSs were prepared with different compositions of phenyltriethoxysilane (PhTES) (10 %, 15 %, 20 %, and 30 %) in silica precursors. The adsorption attractions for BPA were Ph-MS30 > Ph-MS20 > Ph-MS15 > PhMS10 at pH 6.2 to 7 and temperature 27^{o}C (Kim et al., 2014). Wang et al. (2013) used the sulphuric acid-activated Halloysite (a tubular clay mineral) as an adsorbent for the removal of pharmaceutical compounds and achieved 60 % removal efficiency. In their further study, they examined the performance of sediment (sediment affected by varying concentrations of antibiotics adorable species) on adsorption of sulfamethoxazole (SMX) and OFL at different pH and 25^{o}C temperature and determined its adsorption kinetics. Also, the removal of beta-blockers from aqueous media was studied by graphene oxide. Likewise, adsorption studies of carbamazepine and sulfamethoxazole pharmaceuticals have been examined by using CNTs (Cai et al., 2014; Zhang et al., 2011a). On other hand, the adsorption of certain lactam antibiotics such as amoxicillin, cephalexin, cefadroxyl and ampicillin from aqueous media has been studied using several polymeric adsorbents to extract and purification of bioproducts. Recently, it is explored that the use of Lewatit MP500 resin for the removal of sulfamides, sulfamethoxazole and sulfamethazine antibiotics (Fernandez et al., 2014). Use of aluminum and iron nanoparticles as adsorbents for the removal of a variety of pharmaceuticals (Arslan-Alaton and Olmez-Hanci, 2017). All these different adsorbents categories are used for the removal of antibiotics and their performances are summarized below in Tables 2.1, 2.2 and 2.3.

Table 2.1. The results obtained for the removal of pharmaceutically active compounds (PACs) by using natural adsorbents.

Name of Adsorbent	Adsorbate	Optimum purposes	Optimum conditions	Optimum value	References
Desilicated Rice Husk (DRH)	Ciprofloxacin (CPX)	Adsorption capacity	Initial concentration = 314.8 mg/L, pH = 7.92, time = 306.9 min and adsorbent dosage = 0.40 g/L	454.68 mg/g	Zhang et al. (2017)
Grape stalk (GS)	Caffeine	Adsorption capacity	Initial concentration = 20 mg/L, pH = 2, time = 40 min and adsorbent dosage =	89.2 mg/g	Portinho et al. (2017)

			25 g/L		
Rice husk ash (RHA)	Ofloxacin (OFL)	Removal efficiency	Initial concentration = 62.5 mg/L, pH = 6, time = 430 min and adsorbent dosage = 7.94 g/L	79.71 %	Kaur et al. (2021a)
Different biochars: Pig manure biochar (BC-PM), pine wood biochar (BC-PW)	Diclofenac	Removal efficiency	Initial concentration = 2 mg/L, pH = 6.5, time = 48 h and adsorbent dosage = 0.1 g/L	BC-PM 99.6 % BC-PW 99.8 %	Lonappan et al. (2018)
Bone char	Naproxen	Adsorption capacity	Initial concentration = 50, 100, 200 mg/L, pH = 5-7, time = 24 h and adsorbent dosage = 10 mg/L	3.2 mg/g	Reynel-Avila et al. (2015)
Cellulose from Flax Noil (CFN), Quaternized Cellulose from Flax Noil (QCFN)	Amoxicillin (AMX)	Adsorption capacity	Initial concentration = 80 mg/L, pH = 10, time = 10 h and adsorbent dosage = 0.4 g/L at 25^{o}C temperature	183.14 mg/g QCFN>CFN	Hu and Wang, (2016)
Rice husk	Metronidazole (MNZ)	Removal efficiency	Initial concentration = 100 mg/L, pH = 7, time = 90 min and adsorbent dosage = 3 g/L at 27^{o}C temperature	96.4 %	Azarpira and Balarak, (2016)
Maize stalks	Tetracycline (TC)	Removal efficiency	Initial concentration = 100 mg/L, pH = 7, time = 90 min and adsorbent dosage = 2.5 g/L	85.5 %	Balarak et al. (2016)
Rice husk ash (RHA)	Tetracycline (TC)	Adsorption capacity	Initial concentration = 20 mg/L, pH = 5, time = 600 min and adsorbent dosage = 2 g/L	8.37 mg/g	Chen et al. (2016)
Date palm leaflets	Ciprofloxacin	Adsorption capacity	Initial concentration = 50-300 mg/L, pH = 6, time = 90 min and adsorbent dosage = 2 g/L at 318 K temperature	133.30 mg/g	El-Shafey et al. (2012)
Grape stalk	Paracetamol	Adsorption capacity	Initial concentration = 20 mg/L, pH = 6,	2.18 mg/g	Villaescusa et al. (2011)

			time = 48 h and adsorbent dosage = 3.3-33.3 g/L at 293 K temperature		
Sunflower seed shells	Atrazine	Adsorption capacity	Initial concentration = 0.005-1 mg/L, pH = 6, time = 240 min and adsorbent dosage = 12 g/L at 298 K temperature	6.34 mg/g	Rojas et al. (2014)
Isabel grape bagasse	Diclofenac sodium	Adsorption capacity	Initial concentration = 30 mg/L, pH = 5, time = 340 min and adsorbent dosage = 0.2 g/L at 295 K temperature	23.77 mg/g	Antunes et al. (2012)
Pomegranate wood-AC	Amoxicillin	Adsorption capacity	Initial concentration = 50-500 mg/L, pH = 6, time = 300 min and adsorbent dosage = 0.8 g/L at 298 K temperature	437 mg/g	Moussavi et al. (2013)
Siris seed pods-AC	Ibuprofen	Adsorption capacity	Initial concentration = 20-120 mg/L, pH = 2-4, time = 240 min and adsorbent dosage = 0.67 g/L at 303 K temperature	378.10 mg/g	Mestre et al. (2007)

Table 2.2. The results obtained for the removal of pharmaceutically active compounds (PACs) by using activated or modified adsorbents.

Name of Adsorbent	Adsorbate	Optimum purposes	Optimum conditions	Optimum value	References
Modified Grape stalk (MGS)	Caffeine (CFN)	Adsorption capacity	Initial concentration = 20 mg/L, pH = 2, time = 30 min and adsorbent dosage = 15 g/L at 25^{o}C temperature	129.6 mg/g	Portinho et al. (2017)
Grape stalk activated carbon (GSAC)	Caffeine (CFN)	Adsorption capacity	Initial concentration = 20 mg/L, pH = 4, time = 30 min and adsorbent dosage = 15 g/L at 25^{o}C temperature	916.7 mg/g	Portinho et al. (2017)
Activated carbon fibers (ACFs)	Caffeine (CFN)	Adsorption capacity	Initial concentration = 500 mg/L, pH = 2-9, time = 240 min and adsorbent dosage = 25 mg in 25 mL solution	155.50 mg/g	Beltrame et al. (2018)

			at temperature 25-55^{o}C		
Activated carbon (olive-waste cakes)	Naproxen, Ketoprofen, and Ibuprofen	Removal efficiency	Initial concentration = naproxen (20 mg/L), ketoprofen (20 mg/L) and Ibuprofen (10 mg/L) pH = 4.12, time = 26 h and adsorbent dosage = 0.3 g/L at temperature 25^{o}C	90.45 % for naproxen, 88.40 % for ketoprofen and 70.07 % for ibuprofen.	Baccar et al. (2012)
Modified Coal Fly Ash (MCFA)	Ciprofloxacin	Adsorption capacity	Initial concentration = 100 mg/L, pH = 5.6, time = 100 min and adsorbent dosage = 4g in 100 mL at temperature 323 K	1.547 mg/g	Zhang et al. (2011b)
Two activated carbons from agricultural wastes: Albizia lebbeck seed pods by KOH (KAC) and K_2CO_3 (KCAC) activation	Cephalexin (CFX)	Adsorption capacity	Initial concentration = 20-100 mg/L, pH = 7, time = 90 min and adsorbent dosage = 0.5 g/L at temperature 323 K	137.02 and 118.08 mg/g by KAC and KCAC	Ahmed and Theydan, (2012)
NaOH-activated carbon guava seeds (AC-GS)	Amoxicillin (AMX)	Adsorption capacity	Initial concentration = 800 mg/L, pH = 4, time = 240 min and adsorbent dosage = 1 g/L at temperature 25 ^{o}C	570.48 mg/g	Pezoti et al. (2016)
Microwave-assisted Activated carbon from cocoa shell (MWCS-1.0)	Sodium Diclofenac (DFC), Nimesulide (NM)	Adsorption capacity	Initial concentration = 10-300 mg/L, pH = 7-8, time = 223.14 min (DCF) and 45.46 min (NM) and adsorbent dosage = 50 mg in 50 mL at temperature 25 ^{o}C	63.47 mg/g (DFC) and 74.81 mg/g (NM)	Saucier et al. (2015)
Biopolymer modified montmorillonite (MMT)–CuO composites: MMT–CuO–Chitosan (Ch),MMT–CuO–Gum ghatti (Gg),	Dichlorvos (DCV)	Removal efficiency	Initial concentration = 80 mg/L, pH= 10, time = 5 h and adsorbent dosage = 1.5 g/L at temperature 30 ^{o}C	MMT–CuO–Ch composite (93.4 %) followed by MMT–CuO–Gg (87.8 %), MMT–CuO (83.2 %) and MMT–CuO–PLA (63.3	Sahithya et al. (2015)

and MMT–CuO–Poly Lactic acid (PLA) (A)				%)	
Raw, Acid and alkali-treated biochar	Tetracycline (TC)	Adsorption capacity	Initial concentration = 50-1000 mg/L, pH = 7, time = 24 h and adsorbent dosage = 5 g/L at temperature 303 K	16.95, 23.26, and 58.82 mg/g by raw, acid and alkali treated biochar	Liu et al. (2012)
MCM-41 impregnated with A zeolite (A-MCM-41)	Tetracycline (TC)	Adsorption capacity	Initial concentration = 100 - 500 mg/L, pH = 3-10, time = 2 h and adsorbent dosage = 0.004 g in 50 mL at temperature 303 K	419 mg/g	Liu et al. (2013)
Modified graphene	Doxycycline (DC)	Adsorption capacity	Initial concentration = 20-140 mg/L, pH = 6, time = 24 h and adsorbent dosage = 0.3g/L at temperature 30 ^{o}C	555.56 mg/g	Chao et al. (2014)
Copper nitrate modified biochar (Cu-BC)	Doxycycline hydrochloride (DOX)	Removal efficiency	Initial concentration = 20 mg/L, pH = 8, time = 24 h and adsorbent dosage = 2 g/L at temperature 25 ^{o}C	93.22 %	Liu et al. (2017)
Activated carbon fibers (ACFs)	Caffeine (CFN)	Adsorption capacity	Initial concentration = 500 mg/L, pH = 7, time = 240 min and adsorbent dosage = 25 mg in 25 mL at temperature 25 ^{o}C	155.50 mg/g	Beltrame et al. (2018)
Commercial Powdered Activated Carbon (PAC) from pine tree (PAC-I), Agricultural Crop Wastes, Coal (PAC-II), Coconut Shell (PAC-III), and Carbon Nanotubes (CNT)	Sulfamethoxazole	Adsorption capacity	Initial concentration = 1 mg/L, pH = 7, time = 2 h and adsorbent dosage = 1-1.5 g/L at 25^{o}C temperature	Higher adsorption capacity by PAC-I and CNT showed 131 mg/g and 29 mg/g than others.	Tonucci et al. (2015)
Powdered activated carbon	Sulfonamide (SAs) and	Removal efficiency	Initial concentration = 10 µg/L, pH = 7, time	90-100 % removal in	Choi et al. (2008)

(PAC): coal based and co-conut based	Tetracycline (TAs)		= 24 h and adsorbent dosage = 0.8 g/L at 25^{o}C temperature	both cases	

Table 2.3. The results obtained for the removal of pharmaceutically active compounds (PACs) by using commercially synthetic adsorbents.

Name of Adsorbent	Adsorbate	Optimum purposes	Optimum conditions	Optimum value	References
Magnetic ion ex-change resins (MIEX resin)	Sulfameth-oxazole (SMX), Tet-racycline (TCN) and Amoxicillin (AMX)	Adsorp-tion ca-pacity	Initial concentration = 20, 100 and 500 µg/L, pH = 7, time = 30 min and adsorbent dosage = 250 µL/50 mL	789.32, 443.18 and 155.15 µg/mL for SMX, TCN and AMX, re-spectively	Wang et al. (2017)
Natural Zeolite (NZ) and Zeolite coated with manganese oxide nanoparticles (CZ)	Cephalexin (CEX)	Removal efficiency	Initial concentration = 10-40 mg/L, pH = 7, time = 120 min and adsorbent dosage = 6 g/L	28 % and 89 % for NZ and CZ re-spectively	Samarghandi et al. (2015)
Graphene oxide (GhO)	Atenolol (ATL) Pro-pranol (PRO)	Removal efficiency	Initial concentration = 60 mg/L, pH = 2, time = 0-24 h and adsor-bent dosage = 1 g/L at 25^{0}C temperature	93 % (ATL) and 68 % (PRO)	Kyzas et al. (2015b)
Organo-montmorillonite: do-decyltrimethyl ammo-nium bromide (DDTMA) and Hexa-decyltrimethyl ammo-nium bromide (HDTMA)	Bisphenol A	Removal efficiency	Initial concentration = 5-500 mg/L, pH = 4-5, time = 12 h and adsor-bent dosage = 0.2-0.3 g/L at 25^{0} C tempera-ture	96.3 % and 98.9 % for DDTMA and HDTMA	Park et al. (2014)
Functionalized multi-walled CNTs (MWCNTs): hydrox-ylized (MH), carbox-ylized (MC), and graphitized (MG)	Ofloxacin (OFL) and norfloxacin (NOR)	Removal efficiency	Initial concentration = 2-700 mg/L of OFL and 2-60 mg/L of NOR, pH = 7, time = 7 d and adsorbent dos-age = 1-3 mg/5-40 mL at 25^{0} C temperature	20-90 % removal of OFL and NOR fol-lowed the order of MH > MG ≈ MC.	Peng et al. (2012)
Multi-walled CNTs: graphitized (MG), car-boxylized (MC) and hydroxylized (MH)	Ofloxacin (OFL)	Removal efficiency	Initial concentration = 10 mg/L, pH = 2-12, time = 7 d and adsor-bent dosage = 0.1-0.3	20 – 90 %	Peng et al. (2012)

			g/L at 25^0 C temperature		
Fe_3O_4/sepiolite magnetic composite (MSEP)	Atrazine	Adsorption capacity	Initial concentration = 2-28 mg/L, pH = 6.5, time = 120 min and adsorbent dosage = 1-3 g/L at 25^0 C temperature	15.9 µg/m^2	Liu et al. (2014)
Different carbon materials: AC-F400, AC-PS, AC-RH, CNF and MWNT	Carbamazepine, (CBZ) and Ciprofloxacin (CPX)	Adsorption capacity	Initial concentration = 100 mg/L, pH = 7, time = 4h and adsorbent dosage = 2-3 g/L at 30^0 C temperature	242 mg/g and 264 mg/g for CBZ and CPX respectively	Alvarez-Torrellas et al. (2017)
Goethite	Diclofenac (DCF)	Adsorption capacity	Initial concentration = 250-2000 µg/L, pH = 5-10, time = 5-2880 min and adsorbent dosage = 20 g/L at 25^0 temperature	45.96 µg/g	Zhao et al. (2017)
NaY zeolite	Doxycycline (DC)	Adsorption capacity	Initial concentration = 40-120 mg/L, pH = 2-12, time = 0-24h and adsorbent dosage = 0.02 g/L at temperature 30°C	252.12 mg/g	Ali et al. (2017)
Graphene Oxide (Gho)	Beta-blockers: Atenolol (ATL) and propranolol (PRO)	Adsorption capacity	Initial concentration = 60 mg/L, pH = 2, time = 0-24 h and adsorbent dosage = 1 g/L at 25°C temperature	67 mg/g and 116 mg/g for PRO and ATL	Kyzas et al. (2015b)
H67S33-600 (sample with 67% polysiloxane H44 and 33% of sludge pyrolyzed at 500°C), M40T60-600 (sample with 40% of polysiloxane MK and 60% of TEOS and pyrolyzed at 600°C)	Diclofenac (DCF) and Nimesulide (NM)	Adsorption capacity	Initial concentration = 50 mg/L, pH = 7 for DCF and 9 for NM, time = 120 min and adsorbent dosage = 40 mg/L at 25°C temperature	By H67S33-600: 27.18 mg/g and 14.25 mg/g for DCF and NM. By M40T60-600: 41.43 and 26.12 mg/g for	Reis et al. (2016)

				DCF and NM.	
Cellulose fibre (CF), polypyrrole cellulose fibre (PPy)	Potassium diclofenac (PD)	Adsorption capacity	Initial concentration = 0.1 mg/mL, pH = 2-10, time = 1 h and adsorbent dosage = 25.19 mg/L at 25^{o}C temperature	210.07 mg/g and 50.33 mg/g by PPy and CF	Pires et al. (2017)
Biopolymer modified MMT-CuO composites: MMT-CuO-Ch (modified montmorillonite CuO chitosan), MMT-CuO-Gg (Gum ghatti), MMT-CuO, MMT-CuO-PLA (poly-lactic acid)	Dichlorvos (DCV)	Removal efficiency	Initial concentration = 20-100 mg/L, pH = 3-12, time = 1-12 h and adsorbent dosage = 0.5-3.0 g/L at temperature from 20-50^{o}C	MMT-CuO-Ch (93.4 %), MMT-CuO-Gg (87.8 %), MMT-CuO (83.2 %), MMT-CuO-PLA (63.3 %).	Sahithya et al. (2015)
Magnetic Chitosan Grafted Graphene Oxide Nanocomposite (MCGO)	Ciprofloxacin (CIP)	Adsorption capacity	Initial concentration = 20 mg/L, pH = 5, time = 8 h and adsorbent dosage = 10 mg/L in 30 mL at 25^{o}C temperature	282.9 mg/g	Wang et al. (2016)
NaY Zeolite	Doxycycline (DC)	Adsorption capacity	Initial concentration = 40-120 mg/L, pH = 12, time = 10 h and adsorbent dosage = 2 g/L at 30^{o}C temperature	252.12 mg/g	Ali et al. (2017)
Graphene nanosheet (GNS)	Doxycycline (DC)	Adsorption capacity	Initial concentration = 10-100 mg/L, pH = 6-7, time = 200 min and adsorbent dosage = 0.010 g in 10 mL at 25^{o}C temperature	110 mg/g	Rostamian and Behnejad, (2018)
Mesoporous silica	Doxycycline (DC)	Adsorption capacity	Initial concentration = 5-450 mg/L, pH = 7, time = 6h and adsorbent dosage = 2 g/L at 25^{o}C temperature	1123.55 mg/g	Brigante and Avena, (2016)
Graphene oxide	Doxycycline (DC)	Adsorption capacity	Initial concentration = 0-100 mg/L, pH > 4, time = 0.2 h and ad-	35.50 mg/g	Lin et al. (2013)

			sorbent dosage = 2 g/L at 25^{o}C temperature		
Magnetic activated carbon (MAC) iron(III)/cobalt(II) benzoates (MAC-1) and iron(III)/cobalt(II) oxalates (MAC-2)	Amoxicillin (AMX) and Paracetamol (PCT)	Adsorption capacity	Initial concentration = 70-2000 mg/L, pH = 4-10, time = 1-300 min and adsorbent dosage = 30 mg in 50 mL solution at temperature 25-50^{o}C	280.9 and 444.2 mg/g of AMX by MAC-1 and MAC-2. 215.1 and 399.9 mg/g of PCT by MAC-1 and MAC-2	Saucier et al. 2017
Functionalized nanoclay Composite adsorbent	Naproxen	Removal efficiency	Initial concentration = 10 mg/L, pH = 6, time = 120 min and adsorbent dosage = 1 g/L at temperature 25 ^{o}C	92.2 %	Rafati et al. 2016

2.4. Applications of Adsorption Process

Adsorption is considered as one of the most assured physical technique due to the merits of being convenient, inexpensive, efficient and effective for the adsorption of organic pollutants with no unwanted by-products. Tremendous endeavors have been done for exploring the different types of adsorbents with excellent performances. As a result, numerous natural and engineered materials have been evolved to adsorb pharmaceuticals from the water environment (drinking and waste). Apart from the adsorption process, all other advanced techniques have disadvantages like capital and operational cost and sludge generation (Mashkoor and Nasar, 2020). Thus, it is a widely used method in several types of fields. The use of natural and non-natural waste materials is explored due to the wide availability of surface adsorption sites and large surface areas (Xu et al., 2018). Generally, chemical modification of the adsorbents has higher adsorption capacities as compared to unmodified materials (Kaliannan et al., 2019). Scientists examined the effectiveness of different adsorbents towards pharmaceuticals. Some of the industrial wastes accomplished of removing Pharmaceuticals from wastewater are rice husk ash, bagasse fly ash, grape stalks, Modified coal fly ash, Modified graphene, NaY Zeolite, Alumina etc. These all the materials have a high potential for adsorption which is used in a wide range of applications. The industrial materials have variations in chemical composition which is responsible for high specific surface area and high porosity so it has the great potential to be used as an effective adsorbent. Due to this reason, it is used by various industries

worldwide on a smaller as well as larger scale (Bahrami et al., 2017). The adsorption process not only solves the problem of bio-waste burden but also achieves the goal of "treating waste by waste".

2.5. Applications of Solidification/Stabilization Process

Environmental contamination through the discharge of hazardous waste from various industries has become a serious global issue. The quantity of hazardous solid, as well as industrial waste, is increasing significantly, so its proper management can reduce harmful impacts on the ecosystem. Various technologies have been advanced to decrease the potential of toxic species into the biosphere. Out of these technologies, solidification/stabilization (S/S) by cement binder is the best one for the elimination of adverse effects on the ecosystem. The S/S is generically defined as a chemical and physical alteration technique for dropping the movement of contaminants in wastes by converting them into chemically inert form (Yang and Min, 2008).

This process produces free-standing and monolithic masses with enhanced physical integrity. S/S is applied for dealing with heavy metals, polyaromatic hydrocarbon (PAH), Pesticides, antibiotics and other petroleum products from contaminated sites. The stabilization refers to the conversion of waste contaminants to a more chemically stable form, thereby resulting in the more environmentally acceptable waste form (Gailius et al., 2010). This technique makes alterations in chemicals for reducing the mobility and solubility of contaminants in wastewater and soils. Among various types of S/S binders, cement-based systems are usually evaluated due to relatively cheap, wide-ranging disposal and adaptability. In this technique the cementing material comes in contact with water and tricalcium aluminate hydrates (CSH), rapid settling occurs and produces a rigid structure, developing strength in the mixture and contaminants are binded inside.

Bie et al. (2016) demonstrated that the leaching concentration of heavy metal of Municipal Solid Waste Inceration (MSWI) fly ash reduced significantly after being blended with cement within 32 hours. S/S of heavy metals such as Cd, Cu, Pb, Ni, Zn etc. used different cement binder and water content ratios that are 5 % to 20 % binder dosages and from 14 % to 21 % water contents followed for 28 days. Inorganic wastes and contaminated soils were also treated for 28 days with cementitious or pozzolanic binders (S/S) before landfilling. On the other hand, hazardous and radioactive waste is stabilized with Portland cement for safe disposal into the environment (Stegemann and Zhou, 2009).

Cement-based S/S is used successfully with metals because it makes a strong barrier to the mobilization of metals. We are going to use the S/S process for PhACs waste due to several benefits as compared to other remediation technologies such as electrochemical oxidation process, advanced oxidation process, biodegradation process etc. (Paria and Yuet, 2006). Advantages of S/S are: Relatively low economically and easy for usage and handling, durability both physically and chemically. Subsequently, the S/S with cementitious binders is an important technique for reducing leachability of contaminants: industrial wastes, organic and inorganic wastes, radioactive wastage and contaminated soils before disposal or reuse (Stegemann and Zhou, 2009).

2.6. Summary

Consequently from the review literature, it is concluded that the adsorption studies by using agricultural residues are less comparatively synthetic or commercially available adsorbents. Even agricultural waste has good adsorption properties, less cost and available in large amounts.

2.7. RESEARCH GAPS

Based on the literature discussed above, the following research gaps have been identified:

1. Most of the authors used electro-oxidation techniques for the removal of pharmaceutical compounds, which is associated with drawbacks of high energy consumption, formation of intermediate toxic substances, high capital cost etc. Very few studies are reported on the removal of pharmaceutically active compounds (PACs) by using adsorption technique.
2. Very few studies are available on the adsorption of ofloxacin (OFL), out of which of the majority of adsorbents are synthetic.
3. Disposal study of exhausted adsorbents is quite important, which is not reported in detail for PACs.
4. Any type of solidification study for PACs the agriculture-based adsorbent system is not yet reported.

Chapter – 3

MATERIALS AND METHODS

3.1. GENERAL

This chapter describes the materials and methods that are used for the removal of synthetic pharmaceutical wastewater containing ofloxacin (OFL) and doxycycline hydrochloride (DOX) as model compounds for adsorption purpose. The experimental methodology has been illustrated and the details of the methodology part have been discussed. Fig. 3.1 represents the workflow of the present research work.

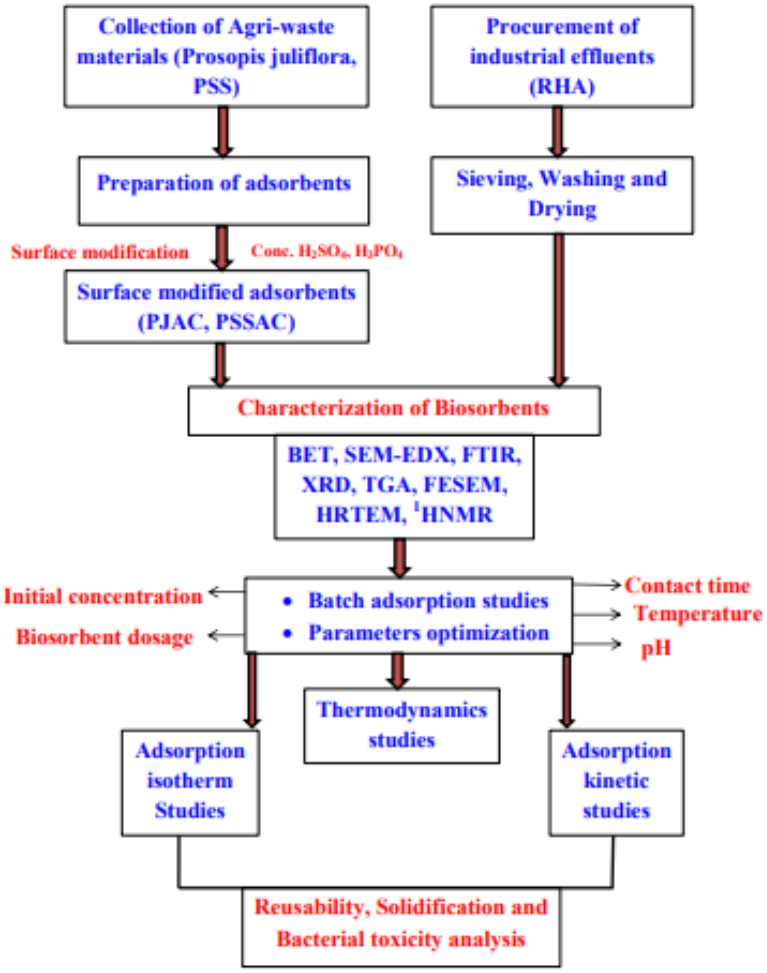

Fig. 3.1. Workflow of the Present Research Work.

3.2. MATERIALS

3.2.1. Wastewater and Chemicals

The synthetic wastewater samples were freshly prepared for each set of experiments at room temperature. A predetermined quantity of antibiotics (ofloxacin and doxycycline hydrochloride) was dissolved in double distilled water with the help of a magnetic stirrer. For the batch mode of the adsorption process, the effects of adsorption parameters such as initial pH, dosage of adsorbent (m), contact time (t) and initial adsorbate concentration (C_0) were studied on the responses; % removal (X_1) and adsorption capacity (mg/g) (X_2) using the central composite design (CCD) based on response surface method (RSM).

The purest powder forms of both antibiotics were obtained from different manufacturing industries**.** Ofloxacin (99.9%) was provided by Shri Ramesth Industries (a unit of Zhen Heal Craft Private Ltd.), Himachal Pradesh, India and doxycycline hydrochloride (99.8%) was procured from Varav biogenesis Private Ltd. Himachal Pradesh, India. The reagents like H_2SO_4 (98%), NaOH (99%) and Muller Hinton Agar (MHA) media were purchased from Himedia Laboratories Pvt. Ltd. India. Microbes, *E.coli* (EC), *Bacillus subtilis (BC), Escherichia coli* (strain K12), *Bacillus halodurans* (strain KG1) and *Bacillus magaterium* MTCC – 1684 were attained from the Department of Biotechnology and Portland cement were obtained from the Department of Civil Engineering, Thapar Institute of Engineering and Technology, Patiala (India).

3.2.2. Selection of different agri-residue adsorbents: Suitable agriculture wastes such as Rice husk ash (RHA), Prosopis juliflora activated carbon (PJAC) and Pumpkin seed shell activated carbon (PSSAC) were used for this study. RHA was obtained from Satyam agro solvex Khanna, Punjab (India). PJAC and PSSAC were prepared in laboratory by simple pyrolysis technique and micro-wave assisted pyrolysis technique respectively. PSSAC and RHA were further functionalized using deep eutectic solvent in a view to improve the adsorptive performance of these agri-residue adsorbents.

3.3. METHODS

3.3.1. Preparation of Activated carbon from Prosopis juliflora

The Prosopis juliflora branches were attained from an alternative energy solution, Yamuna Nagar, Punjab. Consequently, the collected branches were washed with deionized water (DI) water to eliminate dust particles and other impurities. Then cut it into small pieces of ~1-2 cm and dried in sunlight for 6-7 days. This dried matter of Prosopis juliflora was impregnated

with 1:1 H_2SO_4 solution for the surface sites' activation. After that, the resultant material was washed 3-4 times with DI water and overnight dried (~100^oC) in an oven. The oven-dried material was then taken into a crucible and transferred to a muffle furnace at 500^oC. Finally, the activated carbon obtained from Prosopis juliflora was grounded, sieved (100-150 µm) and kept in an airtight container until required. Step by step procedure for preparation is represented in Fig. 3.2.

Fig. 3.2. Methodology for preparation of PJAC.

3.3.2. PSSAC Adsorbent preparation

Pumpkin seeds (Cucurbita moschata Duchesne) were procured from the local market of Punjab, India. Pumpkin seeds were cleaned by using warm water for reducing the dirt particles from the surface of the material. After washing, seeds were oven-dried at 70^oC temperature for 6-7 hours. Now shells of the dried seeds were separated and then it was left under sunlight for 3 days for the maximum moisture removal. Finally, the dried shells were grinded, crushed and sieved to 20-30 mesh fractions. This prepared material was denoted as PSS.

3.3.2.1. Acid activation and microwave-assisted pyrolysis of PSS

The chemical activation of the PSS was done by soaking the powdered PSS in orthophosphoric acid (H_3PO_4). 10 g of PSS powder was blended with 100 ml of 85 % diluted H_3PO_4 solution in a 200 ml flask. Now, the mixture was agitated at 70^oC temperature and 150 rpm speed in a rotary shaker for 6 hours to make sure the complete reaction of H_3PO_4 solution with PSS.

After a predefined time, the mixture was filtered and cleaned using deionized water till the leachate pH approached ~ 6. Next, activated PSSAC was dried in an air-drying oven and put in a desiccator. Finally, the chemically-treated PSS was pyrolyzed using microwave-assisted pyrolysis technique at 500-600 W for 8-10 minutes under the N_2 environment with a flow rate of 100 mL/min (Danish et al., 2014; Kunquan et al., 2010). This pyrolyzed pumpkin seed shell activated carbon (PSSAC) was cleaned thoroughly using the hot distilled water up till the pH of the washing solution approached neutral value. Eventually, it was oven-dried for 24 h at 100^{o}C and then kept in an air-tight container for further use in the experimental studies. The schematic representation of the procedure for PSSAC preparation is given in Fig. 3.3.

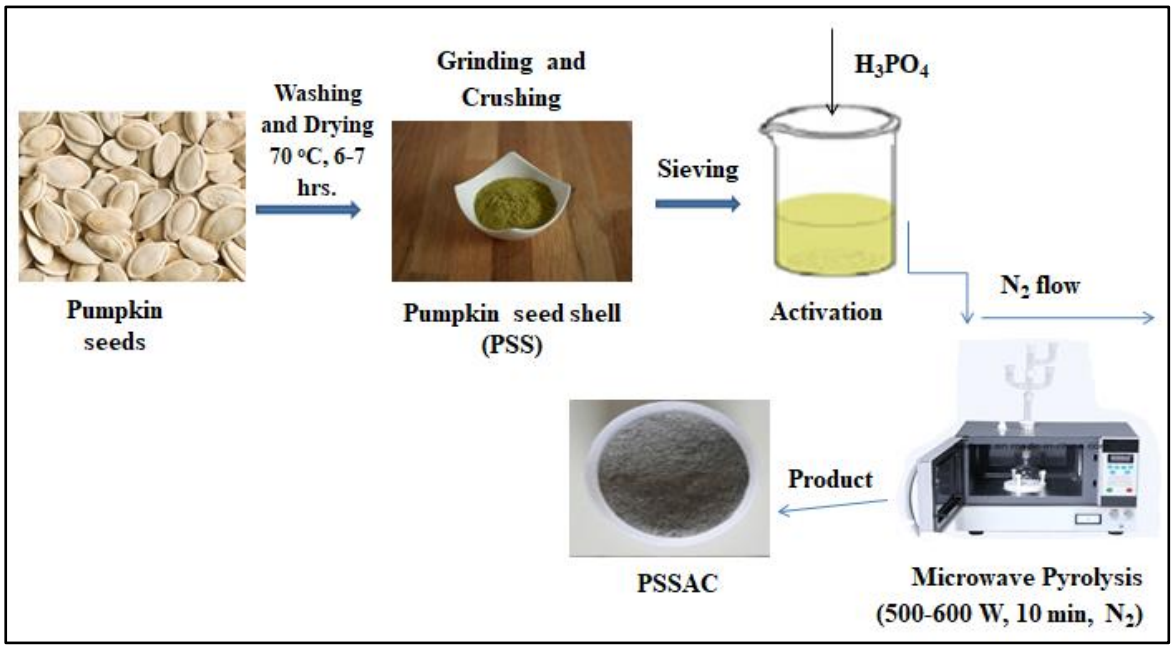

Fig. 3.3. Methodology for preparation of PSSAC.

3.3.3. RHA Adsorbent preparation

RHA, procured from industry was washed with hot water at 80 ˚C and it was dried at 70^{o}C temperature overnight. The dried RHA sample was screened with particle size of 180-600 µm using IS sieves (IS: 437, 1979) and was kept in an airtight container for further use.

3.3.4. Preparation of Deep eutectic solvent functionalized adsorbents

3.3.4.1 . Synthesis of deep eutectic solvent (DES)

Choline chloride-based DES was synthesized using glycolic acid as an hydrogen bond donor (HBD) and choline chloride (ChCl) as hydrogen bond acceptor (HBA), using the same procedure as reported earlier (Sharma et al., 2018). Both components were weighted accurately using a Mettler Toledo electronic balance with the uncertainty of ±0.0001 g. HBD and HBA were taken together into a small glass flask in a 3:1 molar ratio respectively (GC3:1). After proper mixing, the mixture was heated using a thermostatic oil bath with continuous stirring. The oil bath was maintained at 70˚C (±0.1 °C) using a temperature controller (IKA ETS-D5). The mixture of both components melted together and stirred, once enough liquid has resulted. Heating was stopped when the colorless and transparent liquid was formed. It was allowed to cool at room temperature and left overnight to ensure the formation of DES. The prepared DES was stored in glass sealed vials and kept in a moisture-free atmosphere to avoid the humidity effect.

3.3.4.2. DES functionalized PSSAC (DES–PSSAC)

DES–PSSAC was prepared by modifying PSSAC at different DES modification levels by following the method reported in the literature (Hayyan et al., 2015; Smith et al., 2014). The methodology for the preparation of DES–PSSAC is represented in Fig. 3.4. 20 g of dried PSSAC was mixed separately with different amounts of GC3:1 (50 to 120 mL) in 150 mL conical flask with continuous stirring with the help of a magnetic stirrer at 70 °C temperature. Then, the mixture was transferred into 150 ml beaker and sonicated for 3 hours at 65 °C temperature. Afterward, it was allowed to cool at room temperature. The prepared DES–PSSAC was washed 3-4 times using deionized (DI) water and filtered with the help of whatmann No. 1 filter paper. Finally, the resulted material was oven-dried at 100 °C for 24 hours before use, to make sure complete moisture removal (Foo and Hameed, 2011). The prepared DES–PSSAC sample was stored in an airtight glass container for further use in batch adsorption studies.

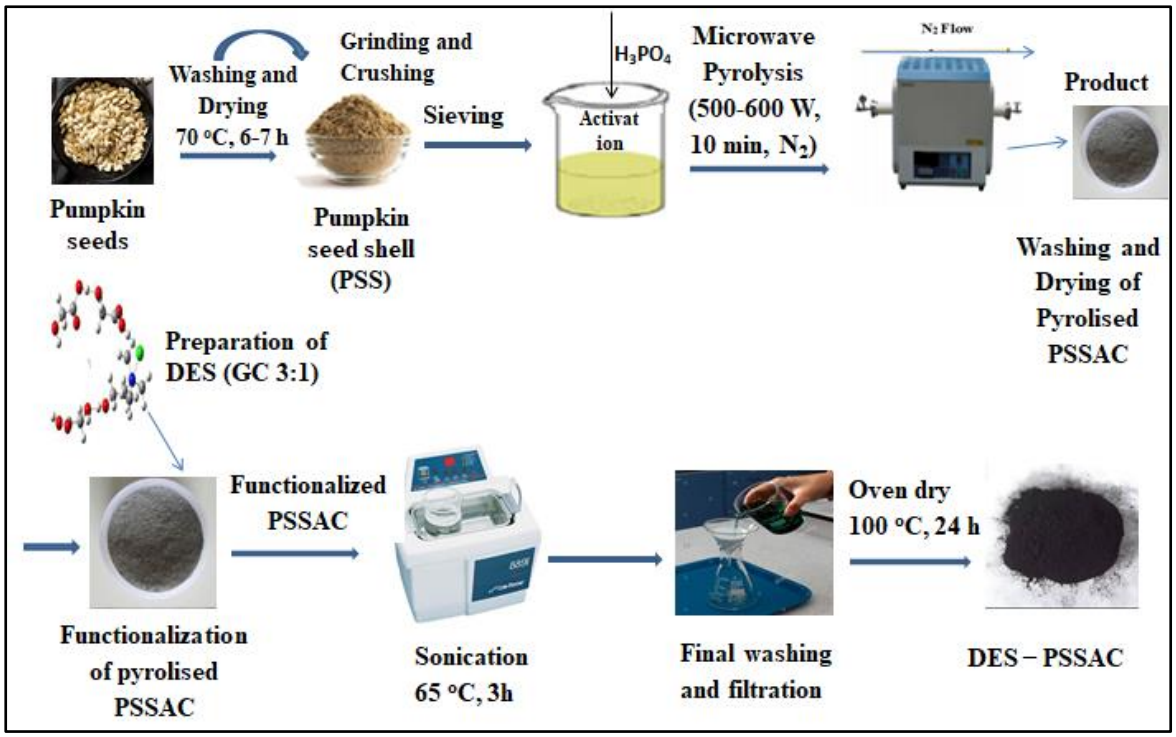

Fig. 3.4. Methodology for preparation of DES–PSSAC.

3.3.4.3. DES functionalized RHA (DES–RHA)

GC3:1 functionalized RHA was prepared by following the method reported in the literature (Pam, 2019). The schematic diagram of a methodology for the preparation of DES–RHA is presented in Fig. 3.5. 20 g of washed and dried RHA was mixed with 100 mL GC3:1 with continuous stirring at 70 °C. The mixture was sonicated for 3 hours at 65 °C. DES–RHA was then washed 3-4 times using distilled water and filtered with whatmann No. 1 filter paper. Finally, it was oven-dried at 100 °C for 24 hours before use, to ensure complete moisture removal.

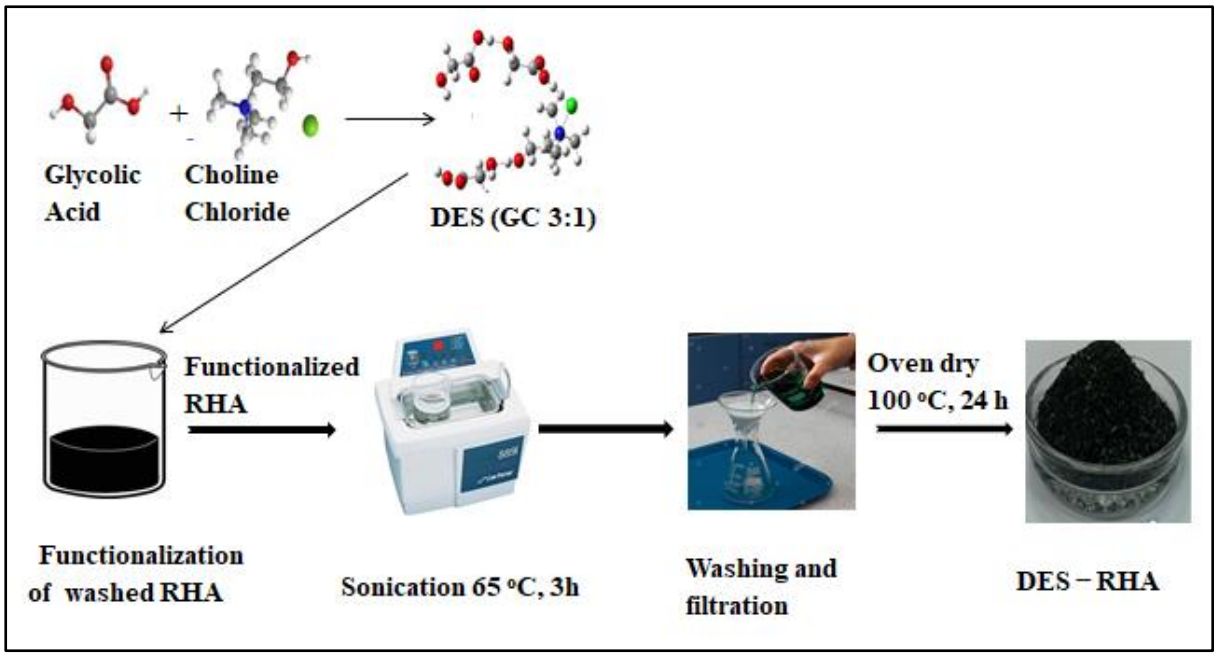

Fig. 3.5. Schematic diagram illustrating the formation of DES–RHA (Pam, 2019).

3.4. INSTRUMENTS AND ANALYTICAL TECHNIQUES

The residual/equilibrium antibiotic concentrations were observed using a dual-beam UV-visible spectrophotometer (model HITACHI U-2000). The UV-visible spectra of OFL and DOX were determined at the wavelength (λ_{max}) of 288 nm and 345 nm respectively using a standard curve. The calibration curves of both antibiotics were prepared by using different concentrations of the known samples and are depicted in Fig. 3.6 a and b. The plots were presented between absorbance versus known concentrations of the solution. The regression equations were applied for the calibration plot of OFL (y = 0.0703 x) and DOX (y = 0.1208 x) enabled us to find out the unknown concentrations of the different samples that were collected from the adsorption process. The value of absorbance was obtained by using the spectrophotometer.

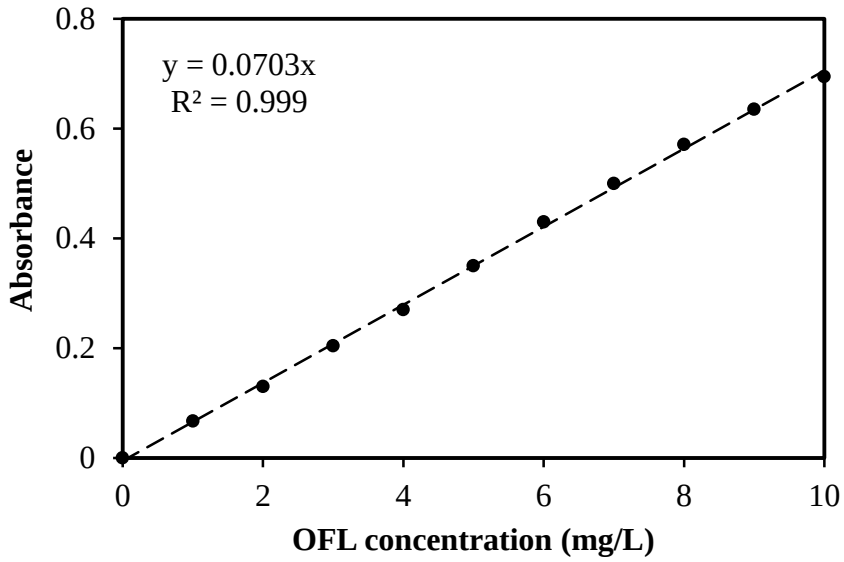

(a)

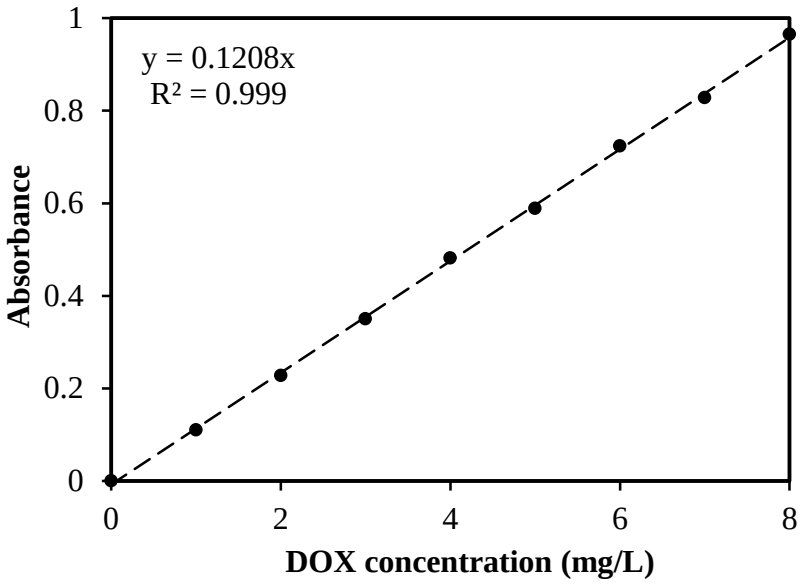

(b)

Fig. 3.6. Calibration curves for (a) OFL and (b) DOX antibiotic.

All the chemical compounds used for adsorption studies were of analytical grade. The reagents were weighed using a Mettler Toledo (AB104-S) scale. According to the requirement, different stock solution concentrations were freshly prepared and pH of the synthetic wastewater was measured through Thermo scientific orion star A111 pH meter. Then use of GeNei SLM–IN–OS– 16, India, incubator shaker for experimental reactions. For the preparation of activated carbon adsorbent from the raw waste by using the microwave-assisted pyrolysis (TA *Model* 2050). Moreover, for the functionalization of the adsorbent by using the *Model* 150VT *Ultrasonic* Homogenizer sonicator.

The morphological and chemical characteristics of the selected adsorbents were characterized by using different analytical techniques. The morphological analysis was accomplished with the help of SEM (EDX) and high-resolution FESEM (JEOL JSM-7500F). Moreover, for a better understanding of the morphology, high-resolution images were taken using TECNAI G2 F20 transmission electron microscope. X-ray diffraction (XRD) pattern was obtained by Bruker D8-Advance X-ray diffractometer (Bruker, Germany), at 2θ (10-90°) with Cu as the object and Ni as the filter media with $\lambda = 1.541$ Å having Kα radiations. The specific surface area was obtained by using the BET technique, and the pore volume (total) was determined at a relative pressure of about 0.95 in the presence of liquid nitrogen. The pore size was evaluated via the Barrett–Joyner–Halenda (BJH) method and pore volume were calculated with the t-plot method. Before gas adsorption measurements, the sample was degassed at 300 °C under vacuum for 3 h, and the adsorption-desorption isotherms were measured at 77 K (Micromeritics/Gemini-2372). Also, Fourier-transform infrared spectroscopy (FTIR) spectra were determined with the help of Nicolet 6700 spectrometer, the USA in the 4000 – 400 cm^{-1} wavenumber range.

The synthesized DES (GC 3:1) was characterized to evaluate its properties and confirm the hydrogen bonding between the original components of DES. To check the thermal stability of prepared GC 3:1, TGA analysis was performed (PerkinElmer, STA6000). The moisture content of GC 3:1 was also examined employing the Karl Fischer titration method (Esico, 1760). ^{1}HNMR and FT-IR analysis was performed to ensure the H-bonding between glycolic acid and ChCl. The ^{1}HNMR of the prepared DES (GC3:1) was determined by operating Bruker AVANCE Neo 500 MHz NMR spectrometer at room temperature. The DES sample, for NMR analysis, was made by dissolving 25 mg of the DES in 0.5 mL of DMSO in a 5 mm NMR tube. The homogeneous mixture of GC3:1 and DMSO were made using a vortex mixer.

The point of zero charge (pH_{pzc}) which is a critical factor and strongly influences the surface charge of the material was also evaluated. pH_{pzc} of the adsorbents were evaluated by salt addition technique (Mahmood et al., 2011). In this method, 40.0 mL of 0.1 M KCl solution was taken in eleven different conical flasks of 100 mL capacity. The pH of the solutions was maintained at different values (2 to 12) by utilizing 0.1 M H_2SO_4 and 0.1 M NaOH as needed. 0.2 g of the adsorbent samples were introduced to every eleven conical flasks. These solutions were agitated for 24 h in a rotary shaker at room temperature and 200 rpm. Once the settling was done, the pH of the supernatant was checked in each conical flask. The deviation between the $pH_{initial}$ and pH_{final} was evaluated and the point at which ΔpH is zero was considered as pH_{pzc} of the adsorbent.

3.5. EXPERIMENTAL PROCEDURE AND ANALYSIS

3.5.1. Use of CCD/RSM model for Batch Adsorption Process

Response surface methodology (RSM) is a static analytical method that shows the relationship between dependent and independent variables while taking more than one response to determine experimental studies. It includes variations within ranges for the optimization of different selected parameters. This method is also valuable for reducing cost and saving time by minimizing the number of experimental reactions (Box and Behnken, 1960). There are many investigational design models, such as pentagonal, Central Composite Designs (CCD), Hexagonal, Box–Behnken Designs (BBD), Doehlert Matrix (DM) and so on. The popularity of the CCD/RSM model on a large scale for adsorption studies has been preferred (Witek-Krowiak et al., 2014). In RSM, designing involves mainly three steps: (a) determine the interaction between dependent – independent variables (b) Then selecting the suitable model from RSM design expert software (c) Finally, implementation of experimentations and calculating valuable results.

3.5.2. Design of Experiments and Optimization

Experiments for the adsorption of the antibiotic on adsorbent were designed and performed by Central composite design (CCD) based on response surface methodology (RSM). The RSM is a statistical tool that facilitates in designing of experiments with a reduced number of experiments, analysis of the interaction between parameters on responses, and optimization of the process parameters for required responses (Soo et al., 2004). pH (2–10), adsorbent dosage (0.5–2.5 g/100 mL), adsorbate concentration (10–90 mg/L), and time (10–750 min) coded with

five-level CCD were considered as independent adsorption process variables, while % antibiotic removal (X_1) and antibiotic adsorption capacity (X_2) were selected as responses.

The following quadratic model was applied for the experimental data fittings, analysis, and optimization of process parameters (Eq. 3.1).

$$X = \psi_0 + \sum_{i=1}^{k} \psi_i x_i + \sum_{i=1}^{k} \psi_{ii} x_i^2 + \sum\sum_{i<j} \psi_{ij} x_i x_j + D_r \qquad \textbf{(3.1)}$$

Where, ψ_0: constant-coefficient; $\psi_{i,}$, ψ_{ii}, ψ_{ij}: Interaction coefficients; x_i and x_j: Variables; D_r: error.

Analysis of variance (ANOVA) was used for the parameter interaction analysis. Further, the model adequacy was assessed by adequate precision, Studentized residuals plots, normal probability plots, coefficient of determination (R^2), predicted R^2 and adjusted R^2, and F and P values.

A Multi-response optimization tool was applied for the optimization of two responses, X_1 and X_2, using the desirability function of RSM. The Multi-response optimization tool in RSM optimizes the responses depending on the set target. The target may be set as smaller the best (STB); larger the best (LTB) and nominal the best (NTB) (Kushwaha et al., 2011; Sangal et al., 2013). Whereas, the desirability function converts the individual desirability (d_i: 0–1) of the responses, X_1 and X_2, into one single desirability value of the system. In this study, the LTB type target was set for the responses X_1 (% antibiotic Removal) and X_2 (antibiotic adsorption capacity) optimization.

3.5.3. Adsorption of Batch Experiments and Data Analysis

In the present study, a total of 30 experiments in the batch mode were conducted as designed by CCD/RSM, and % antibiotic removal (X_1) and adsorption capacity (X_2) were measured. For each set of experiments, in 100 ml antibiotic solution of specified initial concentration and previously adjusted desired pH known dose of adsorbent (as per design matrix) was added. The mixture was then agitated at a constant speed of 150 rpm and 303 K temperature in a temperature-controlled orbital shaker incubator (Remi Elektronik Ltd., India; CIS-24 Plus). For initial pH adjustment, 0.1 N H_2SO_4 and 0.1 N NaOH solutions were used. The maximum absorption of OFL and DOX was found at λ_{max} = 288 nm and λmax = 345 nm respectively. For each set of experiments, after the equilibrium/predetermined time of the adsorption process, the mixture was drawn and the adsorbent was separated by filtration. Further, the ab-

sorbance of the filtrate was observed using a UV-visible spectrophotometer (Electronic Corporation India Ltd.), and equilibrium/residual adsorbate concentration was evaluated from the calibration curve. Adsorbate % removal (X_1) and adsorption capacity (X_2) of adsorbent was then calculated using the following relation:

$$\%\ Removal\ (X_1) = \frac{(C_0 - C_f)}{C_0} \times 100 \qquad \textbf{(3.2)}$$

Furthermore, the equilibrium adsorption capacity, q_e (mg/g) was calculated as:

$$Absorption\ capacity, q_e\ (X_2) = \frac{(C_0 - C_e)}{m} \times V \qquad \textbf{(3.3)}$$

Where, C_o, C_f, and C_e represent the initial, final, and equilibrium adsorbate concentrations (mg/L) in the aqueous phase, respectively, V represents the volume (L) of the adsorbate solution and *m* (g/L) to the mass of adsorbent.

3.5.4. Solidification/Stabilization (S/S) Studies of Exhausted adsorbent

The appropriate management of exhausted adsorbent waste is essential to avoid the release of antibiotics in ecosystems and its adverse impacts on human beings. For this purpose, the solidification/stabilization (S/S) technique was adopted due to its well-known advantages (Kogbara et al., 2013). Loaded adsorbent (having different adsorbate concentrations) and Portland cement were mixed in different mass ratios (Table 3.1) to observe the effect of binder on the leachability behavior of adsorbate. For this purpose, loaded adsorbent and cement were mixed using the required amount of water to make the paste. The beads of approximately 2 cm diameter were made and incubated at room temperature for 24 h. The incubated beads were then soaked in 100 ml distilled water for 15 days maintaining water level throughout the experimentation. After 15 days, the concentration of adsorbate in water was measured using a UV-visible spectrophotometer to observe the leachability of the adsorbate. Step by step procedure for the S/S process is represented in Fig. 3.7.

The capsulation percentage of adsorbate was calculated using the following relation:

$$Capsulation\ percentage = \frac{(C_a - C_l)}{C_a} \times 100 \qquad \textbf{(3.4)}$$

Where, C_a and C_l represent the adsorbate concentrations (mg/L) in adsorbent and leachate respectively.

Table 3.1. Different combinations of exhausted adsorbent and cement for solidification study.

Sample No.	Mass of adsorbent + cement in the mixture	Mass ratio of adsorbent to cement
1	1 g adsorbent + 5 g cement	1:5
2	2 g adsorbent + 4 g cement	1:2
3	3 g adsorbent + 3 g cement	1:1
4	4 g adsorbent + 2 g cement	2:1
5	5 g adsorbent + 1 g cement	5:1

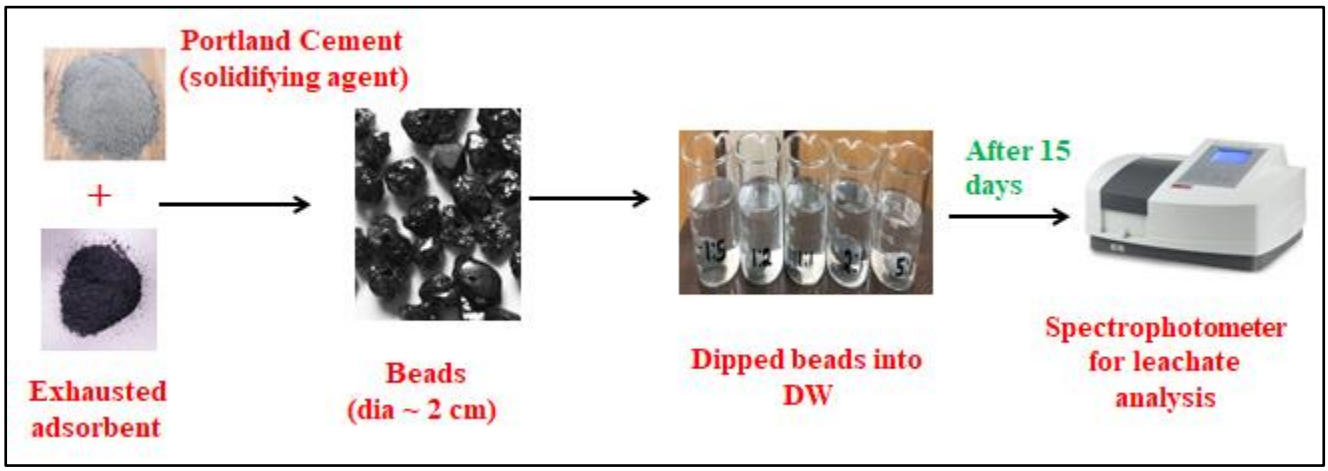

Fig. 3.7. Various steps involved in S/S process procedure.

3.5.5. Bacterial Toxicity Test

After solidification, the toxicity of leachate samples was also determined by bacterial toxicity analysis using the agar cup method (Tambe et al., 2001). The use of different types of microbial strains (procured from the department of biotechnology, Thapar Institute of Engineering & Technology, Patiala) was revived in nutrient broth. Mueller and Hinton agar (MHA) was sterilized and 25 mL media was poured in Petri plates. The 24 h old culture was spread on agar plates. Further, four to five holes were made in each plate with the help of a cork borer. 0.25 µL of each leachate sample from various experiments were added to each hole. Plates were then incubated at 35 ± 0.1^{0}C for 24 h, and observed the zone of inhibition through bacterial growth. Similarly, toxicity analysis of adsorbate solutions of different concentrations (0.1–10 ppm) was also studied for comparison purposes with leachate toxicity. Step by step procedure for the toxicity assessment process is represented in Fig. 3.8.

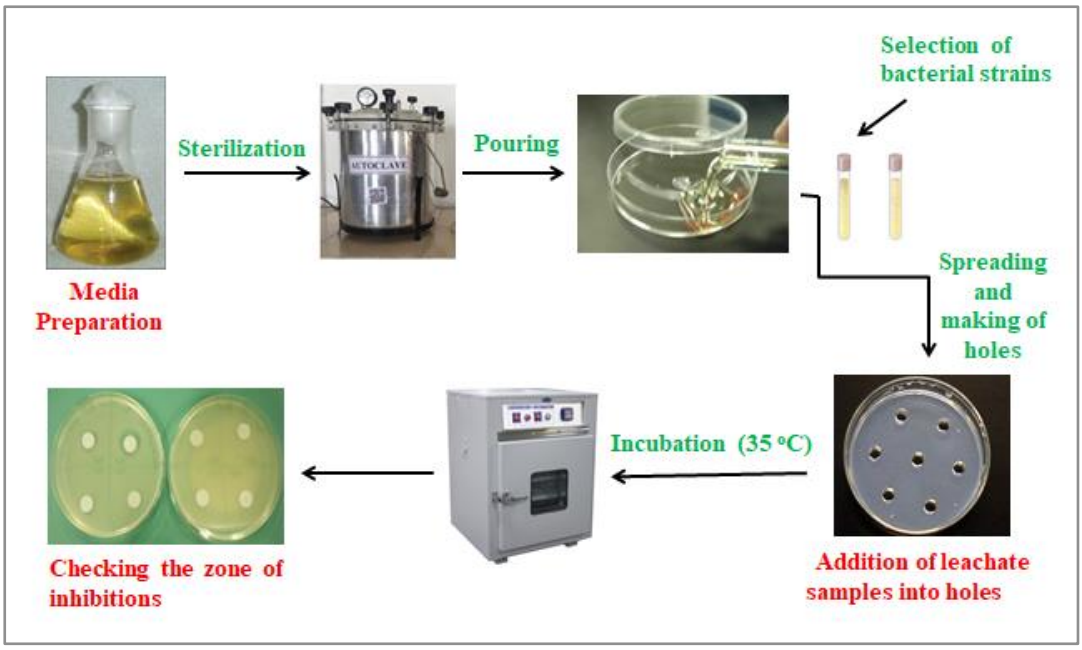

Fig. 3.8. Various steps involved in toxicity assessment of leachate.

3.5.6. Reusability studies

The reusability studies of the adsorbents were examined from three to five cycles by two methods. First is the adsorption/desorption process was studied at three different temperatures like 100, 150 and 200 ^{o}C. In this process, the used adsorbent was revived at different temperatures in a hot air oven overnight. Afterward, the adsorption process was accompanied in a shaker with an agitation rate of 150 rpm for 12 hours at optimized conditions. In the second method, it involves the use of NaOH as a desorbing agent to remove the adsorbed adsorbate from the adsorbent surface. For adsorption studies, 0.25 g of adsorbent was included in 50 mL of adsorbate solution having the original concentration of adsorbate in the orbital shaker with an agitation speed of 150 rpm for 1 h. After then, the adsorbate-loaded adsorbent was separated by filtration and adsorbed amount q (mg/g) was determined using a UV-vis spectrophotometer. For desorption, the adsorbate-loaded adsorbent was frequently washed with distilled water to eliminate any unadsorbed adsorbate molecules. Now, 0.05 M NaOH solutions were added and stirred at 150 rpm for one hour. Additionally, the revived adsorbent was separated by filtration, repetitively washed, finally dried at 100^{o}C for 2–3 h and kept in an airtight container for next adsorption-desorption cycles.

Chapter – 4

ADSORPTION OF OFL AND DOX USING AGRI-RESIDUE BASED ADSORBENTS

4.1. GENERAL

This chapter deals with the results of adsorption process that is used for the removal of pharmaceutical compounds from aqueous medium. It involves Ofloxacn (OFL) and Doxycycline hydrochloride (DOX) antibiotics as a model compounds. It presents the performance of different agri-residue based adsorbents (RHA, PJAC, PSSAC) for adsorption of antibiotics (OFL and DOX). It includes the effect of relevant operating parameters on performance of different adsorbents. Kinetics, isotherms, S/S, bacterial toxicity and reusability studies of these adsorbents are also summarized in this chapter.

4.2. BATCH ADSORPTIVE REMOVAL OF WASTEWATER COMPRISING OFL BY RHA

4.2.1. Adsorbent Characterization

The Brunauere Emmette Teller (BET) surface area and Barrette Joynere Hanlenda (BJH) adsorption/desorption surface area of RHA was found to be 32.6 and 10.96 m^2/g, respectively. The average BET pore diameter was found 6.5 nm, indicating that RHA is mesoporous and appropriate adsorbent for the adsorption of OFL having a high molecular weight (Bahrami et al., 2016). The XRD spectra (Fig. 4.1) of bare RHA showed a single diffuse band centered at around 22°. This indicates that the silica in the sample was in an amorphous state. Although weak peaks at 21°, 27° and 31°, 36°, 68° were identified as trydimite and cristobalite phases respectively (Azmi et al., 2016). No change was observed in the XRD spectra of OFL loaded RHA (Fig. 4.1).

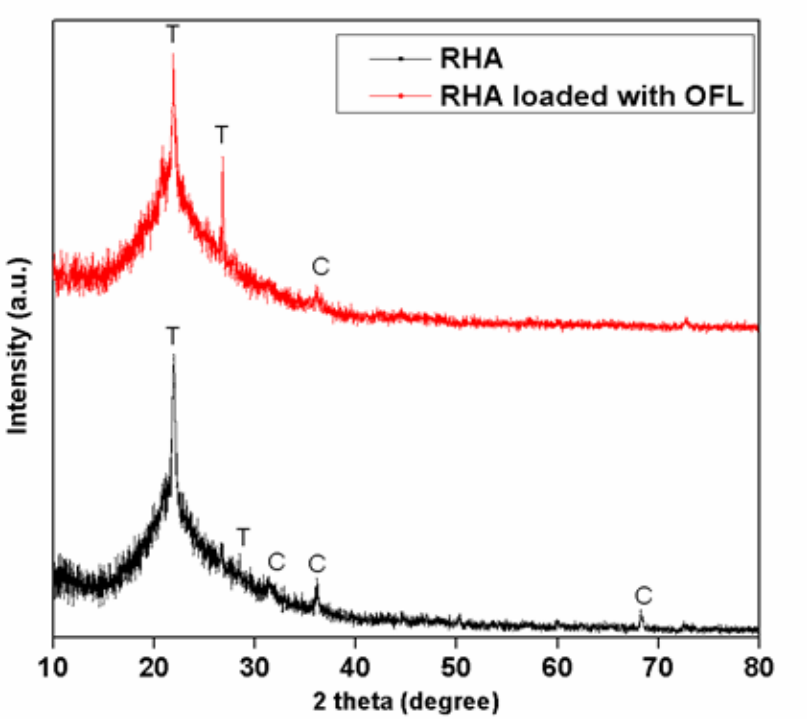

Fig. 4.1. X-ray diffraction (XRD) analysis of bare RHA and RHA loaded with OFL (Trydimite – T, Cristobalite – C).

FTIR (Fourier transform infrared) spectra provide the information of various existing functional groups. FTIR spectra of bared and OFL-loaded RHA are presented in Fig. 4.2. A broader peak between 3000 to 3700 cm^{-1} is attributed to the existence of free and hydrogen-bonded OH group and Si-OH, owing to adsorbed water on the surface (Srivastava et al., 2006; Abou-Mesalam, 2003). A broader, but not intensive, the peak can be seen at 1636 cm^{-1} is due to the carbonyl groups stretching from aldehydes and ketones. Another broader and intense peak at 1092 cm^{-1} represents the Si–O–Si and –C–O–H stretching and –OH deformation. However, comparatively lower intense and narrow peaks at ≈ 795 and 469 cm^{-1} are attributed to the Si–H (Srivastava et al., 2006). Shifting in all the peaks can be seen in Fig. 4.2 due to the loading of OFL on RHA, which indicates that the functional groups present on the surface of RHA are participating in the adsorption.

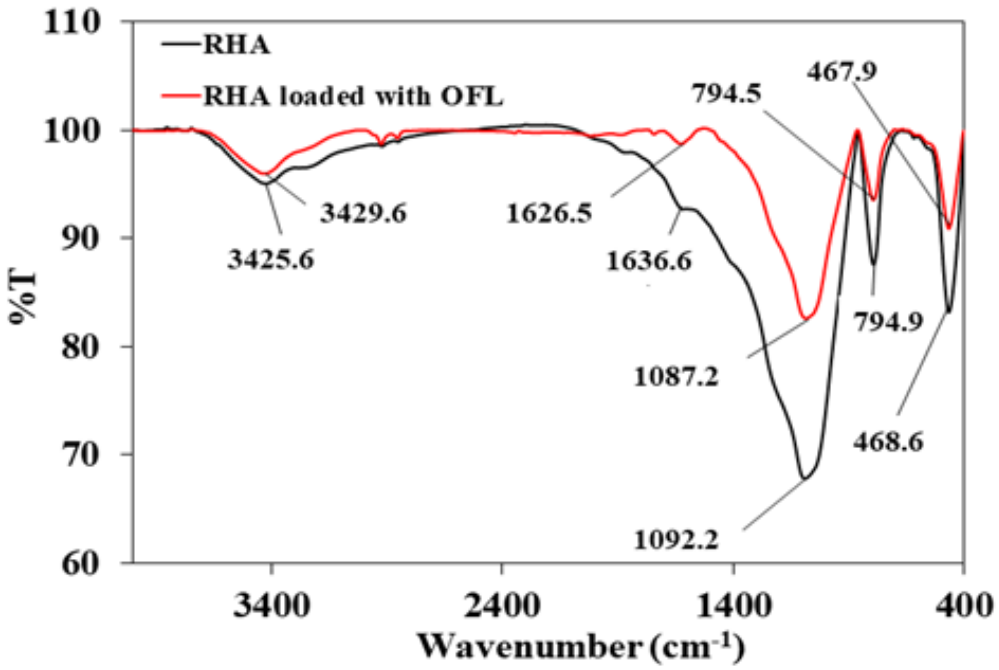

Fig. 4.2. FTIR spectra of RHA and RHA loaded with OFL.

4.3. Model fitting and Statistical Analysis

Experiments advocated as per CCD (Table 4.1), were performed and responses (X_1) and (X_2) were determined. Experimental results with process parameters were then statistically analyzed using RSM Design expert 13 (DX10). Sequential F-test, model summary statistics, and subsequent ANOVA (Table 4.2) analysis suggested a quadratic model fit the experimental data. The adequate precision, 35.509 and 34.373, for the responses X_1 and X_2, respectively, revealed the capability and efficiency of the suggested quadratic model in analyzing variables and responses relation. Further, other tools such as outlier residual plots, Studentized residuals plots, and normal probability (plots are not shown here) well explained the efficiency of quadratic model fittings. Model F- the value of 94.61 and 75.12, for responses X_1 and X_2, respectively, (Table 4.2) supported the significance of the quadratic model. Further, the coefficient of determination R^2, predicted R^2 and Adjusted R^2 showed a good correlation of actual and predicted responses (Table 4.3).

Table 4.1. Experimental design for the adsorption of OFL by RHA.

Std	Run	pH	Dose of RHA (g/L)	OFL conc. (mg/L)	Time (min)	% OFL Removal (X_1)	Adsorption Capacity (X_2)
10	1	8.0	10.0	30.0	565.0	92.85	2.78
25	2	6.0	15.0	50.0	380.0	93.97	3.13
24	3	6.0	15.0	50.0	750.0	85.37	2.84
15	4	4.0	20.0	70.0	565.0	92.57	3.24
5	5	4.0	10.0	70.0	195.0	68.65	4.80
2	6	8.0	10.0	30.0	195.0	71.09	2.13
13	7	4.0	10.0	70.0	565.0	93.40	6.53
28	8	6.0	15.0	50.0	380.0	93.34	3.11
6	9	8.0	10.0	70.0	195.0	59.71	4.18
3	10	4.0	20.0	30.0	195.0	82.28	1.23
4	11	8.0	20.0	30.0	195.0	87.47	1.31
1	12	4.0	10.0	30.0	195.0	74.28	2.22
18	13	10.0	15.0	50.0	380.0	93.48	3.11
14	14	8.0	10.0	70.0	565.0	82.93	5.80
22	15	6.0	15.0	90.0	380.0	85.98	5.15
11	16	4.0	20.0	30.0	565.0	83.52	1.25
16	17	8.0	20.0	70.0	565.0	92.97	3.25
23	18	6.0	15.0	50.0	010.0	55.34	1.84
20	19	6.0	25.0	50.0	380.0	91.28	1.82
30	20	6.0	15.0	50.0	380.0	93.80	3.12
21	21	6.0	15.0	10.0	380.0	87.71	0.58
17	22	2.0	15.0	50.0	380.0	98.91	3.29
26	23	6.0	15.0	50.0	380.0	93.00	3.10
19	24	6.0	05.0	50.0	380.0	67.14	6.41
9	25	4.0	10.0	30.0	565.0	93.19	2.79
12	26	8.0	20.0	30.0	565.0	87.38	1.31
7	27	4.0	20.0	70.0	195.0	89.97	3.14
8	28	8.0	20.0	70.0	195.0	89.87	3.14
29	29	6.0	15.0	50.0	380.0	93.20	3.10
27	30	6.0	15.0	50.0	380.0	93.65	3.12

Table 4.2. ANOVA for the % OFL removal and capacity.

	% OFL removal (X_1)					Adsorption Capacity (X_2)				
Source	**Sum of Squares**	**DF**	**Mean Square**	**F Value**	**Prob > F**	**Sum of Squares**	**DF**	**Mean Square**	**F Value**	**Prob > F**
Model	3504.26	14	250.30	94.61	< 0.0001	62.40	14	4.46	75.12	< 0.0001
A	24.88	1	24.88	9.40	0.0078	0.12	1	0.12	1.98	0.1796
B	582.37	1	582.37	220.12	< 0.0001	21.17	1	21.17	356.87	< 0.0001
C	1.23	1	1.23	0.46	0.5057	33.17	1	33.17	559.08	< 0.0001
D	1008.03	1	1008.03	381.01	< 0.0001	1.93	1	1.93	32.54	< 0.0001
A^2	17.49	1	17.49	6.61	0.0213	4.136×10^{-3}	1	4.136×10^{-3}	0.070	0.7954
B^2	326.15	1	326.15	123.28	< 0.0001	1.58	1	1.58	26.65	0.0001
C^2	64.98	1	64.98	24.56	0.0002	0.14	1	0.14	2.36	0.1455
D^2	879.38	1	879.38	332.39	< 0.0001	1.14	1	1.14	19.18	0.0005
AB	65.15	1	65.15	24.62	0.0002	0.16	1	0.16	2.73	0.1191
AC	37.90	1	37.90	14.33	0.0018	0.12	1	0.12	2.00	0.1777
AD	0.016	1	0.016	0.0059	0.9393	3.473×10^{-5}	1	3.473×10^{-5}	5.853×10^{-4}	0.9810
BC	165.48	1	165.48	62.55	< 0.0001	0.86	1	0.86	14.48	0.0017
BD	418.30	1	418.30	158.11	< 0.0001	1.19	1	1.19	20.05	0.0004
CD	8.80	1	8.80	3.33	0.0882	0.34	1	0.34	5.67	0.0309
Residual	39.69	15	2.65			0.89	15	0.059		
Lack of Fit	38.98	10	3.90	27.79	0.0009	0.89	10	0.089	570.39	< 0.0001
Pure Error	0.70	5	0.14			7.794×10^{-4}	5	1.559×10^{-4}		
Cor Total	3543.95	29				63.29	29			

A: pH, B: dose of RHA (m, g/L), C: OFL conc. (C_0, mg/L), D: Time (t, min)

Table 4.3. Various R-squared values suggested by CCD for different responses.

Responses	R-Squared	Adj R-Squared	Pred R-Squared
% OFL removal (X_1)	0.99	0.98	0.94
Adsorption Capacity (X_2)	0.98	0.97	0.92

Values of "Prob>F" higher to 0.1 designate the parameters in the model insignificant. The significant quadratic model terms from ANOVA were observed as X_1: pH, m, t, pH^2, m^2, C^2, t^2, pH×m, pH×C, m×C, m×t, and X_2: m, C, t, m^2, t^2, m×C, m×t, C×t. Therefore, based on the above, the quadratic model equation can be represented given below.

$$X_1 = 14.9 - (4.04 * pH) + (4.40 * m) + (0.046 * C) + (0.23 * t) + (0.19 * pH^2) - (0.18 * m^2) - (3.85 * 10^{-3} * C^2) - (1.65 * 10^{-4} * t^2) + (0.20 * \text{pH} * \text{m}) - (0.04 * \text{pH} * \text{C}) + (8.50 * 10^{-5} * \text{pH} * \text{t}) + (0.03 * \text{m} * \text{C}) - (5.53 * 10^{-3} * \text{m} * \text{t}) + (2.0 * 10^{-4} * \text{C} * \text{t}) \quad \textbf{(4.1)}$$

$$X_2 = 1.17 - (0.11 * pH) - (0.30 * m) + (0.11 * C) + (8.54 * 10^{-3} * t) + (3.07 * 10^{-3} * pH^2) + (9.60 * 10^{-3} * m^2) - (1.79 * 10^{-4} * C^2) - (5.95 * 10^{-6} * t^2) + (0.01 * \text{pH} * \text{m}) - (2.15 * 10^{-3} * \text{Ph} * \text{C}) - (3.98 * 10^{-6} * \text{Ph} * \text{t}) + (2.32 * 10^{-3} * \text{m} * \text{C}) - (2.95 * 10^{-4} * \text{m} * \text{t}) + (3.92 * 10^{-5} * \text{C} * \text{t}) \quad \textbf{(4.2)}$$

4.4. Effect of Various Parameters and Optimization

Values of responses X_1 and X_2 with various process parameters *i.e.* pH, *t* (min), C_o (mg/L), and *m* (g/L) values for the adsorptive removal of OFL antibiotic are shown in Table 4.1, and the corresponding 3-D response surface graphs obtained from RSM is shown in Fig. 4.3. These plots were further analyzed for individual and interactive effects of the adsorption parameters on responses X_1 and X_2.

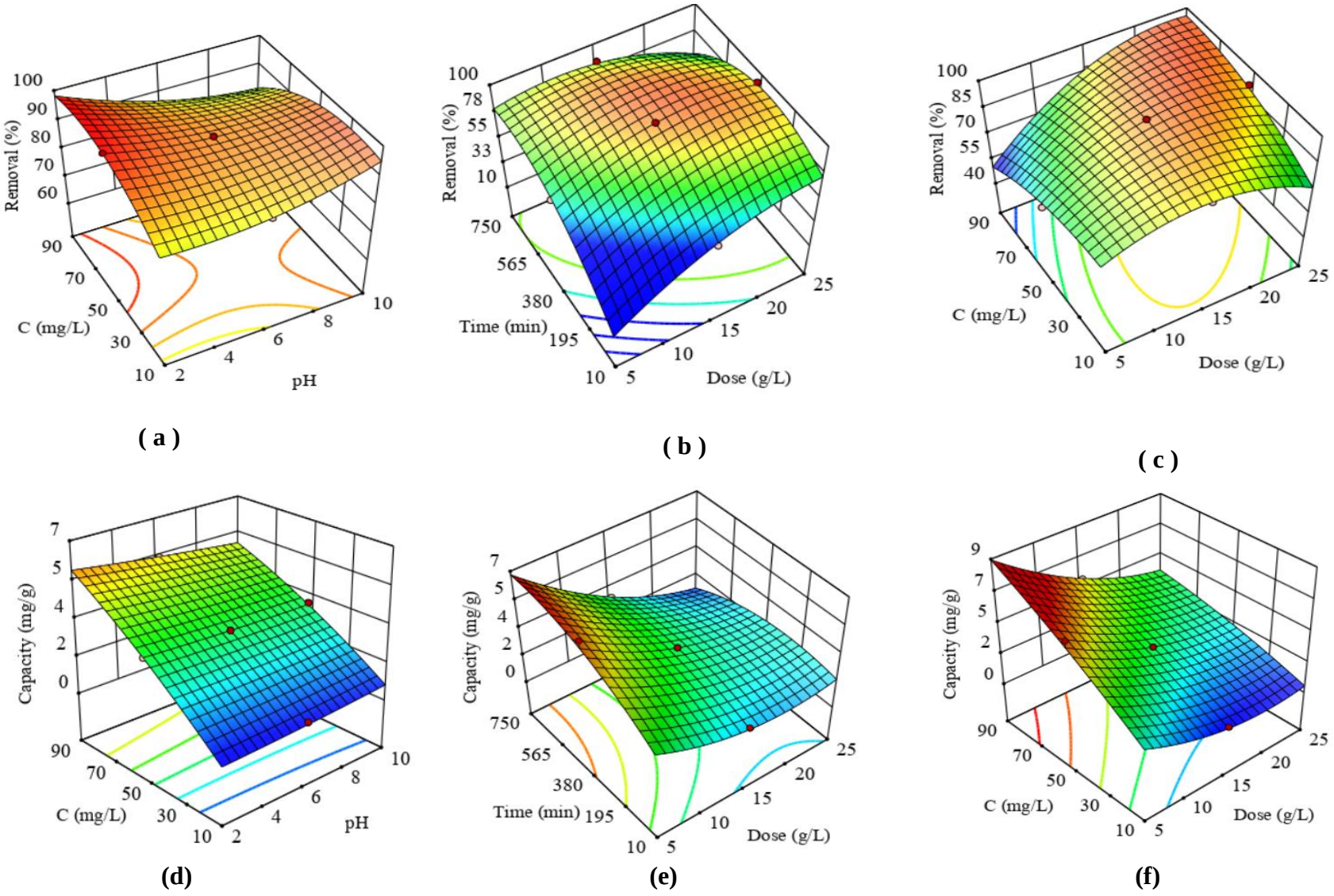

Fig. 4.3. 3D-graph for the adsorptive removal of OFL from aqueous solution (a, b, c) % removal versus pH, OFL concentration, dose, t and (d, e, f) capacity versus pH, OFL concentration, dose, t.

Fig. 4.3 (a-f) shows the interaction of *pH*, *m* (g/L), *t* (min) and *C* (mg/L) on the % OFL removal (X_1) and capacity (X_2), respectively. The simultaneous effects of *pH* and *C* on the responses % OFL removal and capacity are shown in Fig. 4.3 (a) and (d), respectively, at constant *m* and *t* value. At any pH, the % OFL removal was observed increasing sharply with the increase in C value up to more than 90%. However, at higher C, % OFL removal starts decreasing. This indicates that the adsorption of OFL is limited by the adsorbate concentration, and the RHA possesses higher adsorption capacity. Whereas, the capacity was always found increasing at all *pH* with increased *C*. On the other hand, there is no significant change in capacity with pH change at any C value (Fig. 4.3 d). Further, to confirm the presence of silica and integrity of the RHA in respect to the dissolution/precipitation at high pH, elemental analysis through EDX was conducted for both the bare and loaded RHA (Table 4.4). The elemental analysis showed the presence of same elements *i.e.* C, O, Na, Mg, Si, K and Ca in the bare RHA and loaded RHA after adsorption. The presence of Si in loaded RHA after adsorption, with the nearly same weight % explains the wholesomeness of the RHA after adsorption. The slight decrease in the Si weight % value may be due to the loading of Ofloxacin on the RHA which in turn increased the weight % value of C.

Table 4.4. Elemental analysis of bare and loaded RHA.

Elements	Weight %	
	Bare RHA	**Loaded RHA**
C	14.26	20.07
O	51.57	47.73
Na	0.20	0.13
Mg	0.11	0.09
Si	33.24	30.51
K	0.41	1.35
Ca	0.2	0.12

Fig. 4.3 (b) and (e) explains the *m* and *t* interaction on the % OFL removal and capacity, respectively. At lower *m* values, an increase in adsorption time *t* increases the % OFL removal, which becomes nearly constant at higher *t* values. However, at higher *m* values, % OFL removal first in-

creases with *t*, and at higher *t* values, it starts decreasing. This behaviour in % OFL removal at higher *t* values may be due to the desorption of OFL from the RHA at higher *t* values. The capacity was found increasing with t at a lower value of *m*, and capacity was observed first marginally increasing and then after decreasing with t at higher m values (Fig. 4.3 e). This may be because at higher *m* the % OFL removal first increases and then decreases with t value (Fig. 4.3 b).

Fig. 4.3 (c) and (f) describes the interaction of *m* and *C* on the % OFL removal and capacity. % OFL removal decreases with an increase in *C* value at lower *m* value. However, at higher *m*, % OFL removal increases with increased *C*. This change in % OFL removal is due to the higher active sites availability at a higher dose and the adsorption of OFL on RHA can be regarded as adsorbate limiting. Whereas, at lower m, capacity increases with an increase in C, and negligible change were observed in capacity at higher m with increased C value. This indicates the higher adsorption capacity of RHA towards OFL. OFL adsorption on RHA was optimized for maximizing responses X_1 (% Removal) and X_2 (adsorption capacity) by the RSM. The constraints applied for optimization are mentioned in Table 4.5.

Table 4.5. Optimization Constraints applied.

Variables	Goal	Lower Limit	Upper Limit
pH	is in range	6	8
Dose of RHA	minimize	5	25
OFL conc.	is in range	10	90
Time	minimize	10	750
% Removal	maximize	55.34	98.91
Capacity	maximize	0.58	6.53

The optimum values in the study range, as suggested by RSM, were found to be *m* = 7.94 g/L, *t* = 430 min, and *pH* = 6 with responses X_1 and X_2 being 79.54 % and 6.01, respectively. The optimum result from RSM was further validated by conducting three experiments on optimum parameters, and the average value of responses X_1 and X_2 were found to be 79.71 % and 6.28 which is in good agreement with the suggested values (Table 4.6).

Table 4.6. Experimental and predicted responses values comparison at optimized condition (*m* = 7.94 g/L, *t* = 430 min and *pH* = 6, OFL concentration = 62.5 mg/L).

Responses	Predicted value	Experimental value
% removal (X_1)	79.54%	79.71%
Capacity (X_2)	6.01	6.28

4.5. Adsorption Kinetics and Diffusivity

Kinetics of adsorption and hence kinetic parameters are necessary for designing of adsorption columns. At optimum parameters (*m* = 7.94 g/L, *t* = 430 min and *pH* = 6), the kinetics of OFL adsorption on RHA was studied using Pseudo first order and pseudo-second-order kinetic models (Eq. 4.3 and 4.4) at three OFL initial concentration (C_o) 10, 40 and 70 mg/L.

The Pseudo-first-order model is given as (Malik, 2003):

$$q_t = q_e\left[1-\exp\left(-k_f t\right)\right] \qquad \textbf{(4.3)}$$

Where q_t and q_e are the amount of OFL adsorbed (mg/g) at any time (*t*) and at equilibrium, respectively, and k_f is the rate constant (per min).

Pseudo second order model is represented as (Ho and McKay, 1999):

$$q_t = \frac{tk_S q_e^2}{1+tk_S q_e} \qquad \textbf{(4.4)}$$

Where, k_s is the rate constant (g/mg/min).

The initial adsorption rate, h (g/mg/min), is defined as;

$$h = k_s q_e^2 \qquad \textbf{(4.5)}$$

Fitting of experimental data to the kinetic models was performed using nonlinear regression. Herein, Marquardt's percent standard deviation (MPSD) error function was applied. The calculated ki-

netic parameters, coefficient of determination (R^2) and error values as MPSD are presented in Table 4.7 and fitting is shown in the Fig. 4.4.

Table 4.7. Kinetic parameters for ofloxacin (OFL) adsorption on RHA at optimized parameters (*m* = 7.94 g/L, *t* = 430 min and *pH* = 6).

	C_0 (mg/L)		
	10	**40**	**70**
Pseudo first order			
k_f (min^{-1})	0.0136	0.0054	0.0051
$q_{e,exp}$ (mg/g)	0.964	2.90	4.34
$q_{e,cal}$ (mg/g)	0.963	2.95	4.39
R^2 (non-linear)	0.997	0.998	0.999
MPSD	19.96	18.84	8.015
Weber Morris			
$k_{id1(mg/g\ min^{1/2})}$	0.070	0.154	0.223
I_1	0.053	0.348	0.512
R^2	0.973	0.9991	0.997
$k_{id2(mg/g\ min^{1/2})}$	0.005	0.018	0.038
I_2	0.821	2.418	3.269
R^2	0.625	0.842	0.735

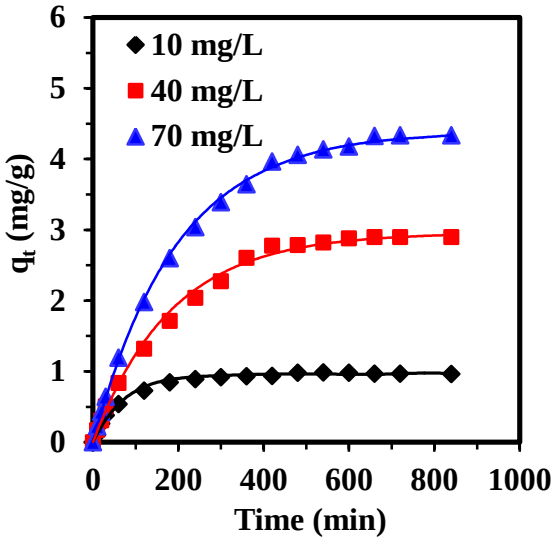

Fig. 4.4. Kinetics of OFL adsorption on RHA at optimized parameters (*m* = 7.94 g/L, *t* = 430 min and *pH* = 6). (Experimental results are shown by data points, Solid line shows pseudo-first-order kinetic model fitting)

High R^2, low MPSD values at all C_o values (10, 40, and 70 mg/L) for Pseudo first-order kinetic model fitting concludes the suitability of the pseudo first-order kinetic model for OFL adsorption on RHA. From Table 4.7, it is observed that the q_e and k_f values were found increasing with C_o, indicating the adsorption is limited by the adsorbate concentration of OFL antibiotic. Pseudo second order kinetic modeling was also performed and experimental data were found in good agreement at lower OFL concentration. However, at higher concentrations very poor fitting was observed (not shown here).

Further, the adsorption process is controlled by the intra-particle diffusion when adsorbate is present in high concentration and adsorbents are of larger particle sizes (Aravindhan et al., 2007). During adsorption of OFL on RHA, Intra-particle diffusion may be the rate-controlling, since RHA is granular. The intra-particle diffusion model is expressed by the following equation (Weber and Morris, 1963):

$$q_t = k_{id} t^{0.5} + I \qquad \textbf{(4.6)}$$

Where k_{id}: intra-particle diffusion rate constant (mg/g $min^{1/2}$); I: intercept representing the boundary layer thickness on RHA. The larger the intercept, the thicker is the boundary layer (Kavitha

and Namasivayam, 2007) Plot of q_t vs. $t^{1/2}$, if linear, intra-particle diffusion controls the process. In the present study, two linear portions can be seen (Fig. 4.5). The first linear part shows the gradual reach of adsorption equilibrium, however, the second part is attributed to the final adsorption equilibrium stage originated due to lower intraparticle diffusion owing lower OFL concentration left (Gercel et al., 2007). Also, for these linear parts, intercepts I_1 and I_2 are not zero (Table 4.7), which indicates surface adsorption is also controlling the adsorption rate of OFL on RHA. Further, $K_{id,1}$ and $K_{id,2,}$ slopes of the linear portions (Table 4.7), were found increasing with C_o due to increased driving force and adsorption of OFL in meso and micropores of RHA.

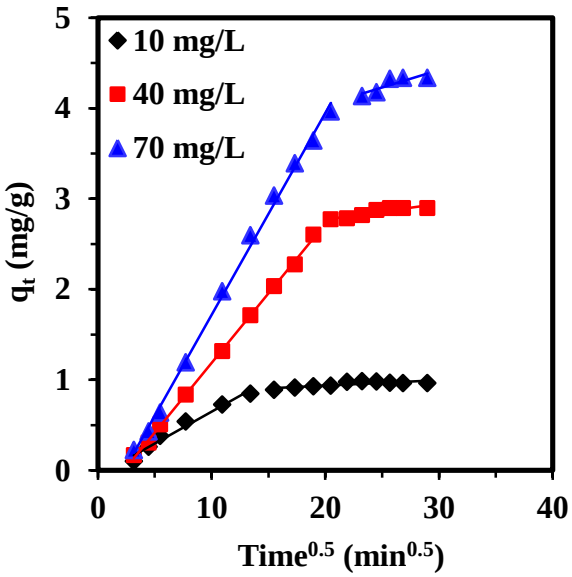

Fig. 4.5. Weber–Morris plot for the adsorption of OFL by RHA at optimized parameters (*m* = 7.94 g/L, *t* = 430 min and *pH* = 6).

4.6. Isotherm Modelling and Thermodynamics

Adsorption isotherms provide the necessary information for adsorption system designing. For this purpose, various isotherms such as Langmuir, Redlich-Peterson (R-P), and Tempkin (Belhachemi and Addoun, 2011) isotherms (Table 4.8) were studied and analyzed for the adsorption of OFL on to RHA at 288-318 K temperatures (T) with C_0 = 5-70 mg/L. All the other experiments were conducted at optimum conditions (m = 7.94 g/L, t = 430 min and pH = 6).

Table 4.8. Isotherms and Thermodynamics parameters for OFL adsorption on RHA at optimized parameters (*m* = 7.94 g/L, *t* = 430 min and *pH* = 6).

ISOTHERMS

Langmuir $q_e = \frac{q_m K_L C_e}{1+K_L C_e}$

T (K)	K_L (L/mg)	q_m(mg/g)	R^2	CHI^2
288 K	0.0574	5.6833	0.982	0.440
303 K	0.0597	7.2162	0.989	0.399
318 K	0.0709	8.4785	0.982	0.773

Redlich-Peterson $q_e = \frac{K_R C_e}{1+a_R C_e^{\beta}}$

T (K)	K_R (L/g)	a_R (L/mg)$^{1/\beta}$	β	R^2	CHI^2
288 K	0.5014	0.1641	0.887	0.988	0.291
303 K	0.4450	0.0773	0.936	0.987	0.423
318 K	0.6048	0.0744	0.987	0.982	0.779

Temkin $q_e = \left(\frac{RT}{B_T}\right) ln(K_t C_e)$

T (K)	K_T(L/mg)	B_T (J/mol)	R^2	CHI^2
288 K	1.0623	0.990	0.992	0.195
303 K	0.7950	1.4191	0.995	0.190
318 K	0.9267	1.6928	0.993	0.397

Thermodynamic Parameters $lnK_D = \frac{-\Delta G^0}{RT} = \frac{\Delta S^0}{R} - \frac{\Delta H^0}{R}\frac{1}{T}$

T (K)	K x 10^{-3} (L/kg)	ΔG^0 (kJ/mol)	ΔH^0 (kJ/mol)	ΔS^0(J/mol)
288 K	569.1775	-15.191		
303 K	1370.7379	-18.196	35.205	175.392
318 K	2266.8332	-20.427		

Further, the experimental isotherm data were then fitted to various isotherm models using nonlinear regression techniques (Fig. 4.6). CHI^2 error function was used for this purpose and the estimated isotherm parameters with R^2 and CHI^2 error values are presented in Table 4.8.

It can be observed that, at a higher T value, OFL adsorption capacity is higher, which indicates the endothermic nature of OFL adsorption onto RHA (Fig. 4.6). At higher T value, new active surface creation and increased intra-particle diffusion enhance the adsorption capacity (Rameshraja et al., 2012). From Table 4.8, Temkin isotherm was found best fitting the experimental isotherm data with the highest R^2 and lowest CHI^2 values at all the temperatures (Table 4.8). However, other isotherms, Langmuir and R-P are also in good agreement. q_m and K_L of Langmuir isotherm explain the affinity of OFL to the RHA (Acar and Eren, 2006). Increasing *T* value from 288-318 K, increases the q_m and K_L values 5.68-8.48 mg/g and 0.0574-0.0709 L/mg, respectively, indicating strong affinity and hence strong bonding of OFL molecule to RHA. β, R-P isotherm model's parameter, was found between 0-1, which signifies favorable OFL adsorption on to RHA (Lakshmi et al., 2009).

Table 4.8 represents thermodynamic parameters at different temperatures calculated from classical thermodynamics. A positive value of ΔH^o and ΔS^o indicates the endothermic and favorable adsorption (Sharma, 2011) and the negative ΔG^o concludes spontaneous nature of OFL adsorption onto RHA (Kushwaha et al., 2010b).

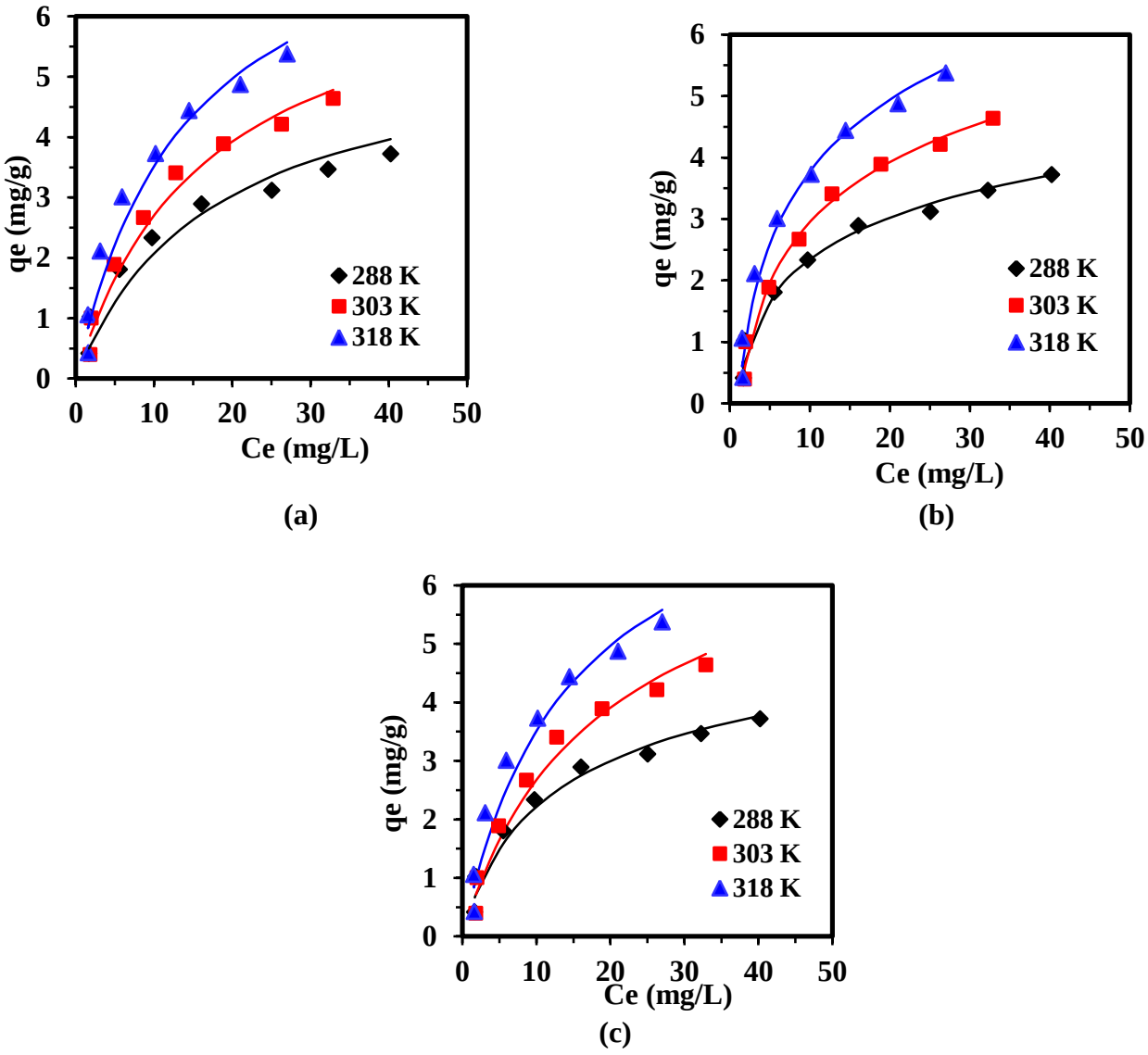

Fig. 4.6. Equilibrium adsorption isotherms for OFL adsorption on RHA at optimized parameters (*m* = 7.94 g/L, *t* = 430 min and *pH* = 6) (a) Langmuir isotherm model (b) Tempkin isotherm model (c) RP isotherm model. Experimental data points are given by symbols and the lines predicted by the isotherm model.

4.7. Solidification/Stabilization and toxicity test

The leachability of OFL from the solidified adsorbent, as explained above in chapter 3, the solidified beads were examined by measuring the OFL concentration in leachate and the capsulation percentage of OFL was calculated. Results depicted in Fig. 4.7 indicates that cement could successfully stabilize the OFL present in the exhausted adsorbent. Even at a higher OFL to cement ratio (5:1) significant amount of OFL (> 95%) was encapsulated for all three studied adsorbent concentrations.

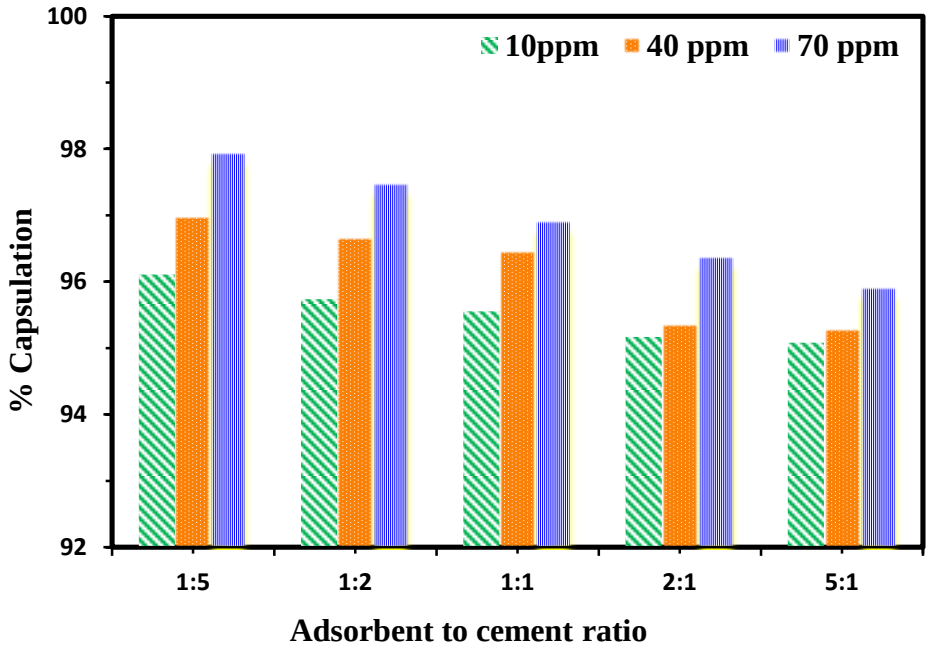

Fig. 4.7. % Capsulation of OFL in cement for different adsorbent to cement mass ratios.

To ensure the safe disposal of stabilized adsorbent, further toxicity analysis of leachate was performed using the agar cup method. The toxicity of prepared OFL solutions of different concentrations (0.1–10 ppm) was also studied for comparison purposes. For prepared OFL solutions, the maximum zone of inhibition (around the agar cup) was observed 28 mm and 25 mm for *E.coli* and *Bacillus subtilis* respectively, obviously, for 10 ppm OFL solution, (Fig. 4.8 (a and b). The minimum inhibition observed in *E.coli* and *Bacillus subtilis* were 12 mm (for 0.4 ppm OFL) and 11

mm (for 1 ppm OFL), respectively. No zone of inhibition was found for OFL concentration less than 0.4 ppm for *E.coli* and less than 1 ppm for *Bacillus subtilis*. The results for toxicity analysis of leachate are represented in Fig. 4.8 (c) and (d). It can be seen that no inhibition in the growth of *E.coli* and *Bacillus subtilis* was observed on plates, which indicated that a sufficient amount of OFL was not present in the leachate to kill the growth of bacteria around the agar cup. This study concludes that the exhausted/OFL loaded RHA encapsulation/stabilization with cement can be a better approach to fix the exhausted/loaded OFL RHA.

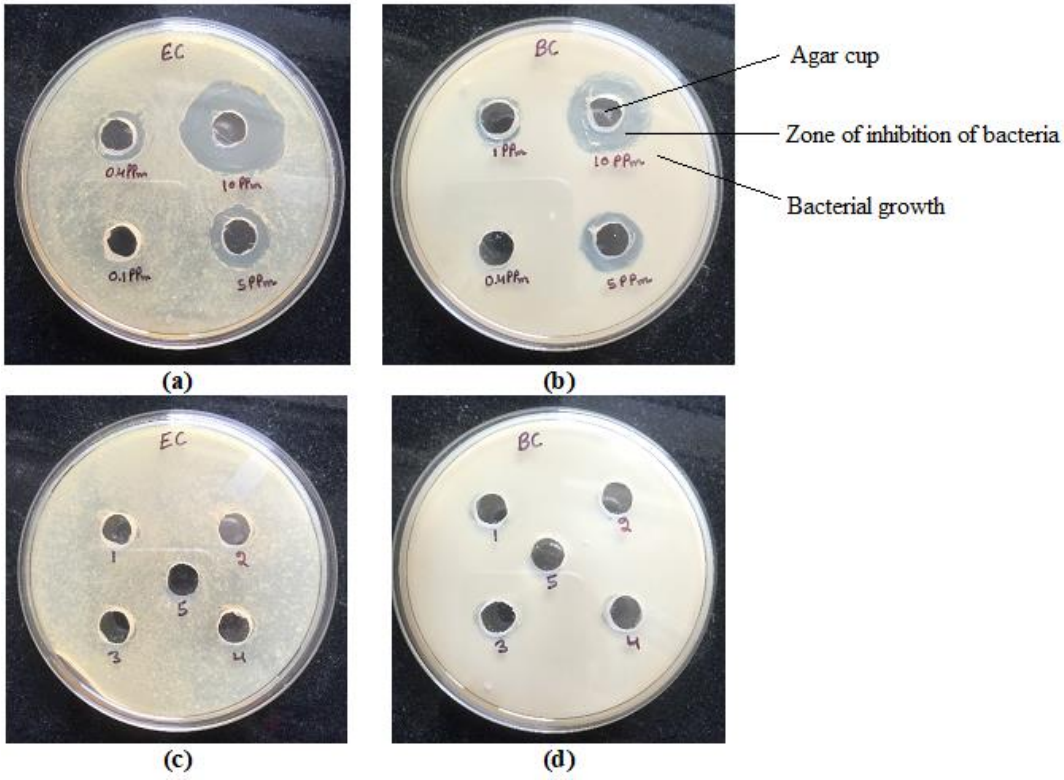

Fig. 4.8. Zone of inhibition on *E.coli* (EC) and *Bacillus subtilis* (BC) bacterial strains (a) for OFL samples on *E.coli* (b) for OFL samples on *Bacillus subtilis* (c) for leachate on *E.coli* (b) for leachate on *Bacillus subtilis.*

4.8. BATCH ADSORPTIVE REMOVAL OF WASTEWATER COMPRISING DOX BY RHA

4.8.1. Characterization of the RHA

The FTIR spectrum of fresh RHA and DOX loaded RHA are shown in Fig. 4.9. Before adsorption, the presence of a wide peak amid 3100 to 3700 cm^{-1} is recognized as the both free and H-bonded OH bands present on the exterior of RHA (Srivastava et al., 2006). In the RHA sample, the predominantly noticeable peaks correlate with the Si-O, Si-H and Si-O-Si groups at regions 1095.1 and 795.8 cm^{-1} respectively. According to the reported literature, the main component of RHA is silicon that exists in the form of SiO_2. After the adsorption process, shifting in peaks from 1095.3 to 1092.3 cm^{-1} and 795.8 to 794.7 cm^{-1} changes the deformation of Si-O, Si-H groups that shows the slight changes observed in peak patterns after loading of the antibiotic (Abou-Mesalam, 2003). This points out that DOX antibiotic has been positively performed. XRD diffraction patterns (Fig. 4.10) of blank RHA showed SiO_2, cristobalite and Trydimite. On the other hand, some sharp and narrow peaks seen in the loaded sample at 2 theta 20.25 and 37.2 explain the amorphous nature of RHA due to the presence of SiO_2 and cristobalite. These were the deviations observed between blank RHA and loaded RHA adsorbent. The specific surface area of the DOX was evaluated by using the nitrogen adsorption-desorption method well-established on the BET model at temperature 77 K in the presence of liquid nitrogen. As a result, the specific surface area and average BET pore diameter of adsorbent were evaluated as 32.6 m^2/g and 6.5 nm, respectively. Thus, it indicates the mesoporous nature of RHA due to $d < 20\ A^0$ and proves to be a suitable adsorbent for the sorption. Moreover, the SEM-EDX pattern of RHA and DOX-RHA are shown in Fig.4.11. The particles have well-arranged pattern on the external surface of RHA which is shown in Fig. 4.11 (a), the internal surface of particle is highly porous and fibrous in nature. Therefore, the existence of mesopores and macropores is supportive for the sorption of DOX molecules on their surface. Fig. 4.11 (c) represents that all the pores are filled with DOX adsorbate and it forms a well-structured network on the RHA surface. Furthermore, the EDX spectrum of both samples (Fig. 4.11 (b, d)) indicates that the major constituents of RHA are silica and oxygen that are accumulated as SiO_2. The main differences are seen in these both (Si and O) components and some other components were also found in lesser concentrations as shown in figures (Fig. 4.11 (b, d)).

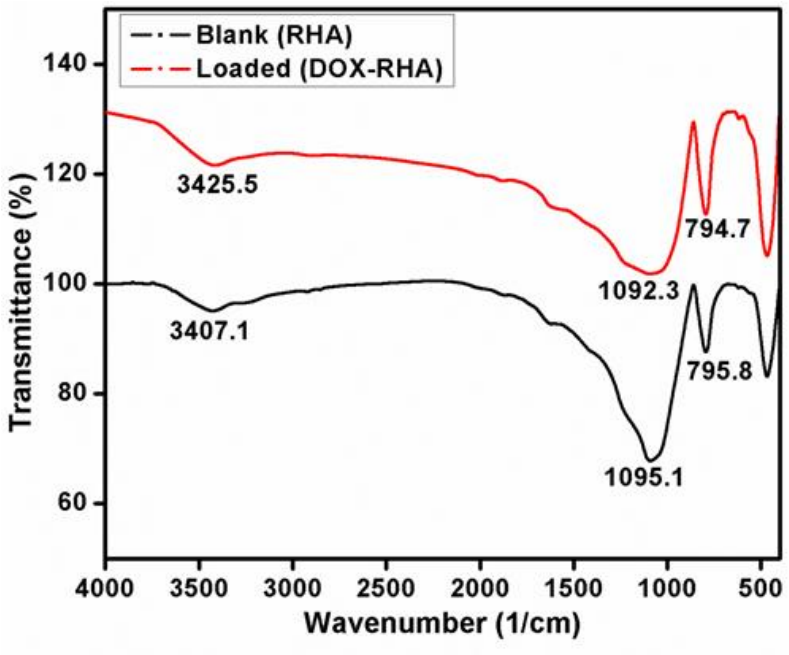

Fig. 4.9. FTIR spectra of RHA and DOX loaded RHA.

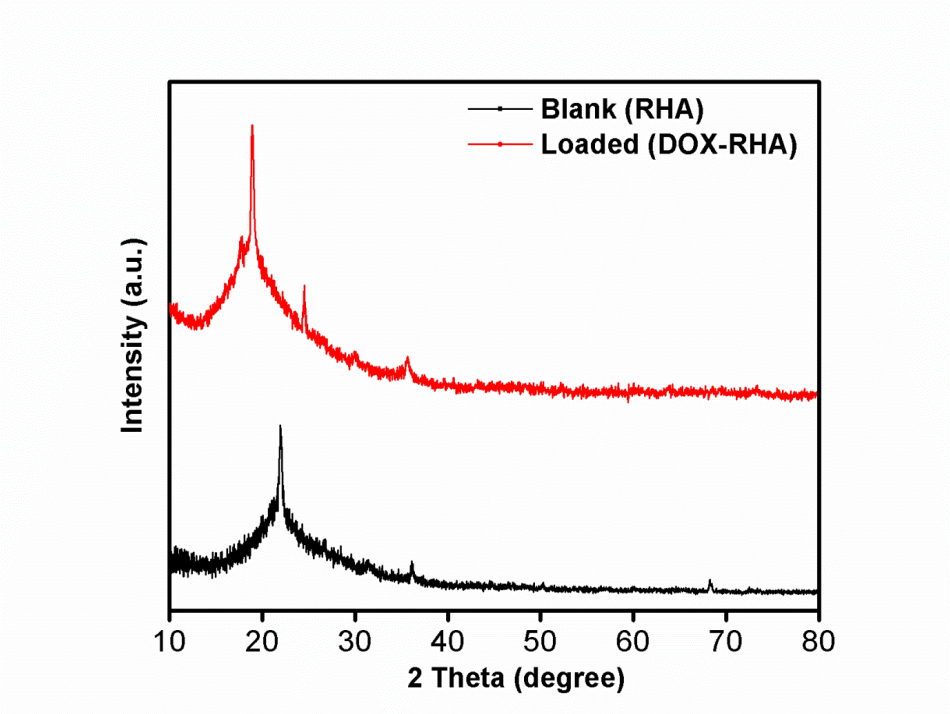

Fig. 4.10. X-ray diffraction (XRD) analysis of blank RHA and DOX – RHA loaded.

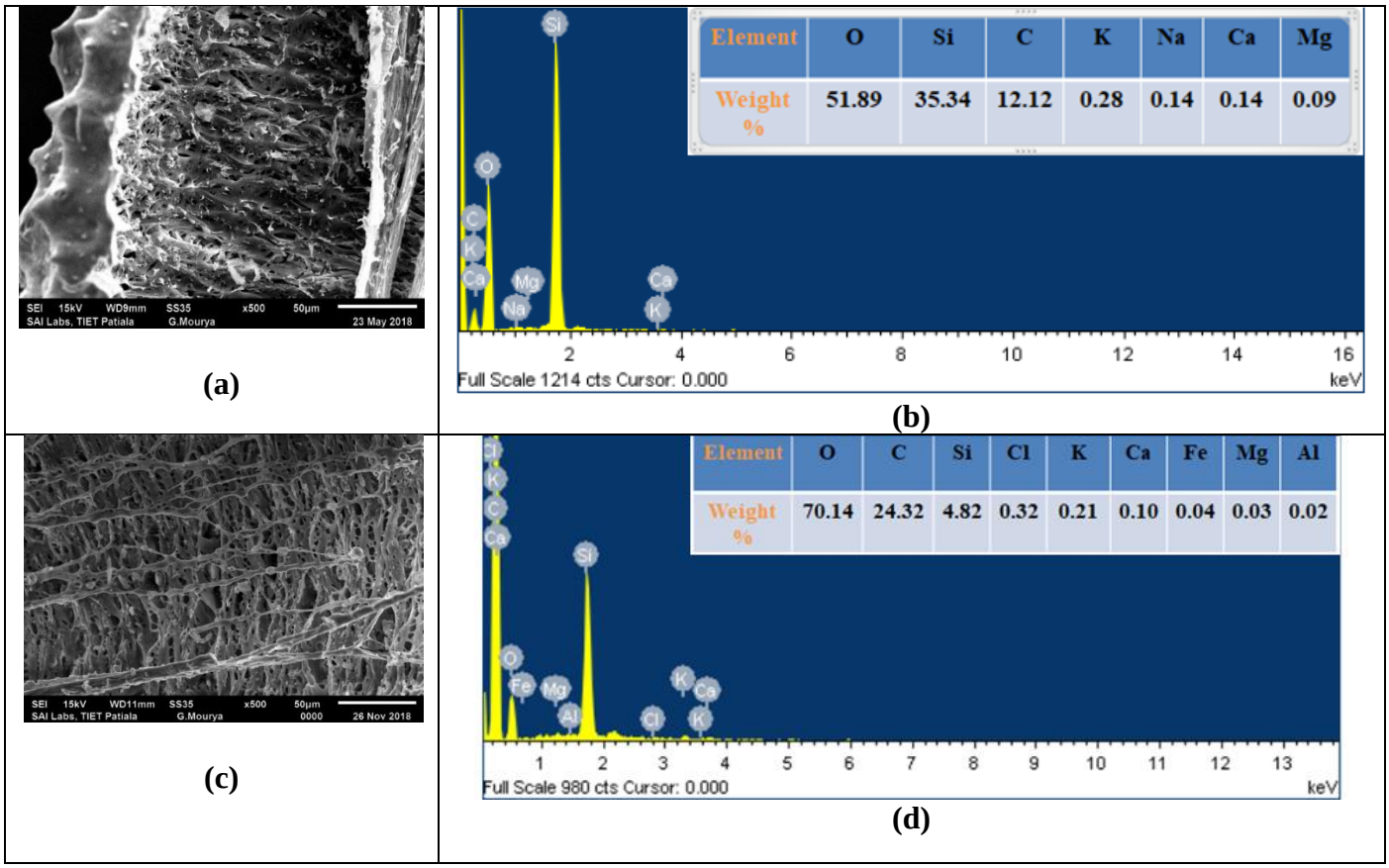

Fig. 4.11. SEM-EDX analysis of RHA and DOX loaded RHA (a, b, c and d).

4.9. Model suitability and statistical investigation

The experimental runs suggested by the CCD model of RSM were completed, and the responses (X_1) and (X_2) were calculated (Table 4.9). The statistical analysis results of experimental data were found using the variance of the ANOVA table generated by the RSM. It involves a sum of squares, F-value, probability values etc., these were analyzed (Table 4.10) and it was recommended by the sum of squares (sequential model) that the quadratic model was the most suitable for the experimental data. The calculated values of 52.36 and 25.11 were found for acceptable precision of both responses (X_1) and (X_2) individually. On the other hand, the model F – values for X_1 and X_2 were 148.87 and 37.17 as listed in table 4.10.

Table 4.9. Design of Experimentation for the adsorption of DOX by RHA.

Std	Run	pH	Dose (g/L)	DOX conc. (mg/L)	Time (min)	% DOX Removal (X_1)	Adsorption Capacity (X_2)
14	1	8.0	10.0	70.0	565.0	96.66	6.76
3	2	4.0	20.0	30.0	195.0	91.70	1.37
11	3	4.0	20.0	30.0	565.0	92.21	1.38
4	4	8.0	20.0	30.0	195.0	90.67	1.36
18	5	10.0	15.0	50.0	380.0	95.31	3.17
25	6	6.0	15.0	50.0	380.0	94.08	3.13
22	7	6.0	15.0	90.0	380.0	95.88	5.75
9	8	4.0	10.0	30.0	565.0	94.42	2.83
27	9	6.0	15.0	50.0	380.0	94.21	3.14
12	10	8.0	20.0	30.0	565.0	90.47	1.35
5	11	4.0	10.0	70.0	195.0	98.12	6.86
19	12	6.0	5.00	50.0	380.0	96.87	9.68
1	13	4.0	10.0	30.0	195.0	94.98	2.84
23	14	6.0	15.0	50.0	10.0	95.47	3.18
29	15	6.0	15.0	50.0	380.0	94.28	3.14
24	16	6.0	15.0	50.0	750.0	94.99	3.16
30	17	6.0	15.0	50.0	380.0	94.31	3.14
7	18	4.0	20.0	70.0	195.0	96.86	3.39
10	19	8.0	10.0	30.0	565.0	93.30	2.79
17	20	2.0	15.0	50.0	380.0	96.60	3.22
21	21	6.0	15.0	10.0	380.0	87.64	0.58
20	22	6.0	25.0	50.0	380.0	92.31	1.84
15	23	4.0	20.0	70.0	565.0	95.73	3.35
26	24	6.0	15.0	50.0	380.0	94.13	3.13
8	25	8.0	20.0	70.0	195.0	95.67	3.34
2	26	8.0	10.0	30.0	195.0	93.94	2.81
13	27	4.0	10.0	70.0	565.0	97.14	6.80
16	28	8.0	20.0	70.0	565.0	94.87	3.32
28	29	6.0	15.0	50.0	380.0	94.26	3.14
6	30	8.0	10.0	70.0	195.0	97.69	6.83

Table 4.10. ANOVA tables for the % DOX removal and capacity.

	% DOX removal (X_1)					Adsorption Capacity (X_2)				
Source	**Sum of Squares**	**DF**	**Mean Square**	**F Value**	**Prob > F**	**Sum of Squares**	**DF**	**Mean Square**	**F Value**	**Prob > F**
Model	154.49	14	11.03	148.87	< 0.0001	116.42	14	8.32	37.17	< 0.0001
A	4.58	1	4.58	61.78	< 0.0001	4.491×10^{-3}	1	4.491×10^{-3}	0.020	0.8892
B	30.77	1	30.77	415.17	< 0.0001	52.12	1	52.12	232.97	< 0.0001
C	94.09	1	94.09	1269.34	< 0.0001	48.87	1	48.87	218.40	< 0.0001
D	1.41	1	1.41	19.05	0.0006	3.101×10^{-3}	1	3.101×10^{-3}	0.014	0.9078
A^2	6.31	1	6.31	85.15	< 0.0001	0.017	1	0.017	0.076	0.7872
B^2	0.53	1	0.53	7.19	0.0171	10.45	1	10.45	46.71	< 0.0001
C^2	8.87	1	8.87	119.65	< 0.0001	0.029	1	0.029	0.13	0.7255
D^2	2.45	1	2.45	33.09	< 0.0001	0.026	1	0.026	0.12	0.7375
AB	0.19	1	0.19	2.60	0.1276	1.430×10^{-5}	1	1.430×10^{-5}	6.391×10^{-5}	0.9937
AC	0.24	1	0.24	3.26	0.0913	5.407×10^{-5}	1	5.407×10^{-5}	2.416×10^{-4}	0.9878
AD	0.016	1	0.016	0.22	0.6474	1.589×10^{-6}	1	1.589×10^{-6}	7.101×10^{-6}	0.9979
BC	1.64	1	1.64	22.16	0.0003	4.04	1	4.04	18.05	0.0007
BD	0.16	1	0.16	2.15	0.1633	8.163×10^{-4}	1	8.163×10^{-4}	3.649×10^{-3}	0.9526
CD	0.58	1	0.58	7.86	0.0134	1.965×10^{-3}	1	1.965×10^{-3}	8.782×10^{-3}	0.9266
Residual	1.11	15	0.074			3.36	15	0.22		
Lack of Fit	1.07	10	0.11	12.62	0.0060	3.36	10	0.34	35643.63	< 0.0001
Pure Error	0.042	5	8.47×10^{-3}			4.708×10^{-5}	5	9.416×10^{-6}		
Cor Total	155.60	29				119.78	29			

A: pH, B: dose (m, g/L), C: DOX conc. (C_0, mg/L), D: Time (t, min)

Thus, it supported the value of the quadratic model. So, the final equations are given in the form of following second-order polynomial quadratic model:

$$X_1 = 99.52 - (1.61 * pH) - (0.52 * m) + (0.19 * C) - (6.47 * 10^{-3} * t) + (0.11 * pH^2) + (5.57 * 10^{-3} * m^2) - (1.42 * 10^{-3} * C^2) + (8.73 * 10^{-6} * t^2) + (0.01 * pH * m) - (3.06 * 10^{-3} * pH * C) - (8.58 * 10^{-5} * pH * t) + (3.20 * 10^{-3} * m * C) + (1.07 * 10^{-4} * m * t) + (5.15 * 10^{-5} * C * t) \quad \textbf{(4.7)}$$

$$X_2 = 5.27 - (0.06 * pH) - (0.78 * m) + (0.15 * C) + (6.62 * 10^{-4} * t) - (6.20 * 10^{-3} * pH^2) + (0.02 * m^2) - (8.07 * 10^{-5} * C^2) + (9.01 * 10^{-7} * t^2) + (9.45 * 10^{-5} * pH * m) - (4.59 * 10^{-5} * pH * C) - (8.51 * 10^{-7} * pH * t) - (5.02 * 10^{-3} * m * C) + (7.72 * 10^{-6} * m * t) - (2.99 * 10^{-6} * C * t) \quad \textbf{(4.8)}$$

The close to unity values of R^2, R_{adj}^2 and R_{pre}^2 confirmed that the quadratic polynomial model to signify the positive associations towards both responses. It is shown in table 4.11. Further assessment of the model adequacy has been investigated by plotting actual versus predicted values. Excellent correlation shown in Fig. 4.12 reveals the adequate relationship among the experimental and calculated values (Table 4.12).

Table 4.11. Various statistic R-squared values suggested by CCD for different responses.

Responses	R-Squared	Adj R-Squared	Pred R-Squared
% DOX removal (X_1)	0.99	0.98	0.96
Adsorption capacity (X_2)	0.97	0.94	0.83

Table 4.12. Comparison of experimental and predicted responses values at optimized condition (m = 5 g/L, t = 85.85 min, pH = 6, DOX concentration = 89.73 mg/L).

Responses	Predicted value	Experimental value
% removal (X_1)	99.51%	98.85%
Capacity (X_2)	16.25	17.74

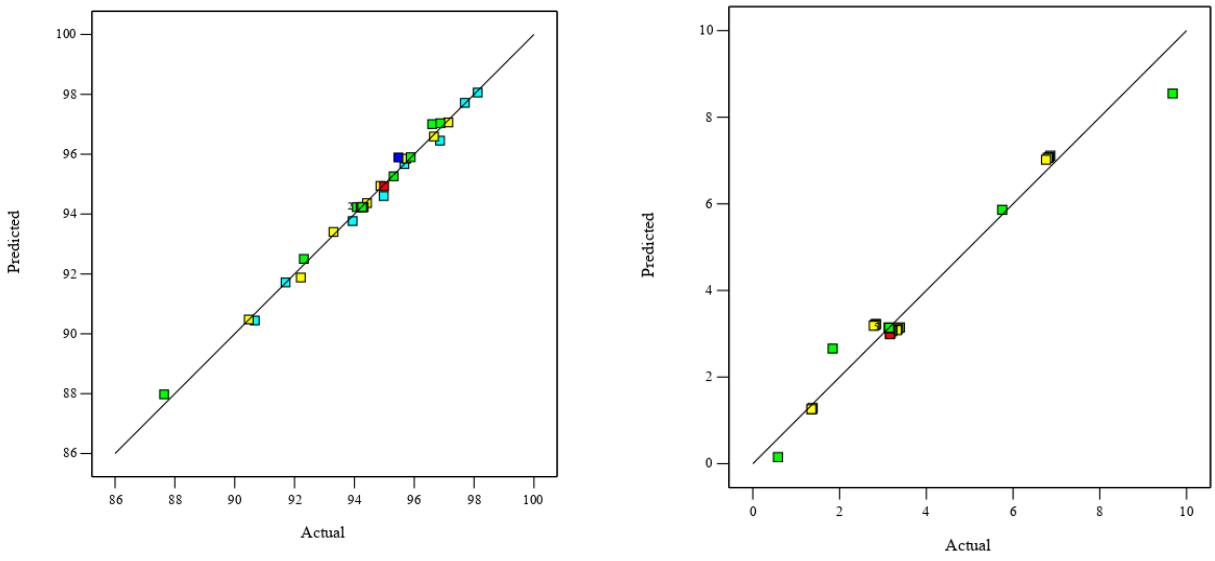

(a) **(b)**

Fig. 4.12. The actual data versus predicted data for (a) Removal (%) and (b) Capacity (mg/g) of DOX.

4.10. Response Surface analysis and optimization

The 3–D response surface plots found from RSM/CCD model for two responses % DOX removal (X_1) and capacity (X_2) with different adsorption parameters i.e., C (mg/L), m (g/L), t (min) and pH values are shown in Fig. 4.13. These graphs illustrate the variations within different dependent and independent parameters which facilitates the analysis for single and simultaneous influence of the parameters on studied responses. The corresponding values of both the responses with these parameters for DOX uptake are summarized in Table 4.9.

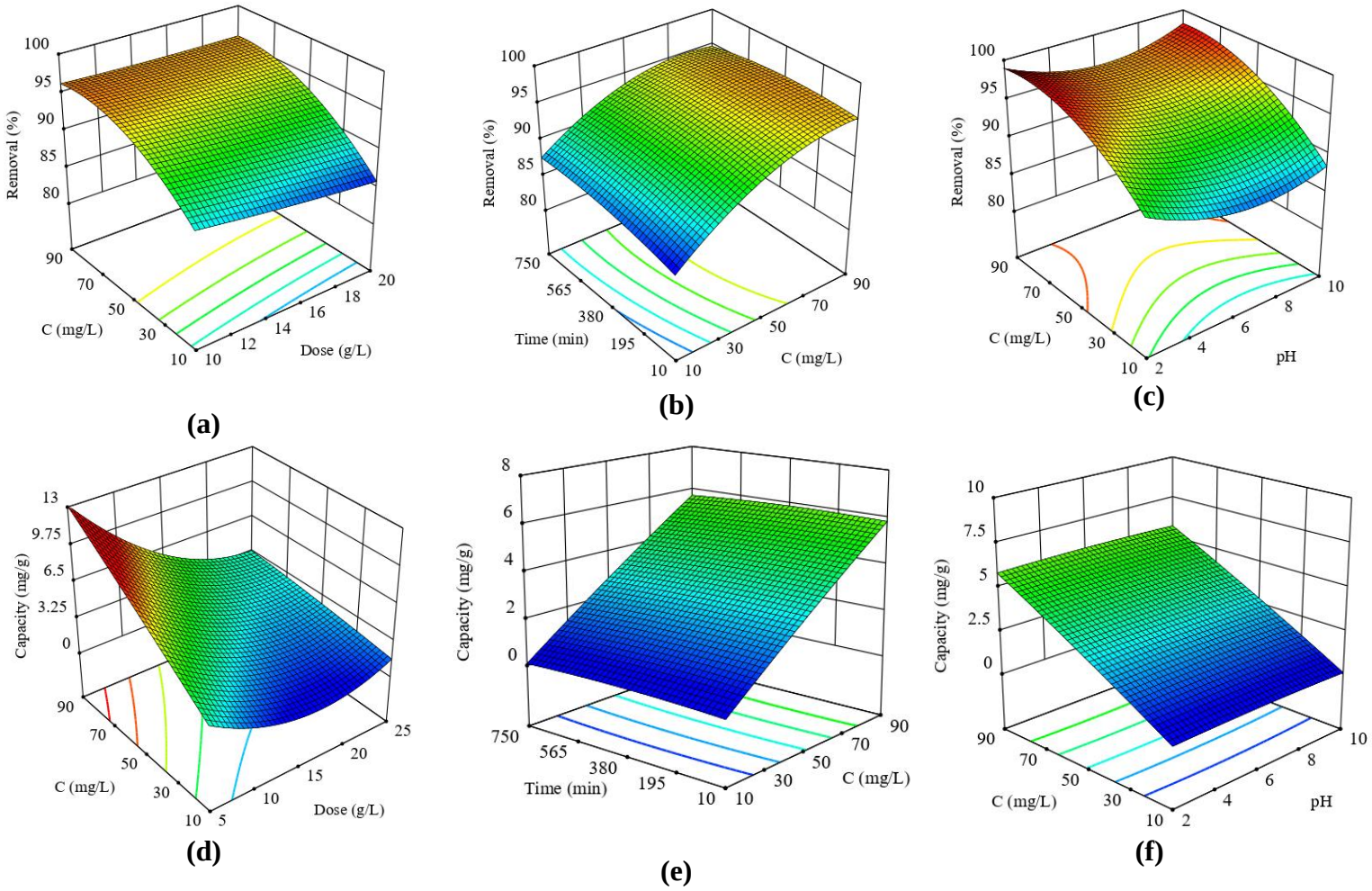

Fig. 4.13. The 3D surface response for the adsorptive uptake of DOX from aqueous solution (a, b, c) % removal vs C, m, t and pH, (d, e, f) capacity vs C, m, t and pH.

Figures 4.13 (a) and (d) represent the interactive influence of C and m on the responses X_1 and X_2 respectively. At any adsorbent dose DOX uptake increases rapidly with enhancement in initial DOX concentration. This increment is continuous for high adsorbent dose but at low dose, % removal becomes ultimately constant at very high DOX concentrations. From fig. 4.13 (d) it may be seen that increasing RHA dosage results in a decreasing adsorption capacity, whereas, it increases with the DOX amount in solution. The maximum DOX removal was observed at the minimum RHA dosage and maximum DOX concentration. At constant RHA dose (5 g/L) and DOX concentration (90 mg/L), a maximum DOX uptake capacity of >13 mg/g was obtained. Further, the relations between DOX initial concentrations (mg/L) and time (min) were studied and is represented in fig. 4.13 (b) and (e). As can be seen from fig. 4.13 (b), DOX removal % enhanced rapidly with increment in its initial concentration till ≈ 80 mg/L, because of larger amount of DOX competing for the available adsorption sites on RHA. Moreover, it was also noted that for very high initial concentrations, less adsorption time favors the DOX uptake, which might be ascribed to the desorption at more adsorption time. The interaction between solution pH and initial concentration of DOX has been exhibited in Fig. 4.13 (c) and (f). As it is evident from figures, when initial DOX concentration increases, the removal rate of DOX by RHA increases significantly regardless of the changes in solution pH. In general, the influence of initial DOX concentration on DOX adsorption is greater than that of solution pH.

In DOX – RHA adsorption, optimization study was also performed for enhancing the performances X_1 and X_2 using the RSM. The optimization restrictions set for this purpose are given in table 4.13. The conditions were evaluated as m = 5 g/L, t = 85.85 minute and pH = 6 with both responses as 99.51 % and 16.25 mg/g respectively. Then further examined the results of responses percentage removal and capacity were 98.85 % and 17.74 mg/g respectively, which are agrees well with the advised values (Table 4.12).

Table 4.13. Optimization Limits applied.

Variables	Goal	Lower Limit	Upper Limit
pH	is in range	6	10
Dose (g/L)	minimize	5	25
DOX conc. (mg/L)	is in range	10	90
Time (min)	minimize	10	750
Removal (%)	maximize	90	100
Capacity (mg/g)	maximize	0.5	10

4.11. Kinetics of DOX adsorption

To understand the kinetics of adsorption between DOX – RHA and calculate the kinetic parameters, pseudo first order and pseudo second order kinetics models were used. It was performed under optimized conditions (pH = 6, m = 5 g/L and time = 85.85 min) at different stock concentrations of DOX (40, 70 and 100 mg/L). These two model equations can be given by the following expressions:

Pseudo Ist order model is represented as (Malik 2003):

$$q_t = q_e\left[1-\exp\left(-k_f t\right)\right] \qquad \textbf{(4.9)}$$

Pseudo 2nd order model is signified as (Ho and McKay 1994):

$$q_t = \frac{tk_S q_e^2}{1+tk_S q_e} \qquad \textbf{(4.10)}$$

The initial adsorption rate, h (g/mg/min), may be calculated with the help of K_s and q_e magnitudes and are given as;

$$h = k_s q_e^2 \qquad \textbf{(4.11)}$$

Where q_e and q_t (mg/g) refers to the equilibrium amount of DOX adsorbed in duration t minues, k_f (min^{-1}) and k_s (g/mg/min) are the reaction constant rates for Pseudo Ist and Pseudo 2nd orders. As shown in Fig. 4.14 (a), initially, sharp increase in sorption takes place due to the availability of high number of the active site on the adsorbent surface and equilibrium was attained within 30 minutes. The experimental data were correlated with these kinetic models with the help of nonlinear regression. It is evident from figure that Pseudo 2nd order kinetic model fitted better with the experimental values than Pseudo Ist order model. All the evaluated kinetic parameters, R^2 and error values are listed in Table 4.14. High R^2 values and low MPSD error at all concentrations (40, 70 and 100 mg/L) confirms that DOX sorption on the RHA follows the second order kinetics.

In addition, the Intra-particle diffusion (IPD) model was utilized to analyse the rate-controlling step in the DOX-RHA adsorption process. The IPD model is represented by following equation (Weber and Morris 1963):

$$q_t = k_{id} t^{0.5} + I \qquad \textbf{(4.12)}$$

Where k_{id} (mg/g min$^{1/2}$) denotes to IPD rate constant and I (mg/g) is the intercept of intraparticle diffusion plot, which also represents the width of boundary layer. In the Weber and Morris plot, if the q_t vs $t^{1/2}$ graph is linear and it crosses through the origin, it confirms that sorption is controlled

solely by internal diffusion. The process of the DOX sorption on surface can be confirmed in two steps by the Weber and Morris plot in fig. 4.14 (b). The initial step represents the quick adsorption due to the higher number of active sites on the sorbent surface. This is denoted as intra-particle diffusion mechanism. The second part diminishes the intraparticle diffusion and attains the ultimate stability point as represented in the 2nd linear fragment in the figure. The second segment of the curves showed the equilibrium diffusion process. So it can be said that the kinetic sorption process of DOX antibiotic onto RHA follows a multistep mechanism. The magnitude of IPD parameters k_{id} and I are listed in Table 4.14.

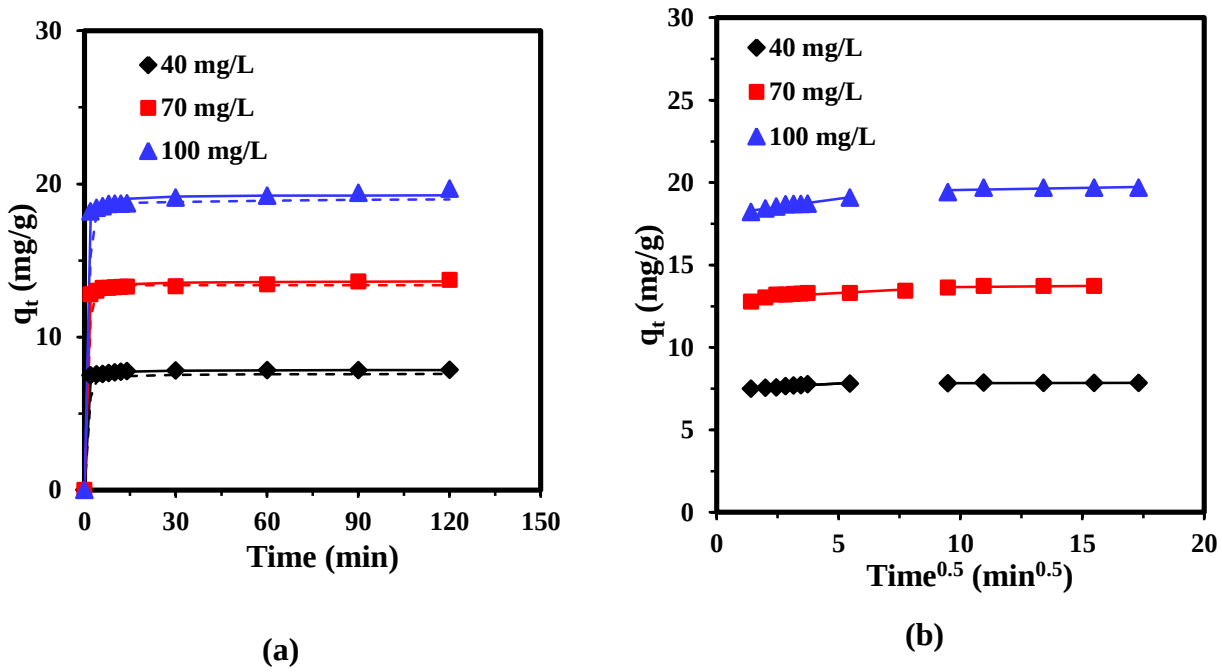

Fig. 4.14. (a) Pseudo-first and second-order adsorption kinetics at different initial concentrations (b) Weber–Morris plot versus t for DOX removal by RHA.

Table 4.14. Kinetic model parameters for DOX adsorption on RHA at optimized parameters (m = 5 g/L, t = 85.85 min and pH = 6).

	C_0 (mg/L)		
	40	**70**	**100**
Pseudo first order			
k_f (min^{-1})	1.190	0.910	0.802
$q_{e,exp}$ (mg/g)	7.849	13.716	19.694
$q_{e,cal}$ (mg/g)	7.794	13.370	19.200
R^2 (non-linear)	0.988	0.992	0.990
MPSD	16.91	6.157	8.695
Pseudo second order			
k_s (g/mg/min)	0.580	0.360	0.276
h (mg/g/min)	35.771	67.042	102.622
$q_{e,cal}$ (mg/g)	7.853	13.644	19.287
R^2 (non-linear)	0.999	0.999	0.998
MPSD	0.928	3.790	7.315
Weber Morris			
k_{id1} (mg/g $min^{-1/2}$)	0.081	0.078	0.202
I_1	7.397	12.911	18.011
R^2	0.884	0.644	0.950
k_{id2} (mg/g $min^{-1/2}$)	0.001	0.012	0.026
I_2	7.822	13.546	19.282
R^2	0.326	0.481	0.451

4.12. Isotherm Modelling and Thermodynamics

The adsorption of the DOX on RHA was examined at distinct temperatures and concentrations and the suitability of equilibrium data were evaluated with the various isotherm models as shown in Fig.4.15. Freundlich (Freundlich, 1906), Redlich- Peterson (R-P) (Redlich and Peterson, 1959), and Langmuir isotherms (Langmuir, 1918) are represented by the following equations.

Langmuir model:

$$q_e = \frac{q_m K_L C_e}{1 + K_L C_e} \qquad \textbf{(4.13)}$$

Redlich-Peterson model:

$$q_e = \frac{K_R C_e}{1 + a_R C_e^{\beta}} \qquad \textbf{(4.14)}$$

Freundlich model:

$$q_e = K_F C_e^{1/n} \qquad \textbf{(4.15)}$$

Where, q_e (mg/g) is the specific equilibrium quantity of adsorbate, C_e (mg/L) is the equilibrium concentration of adsorbate, q_m (mg/g) is the maximum adsorption uptake. K_L, K_F, a_R, K_R are constants, and "n" represents to the empirical constant.

The isotherm studies were performed at a temperature range of 288-318 K with DOX initial concentration of 40 - 300 mg/L. These experiments were directed at optimum conditions as m = 5 g/L, time = 85.85 minutes and pH is 6. As displayed in Fig. 4.15, with the enhancement in temperature, the sorption rate increased due to the endothermic type of the operation. The non-linear fitting was performed and the experimental data suits well with the Langmuir, Freundlich and R-P isotherm models with the high R^2 values. The values of parameters relevant to different isotherm models and correlation coefficient values are given in table 4.15. The high R^2 values represent stronger interactions between adsorbate – adsorbent and as the value of β lies between 0-1 for R-P isotherm it signifies that the sorption of DOX on RHA is favorable operation.

The thermodynamic criterion is examined by Van't Hoff equation (Eq. (4.16)).

$$\ln K_d = \frac{-\Delta G^0}{RT} = \frac{\Delta S^0}{R} - \frac{\Delta H^0}{R}\frac{1}{T} \qquad \textbf{(4.16)}$$

Where, K_d is the equilibrium constant, T is the temperature in K, R represents to gas constant in J/mol/K, ΔG° ΔH° and ΔS° and are changes in Gibb's free energy, standard enthalpy and standard entropy.

Moreover, the evaluated thermodynamics parameters for DOX-RHA adsorption are listed in Table 4.15. It is visible from the parameters that, as the temperature increases ΔG^o value increases, which indicates the enhancement in sorption performance at higher temperatures. The positive value of △H° demonstrate that sorption of DOX on adsorbent surface is of endothermic type. Moreover, the

+ ve value of ΔS° approves the increment in the haphazardness of the DOX molecules at the solid-liquid interfaces (Lakshmi et al. 2009). So from the thermodynamic investigation it is concluded that adsorption of DOX on rice husk ash is spontaneous and endothermic process.

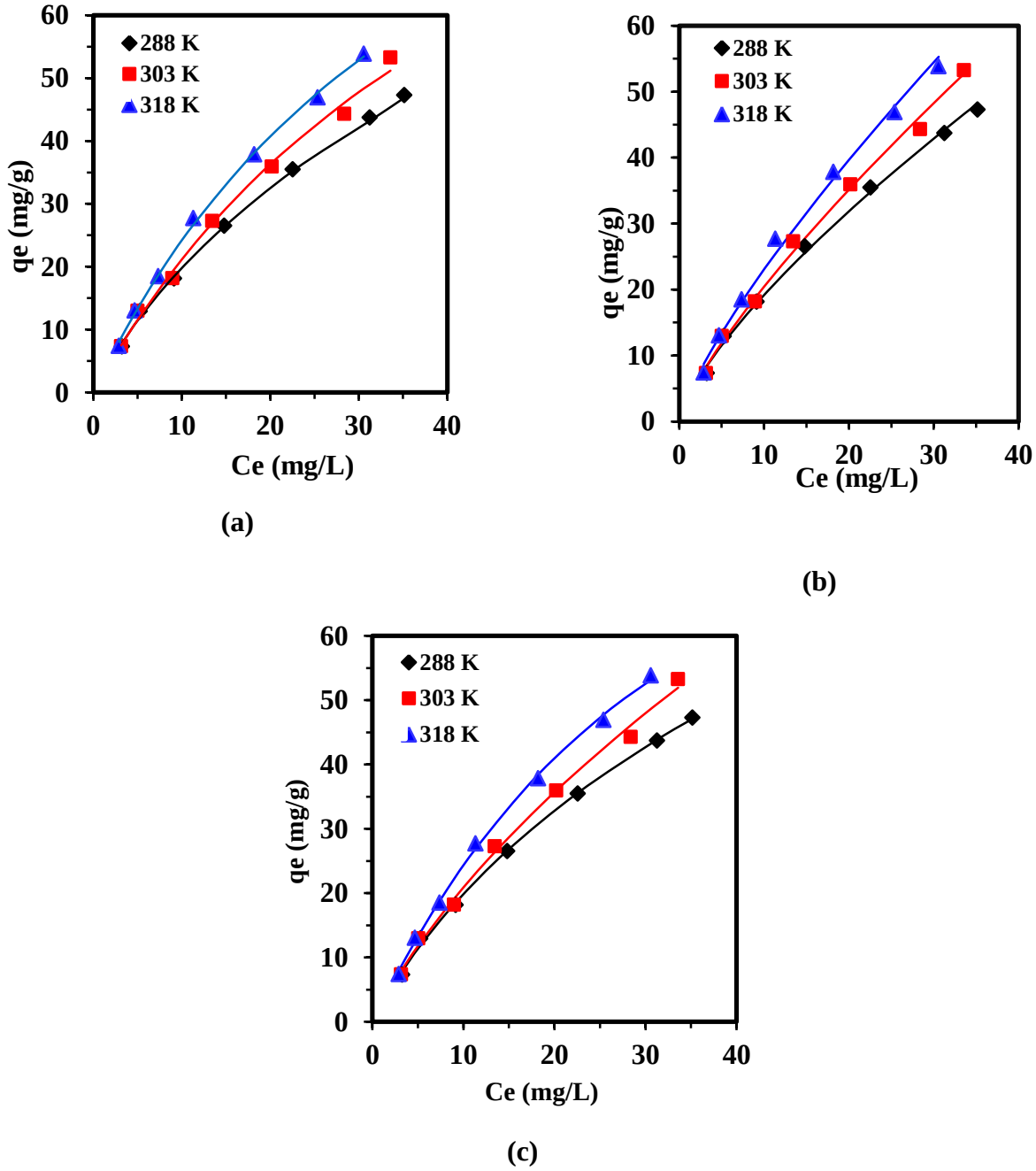

Fig. 4.15. Equilibrium adsorption isotherms for DOX adsorption on RHA at optimized parameters (m = 5 g/L, t = 85.85 min and pH = 6) (a) Langmuir isotherm model (b) Freundlich isotherm model (c) RP isotherm model. Experimental data points given by symbols and the lines predicated by isotherm model.

Table 4.15. Isotherms and Thermodynamics parameters for DOX adsorption on RHA at optimized parameters (m = 5 g/L, t = 85.85 min and pH = 6).

ISOTHERMS

Langmuir $$q_e = \frac{q_m K_L C_e}{1 + K_L C_e}$$

T (K)	K_L (L/mg)	q_m (mg/g)	R^2	CHI^2
288 K	0.036	73.631	0.999	0.137
303 K	0.019	128.934	0.997	0.321
318 K	0.022	130.116	0.997	0.131

Redlich-Peterson $$q_e = \frac{K_R C_e}{1 + a_R C_e^{\beta}}$$

T (K)	K_R (L/g)	a_R (L/mg)$^{1/\beta}$	β	R^2	CHI^2
288 K	2.861	0.077	0.752	0.999	0.136
303 K	3.157	0.133	0.584	0.998	0.320
318 K	2.854	0.012	1.162	0.999	0.122

Freundlich $$q_e = K_F C_e^{1/n}$$

T (K)	K_f (L/mg)	1/n	R^2	CHI^2
288 K	3.541	0.733	0.998	0.307
303 K	3.367	0.783	0.997	0.394
318 K	3.797	0.783	0.997	0.524

Thermodynamic Parameters $$\ln K_D = \frac{-\Delta G^0}{RT} = \frac{\Delta S^0}{R} - \frac{\Delta H^0}{R}\frac{1}{T}$$

T (K)	K x 10^{-3} (L/kg)	ΔG^0 (kJ/mol)	ΔH^0 (kJ/mol)	ΔS^0 (J/mol)
288 K	1.985	-18.182		
303 K	2.069	-19.234	6.226	84.519
318 K	2.544	-20.733		

4.13. Mechanism of Adsorption

The amphoteric quality of DOX permits the presence of several ionic species at distinct ranges of pH. The point of zero charges of RHA was evaluated as 8.1. On the other hand, DOX shows three pKa values (pK_1 =3.5, pK_2 = 7.7, pK_3 = 9.5) (Gao et al. 2012). RHA has predominantly +ve charge at pH < pHpzc and -ve charge when pH > pHpzc. At acidic pH, the interactions between the RHA and DOX are weak due to the presence of the same charges on both compounds. Under neural conditions, the greater removal is obtained at that point because of the interactions between the RHA^+ and DOX^o forms. At this pH, it shows that the H-bonding and electrostatic interactions are responsible for the adsorption of DOX by RHA as shown in Fig. 4.16. Further, the existence of electrostatic interactions are there amid the -OH and ketone groups of the DOX and silane groups present in the RHA. On the other hand, the formation of H-bonding takes place among the –OH and amine groups of the doxycycline molecule and O_2 in the siloxane groups on the RHA adsorbent.

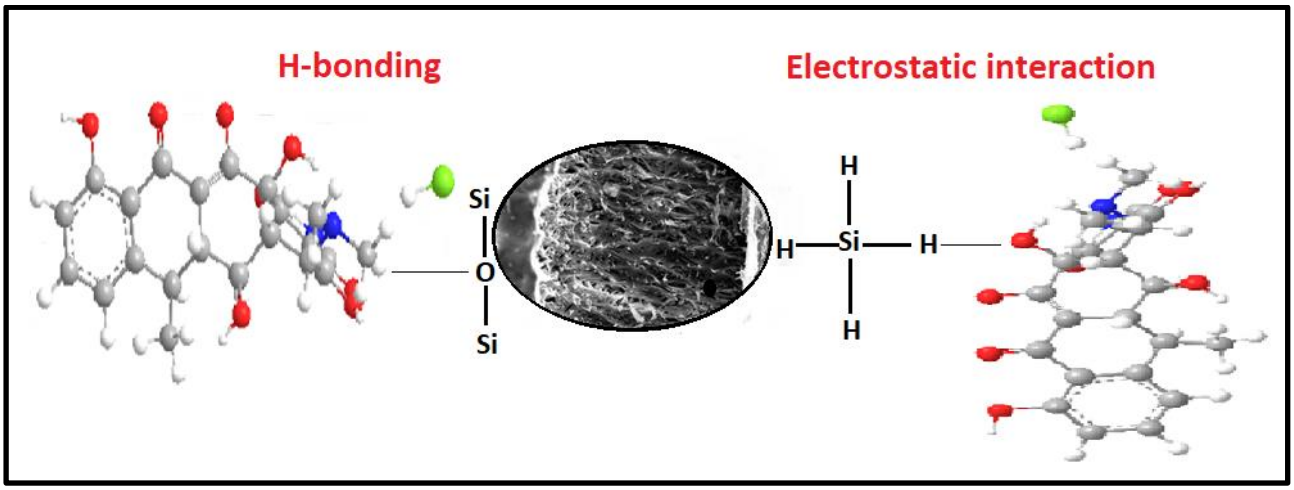

Fig. 4.16. Adsorption mechanism for DOX on RHA surface.

4.14. Solidification/Stabilization performance and toxicity tests

To ensure the safe disposal of exhausted adsorbent, it is necessary to capsulate the antibiotic present in it to avoid its further mixing in the atmosphere. Results of solidification study are shown in fig. 4.17, which shows that for all the studied concentrations (40, 70, and 100 mg/L) the encapsulation percentage was > 98 %. Above results demonstrate that Portland cement can be used as potential solidifying agent for almost complete encapsulation of antibiotics present in exhausted adsorbents.

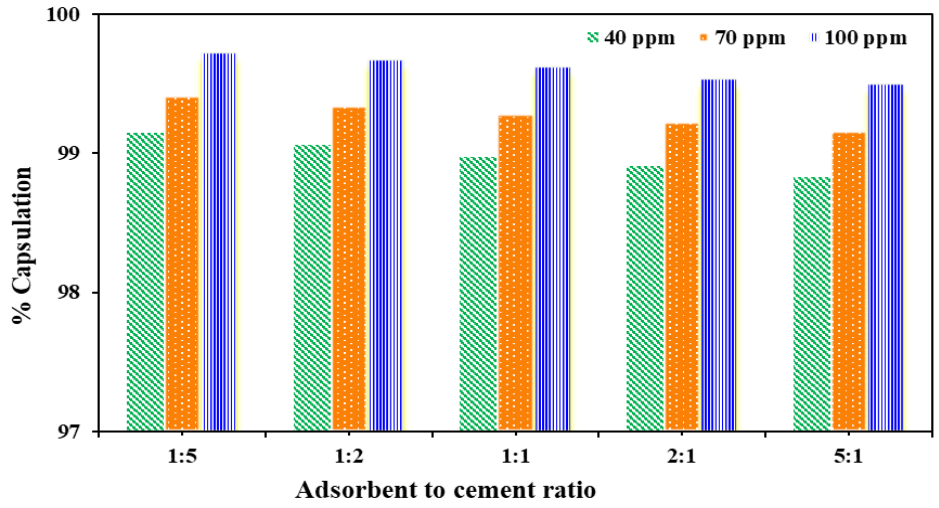

Fig. 4.17. % Capsulation of DOX in cement for different adsorbent to cement mass ratios.

The leachate was further tested to evaluate its toxicity for possible presence of DOX into it. The comparative zone of inhibitions were observed on petri plates having EC and BC bacterial strains. From the results, it is evident that higher zones were found at 10 ppm (30 mm, 28 mm) and lower at 0.1 ppm for EC and 1 ppm for BC (11mm, 14 mm) in both cases EC and BC (Fig.4.18 (a & b)). In Fig. 4.18 (c) and (d), there were no inhibition zones seen in the growth of EC and BC bacterial plates. Therefore, it is indicated that S/S process is a viable method for handling exhausted adsorbents as it could successfully capsule the antibiotic and no harmful effects against the selected bacterial strains were observed.

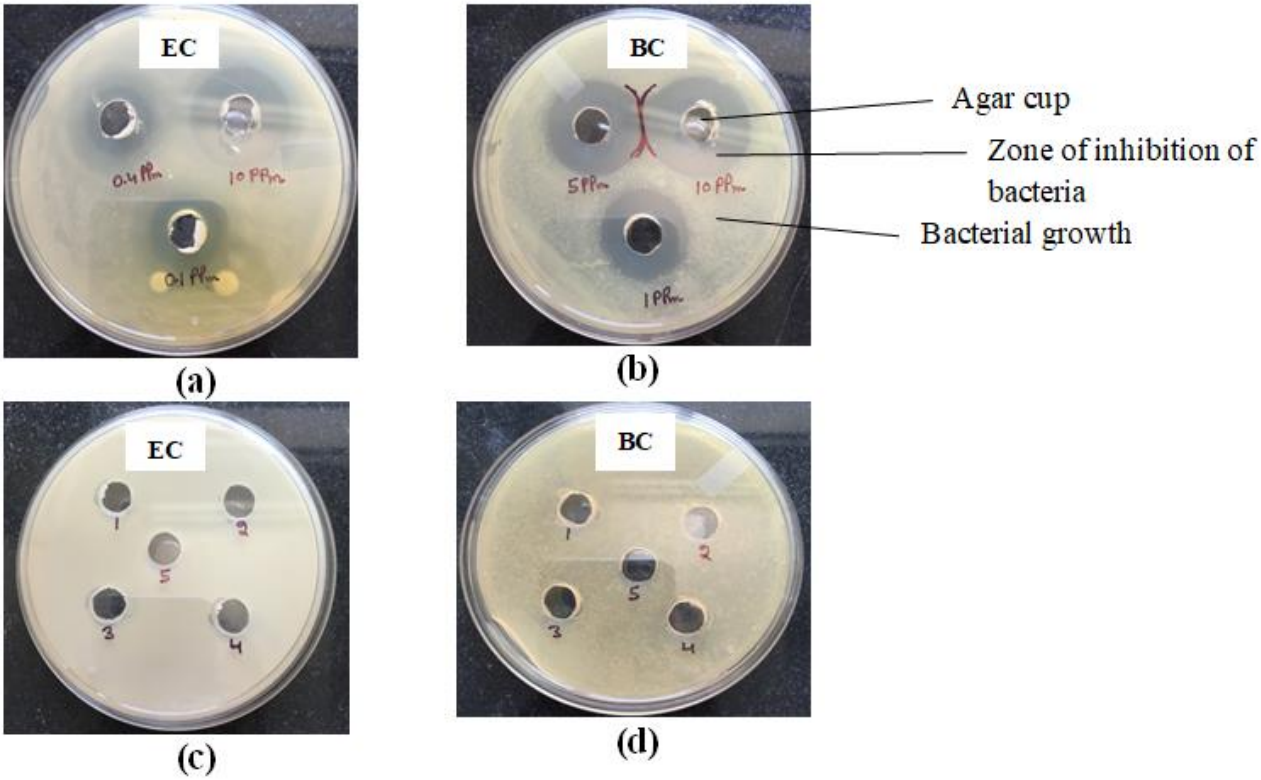

Fig. 4.18. Zone of inhibition on *E.coli* (EC) and *Bacillus subtilis* (BC) bacterial strains (a) for DOX samples on *E.coli* (EC) (b) for DOX samples on *Bacillus subtilis* (BC) (c) for leachate on *E.coli* (d) and *Bacillus subtilis*.

4.15. BATCH ADSORPTIVE REMOVAL OF WASTEWATER COMPRISING OFL BY PJAC

4.15.1. Prosopis juliflora based activated carbon characterization

Fig. 4.19 represents the XRD spectrum of PJAC and OFL loaded PJAC. The XRD patterns were obtained to explain the nature of PJAC adsorbent, i.e. amorphous or crystalline. A high intensity peak seen at ~ 26 (2θ) and low intensity peaks at ~ 31 and 42 (2θ) regions designate the crystalline behavior of the adsorbent (Kumar and Tamilarasan, 2017). Some variations were observed in the loaded sample (PJAC-OFL) due to the deformation in structure of adsorbent after the adsorption of OFL.

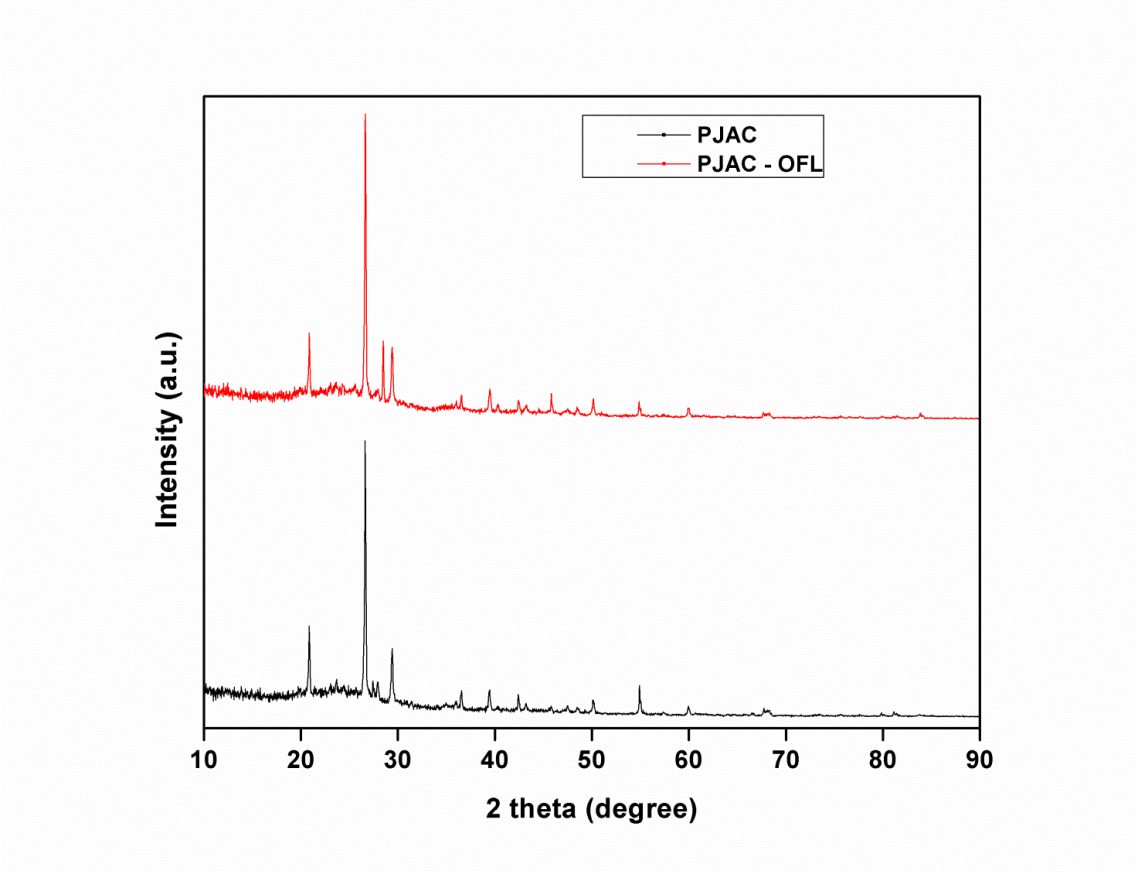

Fig. 4.19. X-ray diffraction (XRD) analysis before and after loading of OFL onto PJAC.

The FTIR spectral examination of PJAC was designated at 1026.4, 1636.04 and 3431.5 cm^{-1} while OFL loaded PJAC showed absorption at 1033.4, 1501.2 and 3398.2 cm^{-1}. As depicted in fig. 4.20, the differences between the peak intensities were found to be 7, 134.84 and 33.3 cm^{-1} respectively. These seen changes confirms the complexation of OFL with the existing functional groups present on the PJAC surface. For PJAC, peaks at 1026, 1636, 2102 and 3431 cm^{-1} indicates to C–O, C=C

stretch, N-H stretching and O-H functional group respectively (Kezerle et al., 2018). Conversely, peaks at 1033.4, 1501.2 and 3398.2 cm^{-1} direct the presence of C-O, C=C and O-H functional groups. So, the main identified functional groups are C=C, C-O, N-H and O-H. It has resulted that the observed functional groups are involved in the sorption of the main compound (OFL) on the adsorbent surface.

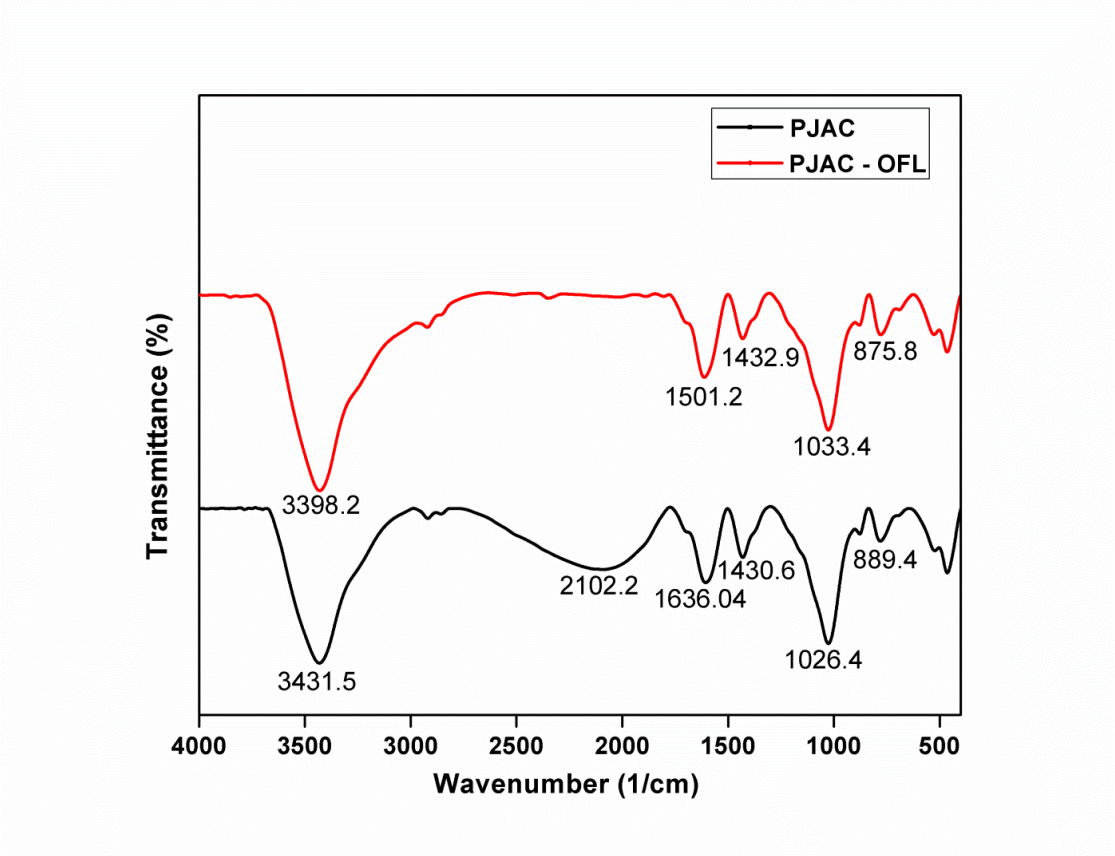

Fig. 4.20. FTIR spectra of PJAC and PJAC − OFL.

The SEM and EDX images of PJAC and OFL loaded PJAC are shown in fig. 4.21. SEM pictures of PJAC adsorbent represent the crystalline and porous texture on its surface as shown in fig. 4.21 (a). From the SEM pictures of OFL loaded PJAC (Fig. 4.21 (c)) it is evident that all the pores are filled with adsorbate (OFL) molecules after the adsorption. On the other hand, EDX spectrum of both samples is revealed in fig. 4.21 (b, d). While comparing the EDX mapping of both samples, main differences were observed in the peaks of Si, Ca, C and other components which were also found in lesser concentrations as shown in fig.4.21 (b, d). These elements are responsible for the removal of OFL from its aqueous phase. Moreover, porosimetry analysis was done to determine the specific surface area, pore diameter and volume of the PJAC. The BET surface area of PJAC was evaluated

to be 320.49 m^2/g. From the BJH model, the calculated pore volume and pore diameter were evaluated as 0.176 cc/g and 2.65 nm, respectively.

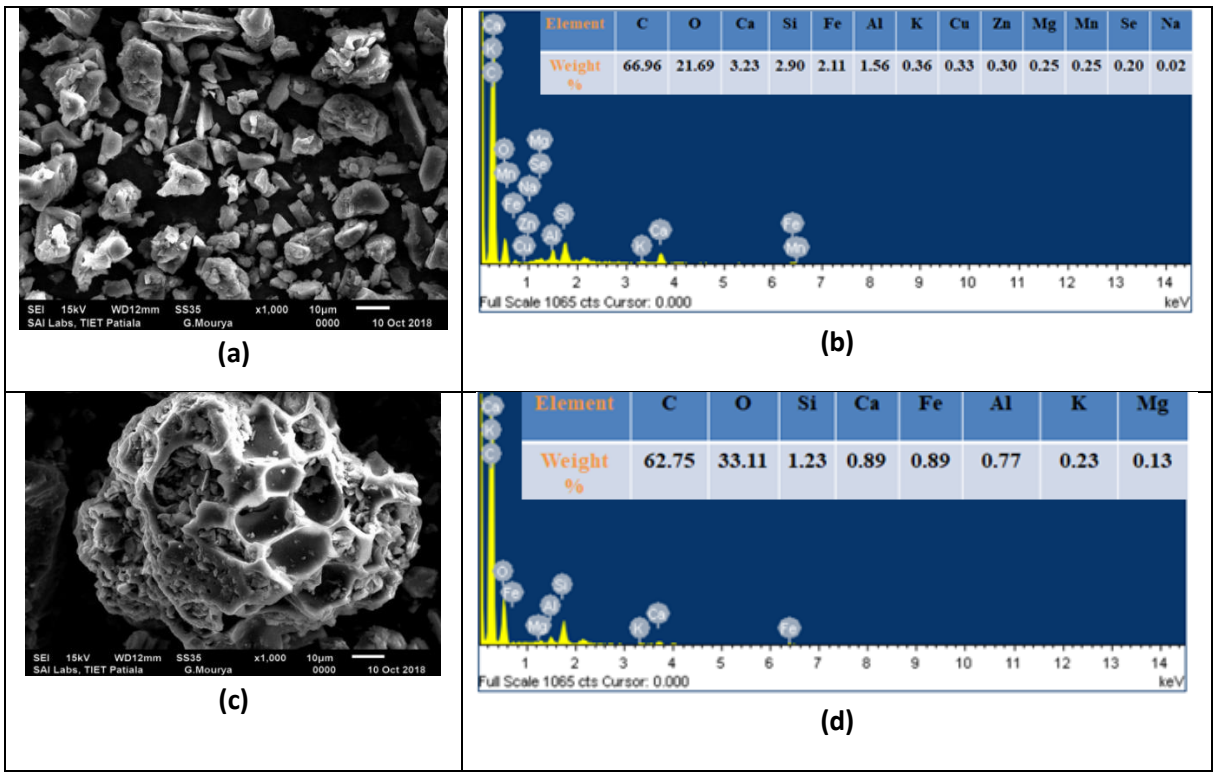

Fig. 4.21. (a, b) SEM-EDX analysis of PJAC (c, d) PJAC loaded with OFL.

4.16. Model result and Statistical analysis

Based on the CCD model the suggested experiments were performed and values of evaluated responses as given in table 4.16. From the RSM generated ANOVA table, the quadratic polynomial regression model was established to calculate the influence of applied independent parameters for both responses (X_1 and X_2).

Table 4.16. Design of experiments for the adsorption of OFL by PJAC.

Std	Run	pH	Dose of PJAC (g/L)	OFL conc. (mg/L)	Time (min)	% OFL removal (X_1)	Adsorption Capacity (X_2)
15	1	4.0	20.0	70.0	565.0	77.87	2.72
13	2	4.0	10.0	70.0	565.0	58.97	4.12
28	3	6.0	15.0	50.0	380.0	72.57	2.41
22	4	6.0	15.0	90.0	380.0	53.42	3.20
5	5	4.0	10.0	70.0	195.0	56.95	3.98
10	6	8.0	10.0	30.0	565.0	68.71	2.06
9	7	4.0	10.0	30.0	565.0	72.61	2.17
4	8	8.0	20.0	30.0	195.0	61.95	0.92
26	9	6.0	15.0	50.0	380.0	72.62	2.42
2	10	8.0	10.0	30.0	195.0	54.80	1.64
18	11	10.0	15.0	50.0	380.0	77.57	2.58
30	12	6.0	15.0	50.0	380.0	72.65	2.42
6	13	8.0	10.0	70.0	195.0	50.65	3.54
16	14	8.0	20.0	70.0	565.0	73.30	2.56
20	15	6.0	25.0	50.0	380.0	78.71	1.57
24	16	6.0	15.0	50.0	750.0	71.57	2.38
1	17	4.0	10.0	30.0	195.0	61.33	1.84
19	18	6.0	5.0	50.0	380.0	44.11	4.41
8	19	8.0	20.0	70.0	195.0	67.26	2.35
25	20	6.0	15.0	50.0	380.0	72.40	2.41
29	21	6.0	15.0	50.0	380.0	72.45	2.41
23	22	6.0	15.0	50.0	10.0	53.65	1.78
21	23	6.0	15.0	10.0	380.0	57.01	0.38
27	24	6.0	15.0	50.0	380.0	72.51	2.41
17	25	2.0	15.0	50.0	380.0	87.42	2.91
12	26	8.0	20.0	30.0	565.0	76.76	1.15
11	27	4.0	20.0	30.0	565.0	83.09	1.24
3	28	4.0	20.0	30.0	195.0	67.23	1.08
14	29	8.0	10.0	70.0	565.0	50.65	3.54
7	30	4.0	20.0	70.0	195.0	76.02	2.66

The final equations for both responses in terms of coded factors are given by following second-order polynomial quadratic model:

$$X_1 = 27.64 - (9.06 * pH) + (2.95 * m) + (0.88 * C) + (0.09 * t) + (0.65 * pH^2) - (0.10 * m^2) - (0.01 * C^2) - (6.90 * 10^{-5} * t^2) + (8.50 * 10^{-4} * \text{pH} * \text{m}) - (9.20 * 10^{-3} * \text{pH} * \text{C}) + (6.27 * 10^{-4} * \text{pH} * \text{t}) + (0.02 * \text{m} * \text{C}) + (7.68 * 10^{-4} * \text{m} * \text{t}) - (7.75 * 10^{-4} * \text{C} * \text{t}) \quad \textbf{(4.17)}$$

$$X_2 = 1.62 - (0.26 * pH) - (0.25 * m) + (0.10 * C) + (3.45 * 10^{-3} * t) + (0.01 * pH^2) + (5.36 * 10^{-3} * m^2) - (4.14 * 10^{-4} * C^2) - (2.69 * 10^{-6} * t^2) + (4.35 * 10^{-3} * \text{pH} * \text{m}) - (1.56 * 10^{-3} * \text{pH} * \text{C}) + (1.13 * 10^{-5} * \text{pH} * \text{t}) - (9.45 * 10^{-4} * \text{m} * \text{C}) - (1.08 * 10^{-5} * \text{m} * \text{t}) - (1.34 * 10^{-5} * \text{C} * \text{t}) \quad \textbf{(4.18)}$$

Experimental data were analyzed from the ANOVA table, and the findings are displayed in Table 4.17. The significant F-values (3349.83, 26.13) and P-values < 0.0001 (same for both responses) have confirmed the acceptation of the developed polynomial quadratic model equation. The close unity values of R^2 (0.988, 0.986), R_{adj}^2 (0.977, 0.973) and R_{pre}^2 (0.932, 0.920) confirmed that the quadratic polynomial model indicates the positive associations for both responses as shown in table 4.18. The adequate precisions were carried out to be 36.27 and 36.01 (greater than 4), which also identify the reasonable agreement of the developed quadratic polynomial model. Moreover, the model accuracy was also investigated by actual versus predicted plots, shown in fig 4.22 (a, b). The best fitting of the experimental versus predicted data is presented in table 4.19.

Table 4.17. ANOVA and statistical values for batch adsorption of OFL onto PJAC.

	% OFL removal (X_1)					Adsorption Capacity (X_2)				
Source	**Sum of Squares**	**DF**	**Mean Square**	**F Value**	**Prob > F**	**Sum of Squares**	**DF**	**Mean Square**	**F Value**	**Prob > F**
Model	3349.83	14	239.27	90.44	< 0.0001	26.13	14	1.87	76.87	< 0.0001
A	202.42	1	202.42	76.51	< 0.0001	0.29	1	0.29	11.91	0.0036
B	1319.80	1	1319.80	498.83	< 0.0001	8.13	1	8.13	334.71	< 0.0001
C	73.40	1	73.40	27.74	< 0.001	15.21	1	15.21	626.46	< 0.0001
D	430.31	1	430.31	162.64	< 0.0001	0.33	1	0.33	13.73	0.0021
A^2	186.51	1	186.51	70.49	<0.0001	0.15	1	0.15	6.10	0.0261
B^2	194.63	1	194.63	73.56	<0.0001	0.49	1	0.49	20.34	0.0004
C^2	487.03	1	487.03	184.08	< 0.0001	0.75	1	0.75	31.08	<0.0001
D^2	153.26	1	153.26	57.93	< 0.0001	0.23	1	0.23	9.62	0.0073
AB	1.15×10^{-3}	1	1.15×10^{-3}	4.37×10^{-4}	0.9836	0.030	1	0.030	1.25	0.2809
AC	2.17	1	2.17	0.82	0.3795	0.063	1	0.063	2.59	0.1284
AD	0.86	1	0.86	0.33	0.5765	2.81×10^{-4}	1	2.81×10^{-4}	0.012	0.9156
BC	130.15	1	130.15	49.19	<0.0001	0.14	1	0.14	5.89	0.0283
BD	8.09	1	8.09	3.06	0.1009	1.60×10^{-3}	1	1.60×10^{-3}	0.066	0.8009
CD	131.78	1	131.78	49.81	<0.0001	0.040	1	0.040	1.64	0.2203
Residual	39.69	15	2.65			0.36	15	0.024		
Lack of Fit	39.64	10	3.96	399.09	< 0.0001	0.36	10	0.036	3299.08	< 0.0001
Pure Error	0.050	5	9.93×10^{-3}			5.51×10^{-5}	5	1.10×10^{-5}		
Cor Total	3389.51	29				26.49	29			

A: pH, B: dose of PJAC (m, g/L), C: OFL conc. (C_0, mg/L), D: Time (t, min)

Table 4.18. Validation of proposed CCD model by various statistic parameters.

Responses	R-Squared	Adj R-Squared	Pred R-Squared
% OFL removal (X_1)	0.988	0.977	0.932
Adsorption Capacity (X_2)	0.986	0.973	0.920

Table 4.19. Comparison of RSM/CCD experimental and predicted responses values at optimized condition (*m* = 16.23 g/L, *t* = 336 min, *pH* = 6 and OFL concentration = 57 mg/L).

Responses	Predicted value	Experimental value
% removal (X_1)	72.41 %	72.38 %
Capacity (X_2)	2.51	2.54

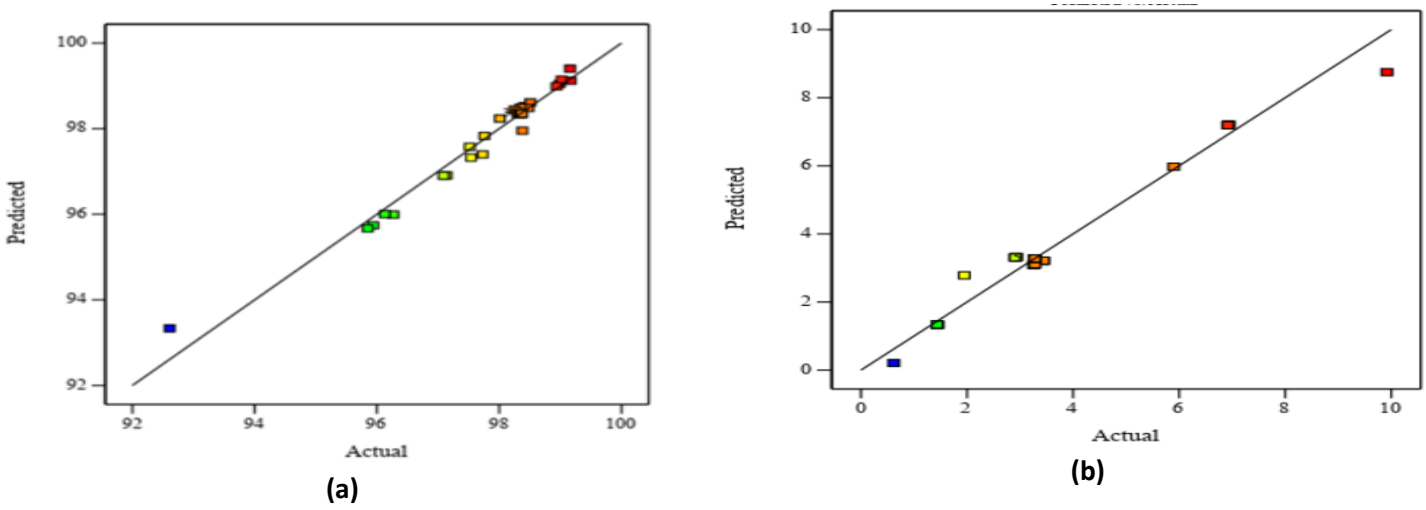

Fig. 4.22. The actual data versus predicted data for (a) % removal (b) capacity (mg/g) of OFL.

4.17. Response Surface analysis

3-D surfaces and contour plots are the graphic illustrations of regression equations and are most useful approach for optimizing the process parameters of the adsorption system. The effects of the relationship between four independent variables i.e., OFL Concentration (mg/L), PJAC mass (g/L), time (min), solution pH and dependent variables are shown in Fig. 4.23.

Fig. 4.23 (a) and (d) represents the interaction effect between PJAC dosage (m) and OFL concentration (C) on the percentage OFL uptake and adsorption capacity. The percentage OFL uptake declines with enhancement in OFL concentration at low PJAC dose. Nevertheless, at higher PJAC

dose, percentage OFL uptake enhances with increase in C value. This variation in OFL removal could be explained by the availability of more adsorption sites at high PJAC dosage so the sorption of OFL on PJAC surface can be regarded as adsorbent restricting.

While, at low PJAC dose, capacity improves with enhancement in original OFL concentration in solution, and minute variation was noticed in capacity at greater dose with enhanced OFL concentration (Fig. 4.23 d). Results demonstrates the greater sorption capacity of PJAC towards OFL.

According to Fig. 6 (b) and (e) the OFL concentration (C) and time (t) interactions on the percentage OFL uptake and sorption capacity shows that at reduced C values, the rise in sorption duration (*t)* enhances the OFL uptake, that attains almost constant value for larger durations. Nevertheless, at high OFL concentrations, % OFL uptake increased firstly and then declines marginally with contact time. This aspect was associated to thedesorption of OFL after equilibrium was attained. On other hand, with the increase of t the capacity was found to increase (Fig. 4.23 e). Possibly this is because when the C value is more the OFL uptake first enhances and afterwards diminishes with time (Fig. 4.23 b). Moreover, it also noted that for very high initial concentrations, less adsorption time favors the OFL uptake, which might be ascribed to the desorption at more adsorption time. Fig. 4.23 (c) and (f), show the simultaneous interaction effects of pH and OFL concentration on responses X_1 and X_2 respectively at fixed PJAC dose and adsorption time.

At a constant pH, the OFL uptake was noticed enhancing continuously with the increment in OFL concentration. Nevertheless, at high initial concentration, OFL uptake appears decreasing with increase in pH. Such pattern shows that the sorption of OFL is restrained by the OFL concentration, and the PJAC acquires greater sorption capacity. While on the contrary, the capacity was observed continuously growing at different *pH* with enhancement in *C* value. Conversely, there is no substantial alteration in adsorption capacity with variation in pH at any OFL concentration (Fig. 4.23 f).

From the above, it is to be noted that out of different parameters, PJAC dose, original OFL concentration, solution pH and sorption time, the interactive effects of initial OFL concentration and PJAC dose was significant on both the responses (X_1 and X_2) as compared to effects of other variates (pH and time).

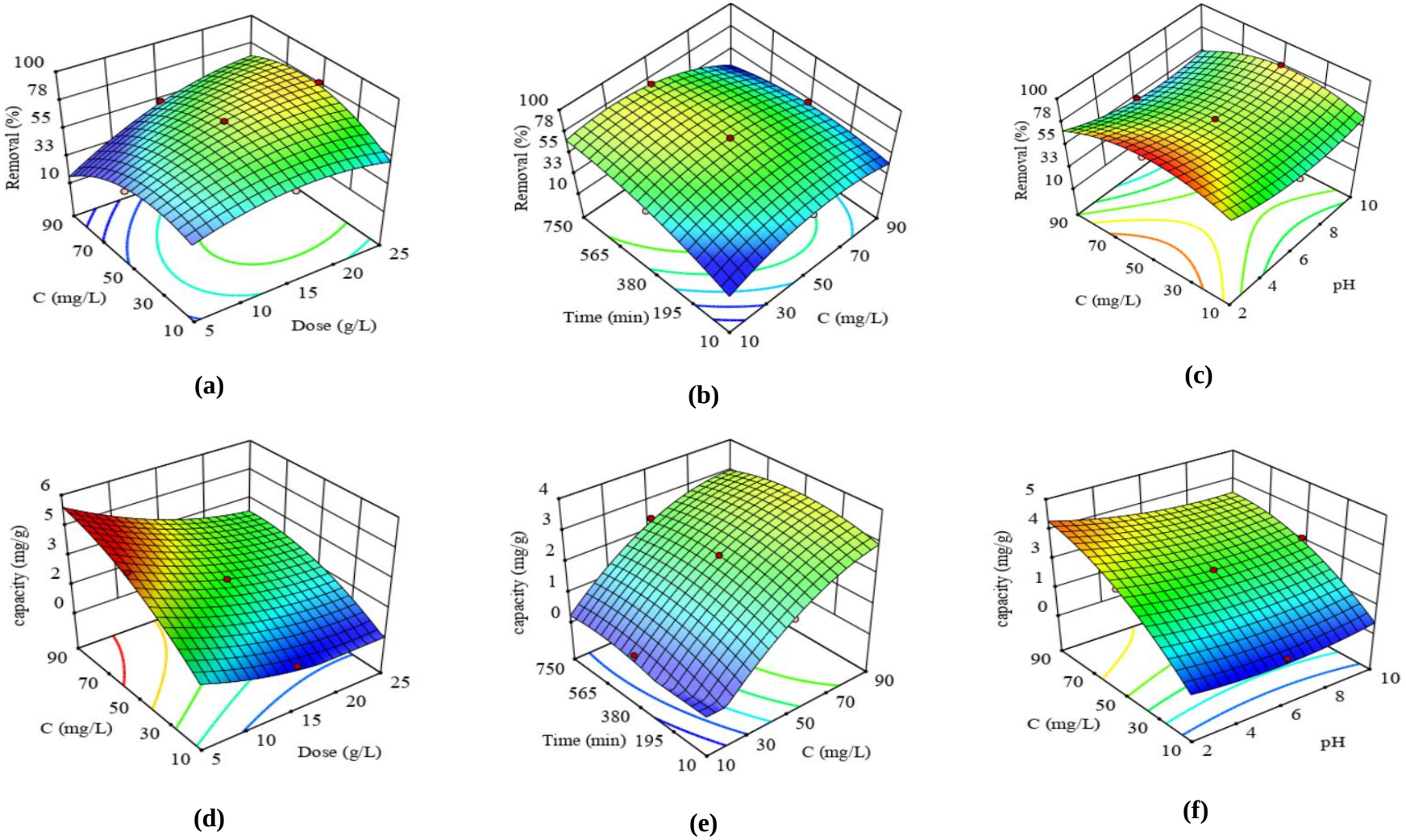

Fig. 4.23. Response surfaces and contour plots for the % removal of OFL (a, b, c) and capacity (d, e, f).

4.18. Adsorption mechanism

The adsorption mechanism of OFL on PJAC has been shown in fig. 4.24. The point of zero charge (pHpzc) of PJAC was found as 8.5. The availability of several functional groups such as C-C, O-H, C=C, C-N and C-O on PJAC surface played a significant role in the sorption of OFL antibiotic. The OFL represents two pKa values, 6.08 (pKa_1) and 8.25 (pKa_2). It is in cationic form (OFL^+) below pH < 6.08, anionic (OFL^-) above pH > 8.25 and in between (8.25< pH >6.08) it exists in non-ionic form (OFL^o) (Goyne et al., 2005). In the present study, maximum OFL uptake was obtained at neural pH. At acidic pH, both OFL and PJAC are positively charged and there is not any possibility of electrostatic interaction between adsorbate and adsorbent molecules. But under neutral conditions (OFL^+) acts as a л electron acceptor (Gao et al., 2019). This OFL^+ behavior causes л - л EDA interactions with the PJAC surface. Moreover, H-bonding between aromatic rings in the OFL molecule and O-H functional groups onto PJAC surface plays an influential role in increasing the adsorption performance. Furthermore, at alkaline conditions (pH > 8.5), both OFL and PJAC are negatively charged. As a result, OFL^- and existing deprotonated functional groups of PJAC express the decrease in OFL uptake. Hence, л - л EDA interactions and H-bonding are the dominating adsorption mechanisms between OFL and PJAC systems.

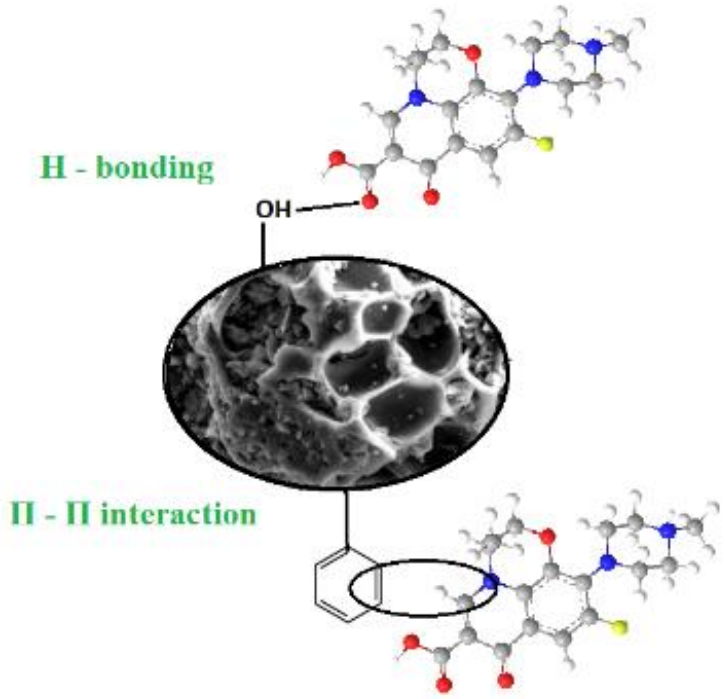

Fig. 4.24. Adsorption mechanism for OFL on PJAC surface.

4.19. Adsorption kinetics, equilibrium and Diffusivity studies

Adsorption kinetic is an imperative aspect to investigate the design of an operative adsorption system and determine the adsorption rate and mechanism of the process. The variations observed in the adsorption capacity of OFL at different time intervals are demonstrated in Fig. 4.25 (a). The adsorption capacity increased quickly in first 60 min due to the availability of many binding sites during the initial stages of the adsorption process. Subsequently, the removal rate becomes slower from 60 to 120 min, and ultimately the equilibrium point was achieved in 240 min. The experimental data were fitted with pseudo-first-order, pseudo-second-order and intraparticle diffusion models as expressed by the following Equations.

Pseudo Ist order model is represented as (Malik, 2003):

$$q_t = q_e\left[1 - \exp\left(-k_f t\right)\right] \qquad \textbf{(4.19)}$$

Pseudo 2nd order model is signified as (Ho and McKay, 1999):

$$q_t = \frac{tk_S q_e^2}{1 + tk_S q_e} \qquad \textbf{(4.20)}$$

Where q_e and q_t (mg/g) refers to the equilibrium quantity of OFL adsorbed at time t (min), k_f (per min) and k_s (g/mg/min) are the reactions constant rates for Pseudo Ist and Pseudo 2nd orders. Fig. 4.25 (a) displays the Pseudo Ist order and Pseudo 2nd order kinetic models. The values for both kinetic models are described in Table 4.20. From comparing the experimental values (R^2) it was detected that adsorption of OFL onto PJAC followed pseudo-second-order kinetics.

Likewise, the intra-particle diffusion model (IDM) is usually used to recognize the rate-controlling diffusion step of the adsorption process, and the equation is expressed as (Weber and Morris, 1963):

$$q_t = k_{id} t^{0.5} + I \qquad \textbf{(4.21)}$$

Where k_{id} (mg/g min$^{1/2}$) is the intra-particle diffusion rate constant and I (mg/g) is the intercept of the intra-particle diffusion plot. Mainly, the sorption system is measured by intra particle model if this plot shows the linear profile passing through the origin. Conversely, the adsorption of OFL onto PJAC represented that intra particle diffusion plots did not move across the origin. Thus, it follows the multi-linearity mechanism of the adsorption process as shown in fig. 4.25 (b). The results rec-

ommended that the sorption process was governed by different steps such as intraparticle diffusion and boundary layer (Lee et al., 2016).

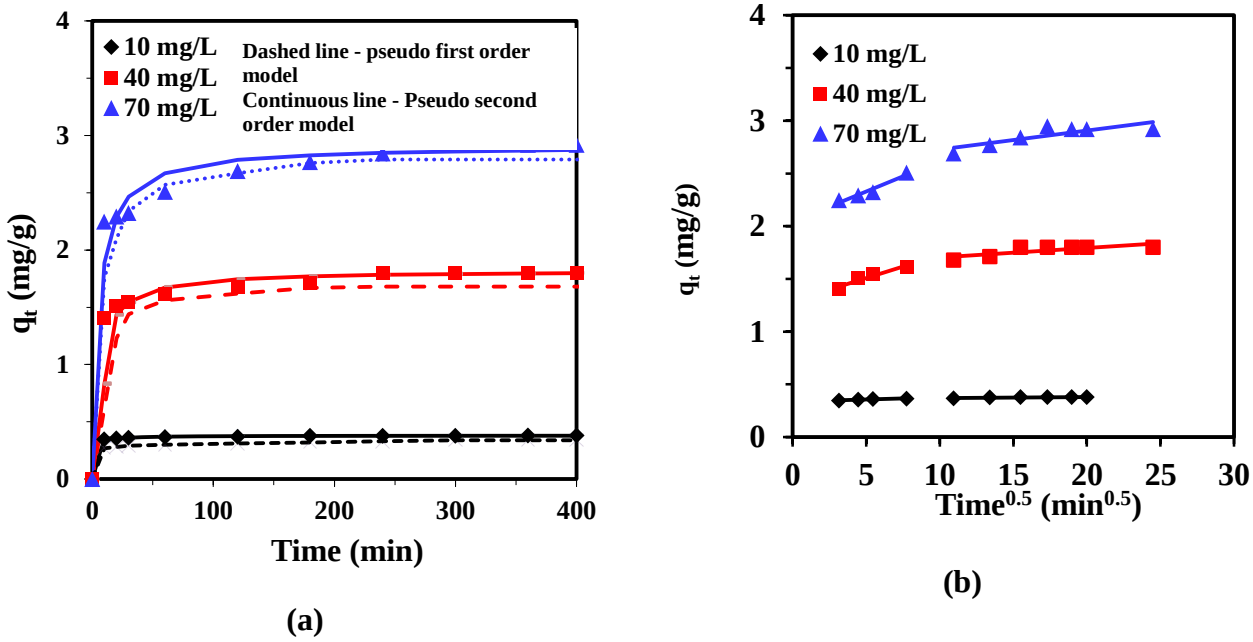

Fig. 4.25 (a) Kinetics of OFL adsorption on PJAC at optimized parameters (m = 16.23 g/L, t = 336 min and pH = 6) (b) Intraparticle diffusion model for the adsorptive removal of OFL by PJAC at optimized parameters (m = 16.23 g/L, t = 336 min and pH = 6).

Table 4.20. Kinetic parameters at different OFL concentrations under optimized parameters (m = 16.23 g/L, t = 336 min and pH = 6).

	C_0 (mg/L)		
	10	**40**	**70**
Pseudo first order			
k_f (min^{-1})	1.20	2.23	6.25
$q_{e,exp}$ (mg/g)	0.379	1.799	2.919
$q_{e,cal}$ (mg/g)	0.376	1.634	2.767
R^2 (non-linear)	0.986	0.972	0.970
MPSD	27.85	23.78	11.61
Pseudo second order			
k_s (g/mg/min)	1.656	0.101	0.062
h (mg/g/min)	0.239	0.338	0.536
$q_{e,cal}$ (mg/g)	0.380	1.822	2.912

R^2 (non-linear)	0.998	0.999	0.999
MPSD	1.97	6.77	4.23
Weber Morris			
k_{id1} (mg/g $min^{-1/2}$)	0.003	0.043	0.057
I_1	0.336	1.288	2.040
R^2	0.868	0.924	0.945
k_{id2} (mg/g $min^{-1/2}$)	0.001	0.009	0.018
I_2	0.358	1.611	2.547
R^2	0.691	0.617	0.694

4.20. Analysis of the adsorption Isotherms and Thermodynamics

Adsorption isotherms are utilized to investigate the dispersion of adsorbate (OFL) amid adsorbent and liquid phase at different temperatures. The equilibrium sorption investigations of OFL on PJAC were carried out at different temperatures (288 K - 318 K) under optimum experimental conditions with diverse original OFL concentrations at 10 to 100 mg/L. Langmuir, (Langmuir, 1918), Redlich and Peterson, (Redlich and Peterson, 1959) and Freundlich isotherm models (Freundlich, 1906) were utilized to evaluate the fitting of the experimental values as given in Eqs. (4.22) – (4.24), respectively.

Langmuir model:

$$q_e = \frac{q_m K_L C_e}{1 + K_L C_e} \qquad \textbf{(4.22)}$$

Redlich-Peterson model:

$$q_e = \frac{K_R C_e}{1 + a_R C_e^{\beta}} \qquad \textbf{(4.23)}$$

Freundlich model:

$$q_e = K_F C_e^{1/n} \qquad \textbf{(4.24)}$$

Where, q_e (mg/g) denotes to specific equilibrium mass of adsorbate, C_e (mg/L) is the equilibrium concentration of adsorbate, q_m (mg/g) is the maximum adsorption uptake. K_L, K_F, a_R, K_R are con-

stants, β represents to the exponent value of which lies in the range of zero to unity (L/mg), and n is the empirical constant. Under optimized conditions, the calculated experimental data were well suited into the Langmuir, Redlich and Peterson and Freundlich isotherm models.

Fig. 4.26 indicates that the non-linear fitting of experimental data with these isotherms and values of associated model variables are given in table 4.21. The magnitude of constants increasing with the rise in temperature, which defines the endothermic behavior of the sorption operation. It occurs due to the presence of C-O and hydroxyl functional groups and heterogeneity of the PJAC adsorbent.

Moreover, the magnitude of thermodynamic parameters analyzed the type of the sorption operation. Three thermodynamic variables, containing Free energy change (ΔG^o), enthalpy change (ΔH^o), entropy change (ΔS^o) were evaluated by employing equations given below:

$$\Delta G_o = -RT \ln K \qquad \textbf{(4.25)}$$

$$\ln K = \frac{\Delta S_0}{RT} - \frac{\Delta H_0}{R}\frac{1}{T} \qquad \textbf{(4.26)}$$

Here T denotes to temperature in Kelvin, *R* stands for universal gas constant (8.314×10^{-3} kJ/mol.K) and $K = (q_e/C_e)$

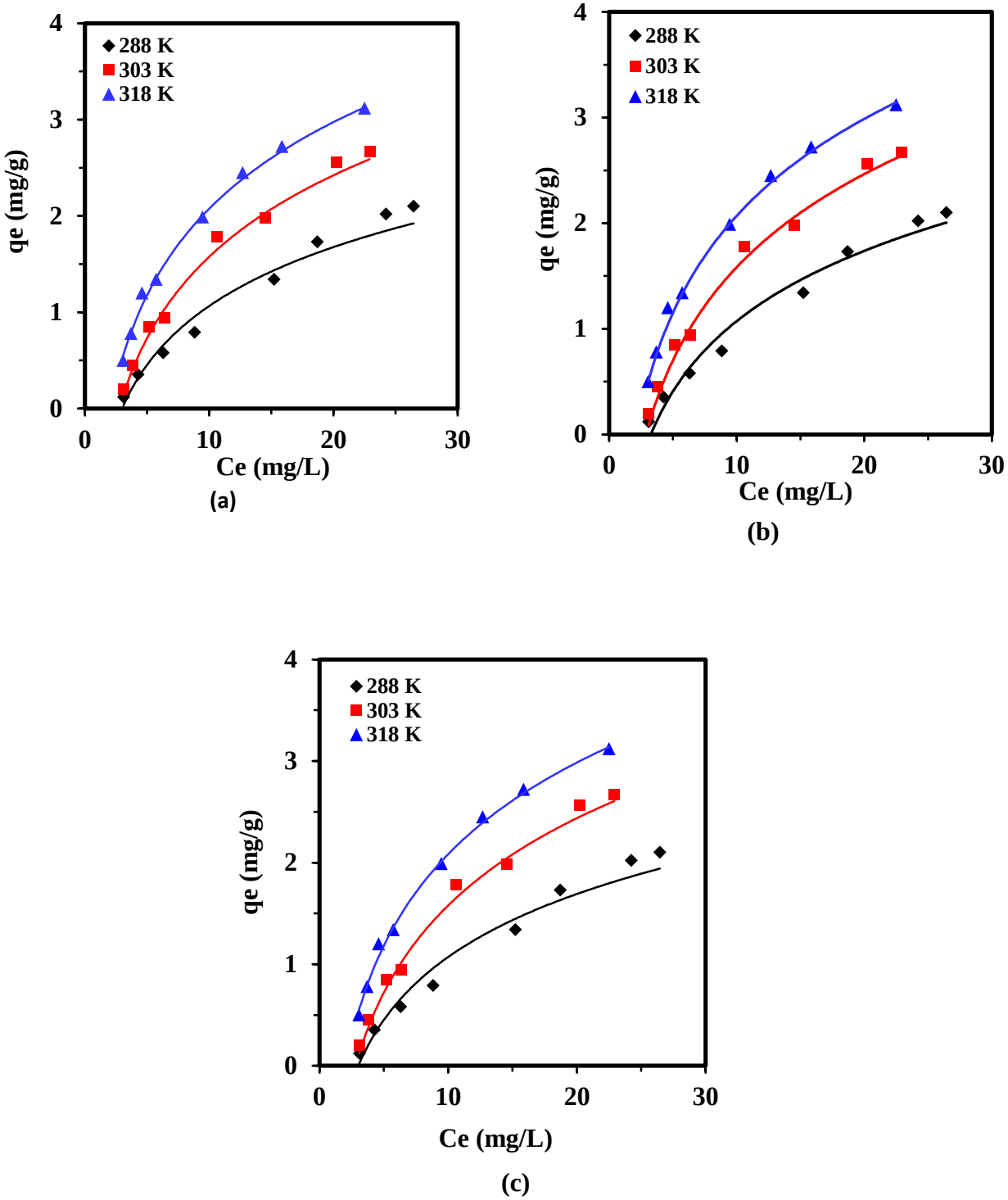

Fig. 4.26. Adsorption equilibrium isotherms at different temperatures for OFL onto PJAC through (a) Langmuir, (b) Freunlich and (c) R-P isotherm model (*m* = 16.23 g/L, *t* = 336 min and *pH* = 6).

Table 4.21. Isotherms studies for OFL adsorption on PJAC at optimized parameters (m = 16.23 g/L, t = 336 min and pH = 6).

ISOTHERMS					
Langmuir	$q_e = \frac{q_m K_L C_e}{1 + K_L C_e}$				
T (K)	**K_L (L/mg)**	**q_m (mg/g)**		**R^2**	**CHI^2**
288 K	2.407	4.982		0.991	0.089
303 K	7.162	12.721		0.992	0.098
318 K	9.188	14.262		0.993	0.064
Freundlich	$q_e = K_F C_e^{1/n}$				
T (K)	**K_F (mg/g) (L/mg)$^{1/n}$**	**1/n**		**R^2**	**CHI^2**
288 K	0.022	1.090		0.991	0.067
303 K	0.058	2.902		0.993	0.076
318 K	0.127	3.429		0.995	0.083
Redlich-Peterson	$q_e = \frac{K_R C_e}{1 + a_R C_e^{\beta}}$				
T (K)	**K_R (L/g)**	**a_R (L/mg)$^{1/\beta}$**	**β**	**R^2**	**CHI^2**
288 K	1.336	10.124	1.12	0.991	0.089
303 K	2.346	20.231	4.916	0.992	0.086
318 K	3.295	22.240	7.696	0.996	0.083

The negative values of ΔG^o at all studied temperatures (Table 4.22) attested that OFL adsorption on PJAC was spontaneous and endothermic by nature. Moreover, the values ΔG^o decreased from -12.27 to -19.72 (KJ/mol) with elevation in temperature and explained the feasibility of sorption operation. The +ve value of ΔH^o showed the endothermic nature. On the other hand, when the enthalpy values exist between 20.0 to 418.4 kJ/mol it resulted that the chemical reactions are the dominating factor in the adsorption process, whereas 20 kJ/mol value directed the physical reaction. Moreover, the positive value of ΔS^o expressed the haphazardness and affinity between the adsorbent and adsorbate.

Table 4.22. Thermodynamics parameters for the adsorption studies of OFL by PJAC (*m* = 16.23 g/L, *t* = 336 min, C_o = 5-70 mg/L and *pH* = 6).

Thermodynamic Parameters	$lnK_D = \frac{-\Delta G^0}{RT} = \frac{\Delta S^0}{R} - \frac{\Delta H^0}{R}\frac{1}{T}$			
T (K)	**K x 10^{-3} (L/kg)**	**ΔG^0 (kJ/mol)**	**ΔH^0 (kJ/mol)**	**ΔS^0 (J/mol)**
288 K	0.168	-12.278		
303 K	0.199	-13.341	58.277	242.211
318 K	1.734	-19.720		

4.21. Effect of solidification on capsulation of OFL and toxicity of leachate

As described in section 2.6, the leachability studies of antibiotic out of the stabilized adsorbent was done and the encapsulation % of OFL was evaluated. Outcome of study is illustrated in fig. 4.27 which shows that Portland cement positively fixed the antibiotic that was existing on exhausted PJAC. For 5:1 mass ratio of adsorbent to cement greater than 95 % encapsulation was obtained at all studied concentrations.

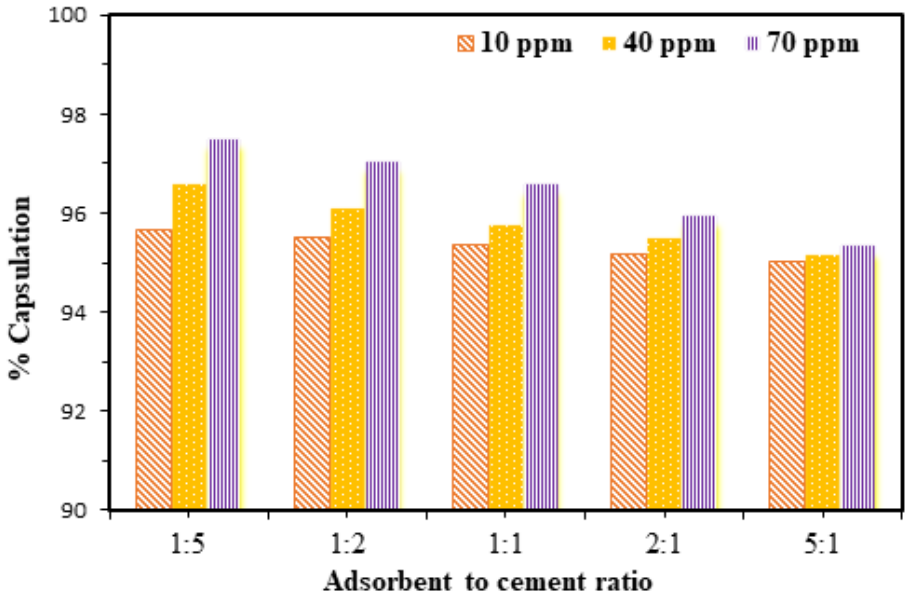

Fig. 4.27. % Capsulation of OFL in cement for different adsorbent to cement mass ratios.

Moreover, the cytotoxicity test was accomplished through agar well diffusion assay against both microbial strains *(Bacillus halodurans* (strain KG1) and *Escherichia coli* (strain K12)). For the toxicity assessment of leachate, difference in zones of inhibition between solutions of known OFL concentration and leachate (after adsorption and solidification) were observed. For this purpose, pure OFL solutions of different concentrations (0.025 to 0.1 ppm) were prepared. The observed zones of inhibition were like, for 0.1 ppm (27 mm and 25 mm), 0.05 ppm (24 mm and 20 mm) and 0.025 ppm (18 mm and 15 mm) in both cases for KG1 and K12 (Figure 4.28 (a & b). On the other hand, there were no zone of inhibition seen in case of leachate solutions. Consequently, it indicates that OFX leachate solution samples did not have any toxicity, as shown in figure 4.28 (c & d), because it didn't present any effect on the bacterial strains plates.

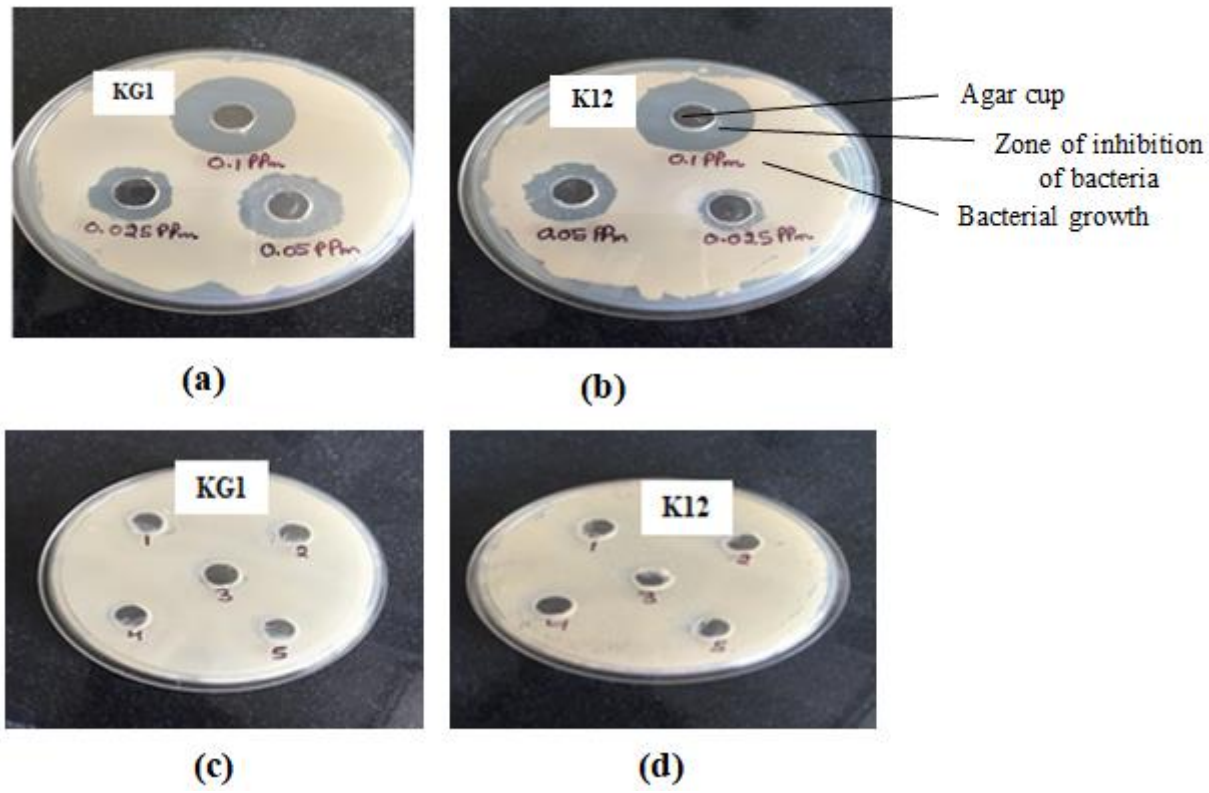

Fig. 4.28. Toxicity assessment by microbes *Bacillus halodurans* (strain KG1) and *Escherichia coli* (strain K12) (a, b) for OFL standard samples, (c, d) for leachates on *Bacillus halodurans* (strain KG1) and *Escherichia coli* (strain K12).

4.22. BATCH ADSORPTIVE REMOVAL OF WASTEWATER COMPRISING DOX BY PJAC

4.22.1. Adsorbent characterization

Micromeritics instrument and software (ASAP 2010) was used to determine the surface area and pore diameter. It was calculated by using nitrogen adsorption-desorption analysis at 77 K. Single point Brunauer-Emmett- Teller (BET) model was used to compute the surface area of PJAC and was found to be 320.49 m^2/g. Pore volume and pore diameter were found as 0.176 cc/g and 2.65 nm, respectively and was determined using BJH model.

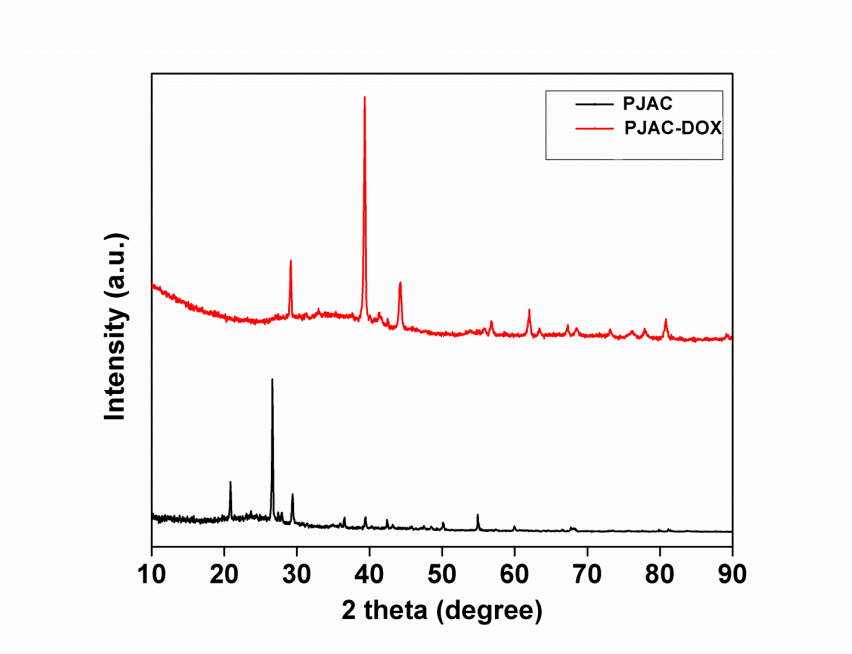

Fig. 4.29. X-ray diffraction (XRD) analysis before and after loading of DOX onto PJAC.

From the XRD diffraction patterns of PJAC (Fig 4.29), presence of Aragonite ($CaCO_3$), Silica (SiO_2), Akdalaite ($(Al_2O_3)_4.H_2O$) and Ca_3Mg (SiO_4) was revealed as the main components. The high and low intensity peaks were observed at 26.23° and 31.12° respectively, which explained the crystalline nature of PJAC due to existence of mainly cristobalite and SiO_2. On the other hand, a typically sharp peak at 2θ = 40.12° presented reformation of N-H functional group onto adsorbent surface reviewed the crystalline calcium-bearing phases in PJAC (Kumar and Tamilarasan, 2017). Additionally, some other narrow peaks also observed in PJAC belongs to SiO_2, cristobalite and CaO. In addition, $CaCO_3$ was also observed at angles 63.22° and 80.21° due to deformation of loaded DOX onto PJAC adsorbent. These were the deviations observed between PJAC and PJAC loaded with DOX (Demeyer et al., 2001).

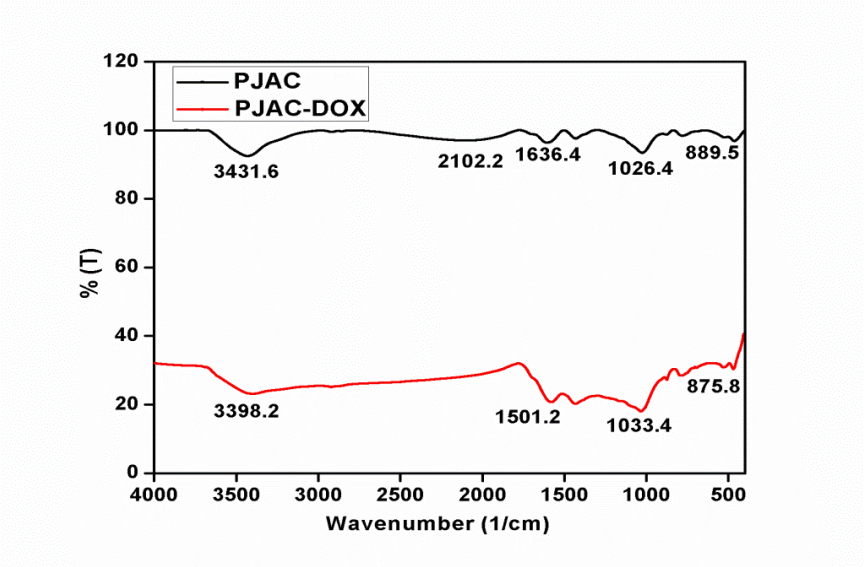

Fig. 4.30. FTIR spectra of PJAC and PJAC loaded with DOX.

FTIR spectra of PJAC and DOX loaded PJAC are presented in Fig. 4.30. The broad bands at the 3600-3100 cm^{-1} region and intensive peak visible at ~1636 cm^{-1} confirms the stretching of C=C group (Ye et al., 2016). A broad band was observed at nearly 2102 cm^{-1} in Prosopis juliflora which was deformed in DOX loaded PJAC sample, this can be assigned to –NH stretching. The bands from ~1505 to 1423 cm^{-1} indicate the presence of branched chain aromatic radicals having strong stretching of N-O nitro compound (Pistorius et al., 2009). In PJAC sample, the intensive band at ~1026 cm^{-1} is possibly representing the polysaccharides, i.e. it could be ascribed to C-O, C=C and C-C-O stretching in cellulose, hemicellulose and lignin (Kezerle et al., 2018). On other hand in DOX loaded PJAC, the shifting in peak in loaded sample at ~1033 cm^{-1} can be corresponded to Si–O–Si vibrations (Noroozifar et al., 2009). Moreover, some narrow peaks at ~700-750 cm^{-1} and ~790-895 cm^{-1} were also observed due to strong bending vibrations of C-H and C=C functional groups. Also, the stretching band at ~565 cm^{-1} can be attributed to the Si-O-Al bonds, and aluminosilicates existing in PJAC. As shown in Fig. 4.30, shifting in the peaks can be dedicated to adsorption of DOX antibiotic onto the PJAC surface.

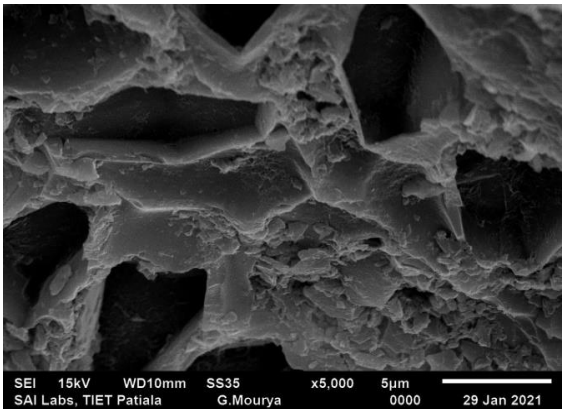

(a)

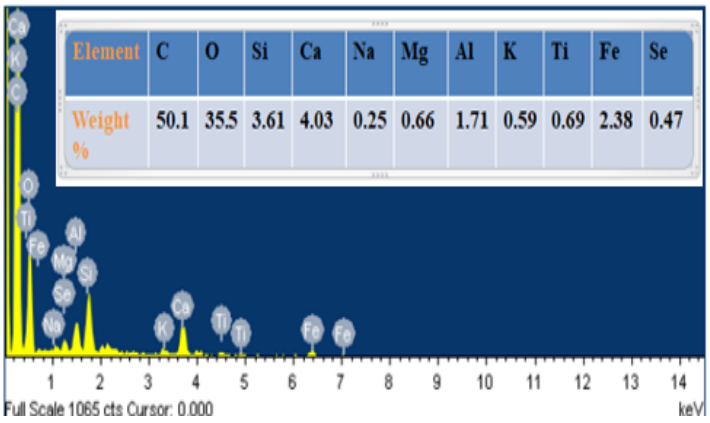

(b)

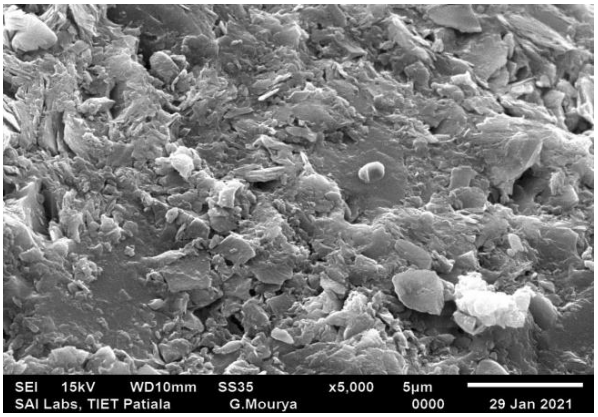

(c)

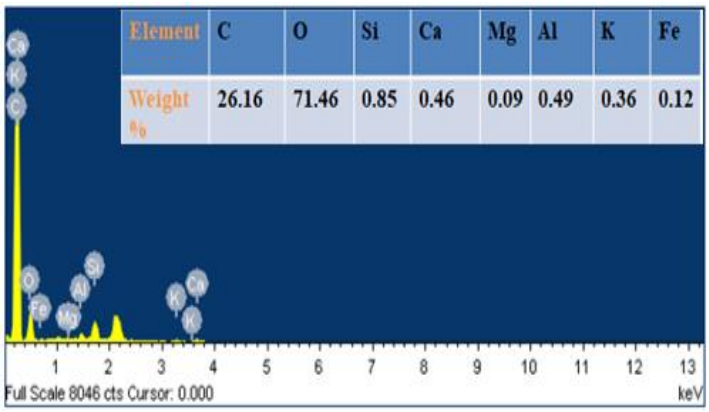

(d)

Fig. 4.31. SEM-EDX analysis of (a, b) PJAC and (c, d) PJAC loaded with DOX.

The morphological and elemental studies of PJAC and DOX loaded PJAC has been explored through scanning electron microscopy (SEM) and energy-dispersive X-Ray (EDX) analysis respectively and is shown in Fig. 4.31 The crystalline porous nature of the PJAC surface can be seen in Fig 4.31 (a). On the other hand, the DOX loaded PJAC surface confirms the deposition of adsorbate layer on the surface of PJAC, which is depicted in Fig. 4.31 (c). Meanwhile, EDX mapping observed is also presented in Fig 4.31 (b). The prominent difference in peaks of C, Ca and Si between PJAC and DOX loaded PJAC samples show the adsorption of DOX antibiotic onto active sites of PJAC surface (Fig. 4.31 (d)). Moreover, SEM analysis (Fig 4.31 (a, c)) proposes that the change in surface structure before and after sorption of DOX and the EDX results also confirm the feasibility of DOX sorption process (Fig. 4.31 (b, d).

4.23. Model validation and diagnostic analysis

The experiments were carried out and the results were statistically analysed by using RSM/CCD model. The investigations suggested as per CCD were 30 (8 axial points, 16 cube points and 6 replicates) with the values of responses X_1 and X_2. The program recommended use of quadratic model for all dependent parameters. The realistic association between DOX and PJAC for both responses X_1 and X_2, in sort of actual factors are stated by second – order polynomial quadratic relationship as given below:

$$X_1 = 94.71 + (0.04 * pH) - (0.24 * m) + (0.18 * C) + (2.63 * 10^{-4} * t) - (0.01 * pH^2) + (1.45 * 10^{-3} * m^2) - (1.68 * 10^{-3} * C^2) + (5.63 * 10^{-7} * t^2) + (4.11 * 10^{-3} * \text{pH} * \text{m}) + (2.11 * 10^{-3} * \text{pH} * \text{C}) - (5.45 * 10^{-5} * \text{pH} * \text{t}) + (1.84 * 10^{-3} * \text{m} * \text{C}) - (1.77 * 10^{-5} * \text{m} * \text{t}) - (3.16 * 10^{-6} * \text{C} * \text{t}) \quad \textbf{(4.27)}$$

$$X_2 = 5.15 + (0.12 * pH) - (0.79 * m) + (0.15 * C) + (9.43 * 10^{-4} * t) - (0.01 * pH^2) + (0.02 * m^2) - (1.16 * 10^{-4} * C^2) - (1.23 * 10^{-6} * t^2) + (3.69 * 10^{-4} * \text{pH} * \text{m}) + (3.46 * 10^{-5} * \text{pH} * \text{C}) - (5.39 * 10^{-7} * \text{pH} * \text{t}) + (5.01 * \text{m} * \text{C}) + (5.79 * 10^{-7} * \text{m} * \text{t}) - (3.09 * 10^{-7} * \text{C} * \text{t}) \quad \textbf{(4.28)}$$

ANOVA results predicted from second order quadric model of response surface shown in Table 4.23 were significant, as directed by the low possibility values (Prob > F < 0.0001). When the values of Prob > F is less than 0.05 it indicate that the model terms are significantly important. On the other hand, for DOX-PJAC, good closeness between R^2 and R^2_{adj} (Table 4.24), confirms a suitable correlation of the polynomial quadratic model to the experimental data. This means that the connection between the independent parameters and both responses are with great significance of the model. Further, to investigate the model adequacy, experimental data were plotted against predicted results for both the responses Fig 4.32 (a, b). Excellent correlations were observed and are listed in Table 25.

Table 4.23. ANOVA for the % DOX removal and capacity.

	% DOX removal (X_1)					Adsorption Capacity (X_2)				
Source	**Sum of Squares**	**DF**	**Mean Square**	**F Value**	**Prob > F**	**Sum of Squares**	**DF**	**Mean Square**	**F Value**	**Prob > F**
Model	51.33	14	3.67	40.63	< 0.0001	119.24	14	8.52	36.32	< 0.0001
A	0.25	1	0.25	2.73	0.1193	2.34×10^{-4}	1	2.34×10^{-4}	9.99×10^{-4}	0.9752
B	4.98	1	4.98	55.23	< 0.0001	53.43	1	53.43	227.84	< 0.0001
C	32.09	1	32.09	355.62	< 0.001	49.97	1	49.97	213.08	< 0.0001
D	3.02×10^{-3}	1	3.02×10^{-3}	0.033	0.8573	8.79×10^{-7}	1	8.79×10^{-7}	3.75×10^{-6}	0.9985
A^2	0.17	1	0.17	1.93	0.1849	0.057	1	0.057	0.24	0.6286
B^2	0.036	1	0.036	0.40	0.5346	10.62	1	10.62	45.30	< 0.0001
C^2	12.53	1	12.53	138.88	< 0.0001	0.059	1	0.059	0.25	0.6224
D^2	0.010	1	0.010	0.11	0.7412	0.049	1	0.049	0.21	0.6554
AB	0.027	1	0.027	0.30	0.5914	2.18×10^{-4}	1	2.18×10^{-4}	9.32×10^{-4}	0.9760
AC	0.11	1	0.11	1.26	0.2786	3.07×10^{-5}	1	3.07×10^{-5}	1.31×10^{-4}	0.9910
AD	6.52×10^{-3}	1	6.52×10^{-3}	0.072	0.7917	6.37×10^{-7}	1	6.37×10^{-7}	2.71×10^{-6}	0.9987
BC	0.54	1	0.54	6.01	0.0269	4.03	1	4.03	17.17	0.0009
BD	4.32×10^{-3}	1	4.32×10^{-3}	0.048	0.8297	4.59×10^{-6}	1	4.59×10^{-6}	1.95×10^{-5}	0.9965
CD	2.19×10^{-3}	1	2.19×10^{-3}	0.024	0.8783	2.09×10^{-5}	1	2.09×10^{-5}	8.94×10^{-5}	0.9926
Residual	1.35	15	0.090			3.52	15	0.23		
Lack of Fit	1.35	10	0.13	173.50	< 0.0001	3.52	10	0.35	4.65×10^{-5}	< 0.0001
Pure Error	3.89×10^{-3}	5	7.78×10^{-4}			3.77×10^{-6}	5	7.55×10^{-7}		
Cor Total	52.69	29				122.76	29			

A: pH, B: dose of PJAC (m, g/L), C: DOX conc. (C_0, mg/L), D: Time (t, min)

Table 4.24. Various R-squared values suggested by CCD for different responses.

Responses	R-Squared	Adj R-Squared	Pred R-Squared
% DOX removal (X_1)	0.97	0.95	0.85
Adsorption Capacity (X_2)	0.97	0.94	0.83

Table 4.25. Experimental and predicted responses values comparison at optimized condition (*m* = 5 g/L, *t* = 120 min and *pH* = 6, DOX concentration = 63 mg/L).

Responses	Predicted value	Experimental value
% removal (X_1)	99.55 %	99.10 %

Capacity (X_2)	10.12	12.44

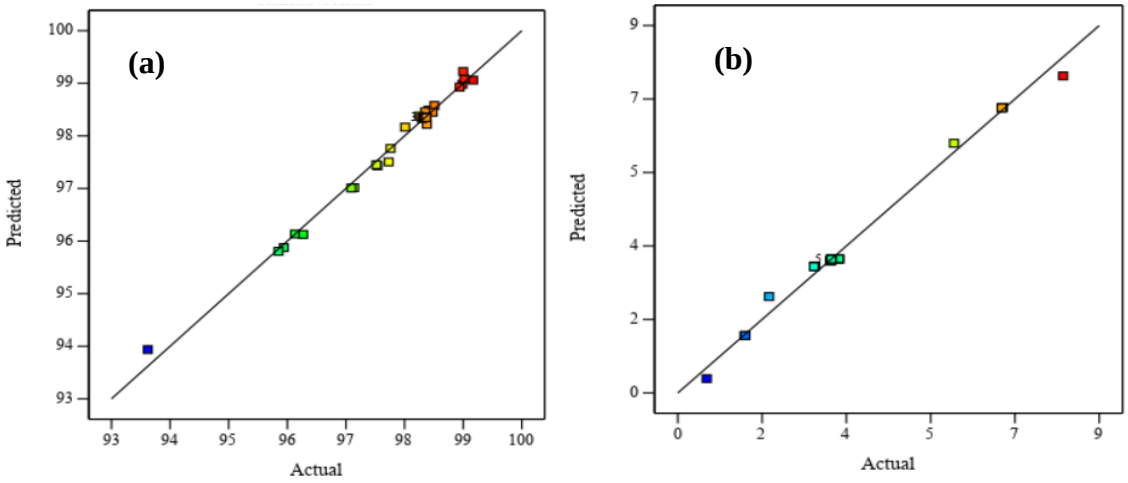

Fig. 4.32. The actual data versus predicted data for (a) removal (%), (b) capacity (mg/g) of DOX.

4.24. Effect of various parameters and optimization

To explore the effects of various adsorption parameters and their interactions on both responses, removal % (X_1) and capacity (X_2), three dimensional (3-D) response surface plots was drawn. The Values of X_1 and X_2 responses with different parameters *i.e.* pH, C (mg/L), dose (g/L) and time (t) are shown in Table 4.26. The experimental results showed the good agreement with the predicted data. Different constraints were applied for the optimization of process parameters are stated in Table 4.27. The 3D graphs obtained were additionally investigated to understand the individual and interactive influence of these parameters on both the responses.

Table 4.26. Range of Variables and Levels of the Design Model.

Factors	Variables	Range of actual and coded variables				
		(-2)	**(-1)**	**(0)**	**(+1)**	**(+2)**
A	pH	2	4	6	8	10
B	Dose of PJAC (g/L)	5	10	15	20	25
C	DOX conc. (mg/L)	10	30	50	70	90
D	Time (min)	10	195	380	565	750

Table 4.27. Optimization Constraints applied.

Variables	Goal	Lower Limit	Upper Limit
pH	is in range	4	8
Dose of PJAC	minimum	10	20
DOX concen-tration	is in range	30	70
Time	minimum	10	565
% removal	maximum	92.61	99.17
Capacity	maximum	0.62	9.92

Fig. 4.33 (a-f) represents the interactive effect of *pH*, *m* (g/L) and *C* (mg/L) on the DOX uptake percentage (X_1) and PJAC capacity (X_2). The coetaneous influence of PJAC dose and DOX concentration on the responses, % DOX uptake and capacity are depicted in Fig. 4.33 a and d, respectively, at constant pH and *t* value. At any PJAC dose, DOX uptake increases with increase in *C* value, but at lower PJAC dose it attains a constant value at nearly 70 mg/L concentration. On the other hand, at high dose, % DOX removal continuously increases with increase in *C* value due to the availability of more adsorption sites. So the adsorption of DOX on PJAC surface can be observed as adsorbate limiting. Conversely, at low PJAC dose, capacity boosts sharply with enhancement in DOX concentration, but at higher dosage this increment was not substantial.

Fig. 4.33 b and e describes the interaction between *pH* and DOX concentration on the % DOX uptake and capacity, respectively. It shows that, at any pH, % DOX uptake increased drastically with an increase in DOX concentration till > 98%. Whereas, at higher concentrations, DOX uptake decreases further. This behavior signifies that the adsorption of DOX is restricted with the DOX amount in solution, and also that PJAC own high adsorption capacity. However, the adsorption capacity was observed rising continuously at each and every *pH* with enhancement in DOX concentration. On the other hand, there is no significant change in capacity with pH change at any C value.

Fig 4.33 (c) and (f) represents the simultaneous effect of the pH and PJAC dose on % DOX uptake and adsorbent capacity. As it is evident from the figure 4.33 (c), at any PJAC dosage, DOX removal increases with increase in solution pH and then declines as solution pH goes beyond 6. Moreover, DOX removal capacity decreases with enhancement in PJAC dosage (Fig 4.33 (f)). DOX adsorp-

tion on PJAC was optimized for maximizing both the responses (percentage removal (X_1) and capacity (X_2)) by the RSM/CCD model. The optimum suggested conditions were found to be *m* = 5 g/L, t = 120 min and pH = 6, showing results X_1 = 99.10% and X_2= 12.44 mg/g respectively. These experiments demonstrate that both results were in good agreement as shown in Table 4.25.

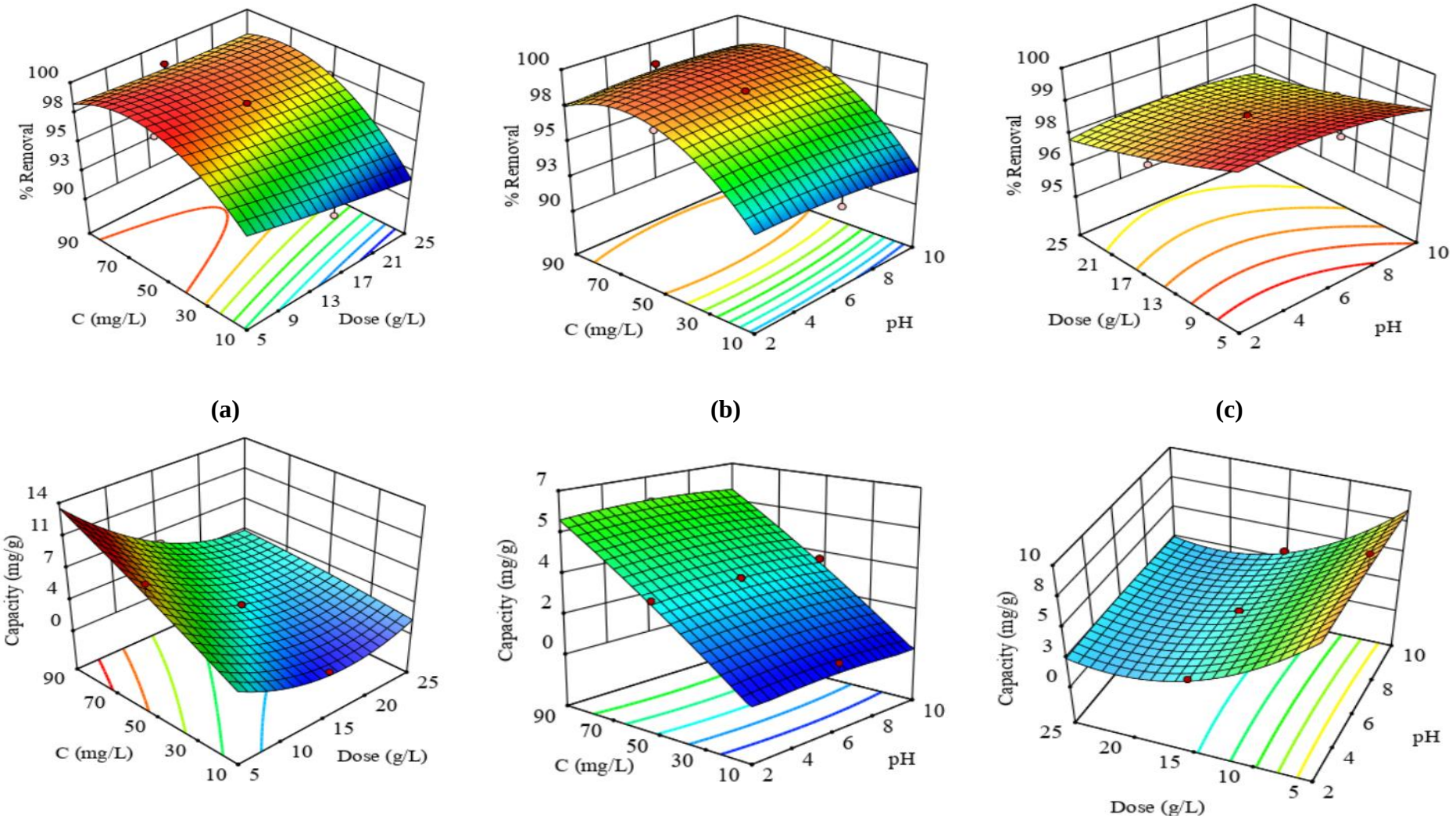

Fig. 4.33. The 3D response surface graph for the % removal of DOX (a, b, c) and capacity (d, e, f) from aqueous solutions.

4.25. Mechanism for adsorption of DOX on PJAC

For elucidating such behaviour of the DOX adsorption on PJAC, solution pH and pH_{ZPC} of PJAC might be very useful. The point of zero charge (pHpzc) of PJAC was found 8.5 (Fig 4.34). Different functional groups such as O-H, C-O, C=C, C-N, C-C present on PJAC surface played important role in the adsorption of DOX. Nearly below 8.5 pH most of the functional groups are protonated and attains +ve charge. Moreover, DOX represents three pKa values (pK_{a1} = 3.5, pK_{a2} = 7.7, pK_{a3} = 9.5) (Gao et al., 2012). DOX has three different ionic forms, it is in protonated form (DOX^{+}) below pH value 3.5, in deprotonated form (DOX^{-}) above 9.5 and in non-ionized form (DOX^{o}) between 7.7 to 9.5 pH. In this study, the maximum removal was obtained at pH 6. As shown in Fig 4.34, when the solution pH goes beyond 2, the DOX removal % increases, it reaches at a maximum at 6 pH and declines further with increase in solution pH. At acidic pH, both DOX as well as PJAC are positively charged and there is no scope of electrostatic interaction between substrate and adsorbent. But at the same time, in the acidic to neutral pH range, cationic (DOX^{+}) as well as zwitterionic (DOX^{o}) forms of doxycycline are л electron acceptors (Ji et al., 2009). These influential л electron acceptors causes л - л EDA interactions with the PJAC. Beyond 8.5 pH when PJAC becomes deprotonated, the electrostatic interaction may cause but in very small pH range. At higher pH, the electrostatic repulsion among DOX^{-} and deprotonated functional groups of PJAC expresses the decrease in DOX uptake. Moreover, hydrogen bonding between aromatic rings in the DOX molecule and hydroxyl group on PJAC surface plays an important role in enhancing the adsorption performance. This adsorption behaviour demonstrates that DOX uptake on PJAC was mainly governed by л - л EDA interactions and hydrogen bonding.

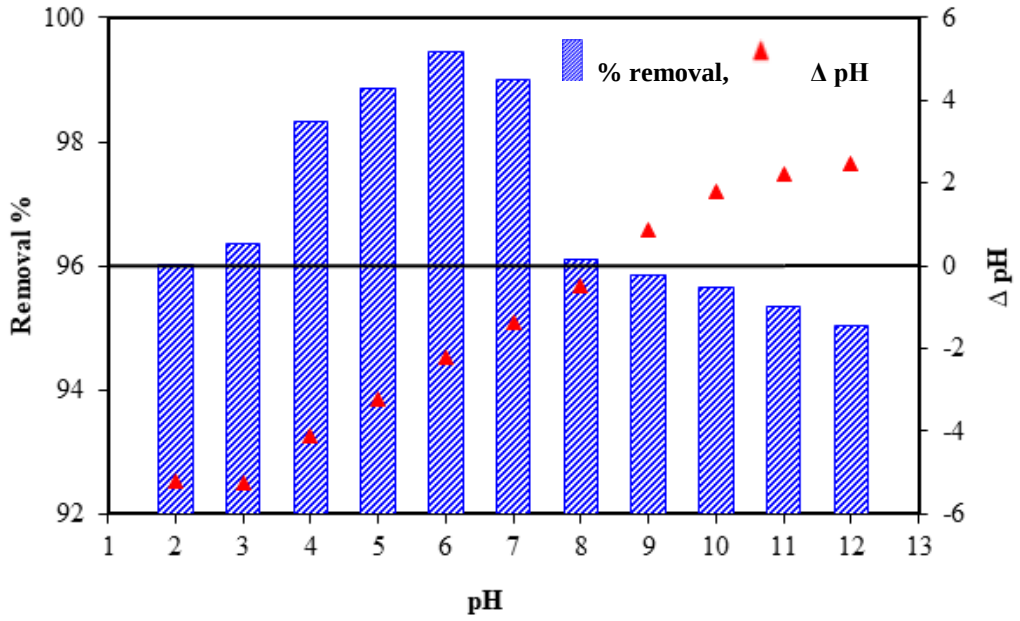

Fig. 4.34. Effect of the solution pH on adsorption efficiency of DOX by PJAC and zeta potentials of DOX, PJAC at different pH, C_0 (DOX) = 63 mg/L, t = 120 min, T = 303 K.

4.26. Sorption Kinetics representation

It is important to evaluate the adsorption kinetics as it can predict the adsorption rate and also can explicate the mechanisms involved in DOX-PJAC adsorption. The adsorption time profile of DOX over PJAC was obtained experimentally at three different initial concentrations (*Co*) 40, 70 and 100 mg/L under optimized conditions. The experimental data was fitted with Pseudo first order and Pseudo second order kinetic models using nonlinear regression model and are given below.

Pseudo 1st order model is represented as (Malik, 2003):

$$q_t = q_e\left[1-\exp\left(-k_f t\right)\right] \qquad \textbf{(4.29)}$$

Where q_t and q_e are the amounts of DOX antibiotic (mg/g) at any instant time (*t*) and equilibrium point, respectively, and k_f is the Pseudo 1st order reaction rate constant (per min).

Pseudo 2nd order model can be represented as (Ho and McKay, 1999):

$$q_t = \frac{tk_S q_e^2}{1+tk_S q_e} \qquad \textbf{(4.30)}$$

Where, k_s is the Pseudo 2nd order reaction rate constant (g/mg/min).

The initial adsorption rate, h (g/mg/min), is defined as;

$$h = k_s q_e^2 \qquad \textbf{(4.31)}$$

During the kinetic studies, the adsorption time profile of DOX (adsorption capacity vs time) indicated that equilibrium was attained in 30 min. As shown in fig. 4.35 (a), the kinetic behavior of DOX-PJAC was better described by pseudo – second order model with R^2 ~1 as compared to pseudo 1st order kinetic model. Also, MPSD value for pseudo – second order model fitting was found lower as compared to 1st order kinetic model for all studied concentrations. The evaluated kinetic constraints are listed in Table 4.28 and the experimental data fitting is shown in Fig. 4.35. It is observed that the values of q_e and K_s increases with increase in C_o. Therefore, the adsorption is limited by the original concentration of DOX. The initial adsorption rate h (g/mg/min) was also found rising with increasing in C_o value. This is the further provision of inference that the adsorption is limited by the C_o of DOX in aqueous solution.

For the investigation of diffusion mechanism and the rate governing steps in the course of DOX adsorption on PJAC, the intra-particle diffusion (IPD) model was used. The IPD model equation can be given as following (Weber and Morris, 1963):

$$q_t = k_{id} t^{0.5} + I \qquad \textbf{(4.32)}$$

Where k_{id} and I are constants of intra-particle diffusion model (mg/g min$^{1/2}$) and the boundary layer thickness of an adsorbent. Higher the intercept, greater will be the boundary layer thickness. By the Weber–Morris model for IPD, when the linear plot of q_t vs $t^{0.5}$ passes through origin while joining all the data points, it approves that internal diffusion is the sole rate-controlling step.

The Weber and Morris IPD plot (q_t and $t^{0.5}$) shown in Fig. 4.35 (b), indicates that dispersal pattern of the DOX onto PJAC surface is governed by various steps as it shows two-step linearity and doesn't pass through origin. In first linear segment rate of adsorption enhanced due to presence of vacant porous spaces onto external surface of the PJAC and then achieved the equilibrium due to lower DOX concentrations left behind. In this way, there are two linear curves where first one describes the mesoporous diffusion and the second demonstrating the microspores diffusion of the adsorbent.

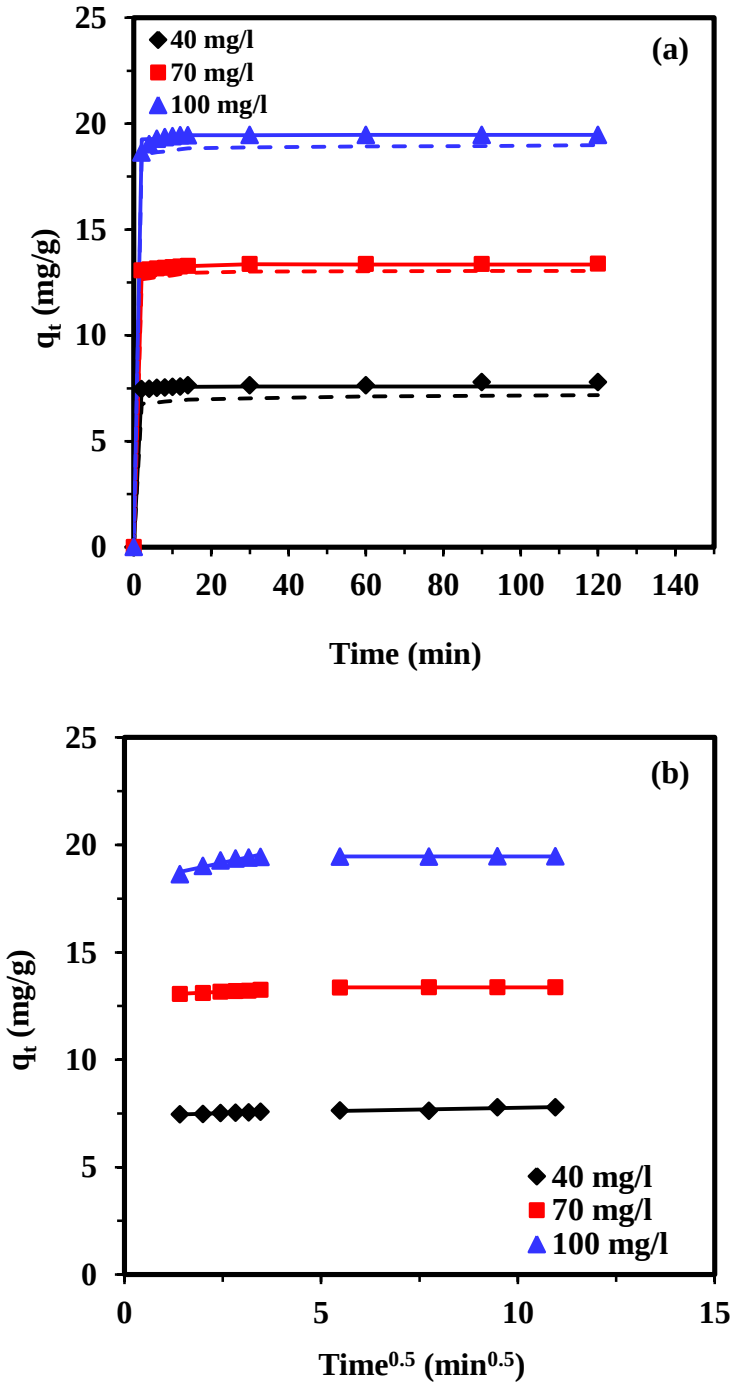

Fig. 4.35. (a) Kinetics of DOX adsorption on PJAC at optimized parameters (*m* = 5 g/L, *t* = 120 min and *pH* = 6) (b) Weber–Morris plot for the adsorptive treatment of DOX by PJAC at optimized parameters (*m* = 5 g/L, *t* = 120 min and *pH* = 6).

Table 4.28. Kinetic parameters for Doxycycline hydrochloride (DOX) adsorption on Prosopis juliflora at optimized parameters (*m* = 5 g/L, *t* = 120 min and *pH* = 6).

	C_0 (mg/L)		
	40	**70**	**100**
Pseuso first order			
k_f (min^{-1})	0.489	4.46	6.85
$q_{e,exp}$ (mg/g)	7.795	13.348	19.415
$q_{e,cal}$ (mg/g)	7.573	13.253	19.41
R^2 (non-linear)	0.999	0.999	0.999
MPSD	29.85	9.664	10.547
Pseuso second order			
k_s (g/mg/min)	7.936	10.23	17.289
h (mg/g/min)	456.422	1800.149	6430.146
$q_{e,cal}$ (mg/g)	7.583	13.26	19.285
R^2 (non-linear)	1	0.999	0.999
MPSD	3.75	0.217	2.189
Weber Morris			
k_{id1} (mg/g $min^{-1/2}$)	0.057	0.0893	0.390
I_1	7.373	12.939	18.194
R^2	0.977	0.992	0.907
k_{id2} (mg/g $min^{-1/2}$)	0.0349	0.002	0.001
I_2	7.421	13.352	19.449
R^2	0.775	0.976	0.991

4.27. Equlibrium isotherms and Thermodynamics

The adsorption isotherms were used to find out the distribution of adsobate (DOX) onto the suface of PJAC with varying temperatures. The equilibrium adsorption experiments were executed at distinct temperatures (288 K, 303 K and 318 K) at optimum conditions and different original DOX concentrations. Freundlich (Freundlich, 1906), Redlich - Peterson (R-P) (Redlich and Peterson, 1959), Langmuir (Langmuir, 1918) and Temkin (Temkin, 1940) isotherms given in Eq. 4.33 to 4.36 respectively, were examined to access the experimental data.

Langmuir isotherm model:

$$q_e = \frac{q_m K_L C_e}{1 + K_L C_e} \quad \textbf{(4.33)}$$

Redlich-Peterson isotherm model:

$$q_e = \frac{K_R C_e}{1 + a_R C_e^{\beta}} \quad \textbf{(4.34)}$$

Freundlich isotherm model:

$$q_e = K_F C_e^{1/n} \quad \textbf{(4.35)}$$

Temkin isotherm model:

$$q_e = \left(\frac{RT}{B_T}\right) ln(K_t C_e) \quad \textbf{(4.36)}$$

Where, q_e (mg/g) is the specific equilibrium amount of adsorbate, Ce (mg/L) is the equilibrium concentration of adsorbate, q_m (mg/g) is maximum sorption capability, K_L, K_F, a_R, K_R are constants, β is the exponent which lies between 0 and 1 (L/mg) and n is the empirical constant. Higher 1/n value indicates, the higher affinity between adsorbent – adsorbate and vice versa. B_T is the variation of adsorption energy (J/mol); k_T is the equilibrium binding constant (L/g) corresponding to the maximum binding energy and R is the universal gas constant (8.314 J/mol-K).

Non-linear fitting of these isotherms with the experimental data are shown in fig. 4.36. The evaluated isotherm parameters, R^2 and CHI^2 error values for different isotherm models are listed in Table 4.29. It is evident from fig. 4.36 that, as the temperature increases, DOX uptake also enhances, this behavior demonstrates that adsorption of DOX on PJAC is of endothermic nature. Out of all the used isotherm models, Langmuir, Freundlich and R-P isotherms fitted better with the experimental data as compared to Tempkin.

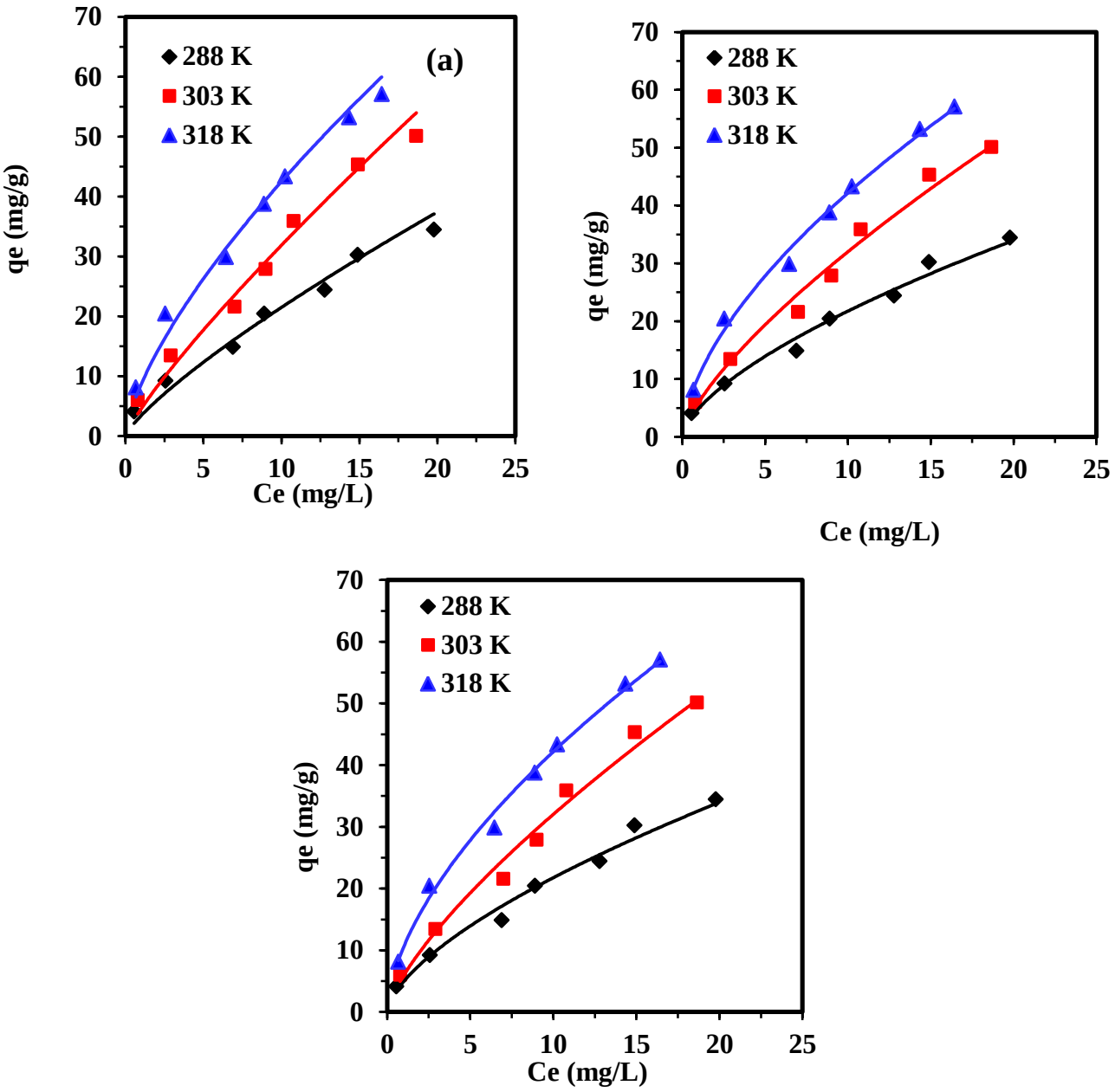

Fig. 4.36. Adsorption equilibrium nonlinear fitted isotherms at different temperatures for DOX onto PJAC (a) Langmuir, (b) Freundlich and (c) RP isotherm model (*m* = 5 g/L, *t* = 120 min and *pH* = 6).

Table 4.29. Isotherms and Thermodynamics parameters for DOX adsorption on Prosopis juliflora at optimized parameters (*m* = 5 g/L, *t* = 120 min and *pH* = 6).

ISOTHERMS

Langmuir $$q_e = \frac{q_m K_L C_e}{1 + K_L C_e}$$

T (K)	K_L (L/mg)	q_m (mg/g)	R^2	CHI^2
288 K	0.059	60.789	0.985	2.137
303 K	0.038	118.81	0.990	2.230
318 K	0.115	81.587	0.984	2.147

Freundlich $$q_e = K_F C_e^{1/n}$$

T (K)	K_F (mg/g) $(L/mg)^{1/n}$	1/n	R^2	CHI^2
288 K	4.951	0.643	0.992	0.679
303 K	6.048	0.724	0.992	0.998
318 K	10.601	0.600	0.997	0.429

Redlich-Peterson $$q_e = \frac{K_R C_e}{1 + a_R C_e^{\beta}}$$

T (K)	K_R (L/g)	a_R $(L/mg)^{1/\beta}$	β	R^2	CHI^2
288 K	8.414	2.610	0.056	0.993	4.683
303 K	29.523	3.980	0.314	0.992	1.067
318 K	40.186	2.859	0.470	0.996	0.488

Temkin $$q_e = \left(\frac{RT}{B_T}\right) ln(K_t C_e)$$

T (K)	K_T(L/mg)	B_T (J/mol)	R^2	CHI^2
288 K	2.753	6.643	0.925	6.292
303 K	1.857	11.042	0.925	9.321
318 K	2.483	13.154	0.960	4.447

Thermodynamic Parameters $$lnK_D = \frac{-\Delta G^0}{RT} = \frac{\Delta S^0}{R} - \frac{\Delta H^0}{R}\frac{1}{T}$$

T (K)	K x 10^{-3} (L/kg)	ΔG^0 (kJ/mol)	ΔH^0 (kJ/mol)	ΔS^0 (J/mol)
288 K	2.405	-18.642	30.167	170.080
303 K	5.620	-21.751		
318 K	7.835	-23.706		

To evaluate the change in energy during the DOX-PJAC adsorption and identify the feasibility of process, thermodynamic study was performed. Different thermodynamic adsorption parameters like enthalpy change (ΔH^o), entropy change (ΔS^o) and free energy change (ΔG^o) were estimated as they provide the information about nature and type of adsorption process. These were estimated with the help of equilibrium adsorption constant (K) using following equations:

$$\Delta G_o = -RT \ln K \qquad \textbf{(4.37)}$$

$$\ln K = \frac{\Delta S_0}{RT} - \frac{\Delta H_0}{R}\frac{1}{T} \qquad \textbf{(4.38)}$$

Where, T is the absolute temperature (K), R is the universal gas constant (8.314×10^{-3} kJ/mol.K) and K ($=q_e/C_e$)

The values of evaluated thermodynamic parameters at different temperatures (288-318 K) are listed in Table 4.30. Positive values of ΔH^o and ΔS^o shows the endothermic nature and favorable DOX adsorption on PJAC. Moreover, negative value of ΔG^o in –ve confirms the spontaneity and feasibility of process.

4.28. Identification of solidification/stabilisation technique and cytotoxicity

For the proper disposal and management of DOX loaded PJAC, it was solidified using the method explained earlier (Kaur et al., 2021a). To study the leachability of DOX from stabilised adsorbent, leachate sample was tested for the DOX concentration using spectrophotometer and encapsulation percentage was calculated using eq. 5. As it is evident from Fig 4.37, Portland cement could successfully stabilize the DOX present in the exhausted PJAC. Even at the highest DOX to cement ratio (5:1) ≈ 99% DOX was encapsulated for all three studied adsorbent concentrations.

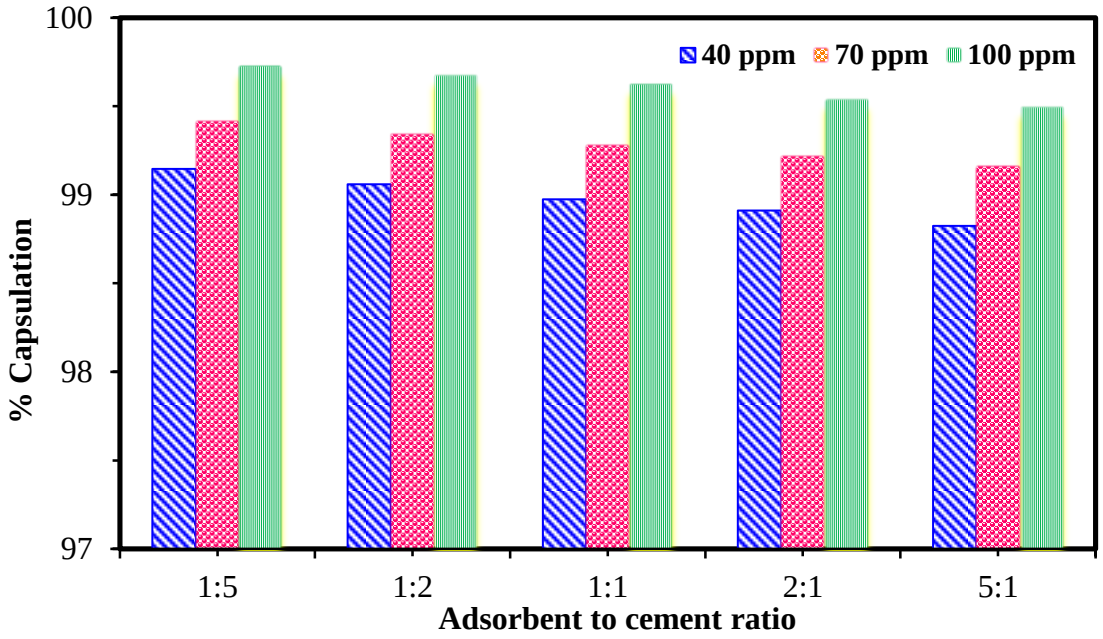

Fig. 4.37. DOX % Capsulation in cement for different adsorbent to cement mass ratios.

Further, to ensure the safe disposal of stabilized PJAC, cytotoxicity test of leachate was performed by using microbial species Escherichia coli (strain K12) and Bacillus halodurans (strain KG1) on MHA media. The zone of inhibition of leachate sample and synthetically prepared DOX solution of known concentrations (0.015 ppm and 0.5 ppm) were determined and compared. The comparative zone of inhibition for leachate and DOX solution are shown in Fig. 4.38. As seen in Fig.4.38 (a, b), for 0.5 ppm DOX solution higher zones were observed (28 mm, 26 mm) and for 0.015 ppm (12 mm, 10 mm) for Escherichia coli and Bacillus halodurans respectively. For the leachate samples no inhibition zone was observed (Fig. 4.38 c, d) in case of both the strains. From this study it can be concluded that Portland cement could successfully encapsulate DOX loaded PJAC can be a better approach to fix the exhausted/loaded DOX-PJAC.

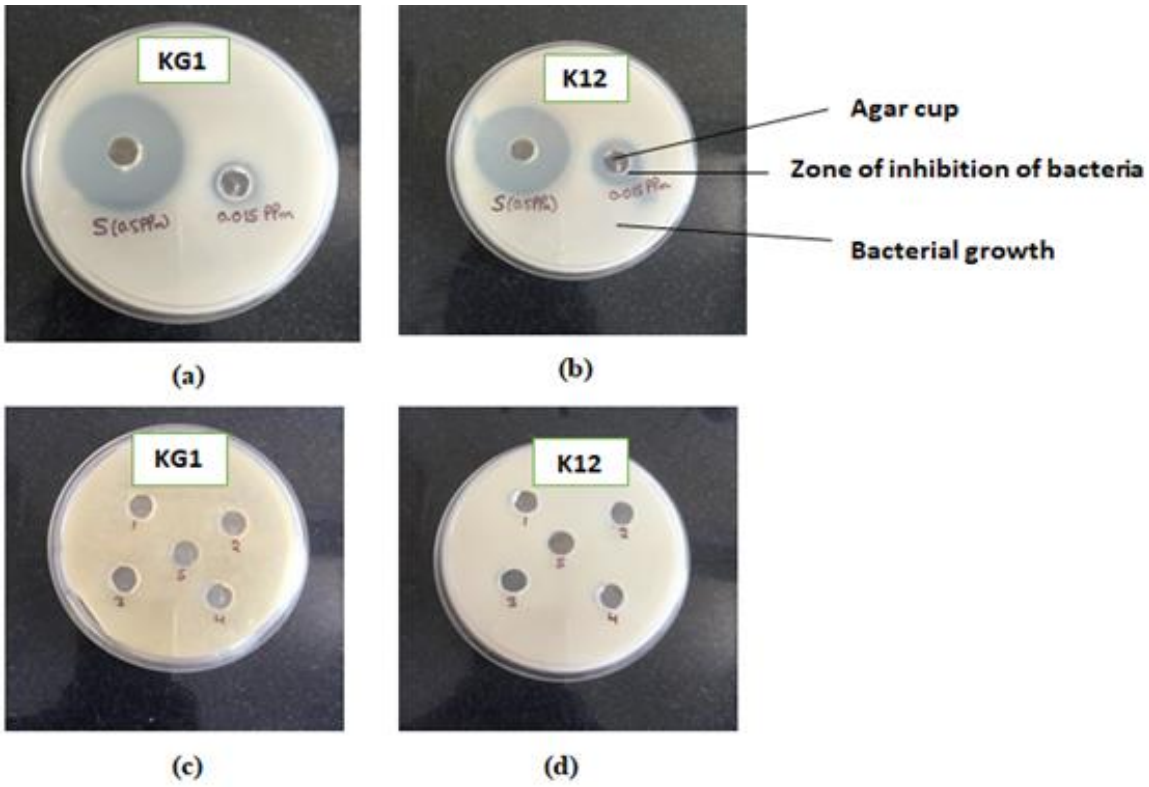

Fig. 4.38. Toxicity assessment by microbes *Bacillus halodurans* (strain KG1) and *Escherichia coli* (strain K12) (a, b) for DOX standard samples, (c, d) for leachates on Bacillus halodurans (strain KG1) and Escherichia coli (strain K12).

4.29. BATCH ADSORPTIVE REMOVAL OF WASTEWATER COMPRISING DOX BY PSSAC

4.29.1. Microwave-assisted pyrolyzed PSSAC characterization

4.29.1.1. Surface chemistry analysis (FTIR)

FT–IR spectral data of PSSAC and DOX adsorbed PSSAC is represented in Fig. 4.39. Because of the existence of functional groups (hydroxyl, sulphonate, phosphate, amino, carboxyl and sulphydryl) on PSSAC surface, it serves as binding spots for the doxycycline hydrochloride molecules. FTIR spectra of PSSAC represents peak at 3024 cm^{-1}, that is attributed to the existence of free and hydrogen-bonded OH groups, peaks visible at 2923 cm^{-1} are credited to the stretching of the methyl group ($-CH_3$). The bands at 1740 cm^{-1} and 1215 cm^{-1} correspond to the stretching frequency of −C=O and −C–N groups. One other sharp band seen at 483 cm^{-1} represents the presence of alkyl and alkynes halides bending vibrations. Moreover, few intense peaks perceived at 2923, 1740, 1215 and 483 cm^{-1} primarily plays the role in the adsorptive uptake (Yuan et al., 2009; Kumar and Randhawa, 2015). In loaded PSSAC spectra, the appearance of an additional peak at 3430 cm^{-1} corresponded to O–H stretching vibrations of H-bonded hydroxyl groups on DOX. Peaks in the regions 2918 cm^{-1} and 1621 cm^{-1} could correlate with the stretching in -NH_2 groups and the presence of C=C stretching vibrations in the aromatic region of DOX (Kumar et al., 2010; Liew et al., 2018). The band near 1167 cm^{-1} corresponds to the strong stretching of the C-O group. Furthermore, the prominent new broadband that emerged at 567 cm^{-1} can be entrusted to the Si-O-Al stretching vibrations and aluminosilicates existing on the adsorbent surface. This band was observed after adsorption, and it is assigned to DOX adsorption on the PSSAC. This indicates that DOX adsorption has successfully been performed.

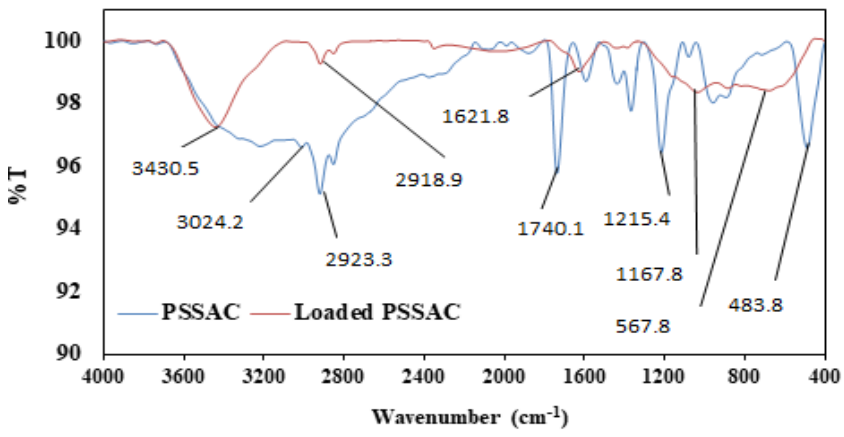

Fig. 4.39. FT -IR spectra of PSSAC and loaded PSSAC.

4.29.1.2. XRD analysis

XRD patterns of bare PSSAC and DOX adsorbed PSSAC were determined employing X-ray diffraction (XRD) with the intensity of diffracted X-ray plotted against 2θ angle and is depicted in Fig. 4.40. The diffraction patterns of PSSAC and loaded PSSAC both represented strong, broad peaks between 20^o to 30^o (2θ), which correspond to the presence of quartz, Kaolinite and illite. Moreover, the presence of aluminophosphates and smectite was developed because of the existence of SiO_2, TiO_2, K_2O, Fe_2O_3, and CaO_2 elements on the adsorbent surface (Treacy et al., 2007). It represents the mesoporous and amorphous nature of the adsorbent. There is not any great difference between the PSSAC and loaded PSSAC samples. A weak peak is seen at 80^o (2θ) in the loaded sample that determines the existence of interactions between the DOX and PSSAC through C=O and -OH functional groups.

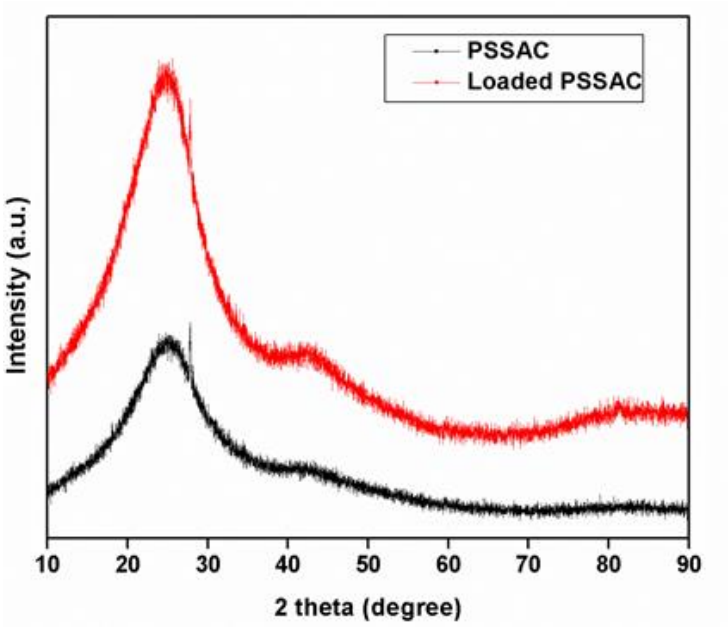

Fig. 4.40. X-ray diffraction (XRD) analysis of PSSAC and loaded PSSAC.

4.29.1.3. BET surface area and FESEM

The N_2 adsorption-desorption measurements for PSSAC was determined at 77 K. In this regard, Brunauere Emmette Teller (BET) surface area of adsorbent was estimated to be 967.89 m^2/g, and it belongs to type IV isotherm as shown in Fig. 4.41. Likewise, the PSSAC adsorbent has a pore diameter of 4.86 nm, and the total pore volume was 0.39 cm^3/g. Moreover, it is worth observing that the PSSAC reveals the mesoporous framework that attests as a suitable material for the adsorption of doxycycline hydrochloride drug.

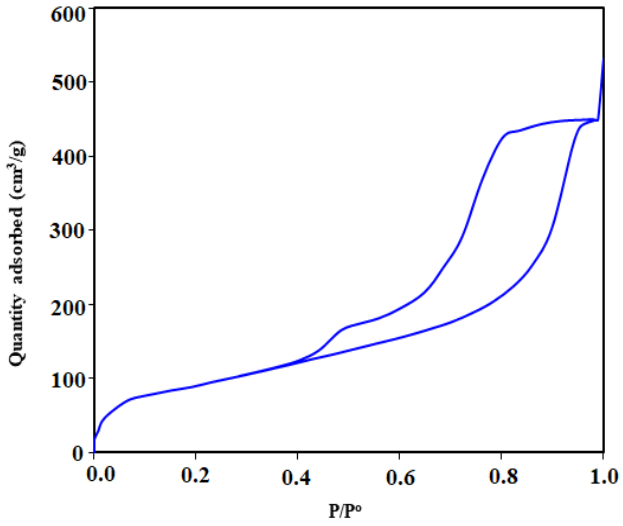

Fig. 4.41. The adsorption/desorption isotherm of N_2 on PSSAC.

FESEM pictures of PSSAC and loaded PSSAC (Fig. 4.42) were tested to detect the surface morphology of the adsorbent. As shown in Fig. 4.42, a uniform pattern of cavities was distributed all over the adsorbent's surface. It indicated the excellent opportunity for the DOX to be adsorbed by the PSSAC. On the other hand, after the loading of DOX, the size of cavities reduced, and their pores got completely filled up by DOX molecules. These two figures conclude that the surface texture of bare PSSAC modifies after the adsorption of DOX.

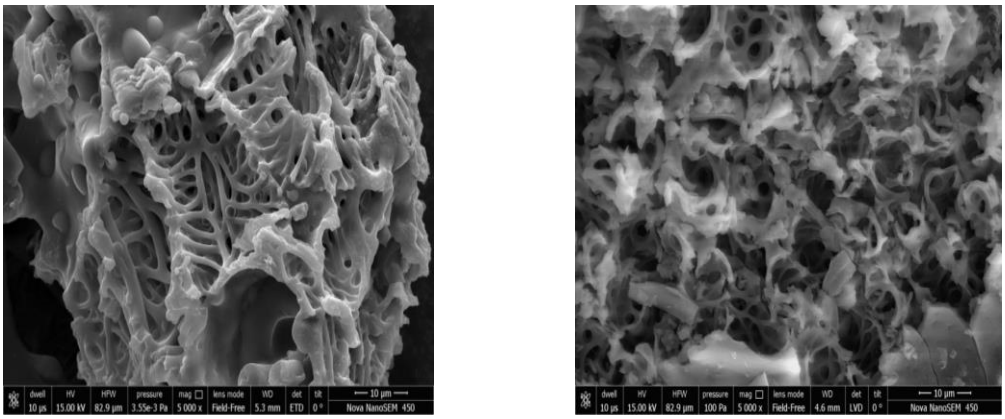

(a) **(b)**

Fig. 4.42. FESEM images for PSSAC and loaded PSSAC (a, b).

4.30. Adsorption experiments

4.30.1. Effect of PSSAC dose on adsorption of DOX

The consequence of PSSAC dose on the adsorptive uptake of DOX was evaluated by keeping other parameters constant (C_o = 25 mg/L, pH = 8, contact time = 600 min). An increment in the dose of adsorbent resulted in enhanced DOX uptake till a definite value, and thereafter the adsorption efficiency becomes almost constant. So the maximum removal rates achieved for PSSAC adsorbent was 85.82% at a DOX dose of 2.5 g/L as depicted in fig. 4.43(a).

At PSSAC dose of more than 2.5 g/L, the incremental DOX uptake was very less because the DOX concentration on the adsorbent surface and in the bulk solution reaches equilibrium with each other. Therefore, the increase in DOX adsorption becomes very less. This is due to the fact that for dose ≥ optimum dose, the removal efficiency mainly depends upon the solution concentration (DOX) and less depends upon the dosage of adsorbent (Mall et al., 2005). From the results, 2.5 g/L adsorbent dosage was considered optimum; thus, further experiments were performed with this optimum PSSAC dose.

4.30.2. Effect of contact time on the DOX adsorption

In adsorption processes, the study of contact time enables the evaluation of the adsorbent efficiency. The time required for complete saturation of the adsorbent by adsorbate is the time at which the highest adsorption is observed. The removal rate of DOX by PSSAC at initial concentration = 25 mg/L, optimized dose = 2.5 g/L and pH = 8 for 600 min is presented in Fig. 4.43(b). It can be observed from the figure that adsorption of DOX was quite rapid in the first 300 min, because of the large number of available vacant active sites and later successively approaches almost stable value.

Rapid adsorption occurs because of high driving forces between the adsorbate and adsorbent molecules (Yu et al., 2003). After 300 min, the adsorption reached an equilibrium state, and with further increase in contact time, there is no additional enhancement in adsorption capacity due to the repulsive forces between the adsorbate and adsorbent molecules (Chakraborty et al., 2011). Based on these results, 300 min time was taken as the equilibrium time for ahead batch adsorption studies.

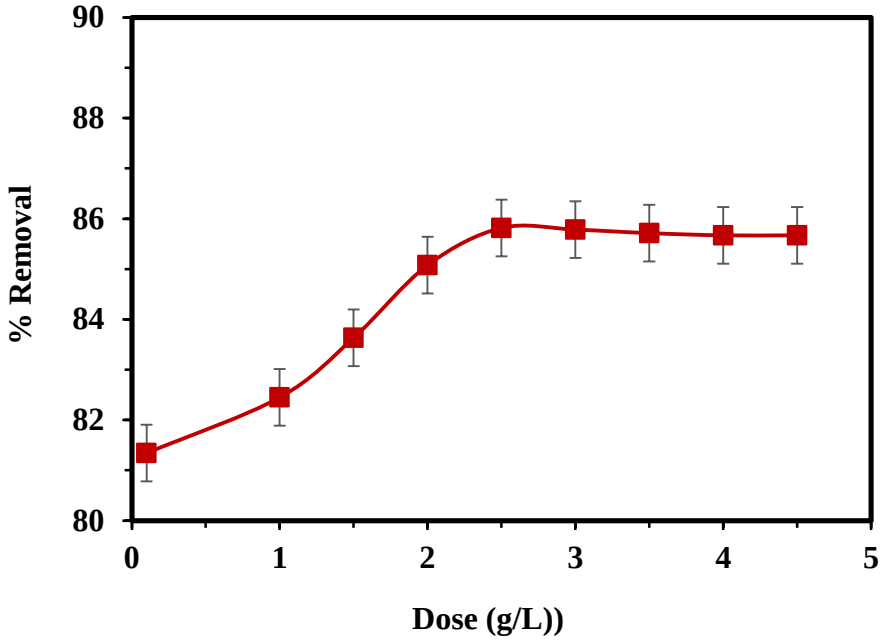

(a)

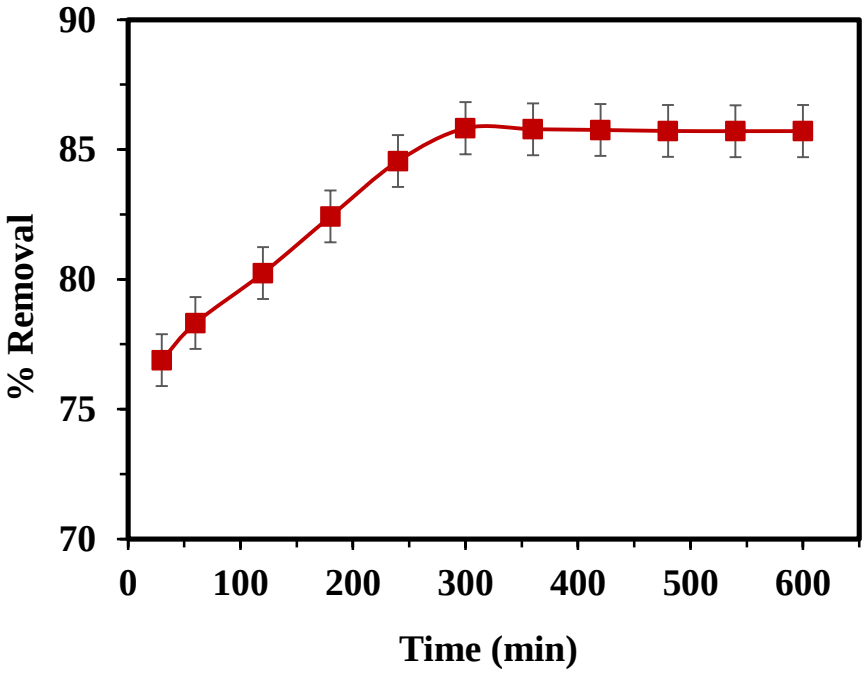

(b)

Fig. 4.43. DOX removal with varying adsorbent dosage at C_o = 25 mg/L, pH = 8, contact time = 600 min (a), Effect of contact time on adsorptive uptake of DOX at C_o = 25 mg/L, dose = 2.5 g/L, pH = 8 (b).

4.30.3. Effect of solution pH on adsorption of DOX

It is a well-known fact that the surface charge of adsorbent and species distribution of adsorbate effects with the variation in the solution pH (Zhang et al., 2012). Hence, its influence on the adsorptive performance of PSSAC for DOX was evaluated, and findings are depicted in Fig 4.44.

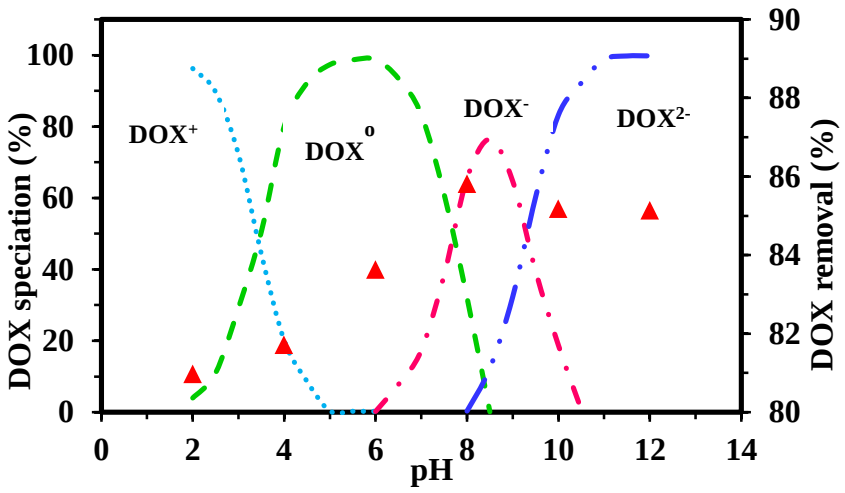

Fig. 4.44. Effect of solution pH on the sorption of DOX on PSSAC (C_o = 25 mg/L, dose = 2.5 g/L, contact time = 300 min at temperature 303 K).

The DOX adsorption on the PSSAC surface was highly pH-dependent. The removal efficiency first enhances and then slowed down with the increment in solution pH, and the highest adsorption performance was obtained at pH 8. The point of zero charges of PSSAC was found 6.1. The presence of various functional groups on PSSAC like carboxyl, hydroxyl, phosphate, amide, amine and sulphonate played significant roles in the adsorption process. Nearly below the neutral pH, the majority of the functional groups is protonated and present the positively charged form. At alkaline pH, due to the deprotonation of functional groups, the surface becomes negatively charged. Moreover, DOX represents three pKa values (pK_{a1} = 3.5, pK_{a2} = 7.7, pK_{a3} = 9.5) (Gao et al., 2012). On the condition of acidic pH, DOX is present in its protonated form, while near the neutral pH, it would be non-ionized, and at alkaline pH (>9.5), the dominant type of DOX is deprotonated. When the pH of the solution increases (>2) initially, the removal percentage enhances slightly; beyond a certain value, it increases and at pH >8, it decreases apparently. In the acidic and neutral pH conditions, the DOX^+ and

DOX^{o} species both are π electron acceptors. The particular efficacious π-electron-acceptors may cause stable π-π EDA interaction with the PSSAC surfaces (Ji et al., 2009). Moreover, at pH >8, the electrostatic repulsion between DOX^{-} species and deprotonated functional groups of PSSAC might describe the decline in adsorption performance. The weak physical forces like H-bonding and van der Waals forces are also participating in the adsorption mechanism. H-bonding causes because of the presence of polysaccharides on the PSSAC surface and aromatic rings in the DOX molecule (Das et al., 2006). Hence, H-bonding and $\pi - \pi$ EDA interactions heavily affected DOX adsorption on PSSAC and the mechanism is represented in Fig. 4.45.

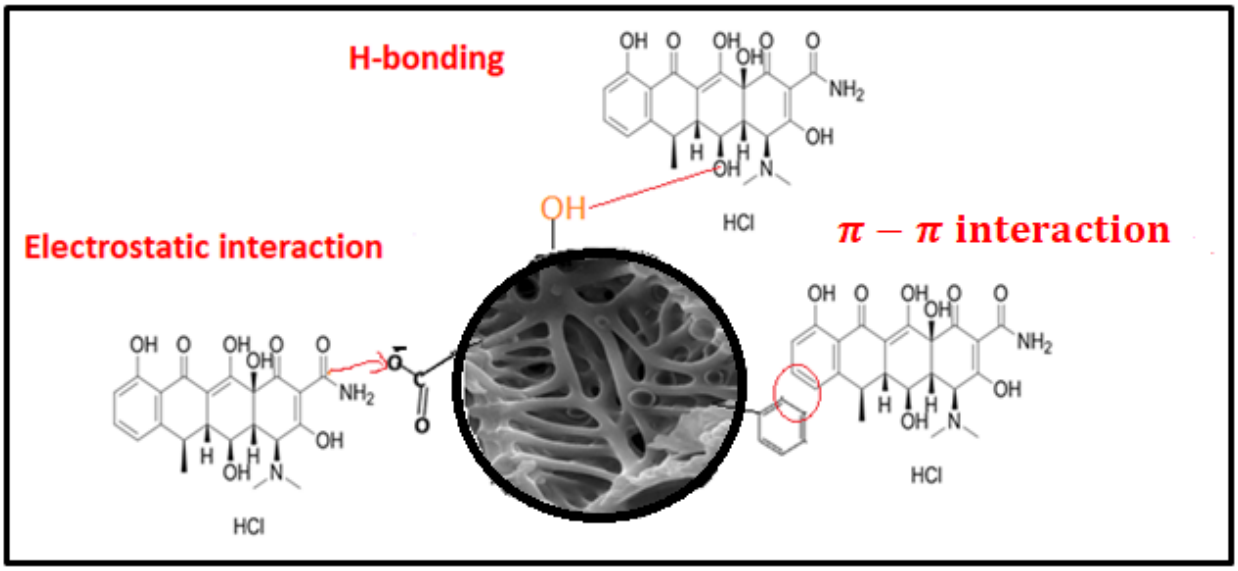

Fig. 4.45. Schematic representation of adsorption mechanism for DOX over PSSAC.

4.31. Adsorption kinetic studies, equilibrium studies and Diffusivity

In the adsorption kinetics study of DOX on the PSSAC, experimental results were fitted with the pseudo 1^{st} order and pseudo 2^{nd} order kinetic models. The model parameters obtained by fitting the experimental results are given in Table 4.30.

The fitting with these models is represented in Fig. 4.46 (a), in which variation in adsorption capacities (q_t) are represented with time. Solid lines represent to the second-order and dotted line to the first order. It is visible that, pseudo 2^{nd} order model fitted better than the pseudo 1^{st} order model because the correlation coefficient (R^2) magnitudes are high for 2^{nd} order model that is close to unity (R^2 = 0.99). Thus, these results suggest that the pseudo 2^{nd} order

kinetic model provided an adequate correlation for DOX adsorption onto the PSSAC (Vivek and Das, 2011).

Table 4.30. Kinetic parameters for adsorption of DOX by PSSAC (*m* = 2.5 g/L, *t* = 600 min and *pH* = 8, orbital shaking at 150 rpm, incubation at 303 K).

	C_0 (mg/L)		
	10	**25**	**50**
Pseuso first order			
k_f (min^{-1})	0.0140	0.0084	0.0250
$q_{e,exp}$ (mg/g)	4.80	8.45	12.49
$q_{e,cal}$ (mg/g)	4.79	8.40	11.01
R^2 (non-linear)	0.995	0.993	0.973
MPSD	10.035	22.928	85.23
Pseuso second order			
k_s (g/mg/min)	0.0030	0.0011	0.0026
h (mg/g/min)	0.088	0.111	0.45
$q_{e,cal}$ (mg/g)	5.45	9.80	13.09
R^2 (non-linear)	0.998	0.997	0.992
MPSD	8.745	11.002	18.583
Weber Morris			
k_{id1} (mg/g $min^{-1/2}$)	0.238	0.4006	0.424
I_1	0.624	0.709	4.685
R^2	0.947	0.986	0.963
k_{id2} (mg/g $min^{-1/2}$)	0.007	0.087	0.0058
I_2	4.625	6.399	12.351
R^2	0.914	0.609	0.954

The intra-particle diffusion (IPD) mechanism was employed for the analysis of the adsorption process of DOX onto PSSAC. The Weber-Morris model for IPD verifies that the internal diffusion is the only rate-controlling step, if the graph between q_t and $t^{1/2}$ passes through all the data points, remains linear and moves across the origin. In the plots of q_t vs $t^{1/2}$ (Fig. 4.46 (b)), two-step linearity was noticed, and it did not move across the origin. Results described that the rate of the adsorption was not controlled by a single adsorption mechanism. The first

phase of the adsorption involves the diffusion of DOX molecules from the external surface of PSSAC into its pores, referred to as intra-particle diffusion, film diffusion/boundary layer diffusion (Abel et al., 2017). As shown in Fig. 4.46 (b), the first region represents the gradual adsorption of DOX and that the intraparticle diffusion is rate-limiting.

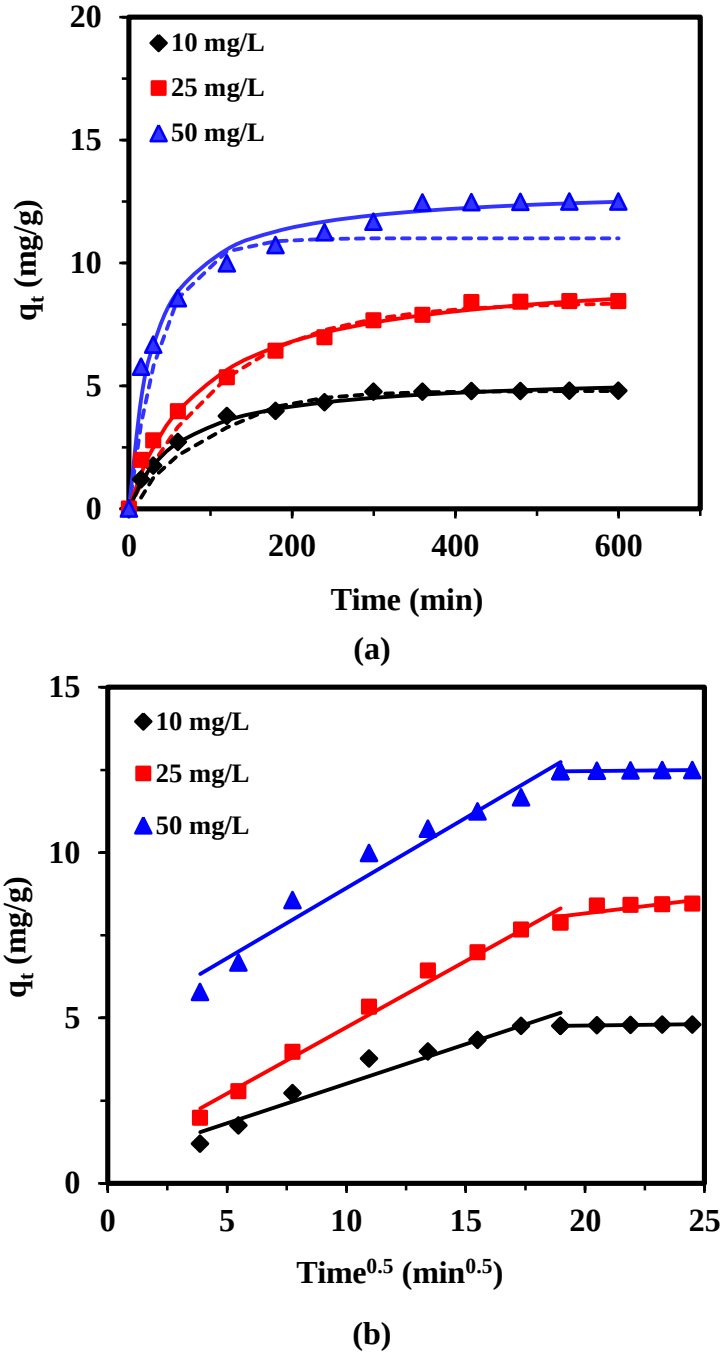

Fig. 4.46. Pseudo-first and second-order adsorption kinetics at different initial concentrations (a) Weber–Morris plot q_t versus $t^{1/2}$ for DOX treatment by PSSAC (b).

Further, quite low DOX concentrations remaining in the solution lessens the intraparticle diffusion and achieves the final equilibrium step of adsorption, as shown by the second linear region in the figure. This adsorption occurred on the interior surfaces of the adsorbent and is called the equilibrium diffusion mechanism. The values of intra-particle diffusion parameters k_{id} and I (slopes and intercepts of linear portions) are given in Table 4.31. The values of $k_{id\,1}$ and $k_{id,2}$ enhances with initial DOX concentration due to the increment in driving force for adsorption. Moreover, because linear lines do not move across the origin, IPD is not the only rate-limiting step involved in the adsorption of DOX on PSSAC. Surface adsorption also controls the adsorption process.

4.32. Adsorption isotherms

The adsorptive uptake of DOX on PSSAC at distinct temperatures in a range of 288 K–318 K and concentrations (10 to 100 mg/L) was investigated and shown in Fig. 4.47. The equilibrium data were fitted with the Langmuir, Freundlich, Temkin and RP isotherm models, and the associated model parameters are presented in Table 4.31. Experimental data displayed good fitting with the Freundlich and R-P isotherm models in comparison with Temkin and Langmuir isotherm models. The findings of the study suggested the multilayer adsorption of DOX on the PSSAC. Moreover, it can be seen from Fig. 4.47; the affinity of DOX on PSSAC was dependent on the reaction temperature. The absorptivity of the DOX was found to increase with an increase in temperature. In general, adsorption is an exothermic process. Nevertheless, when the process is governed by diffusion, also, the adsorption capacity shows enhancement with increment in temperature.

Table 4.31. Langmuir, Freundlich, Redlich-Peterson (R-P) and Temkin isotherm parameters for the adsorption of DOX by PSSAC (*m* = 2.5 g/L, *t* = 300 min and *pH* = 8).

ISOTHERMS

Langmuir $$q_e = \frac{q_m K_L C_e}{1 + K_L C_e}$$

T (K)	K_L (L/mg)	q_m (mg/g)	R^2	CHI^2
288 K	0.074	12.491	0.985	0.282
303 K	0.075	18.464	0.958	0.666
318 K	0.080	26.154	0.990	0.178

Freundlich $$q_e = K_F C_e^{1/n}$$

T (K)	K_F (mg/g) $(L/mg)^{1/n}$	1/n	R^2	CHI^2
288 K	1.907	0.420	0.993	0.07
303 K	2.784	0.424	0.984	0.32
318 K	4.564	0.386	0.992	0.25

Redlich-Peterson $$q_e = \frac{K_R C_e}{1 + a_R C_e^{\beta}}$$

T (K)	K_R (L/g)	a_R $(L/mg)^{1/\beta}$	β	R^2	CHI^2
288 K	2.677	0.870	0.577	0.991	0.073
303 K	3.231	2.372	0.720	0.984	0.322
318 K	5.223	2.823	0.777	0.992	0.245

Temkin $$q_e = \left(\frac{RT}{B_T}\right) ln(K_t C_e)$$

T (K)	K_T(L/mg)	B_T (J/mol)	R^2	CHI^2
288 K	0.903	2.535	0.986	0.201
303 K	0.766	3.980	0.971	0.454
318 K	0.787	5.713	0.997	0.072

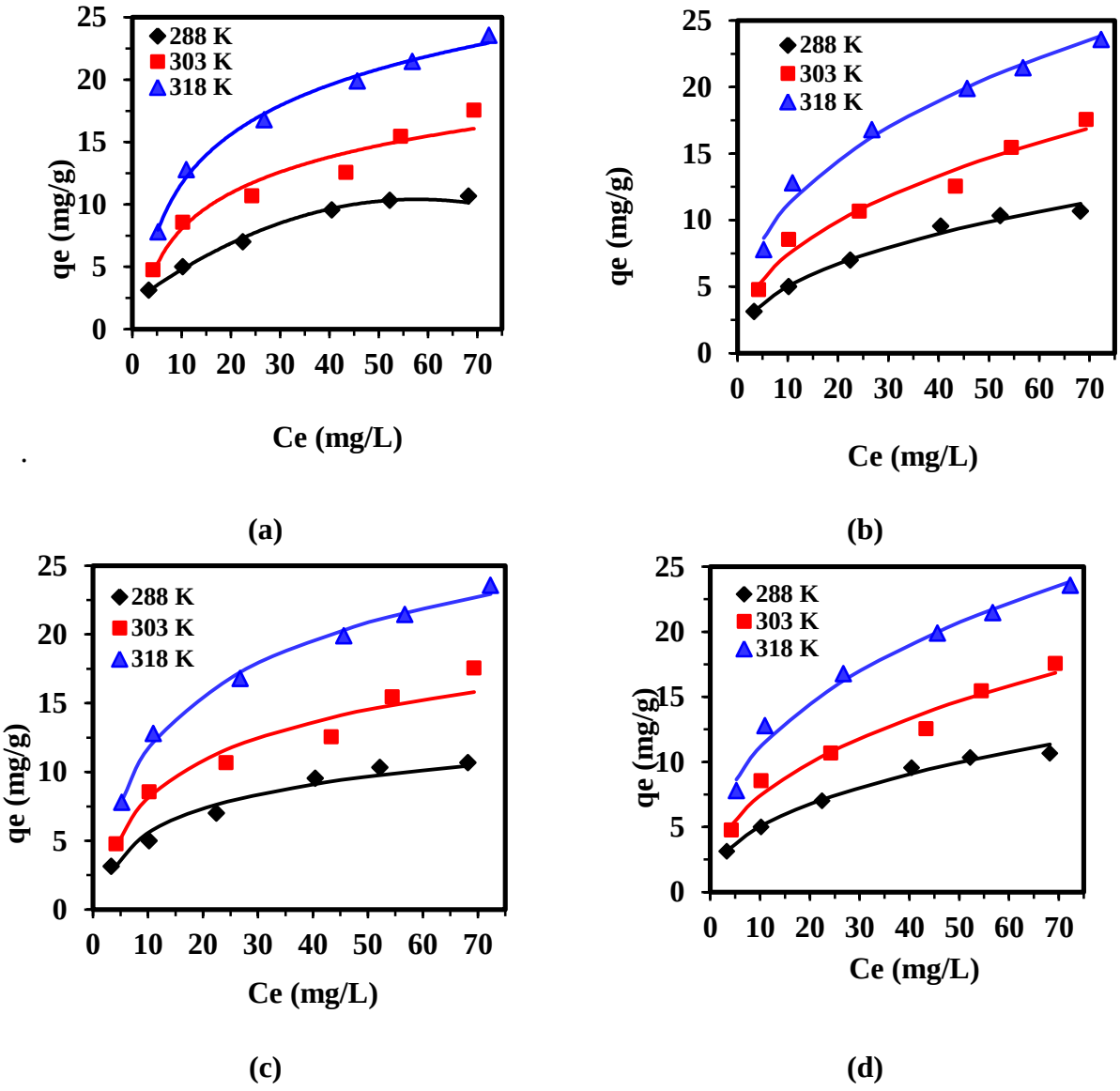

Fig. 4.47. Langmuir, Freundlich, Tempkin and RP isotherm models (a, b, c, and d) plot of DOX by PSSAC at various temperatures.

4.32.1. Thermodynamic study

The corresponding values of thermodynamic parameters are presented in Table 4.32. If ΔH^0 is a positive value, it confirms that the overall adsorption process's behavior is endothermic by nature. In physisorption, the van der Waals interactions are responsible for adsorbate and

adsorbent interactions where the adsorption energy usually lies between 5 to 10 KJ/mol. On the other hand, in chemisorption, the adsorption energy is typically between 30 to 70 KJ/mol. The positive value of ΔS^0 offered the enhancement in the degree of freedom as well as the randomness of adsorbate molecules on the adsorbent surface and an affinity of the PSSAC towards DOX components (Sharma, 2011). Moreover, the decline in a negative value of ΔG^0 with enhancement in temperature designated that DOX uptake on the PSSAC surface was instinctive and thermodynamically favorable. Usually, when the magnitude of ΔG^0 ranges from ⁻20 kJ/mol to ⁻40 kJ/mol type of adsorption is regarded as physisorption, and if less than ⁻40 kJ/mol chemisorption. The evaluated magnitude of ΔG^0, demonstrates that the mechanism involved in this adsorption is physisorption. Hence, from the Thermodynamic study, the adsorption of DOX on PSSAC surface was endothermic and instinctive.

Table 4.32. Thermodynamics parameters for the adsorption studies of DOX by PSSAC (m = 2.5 g/L, *t* = 300 min, C_o = 10-100 mg/L and *pH* = 8).

Thermodynamic Parameters $$lnK_D = \frac{-\Delta G^0}{RT} = \frac{\Delta S^0}{R} - \frac{\Delta H^0}{R}\frac{1}{T}$$

T (K)	K x 10^{-3} (L/kg)	ΔG^0 (kJ/mol)	ΔH^0 (kJ/mol)	ΔS^0 (J/mol)
288 K	6.247	-14.023	14.158	97.112
303 K	0.405	-14.795		
318 K	2.052	-16.983		

4.33. Recyclability of adsorbent

Regeneration studies are very useful to calculate the reusability of adsorbents for its practical applications in distinct areas. Herein, the reusability of exhausted PSSAC was conducted for five adsorption-desorption cycles, as presented in Fig. 4.48. While regenerating, the reduction in adsorption of DOX after 5 adsorption-desorption cycles were 3.48%, 5.71%, 11.48%, 15.39% and 17.37% respectively. These results designate that the PSSAC can be easily recovered and reused. It may also be applied on the industrial scale for the management of pharmaceutical pollutants. The low cost of PSSAC and the possibility of its recoverability makes it an extremely economical adsorbent.

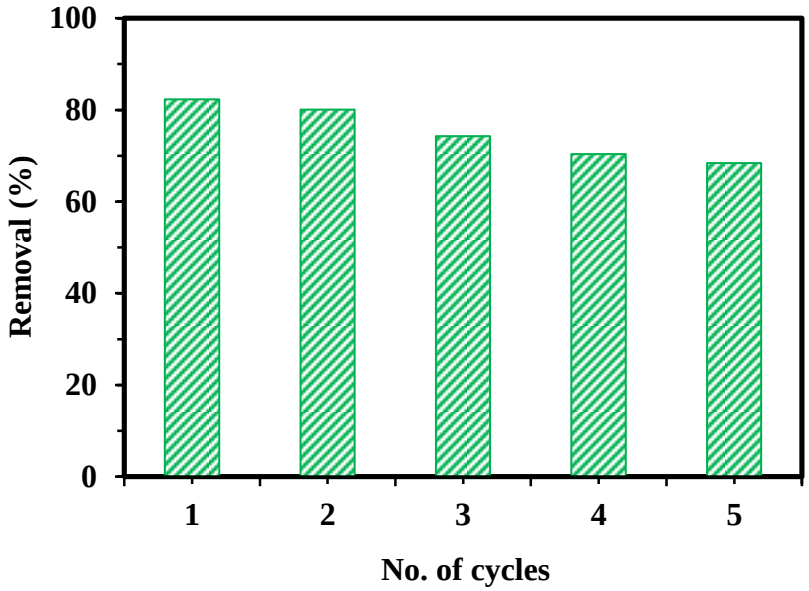

Fig. 4.48. DOX removal by PSSAC up to five adsorption-desorption cycles.

4.34. Comparison of PSSAC with previously studied adsorbents

For comparison purposes, the performance of PSSAC was collated with some previously used adsorbents for the adsorption of DOX. Table 4.33 presents the adsorption capacity of many earlier described adsorbents for DOX uptake from aqueous solutions in a batch process. From the study, it is realistic to propose that the PSSAC bio-sorbent is an appropriate adsorbent for removing antibiotics.

Table 4.33. Comparison of PSSAC with previously studied adsorbents.

Adsorbents	Maximum capacity (mg/g)	References
Cobalt oxide	5.20	Abbas et al., 2019
Raw biochar (BC)	11.48	Liu et al., 2019
Spent black tea leaves (SBTL)	12.53	Hassen et al., 2014
Pomegranate Peel (PP)	18.11	Hassen et al., 2014
Silica Coated Fe_3O_4 MNPs (Fe_3O_4@SiO_2)	21.5	Nooreini and Panahi., 2016
PSSAC	23.6	This study
Graphene oxide	35.50	Lin et al., 2013
Copper nitrate modified biochar (Cu-BC)	52.37	Liu et al., 2017

Chapter – 5
ADSORPTION USING DES FUNCTIONALISED ADSORBENTS

5.1. GENERAL

This chapter covers the study of modified agri-residue adsorbents for adsorption of selected antibiotics (OFL and DOX). Modifications were done by using deep eutectic solvent as functionalization agent. RHA and PSSAC were selected as base materials for DES functionalisation and named as DES-RHA and DES-PSSAC respectively. Further analysis about parameters optimization, kinetics, isotherms and reusability studies of the DES modified adsorbents are also presented in same chapter.

5.2. CHARACTERIZATION RESULTS OF SYNTHESIZED DES

Synthesized DES (GC3:1) was characterized for various relevant properties. The thermal stability of GC3:1 was evaluated using TGA analysis (PerkinElmer, STA6000) and is depicted in Fig. 5.1.

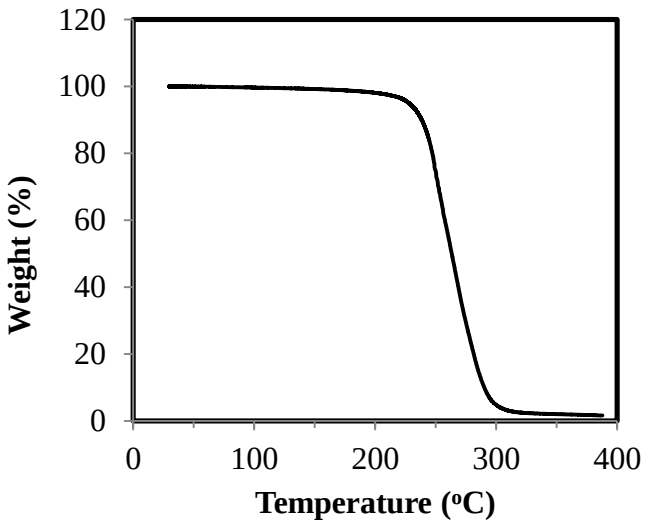

Fig. 5.1. TGA of DES (GC3:1) from 25°C to 400°C temperature at atmospheric pressure.

The TGA analysis has mainly three different steps of mass reduction i.e., removal of moisture content, the discharge of volatile substance and burning of material (Soltani et al., 2015). TGA was performed from 25 ^{o}C to 400 ^{o}C at the heating rate of 10 ^{o}C min^{-1} in N_2 gas envi-

ronment using 25 mg of DES sample. The combustion profiles of GC3:1 represented its high thermal stability. The moisture content of synthesized DES was evaluated using Karl-Fisher titrator (Esico model 1760) and was found as < 0.3 wt %.

To verify the H- bonding between ChCl and glycolic acid, FT-IR was performed, and the spectra are revealed in Fig. 5.2. The bands signify distinctive broadband around 3292 cm^{-1}, which indicates H-bonding among the ChCl and glycolic acid in the DES. In the medium region, intense bands with peaks at 1744, 1173, and 1088 cm^{-1} wavenumbers were noticed. This demonstrates the carbonyl group of glycolic acid and H-bond among the OH group of glycolic acid and Cl^- of ChCl, respectively (Sharma et al., 2018).

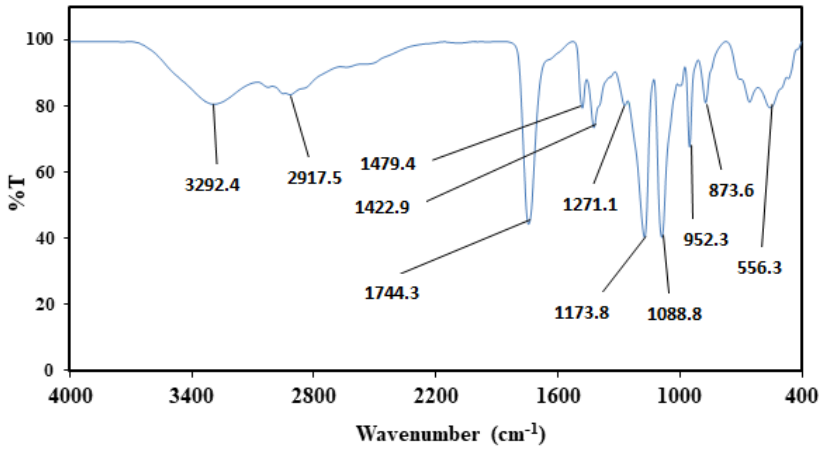

Fig. 5.2. FT-IR spectra of DES (GC3:1).

The structure of prepared DES was determined by ^1H NMR spectra and is shown in Fig. 5.3. Regardless of the dilution of DMSO, the molecular structure of DES was found unaffected. The possible hydrogen bonding in GC3:1 and its optimized chemical structure (using Gaussian 16 software) are represented in Fig. 5.4 (a) and (b), respectively.

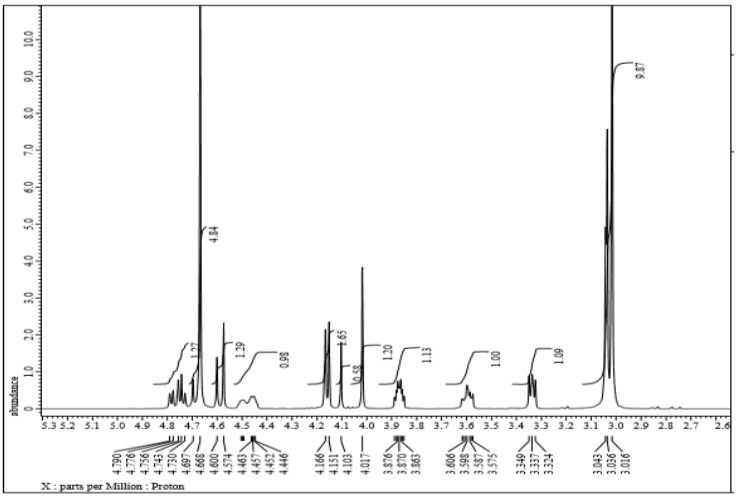

Fig. 5.3. ^{1}H NMR of the synthesized DES (GC3:1).

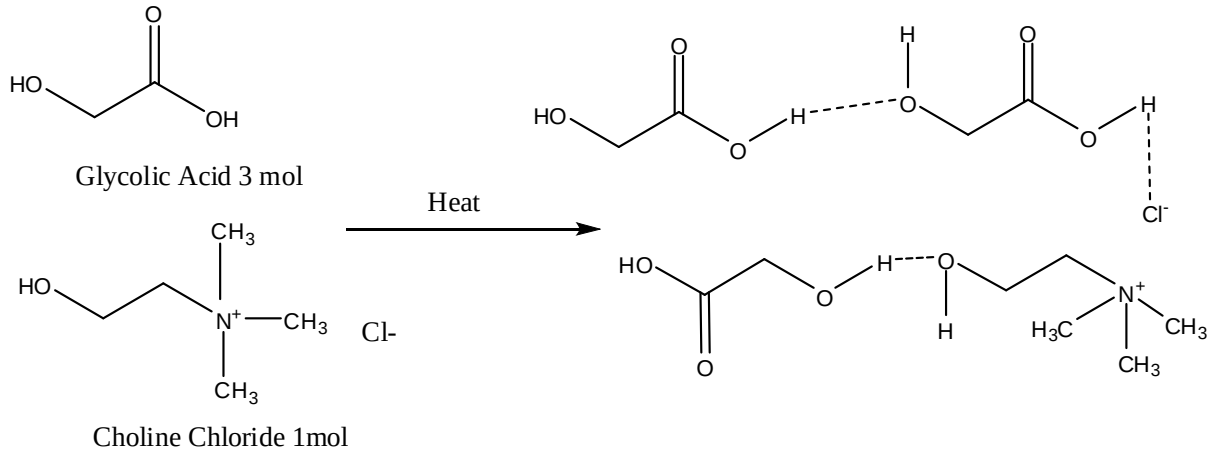

(a)

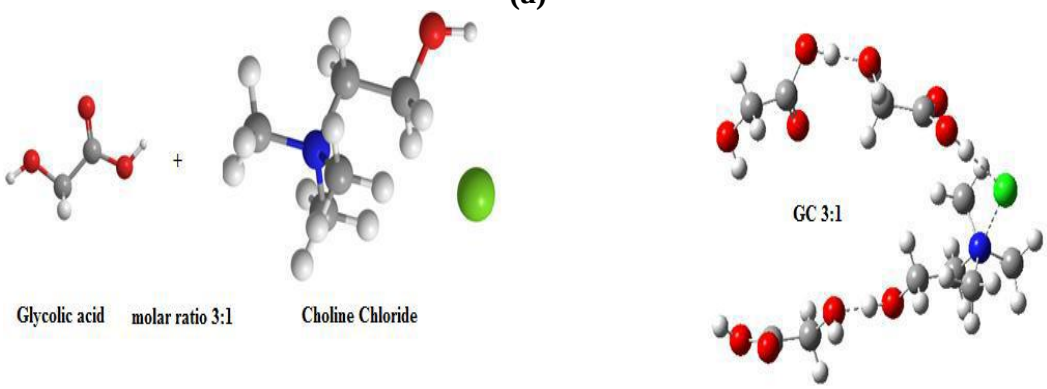

(b)

Fig. 5.4. Hydrogen bonding in GC3:1 (a), Optimized chemical structure (using Gaussian 16 software) (b).

5.3. CHARACTERIZATION RESULTS OF RHA and DES–RHA

5.3.1. FTIR studies

FT–IR spectra of RHA and DES–RHA is illustrated in Fig. 5.5. The presence of a broad peak at 3425 and 3457 cm^{-1} shows the stretching vibration of O–H and Si-OH. In DES–RHA spectra, the existence of a peak at 3002 cm^{-1} is assigned to the coupling of DES with the surface hydroxyl group of rice husk ash. The band around 1092 cm^{-1} is related to Si–O–Si bonding vibrations and at 468 and 794 cm^{-1} to Si–H bonds in RHA. A prominent new peak that appeared in the DES–RHA at 1739 cm^{-1} is due to the presence of -COOH group of glycolic acid on the surface.

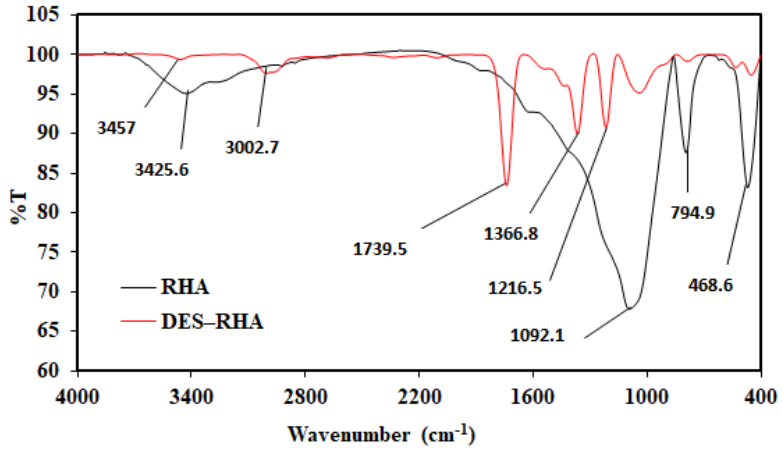

Fig. 5.5. FT-IR spectra of RHA and DES-RHA.

5.3.2. XRD studies

XRD spectra of RHA and DES–RHA samples are represented in Fig. 5.6. The XRD pattern of the samples exhibited wide peaks between 22° and 27° (2θ) for RHA and DES–RHA both, which correspond to the presence of cristoballite (SiO_2). Because of the addition of DES in the RHA matrix, two extra peaks were observed at little high 2θ (around 29.34° and 44.34°) that explain the aggregation of RHA particles with DES because of the existence of functional groups (C=O, -OH) and wrapping of DES onto the RHA surface (Wang et al., 2007). The results indicate that RHA and DES–RHA are having the characteristic of an amorphous, disordered structure that is capable of adsorption of materials (Soltani et al., 2015; Bahrami et al., 2016).

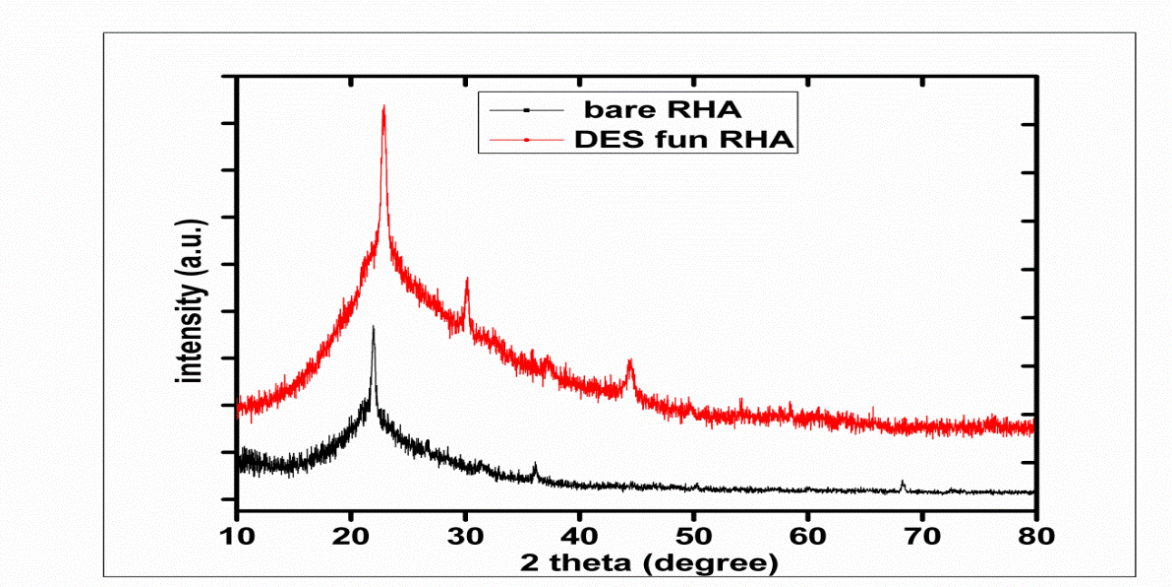

Fig. 5.6. X-ray diffraction (XRD) analysis of bare RHA and DES–RHA.

5.3.3. BET surface area

The specific (BET) surface areas of RHA and DES–RHA was 32.6 m^2/g and 23.12 m^2/g, respectively. As expected, the specific surface area of DES–RHA diminishes as compared to the bare RHA because the condensation of adjoining silanol groups at the pore openings forms siloxane bonds that essentially close the narrower pores. These narrow pores are thus not available for adsorption by nitrogen (Vansant et al., 1995). The average pore diameter was found 6.5 nm, and 1.44 nm, representing that RHA is mesoporous by nature and is an appropriate sorbent for the adsorption of OFL. In addition, the pore volume was decreased from 5.22 to 0.030 cc/g after the functionalization by DES, which is further proof that DES was embedded inside the pore hole of RHA (Gregg and Sing, 1967). The comparative adsorption efficiency of the bare RHA and DES–RHA was examined. It is seen that both adsorbents exhibited different adsorption capacities where the DES–RHA had higher adsorption capacity than RHA.

5.3.4. FESEM, EDX and HR-TEM

FESEM figures of RHA, DES–RHA and OFL adsorbed DES–RHA are depicted in Fig. 5.7. (a, b), (c, d) and (e, f), respectively. The bare surface of RHA possesses a membranous fissure and vesicular nature, which has a plate-like morphology. On the other hand, in the FESEM images of DES–RHA, the agglomerated masses are attached due to hydrogen bonding among ChCl and glycolic acid. This provides evidence of the capability of DES to func-

tionalize RHA without changing physical and chemical properties with non–destructive way. The irregular agglomerations can be perceived for bare RHA while DES–RHA exhibited fewer agglomerative behaviour, which recommends a superior distribution and a greater performance of the DES–RHA adsorbent for OFL removal. There is not any type of definite damage to the structure or morphology after treating the RHA with DES. After adsorption, all the porous surfaces are completely occupied with OFL molecules, as shown in Fig. 5.7 (e, f). The EDX test of washed and dried RHA was performed to analyze its elemental composition and is presented in Table 5.1.

Table 5.1. Elemental analysis of used rice husk ash.

Elements	**C**	**Na**	**Mg**	**Si**	**K**	**Ca**	**O**
Weight %	11.78	0.17	0.10	34.14	0.34	0.17	53.3

Results revealed the presence of different elements such as silica, calcium, sodium, magnesium, potassium, carbon and oxygen. Nevertheless, the highest inorganic constituent present in RHA was silica after oxygen.

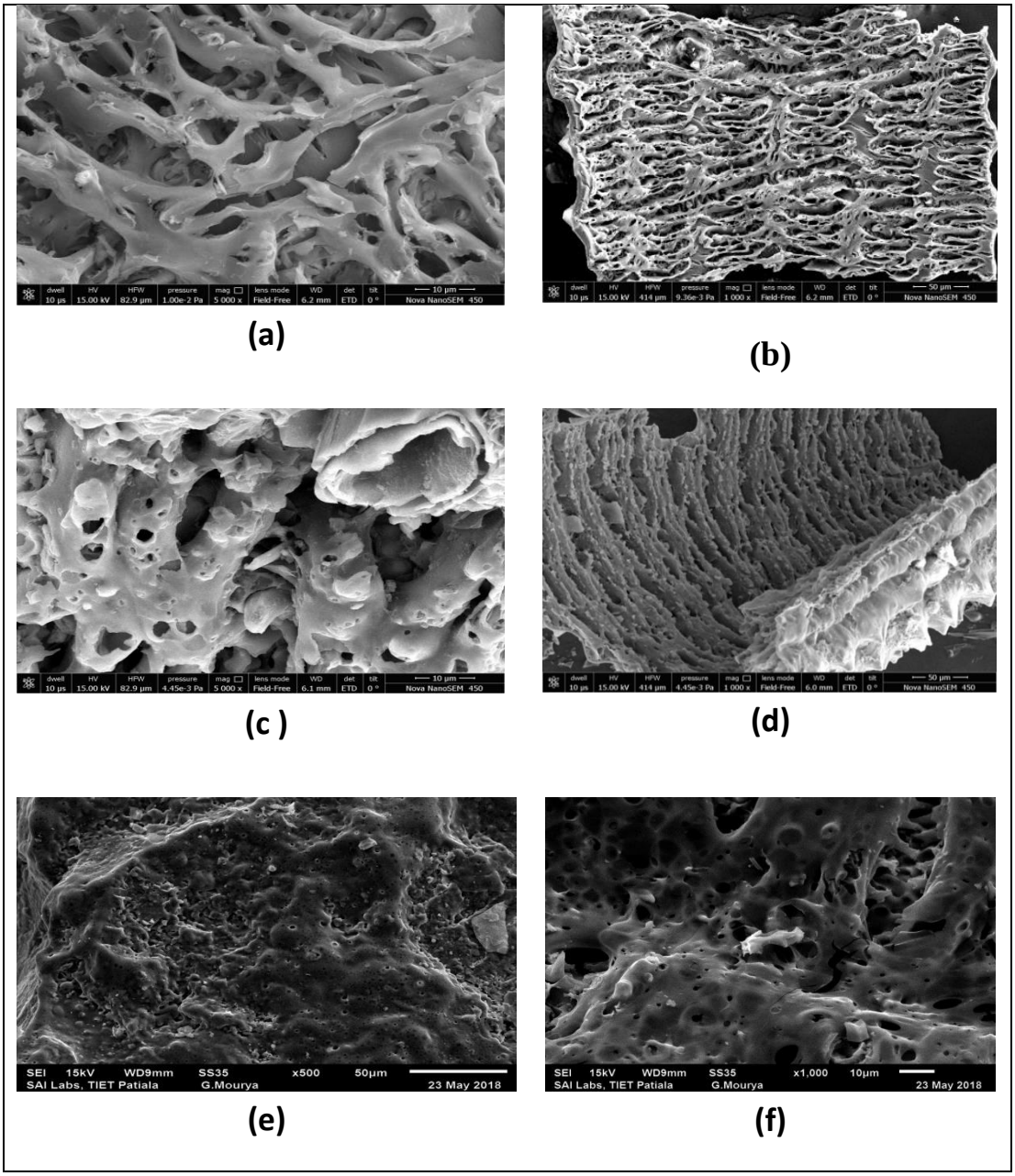

Fig. 5.7. FESEM images for bare RHA (a, b), FESEM images for DES–RHA (c, d), FESEM images after adsorption of OFL (e, f).

For a better understanding of the morphology of RHA and DES–RHA, high-resolution imaging was also recorded. It provided evidence of a successful functionalization of DES over RHA. As shown in Fig. 5.8, in contrast to the TEM micrographs of RHA samples (a), the images of DES–RHA clearly showed a dark texture of DES uniformly covering the entire RHA surface. This uniform distribution of DES activated the surface particles and sorted them together in a uniform manner throughout. Hydrogen bonding onto the RHA surface completely treated the rice husk ash, as shown in Fig. 5.8 (d) and (e). The presence of dark black spots

determines how deep the effect of DES penetrated the rice husk ash matrix without any aggregation. These TEM observations are in agreement with the results from the different characterization results discussed above.

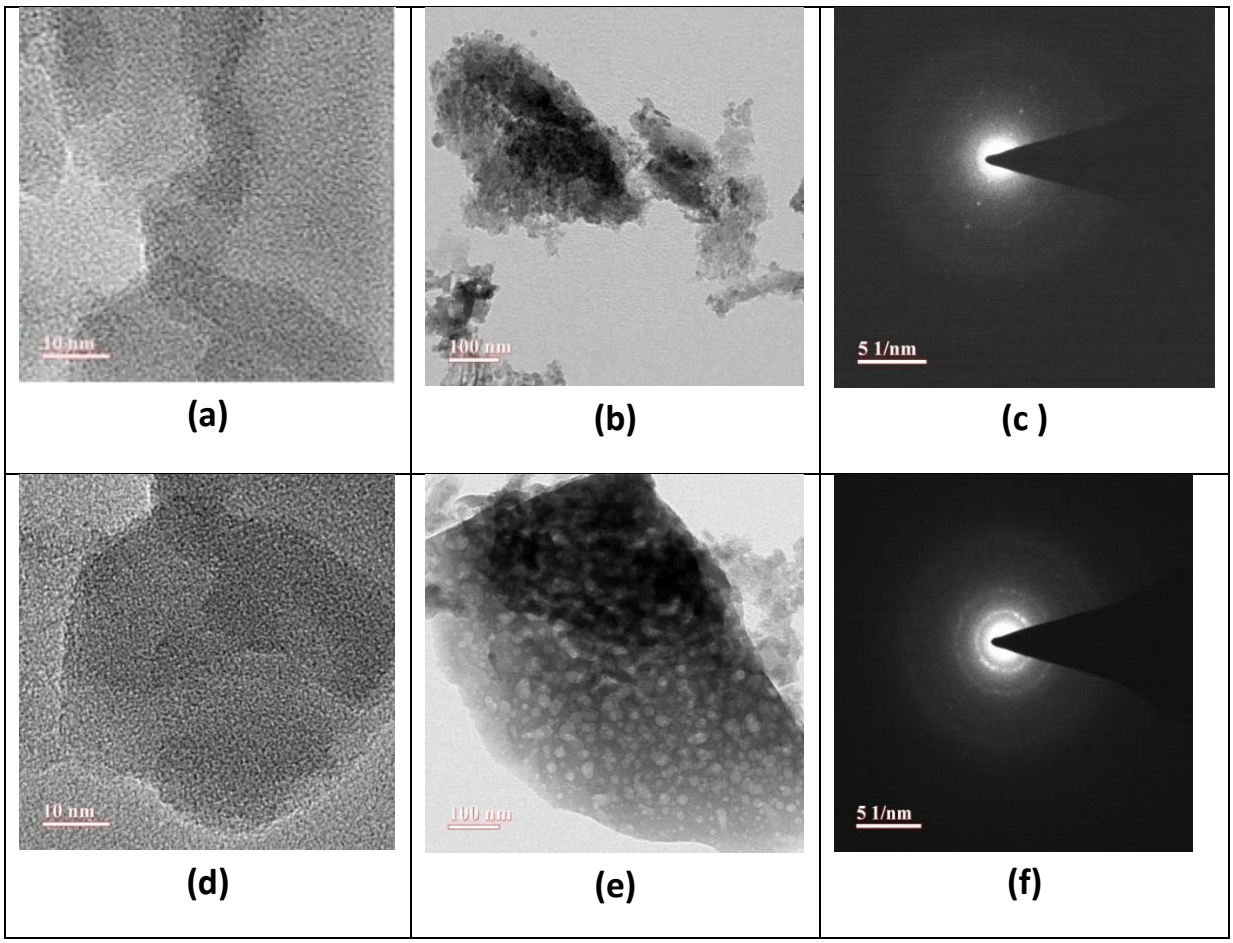

Fig. 5.8. HR-TEM images and SAED patterns of RHA particles (a, b, c), HR-TEM images and SAED patterns of DES–RHA (d, e, f).

5.4. BATCH ADSORPTIVE REMOVAL OF OFL FROM ITS AQUEOUS SOLUTION BY DES-RHA

5.4.1. Optimization of operating conditions

The influences of DES-functionalized RHA dosage, solution pH and adsorption time for the uptake of OFL drug were examined by performing batch adsorption studies. For comparison, results for bare RHA were also represented for all experimental conditions. The effect of different parameters was evaluated, and the experimental condition was optimized. The experiments were repeated twice, and a good reproducibility was achieved with a 5% of average standard deviation.

5.4.1.1. Effect of RHA and DES–RHA dose on OFL removal

The influence of adsorbent dosage on OFL removal efficiency was evaluated for DES–RHA and RHA both, by maintaining remaining variables constant ($C_o = 25$ mg/L, pH = 2, time period = 720 min). Fig. 5.9 represents the % OFL removal with varying adsorbent dosage. An increase in adsorbent dosage leads to increasing active site concentration, which helps to enhance the OFL elimination up to a definite range and thereafter, the removal rate became nearly stable. At dose > 2 g/L for both adsorbents, the gradual OFL removal becomes extremely less as the OFL antibiotic amounts on the adsorbent and in the bulk, solution approaches equilibrium with each other (Yu et al., 2003). Furthermore, DES–RHA represented high removal efficiency, with 77.03% of the OFL using the DES–RHA dose of 2 g/L. On the other hand, at a 2 g/L dose of RHA, the % removal was only 51.51%. Opposite to this, q_e declines as the amount of adsorbent increases (not presented here). Consequently, 2 g/L dosage of DES–RHA was optimum; thus, all the further experimental studies were performed with 2 g/L dosage for DES–RHA and RHA both for OFL removal.

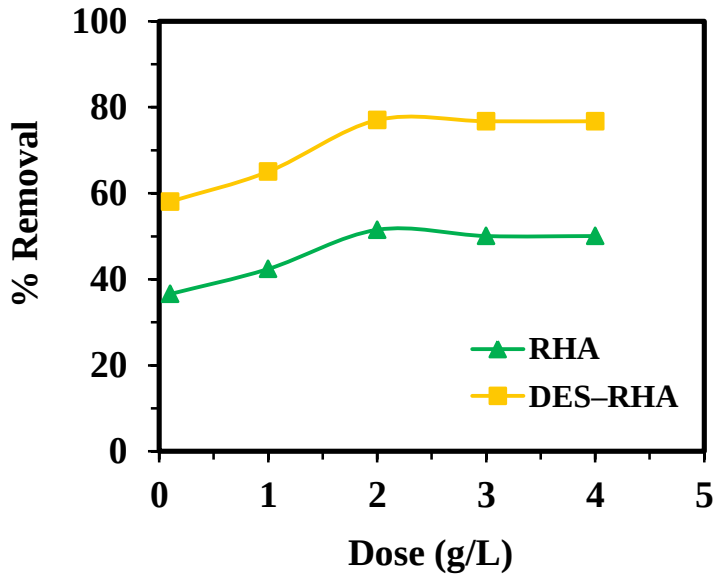

Fig. 5.9. % OFL removal with varying adsorbent dosage at C_o = 25 mg/L, pH = 2, contact time = 720 min.

5.4.1.2. Influence of pH on removal efficiency

The solution pH plays a prominent role in the adsorption process because it can affect the uptake capacity of the adsorbent. The removal of OFL by DES–RHA and bare RHA was determined at distinct solution pH (2 to 10) by keeping other variables constant (C_o = 25 mg/L, the dosage of adsorbent = 2 g/L, time period = 720 min), and the OFL deduction percentage is illustrated in Fig. 5.10.

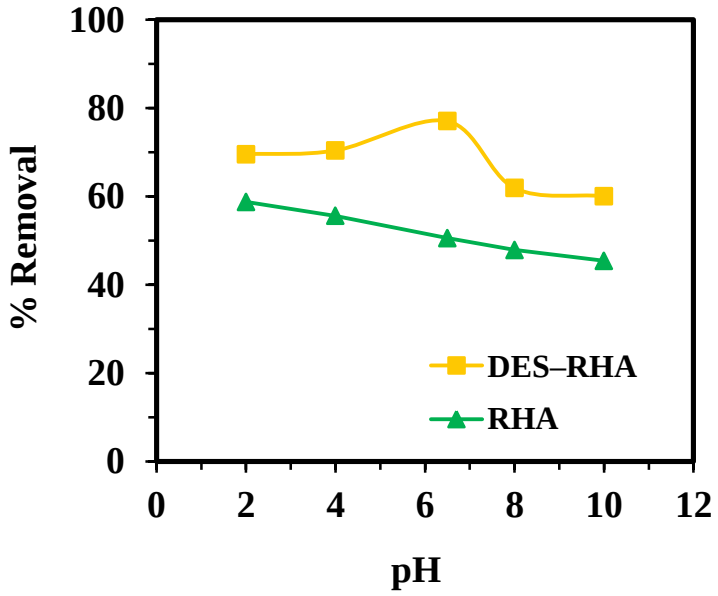

Fig. 5.10. Effect of solution pH on adsorptive uptake of OFL at C_o = 25 mg/L, dose = 2 g/L, contact time = 720 min.

It can be seen that for DES–RHA, with enhancement in pH up to 4, the OFL removal (%) is close to ≈ 70 %. Nevertheless, when pH increased beyond 4, the OFL uptake started rising, being maximum (≈ 77%) at pH = 6.5. Moreover, for pH > 6.5, the OFL elimination (%) was found to reduce and becomes nearly constant to ≈ 61 % at all pH beyond pH = 8. For bare RHA, the maximum OFL removal (%) of ≈ 59 % was observed at pH = 2. However, for all the pH > 2, a continuous decrease in performance was observed. This variation in performance can be attributed to DES functionalization. The acid dissociation constants for Ofloxacin (OFL) are 6.08 (pKa_1) and 8.25 (pKa_2). Therefore, OFL is mainly cationic (OFL^+) for pH < 6.08 and anionic (OFL^-) for pH > 8.25. In-between (6.08 < pH < 8.25), the OFL is a zwitterionic compound (OFL^o) (Goyne et al., 2005). Further, in the aqueous solution of OFL, the distribution of different forms of OFL is not very sharp, and OFL^o formation starts from pH ≈ 4.0 and OFL^- starts from pH ≈ 6.5.

Because DES used in this work is a combination of glycolic acid and ChCl, so it indicates high electronegativity due to the existence of Cl^- ion. As displayed in Fig. 5.10, for pH less than 4, OFL removal is the result of electrostatic forces within DES and OFL^+. As pH rises more (pH > 4), the OFL particles begin to achieve zwitterionic form, and at this pH value (4 ≤ pH ≤ 6.5), electrostatic relationships between DES and OFL reduces because of the few opportunity of OFL^+, and adsorption is directed by H-bonding within OFL^o and DES–RHA combination as shown in Fig. 5.11. This occurs because of the reality that, DES has great H-bonding chances while the adsorbate nature is zwitterionic (Kaur et al., 2018a). Beyond pH > 6.5, the development of OFL^- starts, and subsequently the sorption due to H-bonding weakens causing diminished OFL elimination (%).

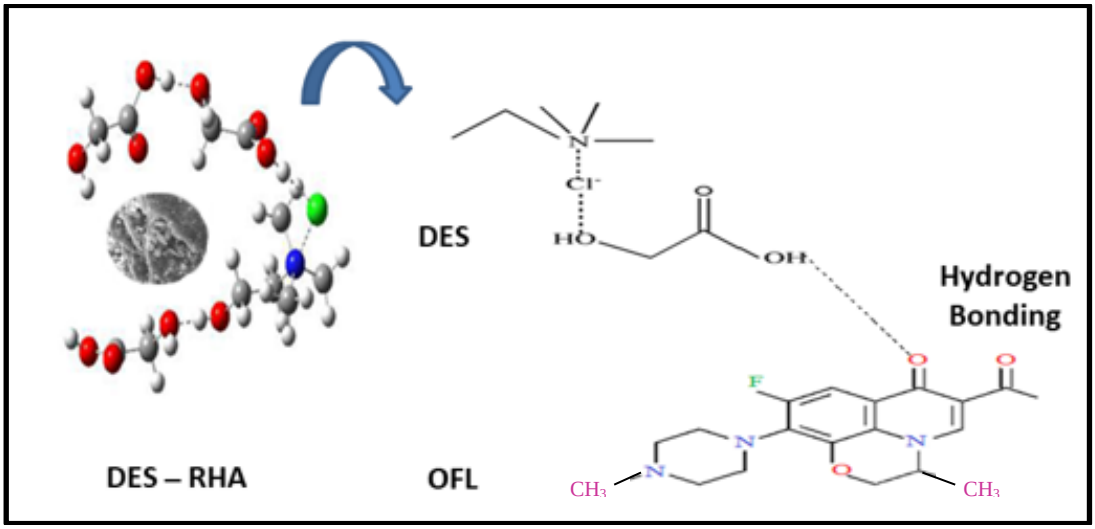

Fig. 5.11. Schematic representation of adsorption mechanism for OFL over DES-RHA via H-bonding.

It is concluded from the outcomes that the highly acidic and nearly neutral pH favours the OFL removal, whereas, at alkaline pH lower OFL removal (%) occurred in both the bare RHA and DES–RHA system. As a result, in the present work, it is proposed that adsorption studies of both adsorbents (RHA and DES–RHA) are pH dependent and performed the major role in the adsorption of OFL. The DES–RHA presented greater removal (77.03 %) than bare RHA. Finally, natural pH range (6.5) was selected for all experiments in this study.

5.4.1.3. Effect of time period on removal efficiency

Fig. 5.12 represents the influence of adsorption time on OFL uptake of DES–RHA and RHA adsorbents. The optimum dose of adsorbents (2 g/L) and pH (6.5) was considered for the study of the effect of time. The time profile of adsorption (Fig. 5.12) represents that adsorption of OFL on DES–RHA was fast. The results showed that OFL uptake increased during the first 480 min and reached the maximum because of the available vacant active adsorbent sites and after 480 min, the adsorption reached an equilibrium state (Chakraborty et al., 2011). From BET analysis results, it is evident that surface area and pore volume of RHA is more than DES–RHA, but the adsorption performance of DES–RHA is superior to RHA. It indicates that the trapping of OFL in pores is not the main adsorption mechanism. Thus, this quick adsorption observed can be attributed to the attraction force among the OFL and DES–RHA (electrostatic interaction among the positively charged adsorbent surface and the negatively charged molecules of OFL at their respective pH).

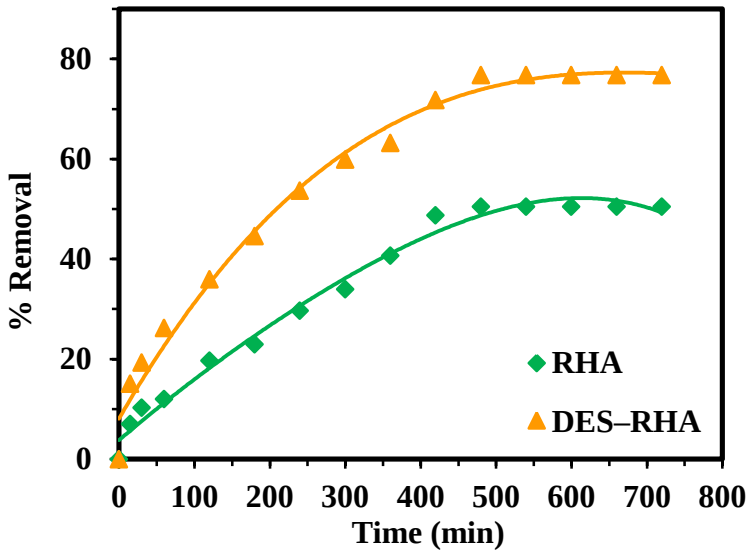

Fig. 5.12. Effect of contact time on adsorptive uptake of OFL at C_o = 25 mg/L, dose = 2 g/L, pH = 6.5.

5.4.2. Kinetic representation

Analyzing the adsorption kinetics is an essential step, to estimate the removal rate of OFL from the water ecosystem and to explore the adsorption procedure. Fitting of experimental findings to the pseudo-first-order and pseudo-second-order kinetic models were performed using nonlinear regression. The data sets and fittings are represented in Fig. 5.13, where the adsorption capacities are plotted against time.

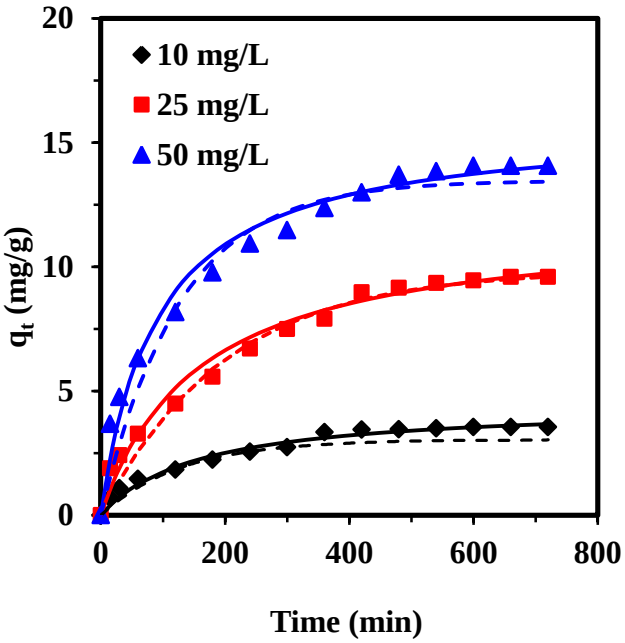

Fig. 5.13. Pseudo-first and second-order adsorption kinetics at different initial concentrations.

The correlation coefficients, R^2 found a good fit with the studied data to the pseudo-first-order and pseudo-second order kinetic studies and resultant model variables are given in Table 5.2. While matching the correlation coefficients R^2 values, it demonstrated that for pseudo-second-order it was close to unity (R^2 = 0.99), which indicates that sorption of OFL on DES–RHA follows pseudo-second-order. The results of the kinetic study indicate that the sorption procedure doesn't only depend on electrostatic interactions within adsorbate and adsorbent, but on other mechanisms as well (hydrogen bonding) (Chaturvedi et al., 2020).

Table 5.2. Kinetic parameters for adsorption of OFL by DES functionalized RHA (*m* = 2 g/ L, *t* = 720 min and *pH* = 6.5, orbital shaking at 150 rpm, incubation at 303 K).

	C_0 (mg/L)		
	10	**25**	**50**
Pseuso first order			
k_f (min^{-1})	0.0077	0.0051	0.0079
$q_{e,exp}$ (mg/ g)	3.54	9.60	14.06
$q_{e,cal}$ (mg/g)	3.04	9.85	13.47
R^2 (non-linear)	0.982	0.993	0.986

MPSD	59.81	31.15	35.93
Pseuso second order			
k_s (g/mg/min)	0.00144	0.00053	0.0007
h (mg/gmin)	0.029	0.075	0.18
$q_{e,cal}$ (mg/g)	4.46	11.89	15.80
R^2 (non-linear)	0.991	0.992	0.992
MPSD	35.95	28.07	36.25
Weber Morris			
k_{id1} (mg/g/min)	0.1588	0.4237	0.5529
I_1	0.1413	0.0582	1.915
R^2	0.986	0.9958	0.9928
k_{id2} (mg/g/min)	0.0184	0.1031	0.0761
I_2	3.0668	6.9018	12.086
R^2	0.9375	0.9628	0.8184

To analyze the diffusion mechanism during the adsorption process of OFL on DES–RHA, The intra-particle diffusion (IPD) model was used to investigate the rate governing steps in the adsorption process. The use of Weber and Morris plot; q_t versus $t^{1/2}$ (Fig. 5.14) approves that adsorption is solely controlled by internal diffusion if the graphs represent linearity and crosses via origin. The mechanism of the OFL adsorption on DES–RHA is explained in two steps as shown in Fig. 5.14.

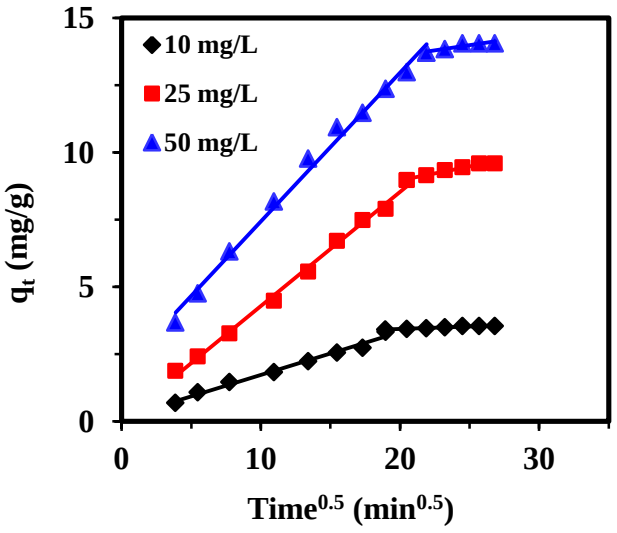

Fig. 5.14. Weber-Morris plot q_t versus $t^{1/2}$ for OFL treatment by DES-RHA.

Where the first step shows the rapid sorption rate because of the presence of a higher no. of active sites on the adsorbent surface. It is called as intra-particle diffusion process (Gercel et al., 2007). Further, intra-particle diffusion diminishes and attains the final equilibrium stage of adsorption as shown by the second linear segment in the figure. This portion of the graph represented the equilibrium diffusion mechanism where OFL molecules slowly diffused through the pores of the DES–RHA and was adsorbed by its internal surfaces. Thus we can say that the adsorption mechanism of OFL follows a multistep mechanism. The magnitude of intra-particle diffusion variables is shown in Table 5.2. Where the obtained values of constants $k_{id,1}$ and $k_{id,2}$ increases with initial OFL concentration because of enhancement in driving force for adsorption process. Furthermore, the linear lines do not cross across the origin. Thus, it is concluded that in the adsorption of OFL on DES–RHA intra-particle diffusion is not the sole rate-limiting step but surface adsorption also plays its role in sorption.

5.4.3. Equilibrium isotherms

The adsorption of the OFL on DES–RHA at several temperatures and concentrations was examined and is represented in Fig. 5.15. The equilibrium data were well suited with the Langmuir, Temkin, RP and Freundlich isotherm models, and the related constraints are listed in Table 5.4. It is recognized from Table 5.3 that except Freundlich isotherm model, all other isotherm models fitted well with the experimental data with the high correlation coefficients (R^2>0.99). The better fitting of experimental data with the Langmuir isotherm model as compared to Freundlich indicates that DES–RHA surface had a large number of adsorption active sites and the adsorption process of the OFL was dominated by monolayer adsorption (Sharma, 2011). It is observed from Fig. 5.15, that the interactions between OFL on DES–RHA was related to reaction temperature. The sorption ability of the OFL improved with the increase of reaction temperature, demonstrating that high temperature is best for enhancing the adsorption capacity.

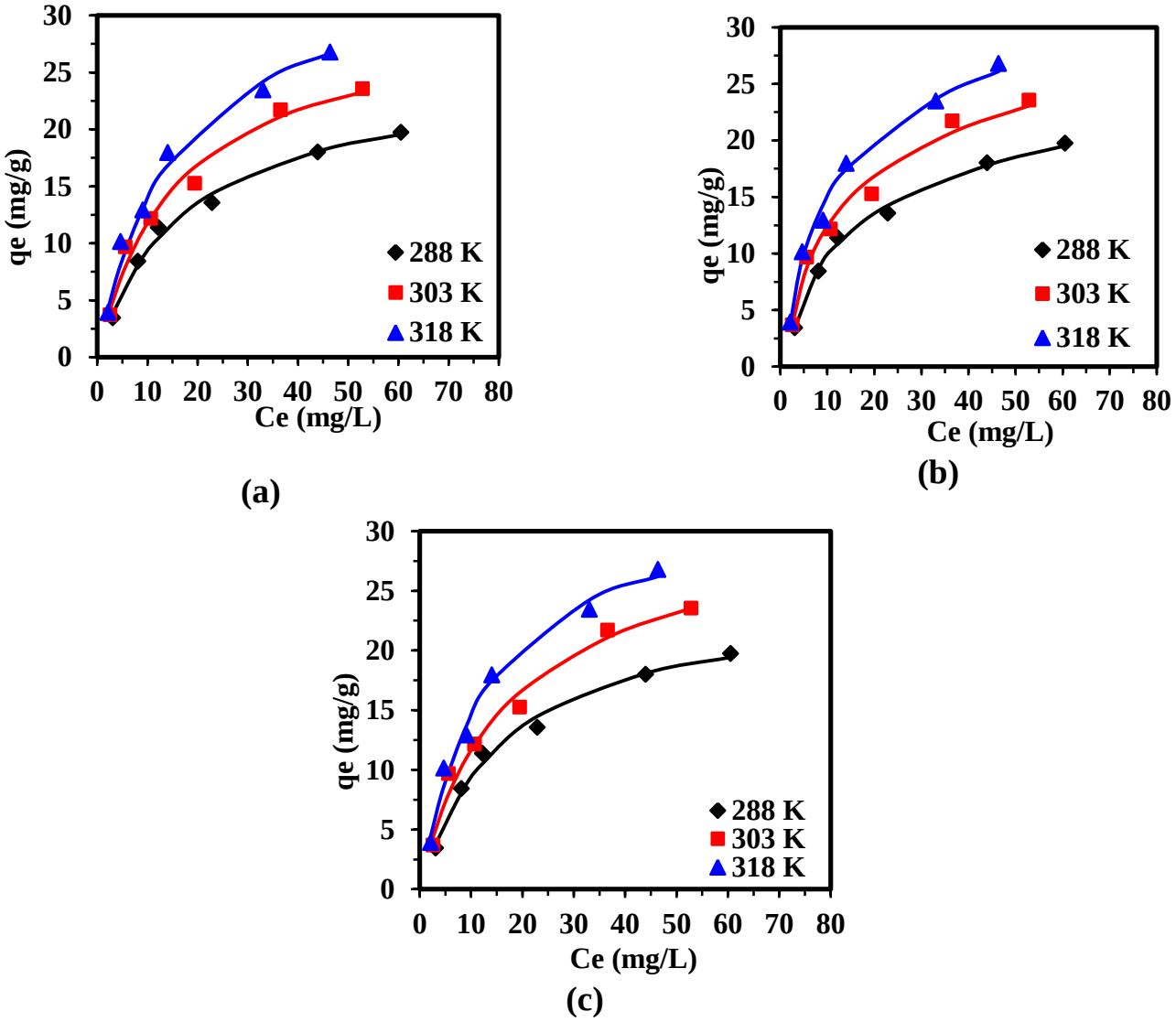

Fig. 5.15. Langmuir, Tempkin and RP isotherm models (a, b, c) plot of OFL sorption on DES-RHA.

Table 5.3. Langmuir, Redlich-Peterson (R-P) and Temkin isotherm parameters for the adsorption of ofloxacin (OFL) by DES functionalized RHA (m = 2 g/L, t = 720 min and pH = 6.5).

ISOTHERMS				
Langmuir	$q_e = \frac{q_m K_L C_e}{1 + K_L C_e}$			
T (K)	**K_L (L/mg)**	**q_m(mg/g)**	**R^2**	**CHI^2**
288 K	0.058	25.097	0.995	0.183
303 K	0.063	30.249	0.990	0.549
318 K	0.063	35.769	0.993	0.516

Freundlich $$q_e = K_F C_e^{1/n}$$

T (K)	K_F(mg/g) (L/mg)$^{1/n}$	1/n	R^2	CHI^2
288 K	2.614	0.509	0.98	0.99
303 K	2.850	0.551	0.98	1.31
318 K	3.492	0.548	0.97	1.67

Redlich-Peterson $$q_e = \frac{K_R C_e}{1 + a_R C_e^{\beta}}$$

T (K)	K_R (L/g)	a_R (L/mg)$^{1/\beta}$	β	R^2	CHI^2
288 K	1.407	0.046	1.046	0.995	0.179
303 K	2.058	0.091	0.929	0.991	0.536
318 K	2.344	0.053	1.063	0.993	0.424

Temkin $$q_e = \left(\frac{RT}{B_T}\right) ln(K_t C_e)$$

T (K)	K_T(L/mg)	B_T (J/mol)	R^2	CHI^2
288 K	0.606	5.419	0.998	0.1
303 K	0.697	6.395	0.992	0.317
318 K	0.795	7.232	0.996	0.228

5.4.4. Thermodynamics

The calculated thermodynamics constraints are mentioned in Table 5.4. The -ve value of ΔG° at each reaction temperature directed that adsorption of OFL on the DES–RHA surface was instantaneous in nature and thermodynamically favorable. Usually, when the ΔG° value ranges between ⁻20 kJ/mol to ⁻40 kJ/mol it indicates that the adsorption process is physisorption by nature. On other hand, when the ΔG° values less than ⁻40 kJ/mol then it follows the chemisorption adsorption process. The determined values of ΔG° are close to ⁻20 kJ/mol, demonstrating that the adsorption mechanism of OFL on DES–RHA is by physisorption. The decrease in ΔG° value with the enhancement in temperature from 288 K to 303 K indicated, increase in adsorption efficiency at high temperatures. Moreover, the +ve value of parameter ΔH° established the endothermic nature of OFL adsorption onto DES–RHA. Furthermore, the increase in the randomness of the adsorbates molecules at the liquid-solid interface was approved by the positive ΔS° values (Sharma, 2011). Thus, from the thermodynamic study, it can be determined that the sorption of OFL on DES–RHA was endothermic and spontaneous by nature.

Table 5.4. Thermodynamics parameters for the adsorption studies of ofloxacin (OFL) by DES functionalized RHA (*m* = 2 g/L, *t* = 720 min, C_o = 10-100 mg/L and *pH* = 6.5).

Thermodynamic Parameters	$lnK_D = \frac{-\Delta G^0}{RT} = \frac{\Delta S^0}{R} - \frac{\Delta H^0}{R}\frac{1}{T}$			
T (K)	K **x 10^{-3} (L/kg)**	ΔG^0 **(kJ/mol)**	ΔH^0 **(kJ/mol)**	ΔS^0 **(J/mol)**
288 K	2151.425	-18.375	27.454	157.481
303 K	2050.013	-19.210		
318 K	6478.243	-23.203		

5.4.5. Reusability of DES–RHA

The exhausted DES–RHA represented very good regeneration behavior (Fig.5.16). After 3 adsorption-desorption cycles, the OFL uptake of DES–RHA was reduced slightly at lower regeneration temperatures. While regenerating at 100 ^oC, 150 ^oC and 200 ^oC temperatures the reduction in removal percentage of OFL after 3 cycles were 14.2%, 18.2% and 26.1% respectively. With the rise in regeneration temperature, a decrease in the removal efficiency of OFL was observed. It may be because of the reduction in the active sites of the DES–RHA surface or slight degradation of DES at high temperatures. These results confirm that DES–RHA has good recycling ability and can be reused repeatedly for the removal of pharmaceutical wastes from industrial effluents.

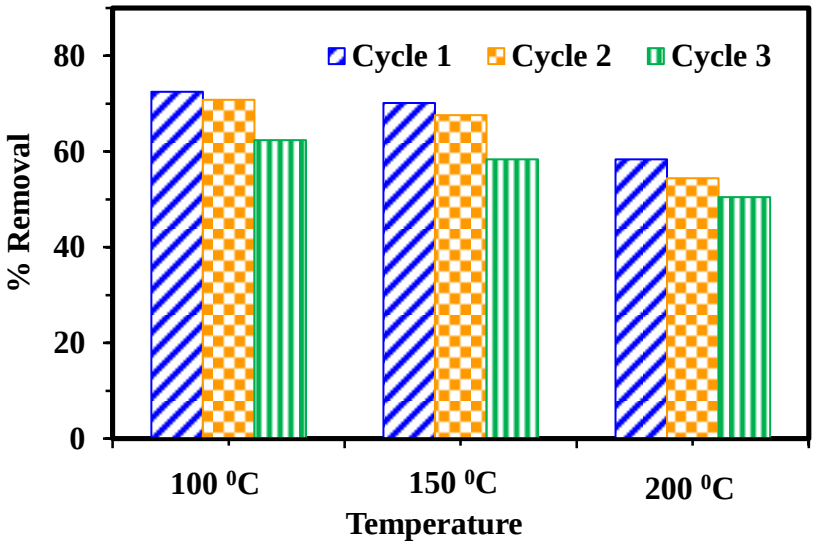

Fig. 5.16. Regeneration tests for heat treatment at temperatures of 100, 150 and 200 ^oC.

5.4.6 Comparative study

The adsorption capacity of DES–RHA was compared with different types of earlier used sorbents for OFL uptake. Table 5.5 represents the OFL removal capacity of DES–RHA with other sorbents reported in the literature. From this study, it is practical to recommend DES–RHA as an appropriate adsorbent for the removal of pharmaceutical waste.

Table 5.5. Comparison of DES–RHA with previously studied adsorbents.

Adsorbents	Removal	References
Zeolite	50%	Liu et al., 2020
Titanium oxide	65%	Wieren et al., 2012
CNTs	20-70%	Peng et al., 2014
ZnO nanoparticles	70%	Dhiman and Sharma, 2016
DES–RHA	77%	This study
Carbon Nanotubes (CNTs)	20-80%	Peng et al., 2012
Moringaoleifera pod husk (MOP)	90.98%	Wuana et al., 2015
HCl-treated sawdust (SD)	96%	Qureshi et al., 2015

5.5. CHARACTERIZATION RESULTS

5.5.1. Surface chemistry analysis (FTIR)

FTIR spectroscopy analysis was performed to recognize the intensities and functional groups existing on the adsorbent surface. Understanding functional groups of adsorbent are quite important because they govern their surface properties. The FTIR spectra of synthesized DES were performed to identify the hydrogen bonding between HBD and HBA and are shown in Fig. 5.17. (inset). The spectra represent characteristic broadband at 3292 cm^{-1} wavenumber, and this designates hydrogen bonding between the glycolic acid and ChCl in the DES. At lower wavenumber, three peaks at regions 1744, 1173, and 1088 cm^{-1} were detected. It confirms that the carbonyl group of glycolic acid and hydrogen bonding between the OH group of glycolic acid and Cl^- of ChCl (Sharma et al., 2019).

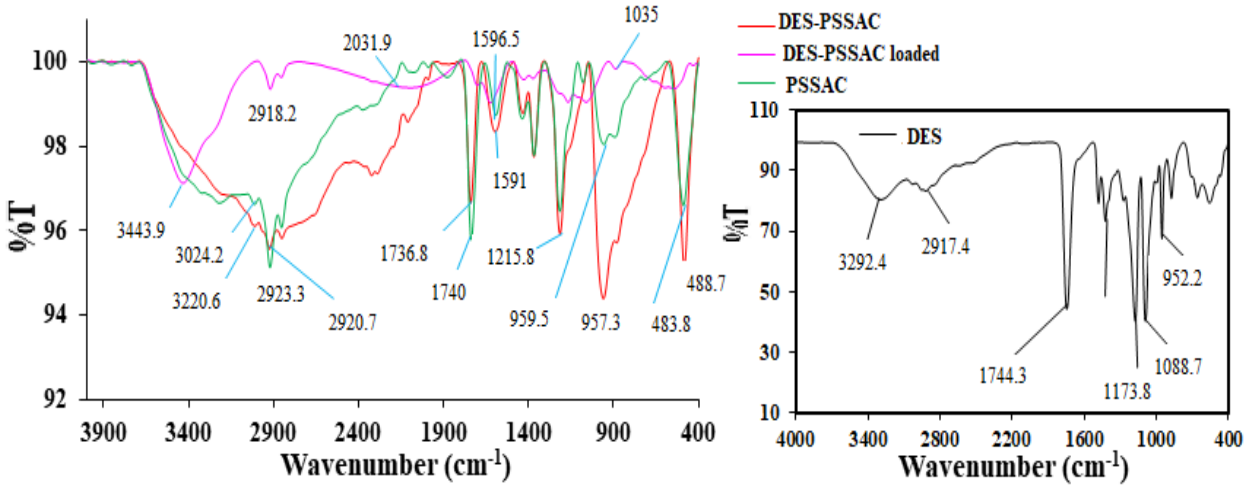

Fig. 5.17. FT-IR spectra of DES–PSSAC, DES–PSSAC loaded, PSSAC and DES (inset).

Besides, FTIR spectra of bare PSSAC were also generated and are depicted in Fig. 5.17. The PSSAC consists of various lipids, proteins, and polysaccharides comprising many functional groups like hydroxyl, amino, carboxyl, sulphydryl, phosphate, and sulphonate can act as binding sites for DOX molecules. The spectrum of PSSAC has a peak at 3024 cm^{-1}, which is ascribed to the presence of a free and hydrogen-bonded OH group. Peaks at 2923 cm^{-1} (−CH_3 stretching), 1740 cm^{-1} (−C=O stretching), 1596 cm^{-1} (−CO-NH bonding vibrations), 1215 cm^{-1} (−C–N stretching vibrations), 959 cm^{-1} (–COOH vibrations) and at 483 cm^{-1} (due to existence of alkyl and alkynes halides bending vibrations) were observed. The strong bands were seen at 2923, 1740, 1215 and 483 cm^{-1} mainly participate in the adsorption process (Yuan et al., 2009; Kumar and Randhawa, 2015).

To discover the changes in the surface characteristics of PSSAC after functionalization and DOX loading, FTIR spectra of DES–PSSAC and DOX loaded DES–PSSAC were generated and are shown in Fig. 5.17. The DES–PSSAC showed almost the same characteristic peaks in the FTIR spectrum as the bare PSSAC, which indicates that various lipids, proteins, and polysaccharides remain intact during the processing steps to form DES–PSSAC. The FT-IR spectrum of DES-PSSAC shows the various major peaks at 2920, 1736, 1215, and 488 cm^{-1}. Peaks at regions 2920 cm^{-1} and 1736 cm^{-1} could correspond to the presence of stretching in -NH_2 groups and the existence of stretching in the −C=O and -COOH groups (Mahapatra et al., 2012).

Furthermore, after the adsorption of DOX, strong and long absorption bands at 3000–3600 cm^{-1} with a maximum at near 3443 cm^{-1} are attributed to O–H stretching vibrations of hydrogen-bonded hydroxyl groups. Some new peaks seen at 3443, 2918, 2031, 1626, and 1035 cm^{-1} were also found on the spectrum (Fig. 5.17). Other peaks could be attributed at 2031 cm^{-1} for NH- stretching and 1035 cm^{-1} for –C–O stretching. One strong band is also seen at about 1626 cm^{-1} due to C=C vibrations in the aromatic region (Zhang et al., 2012; Esmaeli et al., 2013). According to the results, it can be perceived that some peaks were shifted or disappeared, and certain new peaks were also detected while comparing the loaded DES–PSSAC spectrum with DES–PSSAC and bare PSSAC. These changes demonstrate the possible contribution of all the functional groups on the surface of the DES–PSSAC in the adsorption process. Both new and shifted peaks might be due to the formation of bonds between DES–PSSAC and DOX molecules.

5.5.2. XRD analysis

X-ray diffraction (XRD) patterns and phase analysis of DES–PSSAC and DOX loaded DES–PSSAC was studied. The intensity of diffracted X-ray plotted against 2 theta angle for both are represented in Fig. 5.18. The diffraction patterns for the samples showed strong, broad peaks between 20^{o} to 30^{o} (2θ) for DOX-loaded and unloaded DES–PSSAC. The results indicated the presence of smectite, kaolinite, ilitite, and quartz. This was determined by the intensity of peaks that represents the amorphous and microporous nature of the adsorbent. Also, the existence of aluminophosphates and smectite was formed due to the occurrence of elements as SiO_2, TiO_2, K_2O, Fe_2O_3, and CaO_2 on the adsorbent surface (Treacy and Higgins, 2007). Moreover, due to the introduction of DOX into the DES–PSSAC matrix, two additional peaks at slightly higher 2θ (around 43.50^{o} and 84.56^{o}) causing deformation of kaolinite, ilitite, and aluminophosphates compound bond on to the adsorbent surface. These were some deviations observed between the DES–PSSAC and DOX loaded DES–PSSAC.

5.5.3. BET surface area and FESEM

The Brunauere Emmette Teller (BET) surface area and Barrette Joynere Hanlenda (BJH) adsorption/desorption surface area of DES–PSSAC was found to be 629.90 and 322.82 m^2/g, respectively. The average BET pore diameter was found at 2.19 nm, indicating that DES–PSSAC is microporous and an appropriate adsorbent for the adsorption of DOX antibiotic.

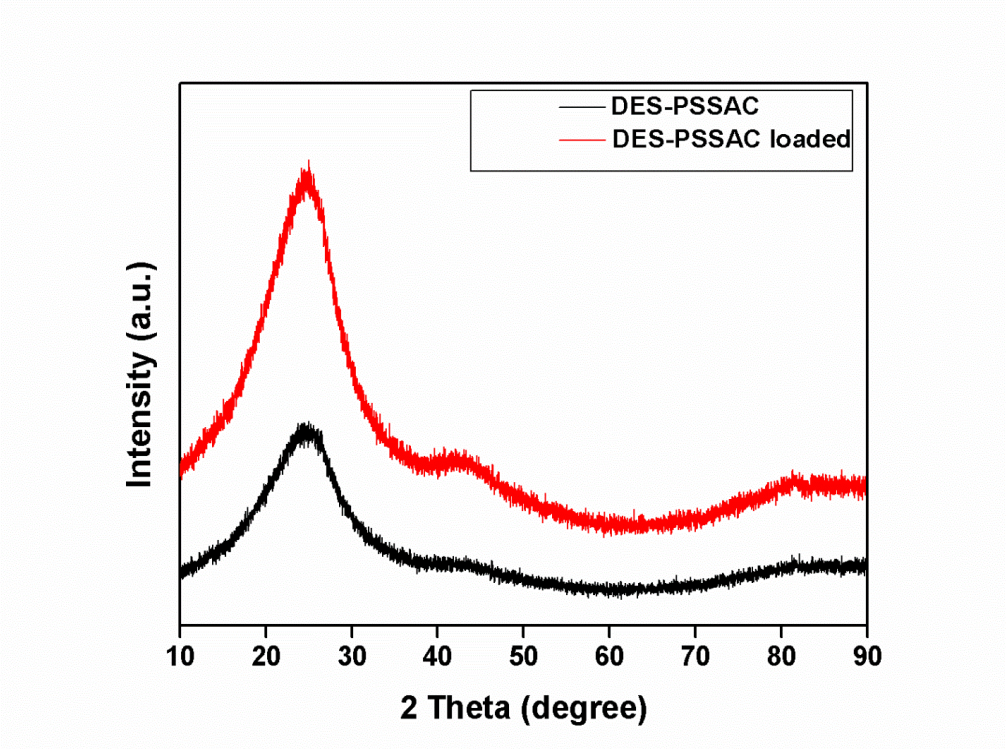

Fig. 5.18. X-ray diffraction (XRD) analysis of DES–PSSAC and DES–PSSAC loaded.

FESEM images of bare PSSAC, DES functionalized PSSAC and DOX loaded DES–PSSAC are shown in Fig. 5.19 (a), (b), and (c), respectively. These were studied to detect the surface morphologies before and after functionalization and adsorption. Fig. 5.19 (a) shows that the whole surface of bare PSSAC was covered with dark black colour cavities. After modifying PSSAC by DES, its deposition on the surface can be observed, as shown in Fig. 5.19 (b). No categorical change in the morphology or structure of PSSAC was observed after functionalization with DES. This indicates that used DES is capable of modifying PSSAC without compromising its basic structure. Before adsorption, DES–PSSAC possesses several heterogeneous pores where there is a good possibility for DOX antibiotic to be trapped and adsorbed. The surface of DOX-loaded adsorbent Fig. 5.19 (c) shows that the complete surface and voids are covered with a layer of antibiotic (Plecas et al., 2004). Therefore it confirms, the better dispersion and higher performance of DES functionalized PSSAC adsorbent for DOX uptake.

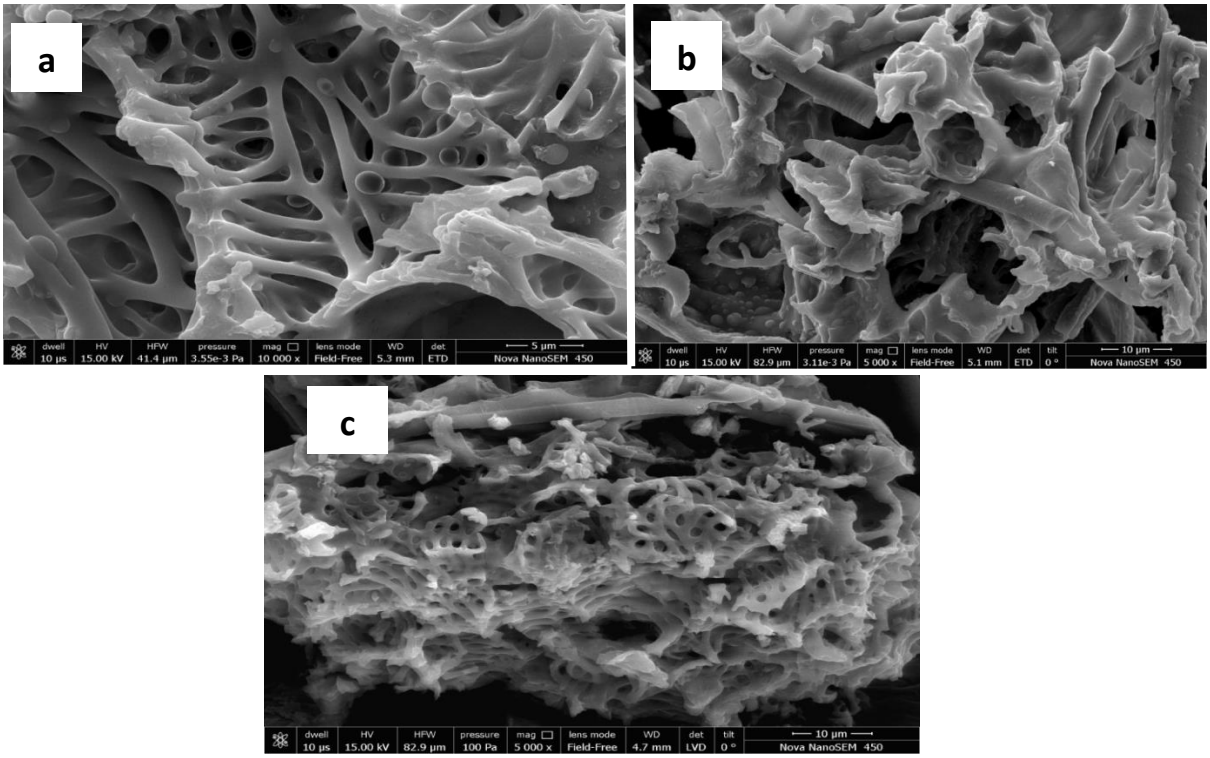

Fig. 5.19. FESEM images for PSSAC (a) DES–PSSAC (b) DES–PSSAC loaded (c).

5.6. OPTIMIZATION OF DES AMOUNT FOR PSSAC FUNTIONALISATION

"DES intercalated PSSAC was prepared by modifying PSSAC at different DES modification levels (2.5 mL/g to 6 mL/g). The adsorption performance of these DES-loaded PSSAC samples were evaluated for DOX uptake. As shown in Fig. 5.20, adsorption capacity for DOX increased continuously as DES concentration increased up to 5 mL/g; beyond this DES loading, no further improvement in performance was observed." This behavior might be due to unavailability of any sites for functionalization beyond 5 mL/g.

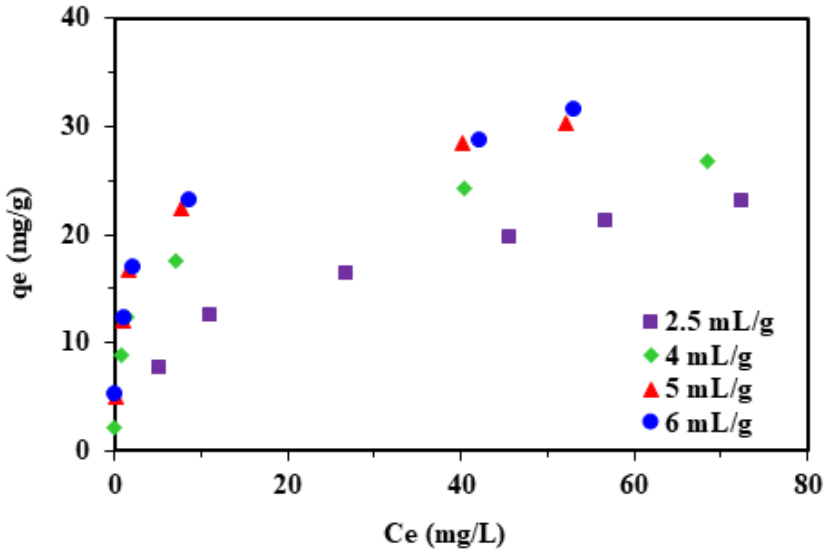

Fig. 5.20. Uptake of DOX by DES–PSSAC functionalized with different DES loading.

5.7. BATCH ADSORPTIVE REMOVAL OF WASTEWATER COMPRISING DOX BY DES-PSSAC

5.7.1. Effect of Different Parameters

5.7.1.1. Effect of adsorbent dosage on DOX removal

The effect of DES–PSSAC dosage on the adsorption performance of DOX was investigated at an initial DOX concentration of 25 mg/L, time = 600 min, agitation rate = 150 rpm, pH = 7.5 and temperature = 303 K, with varying adsorbent dosage from 0.1 to 4 g/L.

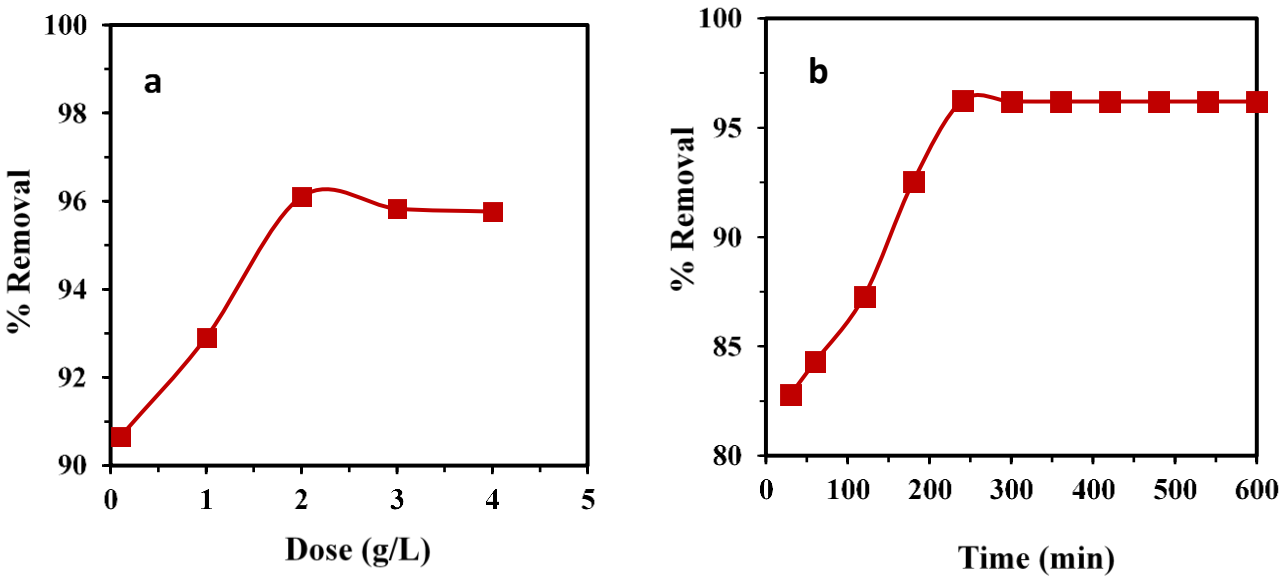

Fig. 5.21. DOX removal with varying adsorbent dosage at C_o = 25 mg/L, pH = 7.5, contact time = 600 min. (a) Effect of contact time on adsorptive uptake of DOX at C_o = 25 mg/ L, dose = 2 g/L, and pH = 7.5 (b).

As shown in Fig. 5.21 (a), an increase in adsorbent dosage resulted in increased DOX removal up to a certain value and after that the removal efficiency remained almost constant. The highest removal obtained was 96.22% at an adsorbent dose of 2 g/L. At a dose > 2 g/L, the DOX removal becomes almost constant as the surface concentration and the bulk solution concentration of DOX antibiotic come to equilibrium with each other. The enhancement in removal percentage with an increase in the adsorbent dose by keeping other parameters constant can be accredited to the higher availability of adsorption sites and larger surface area of the adsorbent. Whereas the amount of free ions in solution remains almost constant (Ozacar and Sengil, 2005; Mall et al., 2005). Opposite to this, the adsorption capacity (q_e) decreases with an increase in the adsorbent dose because of the saturation of adsorption sites during the adsorption process, where the particle-particle interaction leads to aggregation of solid particles that decrease in total surface area of the adsorbent (not shown here) (Lataye et al., 2009). As a result, 2 g/L DES–PSSAC dose was found to be optimum, and further experimental studies were undertaken with this optimum dose for DOX adsorption.

5.7.1.2. Effect of contact time on adsorptive uptake of DOX

The effect of contact time is an important parameter, which enables examination of the adsorbent efficiency for wastewater treatment. The time that takes the adsorbent to be saturated by the adsorbate is the point (time) at which maximum adsorption is noticed. The time-profile for adsorption of DOX on DES–PSSAC was examined at optimized parameters (adsorbent dose = 2 g/L, pH = 7.5, C_o = 25 mg/L and temperature = 303 K) and is presented in Fig. 5.21 (b). Results represent that DOX removal efficiency sharply rose during the first 240 min due to the availability of more vacant active adsorbent sites and then gradually approached a more or less constant value. Therefore, 240 min time can be assumed to be equilibrium time for DOX adsorption onto DES–PSSAC (Yu et al., 2003).

5.7.1.3. Effect of solution pH on adsorptive uptake of DOX

The pH of the aqueous medium is one of the most important controlling parameters of the adsorption processes that could stimulate the adsorbent's adsorption capacity. The effect of solution pH on adsorptive uptake of DOX was investigated at different solution pH ranging from 2 to 12 by keeping rest parameters constant (C_o = 25 mg/L, adsorbent dose = 2 g/L, contact time = 240 min) and the DOX removal efficiency is depicted in Fig. 5.22.

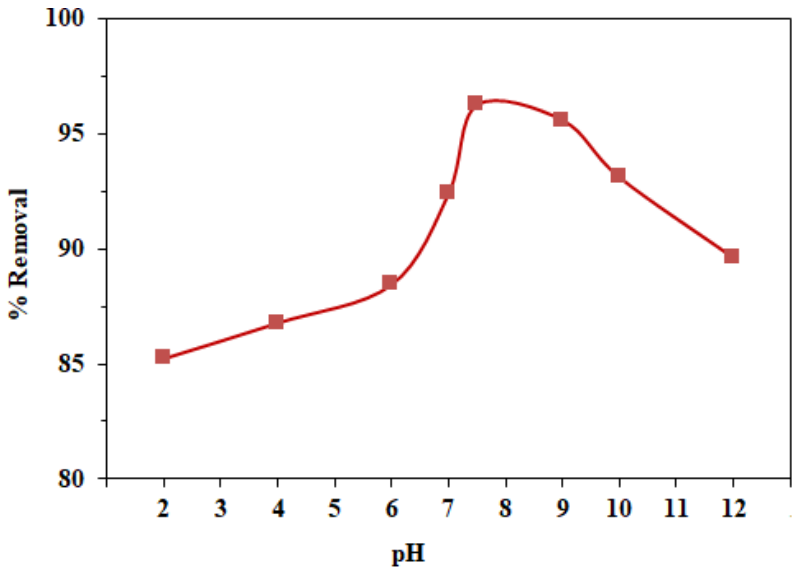

Fig. 5.22. Effect of solution pH on adsorptive uptake of DOX at C_o = 25 mg/L, dose = 2 g/L, contact time = 240 min.

It is evident from the figure that, with an increase in pH up to 4, the DOX removal (%) increment is very less and remains nearly constant to ≈ 85 %. However, for pH > 4, the DOX

removal (%) was found increasing being maximum (≈ 96.3 %) at pH = 7.5. Further, for pH > 7.5, the DOX removal (%) was observed decreasing due to the the same charges on DOX and adsorbent in this pH range.

The molecular structure of DOX shown in Fig. 5.23 represents its amphoteric nature. Due to the presence of different ionizable functional groups like phenol, alcohol and amino groups, DOX exist as cations, anions and zwitterion at different pH. There are three acid dissociation constants for DOX (pKa_1 = 3.5, pKa_2 = 7.7, pKa_3 = 9.5) (Gao et al., 2012). DOX is primarily cationic (DOX^+) for pH < 3.5, and anionic (DOX^-) for pH > 7.7. In between (3.5 < pH < 7.7), DOX is a zwitterionic compound (DOX^o) and at pH > 9.5 it exist as DOX^{2-} in solution. DES which is a mixture of glycolic acid and choline chloride represents high electronegativity due to the presence of chloride anion. As shown in Fig. 5.22, for pH ≤ 4, DOX uptake is due to the electrostatic forces between DES and DOX^+. As pH increases beyond pH > 4, the DOX molecules start attaining zwitterionic form, and in this pH range (3.5 ≤ pH ≤ 7.7), electrostatic interaction between DOX and DES–PSSAC diminishes due to the less availability of DOX^+. Further increase in adsorption efficiency in this pH range indicates that electrostatic interaction is not the only mechanism of adsorption between DOX and DES–PSSAC. In this pH range, adsorption is governed by hydrogen bonding between DOX^o and DES–PSSAC system. This happens due to the fact that GC3:1 DES represents high hydrogen bonding opportunity when the substrate is in zwitterionic form (Kaur et al., 2018).

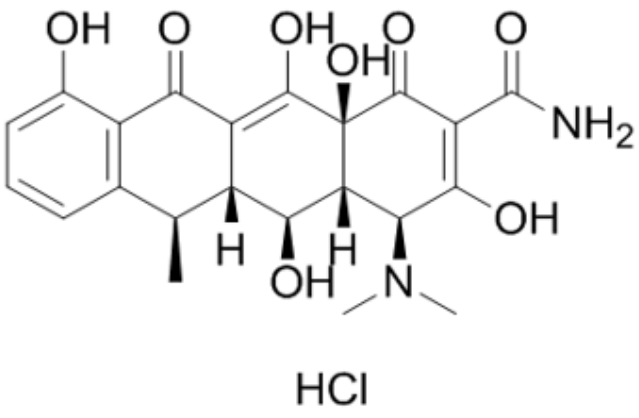

Fig. 5.23. Molecular structure of Doxycycline hydrochloride.

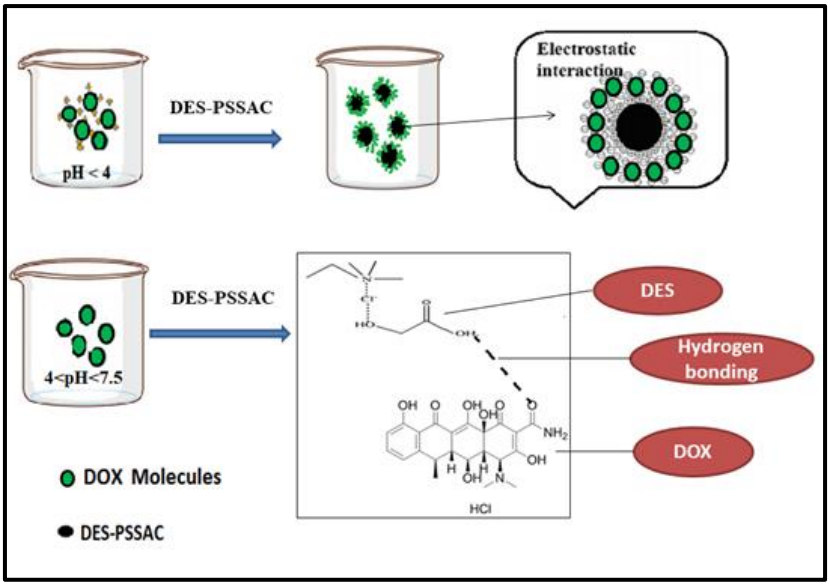

Fig. 5.24. Schematic representation of adsorption mechanism for DOX over DES–PSSAC via H-bonding and electrostatic interaction.

The hydrogen bonding mechanism of DOX^{o} and DES–PSSAC is shown in Fig. 5.24. Beyond pH > 7.7, the formation of DOX^{-} starts, and consequently, the adsorption due to hydrogen bonding weakens, resulting in decreased DOX removal (%). The above results conclude that 7.5 pH favours the DOX removal. Therefore in the present study, it is suggested that sorption studies of DOX on DES–PSSAC is pH-dependent and played the predominant role. Finally, a nearly natural pH value (7.5) was used to carry out further experiments.

Moreover, the FTIR spectra of DES–PSSAC before and after adsorption of DOX are displayed in Fig. 5.17. After adsorption of DOX, the peaks of aromatic C=C bonds shifted from 1620 to 1626 cm^{-1}, indicating that the π–π electron-donor-acceptor interaction between DOX and DES–PSSAC was the significant force for DOX adsorption (Jiang et al., 2016). At alkaline pH, the deprotonated form of DOX was anionic species. The dominant form of DOX would be zwitterionic and cationic species at neutral and lower pH, which were both available and effective π-electron-acceptors, which could induce strong π-π electron-donor-acceptor interaction with the DES–PSSAC.

5.7.2. Representation of adsorption Kinetics and Diffusivity

It is important to explore the adsorption kinetics to predict the rate of removal of DOX from its aqueous solution and understand the adsorption mechanism. The adsorption kinetics experiments were conducted for three different initial concentrations (C_0) 10, 25, and 50 mg/L

at optimized conditions (m = 2 g/L, pH = 7.5) at 303 K temperature and agitation rate of 150 rpm for 600 min. The kinetic studies of DOX adsorption onto DES–PSSAC were examined using pseudo 1st order, (Malik, 2003), pseudo 2nd order (Ho and McKay, 1999) and intra-particle diffusion models (Weber and Morris, 1963). The pseudo 1st and pseudo 2nd non–linear kinetic models were calculated by applying Eqs. 5.1 and 5.2 respectively.

$$q_t = q_e\ [1 - \exp(-K_f\, t)] \qquad \textbf{(5.1)}$$

Where q_t and q_e are the amounts of DOX adsorbed (mg/g) at any time (t) and at equilibrium, respectively, and k_f is the rate constant (per min).

Pseudo 2nd order model is represented as:

$$q_t = \frac{tk_s q_e^2}{1+tk_s q_e} \qquad \textbf{(5.2)}$$

Where, k_s is the rate constant (g/mg/min).

The initial adsorption rate, h (g/mg/min), is defined as;

$$h = k_s\, q_e^{\,2} \qquad \textbf{(5.3)}$$

The experimental results and fitting of the models are represented in Fig. 5.25 (a), where the adsorption capacities (q_t (mg/g)) are plotted against time (t (min)).

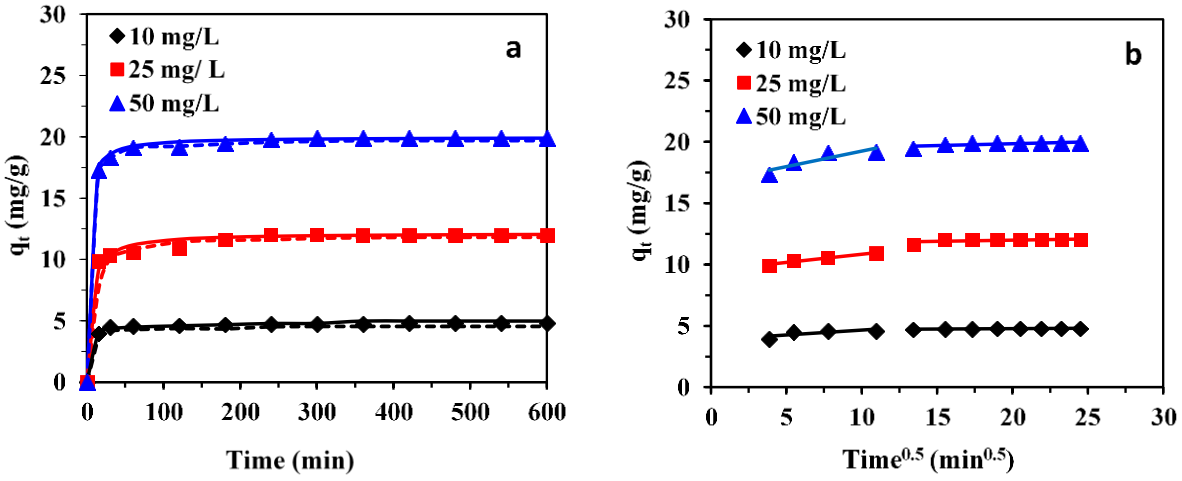

Fig. 5.25. Pseudo-first and second order adsorption kinetics at different initial concentrations (a). Weber–Morris plot q_t versus $t^{1/2}$ for DOX adsorption by DES–PSSAC (b).

At high DOX concentrations, the enhanced removal efficiency was observed. This was likely due to the enhanced driving force from the solution to the adsorbent surface, which enabled the speedy transfer of the DOX to the DES–PSSAC surface.

Table 5.6. Kinetic parameters for adsorption of DOX by DES-PSSAC (*m* = 2 g/L, *t* = 600 min and *pH* = 7.5, orbital shaking at 150 rpm, incubation at 303 K).

	C_0 (mg/L)		
	10	**25**	**50**
Pseuso first order			
k_f (min^{-1})	0.0230	0.0661	0.2300
$q_{e,exp}$ (mg/g)	4.78	12.02	19.89
$q_{e,cal}$ (mg/g)	4.12	12.01	19.89
R^2 (non-linear)	0.993	0.979	0.991
MPSD	20.551	8.795	3.973
Pseuso second order			
k_s (g/mg/min)	0.230	0.0159	0.0219
h (mg/g/min)	4.085	2.350	8.74
$q_{e,cal}$ (mg/g)	4.21	12.14	19.97
R^2 (non-linear)	0.997	0.993	1.00
MPSD	10.798	6.335	2.347
Weber Morris			
k_{id1} (mg/g $min^{-1/2}$)	0.0795	0.136	0.253
I_1	3.8497	9.481	16.71
R^2	0.646	0.940	0.797
k_{id2} (mg/g $min^{-1/2}$)	0.0062	0.0204	0.0296
I_2	4.641	11.578	19.246
R^2	0.747	0.336	0.541

The correlation coefficients (R^2) obtained by fitting the experimental data to the pseudo 1st order and pseudo 2nd order kinetic models, and corresponding model parameters are summarized in Table 5.6. While comparing the R^2 values for both the kinetic models, it indicated that adsorption of DOX on DES–PSSAC favours 2nd order kinetics, because its R^2 values was close to unity. These results suggest that adsorption process doesn't solely depends on electrostatic attraction between DOX and adsorbent, but on other mechanisms also (Vivek and Das, 2011).

Furthermore, to determine the rate-controlling step and intra-particle diffusion (IPD) mechanism, Weber-Morris model was adopted (Abel et al., 2017). The parameters of the Weber-Morris model are usually analyzed by the following equation:

$$q_t = \mathrm{k_{id}} \mathrm{t}^{1/2} + \mathrm{I} \qquad \textbf{(5.4)}$$

Where k_{id}: intra-particle diffusion rate constant (mg/g $\mathrm{min}^{1/2}$); I: intercept representing the boundary layer thickness on DES–PSSAC. The larger the intercept, the thicker is the boundary layer. The Weber-Morris model for IPD confirms that the sole rate-determining step is internal diffusion if the plot of q_t versus $\mathrm{t}^{1/2}$ composed of all data points is linear and passes through the origin. From the Weber-Morris plot shown in Fig. 5.25 (b), two linear regions were observed and it did not pass through the origin. This demonstrates that the adsorption process is governed by more than one mechanism. An initial, steep linear adsorption region was followed by a steady horizontal adsorption region with different rates.

From Fig. 5.25 (b) it is clear that in the first region where the adsorption capacity of DES–PSSAC increased sharply the process was controlled by film diffusion/boundary layer diffusion (Ahmed et al., 2015). Due to the capture of DOX molecules by exterior adsorbent surface. In the second region, the DOX molecules successively passed into the pores of DES–PSSAC and were further trapped by the interior surfaces by equilibrium diffusion mechanism. The values of rate constants of pore diffusion in terms of I_1 and I_2 rise as the initial DOX concentration increases from 10 mg/L to 50 mg/L (Table 5.6). This can be recognized as the high driving force for sorption associated with the high DOX concentration.

5.7.3. Adsorption isotherms

The equilibrium adsorption isotherms have been widely applied to explain how adsorbent interacts with adsorbate and also give a complete description of equilibrium concentration in the reaction system. The batch adsorption isotherm experiments of DOX on DES–PSSAC were carried out at temperatures of 288 K, 303 K, and 318 K. The initial DOX concentration was varied from 10 to 100 mg/L at an adsorbent dose of 2 g/L and pH 7.5. Several isotherm models, Langmuir, (Langmuir, 1918) Freundlich (Freundlich,1906), Temkin (Temkin and Pyzhev, 1940) and Redlich and Peterson (Redlich and Peterson, 1959) were applied to analyse the equilibrium data from the adsorption isotherm experiments, as given in Eqs. (5.5) - (5.8), respectively.

$$q_e = \frac{q_m K_L C_e}{1+K_L C_e} \quad \textbf{(5.5)}$$

$$q_{e} = K_F C_e^{1/n} \quad \textbf{(5.6)}$$

$$q_e = \left(\frac{RT}{B_T}\right) ln(K_t C_e) \quad \textbf{(5.7)}$$

$$q_e = \frac{K_R C_e}{1+a_R C_e^{\beta}} \quad \textbf{(5.8)}$$

Where q_e (mg/g) is the specific equilibrium amount of DOX adsorbate; q_m (mg/g) is the maximal adsorption capacity of DOX on DES–PSSAC adsorbent; K_L (L/mg) indicates the Langmuir constant which is correlated with the adsorption energy; C_e (mg/L) represents the adsorbate (DOX) equilibrium concentration; K_F (L/mg) is the Freundlich constant which associates with the adsorption capacity of DES–PSSAC (mg/g); n (g/L) is an empirical constant that indicates the adsorption effectiveness; B_T is the variation of adsorption energy (KJ/mol); k_T is the equilibrium binding constant (L/g) corresponding to the maximum binding energy. Furthermore, K_R and β are the R–P constants; Where the value of β is equal to 1 and the value of the parameter $a_R C_e^{\beta}$ is much bigger than 1. The ratio of K_R/a_R indicates the adsorption capacity and R is the universal gas constant (8.314 J/mol/K). All these parameters of the isotherm models were evaluated using nonlinear regressions.

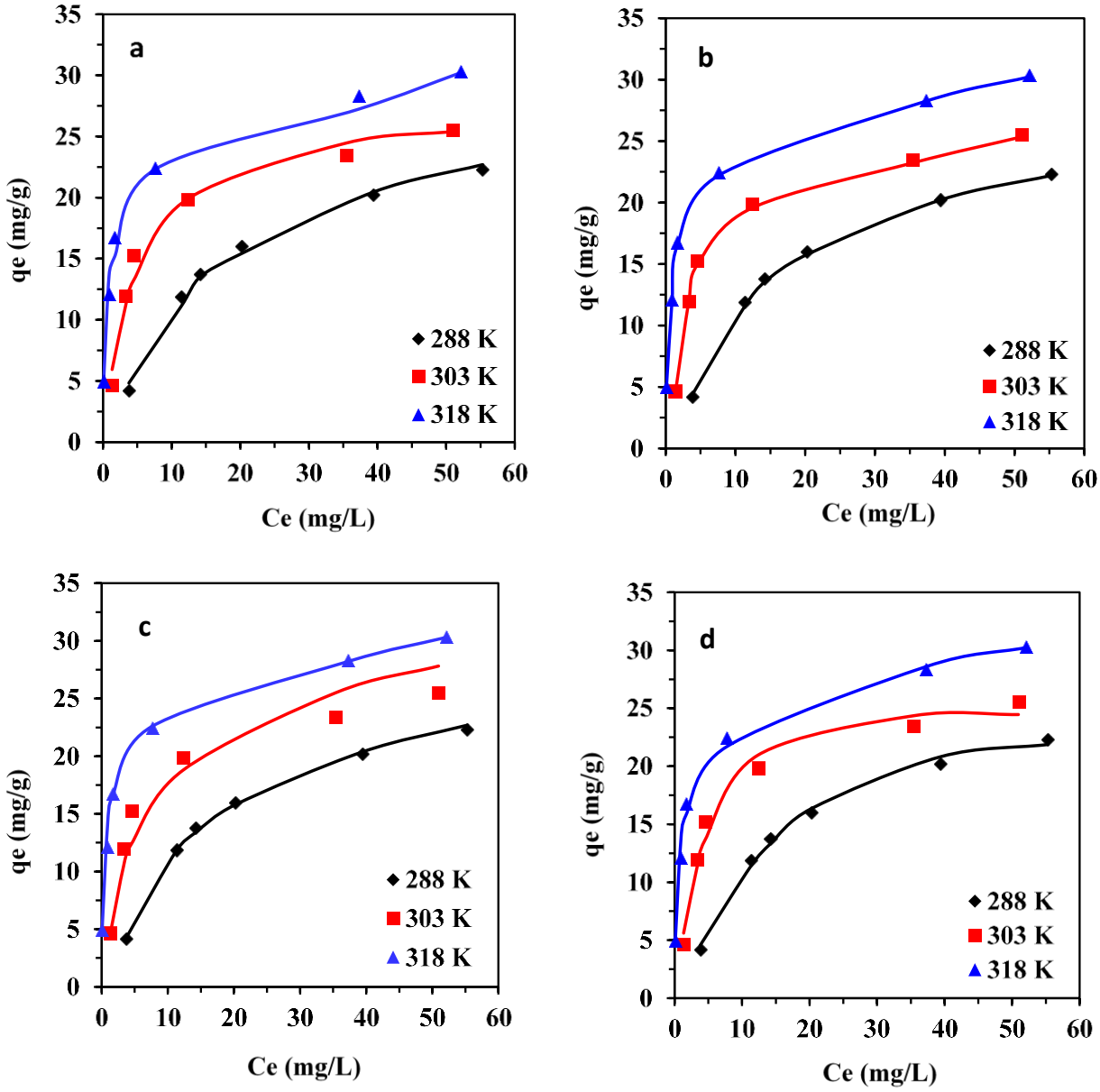

Fig. 5.26. Langmuir (a) Freundlich (b) Tempkin and R-P isotherm(c, d) models plot of DOX adsorption by DES–PSSAC at different temperatures.

The adsorption of the DOX on DES–PSSAC investigated at different temperatures and concentrations are shown in Fig. 5.26 (a, b, c and d). The parameters obtained by fitting of experimental data into Langmuir, Freundlich, Tempkin and R-P isotherm models are summarized in Table 5.7.

Table 5.7. Langmuir, Freundlich, Redlich-Peterson (R-P) and Temkin isotherm parameters for the adsorption of DOX by DES-PSSAC (*m* = 2 g/L, *t* = 240 min and *pH* = 7.5).

ISOTHERMS

Langmuir

$$q_e = \frac{q_m K_L C_e}{1 + K_L C_e}$$

T (K)	K_L (L/mg)	q_m (mg/g)	R^2	CHI^2
288 K	0.048	31.166	0.989	0.177
303 K	0.202	27.878	0.988	0.230
318 K	4.189	17.275	0.991	0.413

Freundlich

$$q_e = K_F C_e^{1/n}$$

T (K)	K_F (mg/g) $(L/mg)^{1/n}$	1/n	R^2	CHI^2
288 K	2.188	0.614	1.0	0.02
303 K	8.295	0.307	1.0	0.05
318 K	13.124	0.219	1.0	0.02

Redlich-Peterson

$$q_e = \frac{K_R C_e}{1 + a_R C_e^{\beta}}$$

T (K)	K_R (L/g)	a_R $(L/mg)^{1/\beta}$	β	R^2	CHI^2
288 K	1.277	0.010	1.337	0.992	0.093
303 K	4.825	0.110	1.123	0.988	0.547
318 K	95.347	5.929	0.839	0.996	0.221

Temkin

$$q_e = \left(\frac{RT}{B_T}\right) ln(K_t C_e)$$

T (K)	K_T(L/mg)	B_T (J/mol)	R^2	CHI^2
288 K	6.853	0.496	0.991	0.3
303 K	6.361	1.557	0.981	1.185
318 K	3.959	39.354	0.997	0.292

It is inferred from the results that adsorption data fitted best with the Freundlich and RP isotherm models as compared to Langmuir and Tempkin isotherms, thereby suggesting multilayer adsorption. The adsorption capacity of the DOX enhanced with the increment in reaction temperature, indicating that high temperature was favorable for the increase of adsorption capacity. The maximum adsorption capacity (q_{max}) was obtained to be 30.35 mg/g.

5.7.4. Thermodynamic study

Temperature is one of the key parameters which can affect the performance of the adsorption process. The thermodynamic study, can express the change in energy during the adsorption process and identify the feasibility of the process. The adsorptive behavior of DOX on DES–PSSAC was evaluated by studying experimental results at different temperature ranges. The thermodynamic adsorption parameters, changes of enthalpy ($\Delta H°$), changes in the entropy ($\Delta S°$), and changes in Gibb's free energy ($\Delta G°$) were evaluated because these are the real indicators for understanding the nature and type of adsorption process. These parameters were determined by the Van't Hoff equation (Eq. 5.9).

$$\ln K_d = \frac{-\Delta G^0}{RT} = \frac{\Delta S^0}{R} - \frac{\Delta H^0}{R}\frac{1}{T} \qquad \textbf{(5.9)}$$

Where K_d is the equilibrium constant, R is the gas constant (8.314 J/mol/K) and T is the temperature (K). The value of ΔH^0 and ΔS^0 can be determined by plotting ln K_d against 1/T as slope and intercept, respectively.

Table 5.8. Thermodynamics parameters for the adsorption studies of DOX by DES-PSSAC (*m* = 2 g/L, *t* = 240 min, C_o = 10-100 mg/L and *pH* = 7.5).

Thermodynamic Parameters $$lnK_D = \frac{-\Delta G^0}{RT} = \frac{\Delta S^0}{R} - \frac{\Delta H^0}{R}\frac{1}{T}$$

T (K)	K x 10^{-3} (L/kg)	ΔG^0 (kJ/mol)	ΔH^0 (kJ/mol)	ΔS^0 (J/mol)
288 K	4.2908	-20.028		
303 K	100.9215	-29.026	110.329	454.98
318 K	321.7605	-33.529		

The evaluated thermodynamics parameters are listed in Table 5.8. The positive value of the parameter ΔH^0 (110.33 kJ/mol) verifies that the adsorption of DOX on DES–PSSAC is an endothermic process. The positive value of ΔS^0 (454.98 kJ/mol/K) proposed the increase in the degree of freedom and randomness mobility of DOX molecules onto the DES–PSSAC surface. Moreover, the negative value of ΔG^0 at all temperatures indicated that the adsorption of DOX on the DES–PSSAC surface was spontaneous and feasible. Generally, if the value of ΔG^0 lies between ⁻20 kJ/mol to ⁻40 kJ/mol then the process is considered as physisorption and for less than ⁻40 kJ/mol chemisorption. The calculated values of ΔG^0 lies between ⁻20 to -33.5 kJ/mol, indicating that the adsorption mechanism of DOX on DES–PSSAC is by physisorption. Thus, it can be concluded that the thermodynamic adsorption study of DOX over DES–PSSAC was spontaneous and endothermic.

5.7.5. Adsorbent regeneration

The regeneration and stability of the adsorbents are very important for their practical application in different fields. Accordingly, the durability of prepared DES–PSSAC was evaluated for the three adsorption-desorption cycles. The regeneration study of exhausted DES–PSSAC was done at different temperatures (100, 150 and 200 ^oC) and adsorption performance was evaluated as shown in Fig. 5.27.

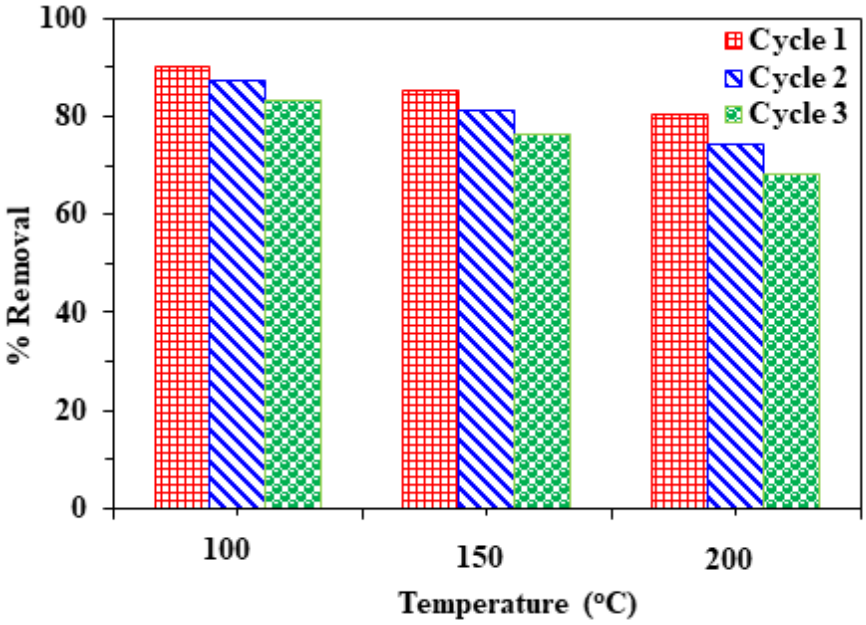

Fig. 5.27. Regeneration tests by heat treatment at different temperatures (100, 150 and 200 ^{o}C) and performance evaluation.

The drop in removal percentage of DOX after 3 cycles for 100, 150 and 200 ^{o}C were 13.11 %, 20.01 % and 28.11 % respectively. It shows that there is not any great loss of adsorption active sites after three runs. Nonetheless, the drop in removal percentage of DOX with an increase in regeneration temperature can be attributed to a slight degradation of DES at high temperatures. Moreover, FTIR spectra of regenerated DES–PSSAC after the third cycle were also generated. The presence of the characteristic bands of the DES at 1736, 1215 and 3222 cm^{-1} in the FT-IR spectra of regenerated DES–PSSAC (Fig. 5.28) represents the stability of the DES modified PSSAC throughout the adsorption/regeneration processes. The regeneration study reveals good stability and reusability of the exhausted DES–PSSAC, which makes it a potentially applicable adsorbent for the treatment of pharmaceutical wastewater.

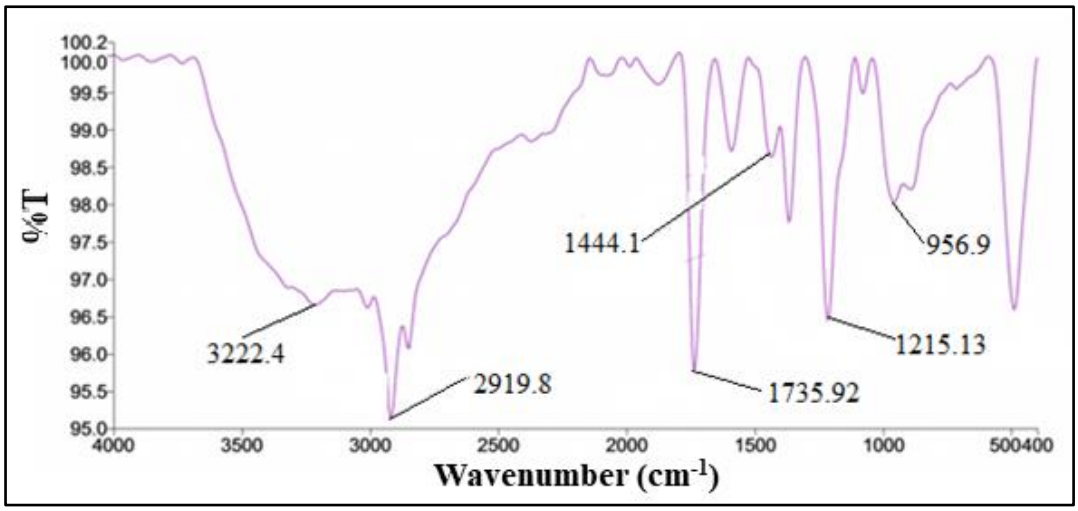

Fig. 5.28. FTIR spectra of regenerated DES–PSSAC.

Chapter – 6

CONCLUSION

The objective of this work was to study the applicability of agri-residue based adsorbents for the uptake of OFL and DOX antibiotics from its aqueous solution. Two different types of adsorbents, *i.e.,* activated carbon derived from agri-residue and DES functionalized activated carbon, were considered for the adsorptive study of different antibiotics. On the basis of results obtained from the present study of pharmaceutical wastewater comprising OFL and DOX antibiotics, the following major conclusions were drawn.

6.1. Adsorption studies of OFL and DOX antibiotics

- The low-cost and abundantly available agri-residues with high silica content, played a significant role in removal of pharmaceutical contaminants from wastewater. Use of such agri-residues will help in solving the problem of bio-waste burden and achieving the goal of "treating waste by waste" simultaneously.
- This study presented the effective removal of model compounds (OFL and DOX) and the appropriate management of exhausted adsorbents by stabilization method using Portland cement as a solidifying agent.
- Optimized conditions for efficient removal of OFL by RHA were pH = 6, m = 7.94 g/L, C_o = 62.5 mg/L and t = 430 min, by PJAC were pH = 6, m = 16.23 g/L, C_o = 57 mg/L and t = 336 min, by DES-RHA were pH = 6.5, m = 2 g/L, C_o = 25 mg/L and t = 480 min.
- Optimized conditions for efficient removal of DOX by RHA were pH = 6, m = 5 g/L, C_o = 89.73 mg/L and t = 85.85 min, by PJAC were pH = 6, m = 5 g/L, C_o = 62.8 mg/L and t = 10 min, by PSSAC were pH = 8, m = 2.5 g/L, C_o = 25 mg/L and t = 300 min, by DES-PSSAC were pH = 7.5, m = 2 g/L, C_o = 25 mg/L and t = 240 min.
- The adsorption capacity of all the combinations was found to increase with increased concentration of adsorbate and temperature, indicating that the adsorption is substrate limiting and endothermic in nature.
- All antibiotic-adsorbent combinations followed pseudo-second-order kinetics except OFL-RHA. Adsorption isotherm data fitted well with the Langmuir, Freundlich, Temkin and R-P isotherm models for OFL and DOX adsorption. Adsorption process was controlled by intra-particle diffusion along with surface diffusion.

- From the thermodynamic study, positive value of ΔS◦ suggested high randomness of the adsorbate molecules at the liquid-solid interface and good affinity between adsorbent and adsorbate. Negative ΔG◦ with increasing magnitude with increased temperature depicted the feasible and spontaneous adsorption of OFL and DOX antibiotics onto adsorbents. The positive value of ΔH^o approves that overall reaction is endothermic.
- This study reveals that, the use of DESs as a functionalization agent can be a good approach for the modification of materials to be applied for the removal of pharmaceutical pollutants. Due to it's distinctive advantages, DESs can be an attractive functionalization agent and replacement for traditional organic solvents and ionic liquids.
- It can be concluded that, adsorption technology could be utilized as an effective technique for the remediation of real pharmaceutical industry wastewater in the common effluent treatment plant (CETP), and if used with traditional treatment technologies, it may achieve the best possible treatment goals at the lowest possible cost.

6.2. Solidification/Stabilisation (S/S), Cytotoxicity assessment and Reusability studies

- By the solidification/stabilisation (S/S) process, almost complete encapsulation of contaminants was achieved. More than 95% OFL and more than 98% DOX was encapsulated in portland cement, which was present in different exhausted adsorbents.
- Moreover, cytotoxicity assessment of leachate from solidified adsorbent, indicated that most of the antibiotic was encapsulated inside the cement and the antibiotic present in leachate was not sufficient to eradicate the growth of selected bacterial strains. This confirmed that stabilization is a safe and effective disposal technique for the proper management of exhausted adsorbents.
- More importantly, the good regeneration capability of exhausted adsorbents proves that these can be utilized as a low-cost and eco-friendly bio-adsorbent to treat pharmaceutical wastewater. For DES functionalized adsorbents, DES-PSSAC and DES-RHA more than 70 % and 50 % removal was achieved respectively till third cycle.
- The high adsorption capacities, good regeneration ability and low-cost of adsorbents exhibited that adsorbents prepared in this study have a wide range of applications for the removal of pharmaceutically active compounds.

FUTURE RECOMMENDATION

- In order to industrially apply DES functionalized adsorbents, more DESs should be explored, which can give high adsorption capacity for pharmaceutical compounds in wastewater. It is also of great importance to further investigate the toxicity and biodegradability of the DESs.
- To find the broad application prospects of argi-residues as adsorbent in the future management of pharmaceutical pollutants, real wastewater should be investigated. Since the toxic nature of wastewater was tested only against the clinical isolates of selected microbes, a comprehensive study dealing with toxicity analysis of actual wastewater using different bioassays test methods could exhibit more reliable and viable results.
- Solidification/stabilisation process should be adopted at industrial scale for safe disposal of bulk exhausted adsorbents and to find its possible use as a building material.
- Pilot and full scale unit can be taken into consideration to evaluate the uptake ability of studied adsorbents for industrial implementations.

REFERENCES

Abbas, R.F., Hami, H.K., Mahdi, N.I., 2019. Removal of doxycycline hyclate by adsorption onto cobalt oxide at three different temperatures: isotherm, thermodynamic and error analysis. International Journal of Environmental Science and Technology 16, 5439–5446.

Abel, S., Nybom, I., Maenpaa, K., Hale, S.E., Cornelissen, G., Akkanen, J., 2017. Mixing and capping techniques for activated carbon based sediment remediation–Efficiency and adverse effects for Lumbriculus variegatus. Water Research 114, 104–112.

Abou-Mesalam, M.M., 2003. Sorption kinetics of copper, zinc, cadmium and nickel ions on synthesized silico-antimonate ion exchanger. Colloids and Surfaces A: Physicochemical and Engineering Aspects 225, 85–94.

Acar, F.N., Eren, Z., 2006. Removal of Cu (II) ions by activated poplar sawdust (Samsun Clone) from aqueous solutions. Journal of Hazardous Materials 137, 909–914.

Agarwal, M., 2005. Effects of air pollution on agriculture: An issue of national concern. National Academy Science Letters 28, 93–106.

Ahmed, M.B., Zhou, J.L., Ngo, H.H., Guo, W., 2015. Adsorptive removal of antibiotics from water and wastewater: progress and challenges. Science of the Total Environment 532, 112–126.

Ahmed, M.J., Theydan, S.K., 2012. Adsorption of cephalexin onto activated carbons from Albizia lebbeck seed pods by microwave-induced KOH and K_2CO_3 activations. Chemical Engineering Journal 211–212, 200–207.

Ahmed, M.J., Theydan, S.K., 2013a. Microporous activated carbon from siris seed pods by microwave-induced KOH activation for metronidazole adsorption. Journal of Analytical and Applied Pyrolysis 99, 101–109.

Ahmed, M.J., Theydan, S.K., 2013b. Microwave assisted preparation of microporous activated carbon from siris seed pods for adsorption of metronidazole antibiotic. Chemical Engineering Journal 214, 310–318.

Ahmed, M.J., Theydan, S.K., 2014. Fluoroquinolones antibiotics adsorption onto microporous activated carbon from lignocellulosic biomass by microwave pyrolysis. Journal of the Taiwan Institute of Chemical Engineers 45, 219–226.

Ali, M.M.M., Ahmed, M.J., 2017. Adsorption behavior of doxycycline antibiotic on NaY zeolite from wheat (*Triticum aestivum*) straws ash. Journal of the Taiwan Institute of Chemical Engineers 81, 218–224.

Alidadi, H., Dolatabadi, M., Davoudi, M., Barjasteh-Askari, F., Jamali-Behnam, F., Hosseinzadeh, A., 2018. Enhanced removal of tetracycline using modified sawdust: optimization, isotherm, kinetics and regeneration studies. Process Safety and Environmental Protection 117, 51–60.

Alvarez-Torrellas, S., Peres, J.A., Gil-Alvarez, V., Ovejero, G., Garcia, J., 2017. Effective adsorption of non-biodegradable pharmaceuticals from hospital wastewater with different carbon materials. Chemical Engineering Journal 320, 319–329.

Amorim, K.P., Romualdo, L.L., Andrade, L.S., 2014. Performance and kinetic-mechanistic aspects in the electrochemical degradation of sulfadiazine on boron-doped diamond electrode. Journal of Brazilian Chemical Society 25, 1484–1492.

Ania, C.O., Bandosz, T.J., 2006. Metal-loaded polystyrene-based activated carbons as dibenzothiophene removal media via reactive adsorption. Carbon 44 (12), 2404–2412.

Antunes, M., Esteves, V.I., Guegan, R., Crespo, J.S., Fernandes, A.N., Giovanela, M., 2012. Removal of diclofenac sodium from aqueous solution by Isabel grape bagasse. Chemical Engineering Journal 192, 114–121.

Arami, M., Limaee, N.Y., Mahmoodi, N.M., Tabrizi, N.S., 2005. Removal of dyes from colored textile wastewater by orange peel adsorbent: Equilibrium and Kinetic studies. Journal of Colloid and Interface Science 288, 371–376.

Aravindhan, R., Rao, J.R., Nair, B.U., 2007. Removal of basic yellow dye from aqueous solution by adsorption on green algae: Caulerpa scalpelliformis. Journal of Hazardous Materials 142, 68–76.

Arslan-Alaton, I., Dogruel, S., 2004. Pre-treatment of penicillin formulation effluent by advanced oxidation processes. Journal of Hazardous Materials B 112, 105–113.

Arslan-Alaton, I., Olmez-Hanci, T., 2017. The Use of Al and Fe Nanoparticles for the Treatment of Micropollutants. Nanotechnologies for Environmental Remediation 61–114.

Aydin, A.H., Bulut, Y., Yavuz, O., 2004. Acid dyes removal using low cost adsorbents. International Journal on Environment Pollution 21, 97–104.

Azarpira, H., Balarak, D., 2016. Rice husk as a Biosorbent for Antibiotic Metronidazole Removal: Isotherm Studies and Model validation. International Journal of ChemTech Research 9 (7), 566–573.

Azmi, M.A., Ismail, N.A.A., Rizamarhaiza, M., Hasif, W.M., Taib, H., 2016. Characterization of Silica Derived from Rice Husk (Muar, Johor, Malaysia) decomposition at different temperatures. AIP Conference Proceedings 1756, 020005.

Baccar, R., Sarra, M., Bouzid, J., Feki, M., Blanquez, P., 2012. Removal of pharmaceutical compounds by activated carbon prepared from agricultural by-product. Chemical Engineering Journal 211–212, 310–317.

Bahrami, A., Simon, U., Soltani, N., Zavareh, S., Schmidt, J., Pech-Canul, M.I., Gurlo, A. 2017. Eco-fabrication of hierarchical porous silica monoliths by ice-templating of rice husk ash. Green Chemistry 19 (1), 188–195.

Bahrami, A., Soltani, N., Pech-Canul, M.I., Gonzalez, L.A., 2016. Development of metal-matrix composites from industrial/agricultural waste materials and their derivatives. Critical Reviews in Environmental Science and Technology 46 (2), 143–208.

Balarak, D., Mostafapour, F.K., Azarpira, H., 2016. Adsorption isotherm studies of tetracycline antibiotics from aqueous solutions by maize stalks as a cheap biosorbent. International Journal of Pharmacy and Technology 8, 16664–16675.

Bansal, P., Verma, A., Aggarwal, K., Singh, A., Gupta, S., 2016. Investigations on the degradation of an antibiotic Cephalexin using suspended and supported TiO_2: Mineralization and durability studies. The Canadian Journal of Chemical Engineering 94 (7), 1269–1276.

Barreto, L.S.S., Ghisi, E., Godoi, C., Oliveira, F.J.S., 2020. Reuse of ornamental rock solid waste for stabilization and solidification of galvanic solid waste: Optimization for sustainable waste management strategy. Journal of cleaner production 275, 122996.

Batzias, F., Sidiras, D., Schroeder, E., Weber, C., 2009. Simulation of dye adsorption on hydrolyzed wheat straw in batch and fixed-bed systems. Chemical Engineering Journal 148, 459–472.

Belhachemi, M., Addoun, F., 2011. Comparative adsorption isotherms and modeling of methylene blue onto activated carbons. Applied Water Science 1, 111–117.

Beltrame, K.K., Cazetta, A.L., de Souza, P.S.C., Spessato, L., Tais, L., Almeida, S.V.C., 2018. Adsorption of caffeine on mesoporous activated carbon fibers prepared from pineapple plant leaves. Ecotoxicology and Environmental Safety 147, 64–71.

Bie, R., Chen, P., Song, X., Ji, X., 2016. Characteristics of municipal solid waste incineration fly ash with cement solidification treatment. Journal of the Energy Institute 89, 704–712.

Boeckel, T.P., Gandra, S., Ashok, A., Caudron, Q., Grenfell, B.T., Levin, S.A., Laxminarayan, R., 2014. Global antibiotic consumption 2000 to 2010: an analysis of national pharmaceutical sales data. The Lancet Infectious Diseases 14 (8), 742–750.

Box, G.E.P., Behnken, D.W., 1960. Some new three level designs for the study of quantitative Variables. Technometrics 2, 455–475.

Brigante, M., Avena, M., 2016. Biotemplated synthesis of mesoporous silica for doxycycline removal. Effect of pH, temperature, ionic strength and Ca^{2+} concentration on the adsorption behavior. Microporous and Mesoporous Materials 225, 534–542.

Brown, K.D., Kulis, J., Thomson, B., Chapman, T.H., Mawhinney, D.B., 2006. Occurrence of antibiotics in hospital, residential and dairy effluent, municipal wastewater and the Rio Grande in New Mexico. Science of the Total Environment 366, 772–783.

Cai, N., Larese-Casanova, P., 2014. Sorption of carbamazepine by commercial graphene oxides: A comparative study with granular activated carbon and multiwalled carbon nanotubes. Journal of Colloid and Interface Science 426, 152–161.

Chakraborty, S., Chowdhury, S., Papita, P.D., 2011. Adsorption of Crystal Violet from aqueous solution onto NaOH-modified rice husk. Carbohydrate Polymers 86, 1533–1541.

Chao, Y., Zhu,W., Wu, X., Hou, F., Xun, S., Wu, P., Ji, H., Xu, H., Li, H., 2014. Application of graphene-like layered molybdenum disulfide and its excellent adsorption behavior for doxycycline antibiotic. Chemical Engineering Journal 243, 60–67.

Chaturvedi, G., Kaur, A., Umar, A., Khan, M.A., Algarni, H., Kansal, S.K., 2020. Removal of fluoroquinolone drug, levofloxacin from aqueous phase over iron based MOFs, MIL-100(Fe). Journal of Solid State Chemistry 281, 121–129.

Chen, Y., Wang, F., Duan, L., Yang, H., Gao, J., 2016. Tetracycline adsorption onto rice husk ash, an agricultural waste: Its kinetic and thermodynamic studies. Journal of Molecular Liquids 222, 487–494.

Choi, K.J., Kim, S.G., Kim, S.H., 2008. Removal of tetracycline and sulfonamide classes of antibiotic compound by powdered activated carbon. Environmental Technology 29, 333–342.

Choudhary, M., Singh, D., Devnani, G.L., Mishra, A., 2021. Impact of various surface modifications on agro waste rice husk and its reinforced polymer composites. Materials Today: Proceedings DOI: https://doi.org/10.1016/j.matpr.2021.01.187

Chowdhury, S., Mishra, R., Saha, P., Kushwaha, P., 2011. Adsorption thermodynamics, kinetics and isosteric heat of adsorption of malachite green onto chemically modified rice husk. Desalination 265, 159–168.

Chuudhary, R., Chaudhari, P.K., 2017. Removal of pollutants of coking wastewater by adsorption. Desalination and Water Treatment 75, 45-57.

Collier, N.C., Milestone, N.B., Hill, I.M., Godfrey, I.M., 2006. The disposal of radioactive ferric floc. Waste Management 26, 769–775.

Crini, G., Lichtfouse, E., 2019. Advantages and disadvantages of techniques used for wastewater treatment. Environmental chemistry letters 17, 145–155.

Danish, M., Hashim, R., Ibrahim, M.N.M., Sulaiman, O., 2014. Optimization study for preparation of activated carbon from Acacia mangium wood using phosphoric acid. Wood Science and Technology 48, 1069–1083.

Das, S.K., Bhowal, J., Das, A.R., Guha, A.K., 2006. Adsorption behavior of Rhodamine B on Rhizopus oryzae biomass. Langmuir 22, 7265–7272.

Demeyer, A., Nkana, J.C.V., Verloo, M.G., 2001. Characteristics of wood ash and influence on soil properties and nutrient uptake: an overview. Bioresource Technology 77, 287–295.

Deng, W., Li, N., Zheng, H., Lin, H., 2016. Occurrence and risk assessment of antibiotics in river water in Hong Kong. Ecotoxicology and Environmental Safety 125, 121–127.

Dhiman, N., Sharma, N., 2016. Adsorption potential of ZnO nanoparticles for ofloxacin hydrochloride from aqueous solutions. International Journal of Advanced Technology in Engineering and Science 4, 1–10.

Dureja, H., Madan, A.K., 2007. Adsorption in pharmacy: A review. Drug Delivery Technology 7(8), 58–64.

El-Ghenymy, A., Garrido, J.A., Rodriguez, R.M., Cabot, P.L., Centellas, F., Arias, C., Brillas, E., 2013. Degradation of sulfanilamide in acidic medium by anodic oxidation with a boron-doped diamond anode. Journal of Electroanalytical Chemistry 689, 149–157.

El-Shafey, E.I., Al-Lawati, H., Al-Sumri, A.S., 2012. Ciprofloxacin adsorption from aqueous solution onto chemically prepared carbon from date palm leaflets. Journal of Environmental Sciences 24, 1579–1586.

El-Zahhar, A.A., Awwad, N.S., El-Katori, E.E., 2014. Removal of bromophenol blue dye from industrial waste water by synthesizing polymer-clay composite. Journal of Molecular Liquids 199, 454–461.

Esmaeli, A., Jokar, M., Kousha, M., Daneshvar, E., Zilouei, H., Karimi, K., 2013. Acidic dye wastewater treatment onto a marine macroalga, *Nizamuddina zanardini* (Phylum: Ochrophyta). Chemical Engineering Journal 217, 329–336.

Fernandez, A.M.L., Rendueles, M., Diaz, M., 2014. Competitive retention of sulfamethoxazole (SMX) and sulfamethazine (SMZ) from synthetic solutions in a strong anionic ion exchange resin. Solvent Extraction and Ion Exchange 32, 763–781.

Fernandez-Sanroman, A., Acevedo-García, V., Pazos, M., Sanromán, M.A., Rosales, E., 2020. Removal of sulfamethoxazole and methylparaben using hydrocolloid and fiber industry wastes: Comparison with biochar and laccase-biocomposite. Journal of Cleaner Production 271, 122436.

Fick, J., Soderstrom, H., Lindberg, R.H., Phan, C., Tysklind, M., Larsson, D.G., 2009. Contamination of surface, ground, and drinking water from pharmaceutical production. Environmental Toxicology and Chemistry 28 (12), 2522–2527.

Foo, K.Y., Hameed, B.H., 2011. Preparation of activated carbon from date stones by microwave induced chemical activation: Application for methylene blue adsorption. Chemical Engineering Journal 170, 338–341.

Francis, P.S., Adcock, J.L., 2005. Chemiluminescence methods for the determination of Ofloxacin. Analytica Chimica Acta 541, 3–12.

Freundlich, H.M.F., 1906. Uber die adsorption in losungen. Journal of Physical Chemistry 57, 385–470.

Gailius, A., Vacenovska, B., Drochytka, R., 2010. Hazardous Wastes Recycling by Solidification/Stabilization. Materials science (Medziagotyra) 16, 165–169.

Gamiz, B., Pignatello, J.J., Cox, L., Hermosin, M.C., Celis, R., 2016. Environmental fate of the fungicide metalaxyl in soil amended with composted olive-mill waste and its biochar: An enantioselective study. Science of the Total Environment 541, 776–783.

Gao, B., Li, P., Yang, R., Li, A., Yang, H., 2019. Investigation of multiple adsorption mechanisms for efficient removal of ofloxacin from water using lignin-based adsorbents**.** Scientific Reports 9, 637.

Gao, Y., Li, Y., Zhang, L., Huang, H., Hu, J., Shah, S.M., Su, X., 2012. Adsorption and removal of tetracycline antibiotics from aqueous solution by graphene oxide. Journal of Colloid and Interface Science 368 (1), 540–546.

Gercel, O., Ozcan, A., Ozcan, A.S., Gercel, H.F., 2007. Preparation of activated carbon from a renewable bio-plant of Euphorbia rigida by H_2SO_4 activation and its adsorption behaviour in aqueous solutions. Applied Surface Science 253, 4843–4852.

Ghaemi, M., Absalan, G.H., 2015. Fast removal and determination of doxycycline in water samples and honey by Fe_3O_4 magnetic nanoparticles. Journal of the Iranian Chemical Society 12, 1–7.

Gobel, A., McArdell, C.S., Joss, A., Siegrist, H., Giger, W., 2007. Fate of sulfonamides, macrolides and trimethoprim in different wastewater treatment technologies. Science of the Total Environment 372, 361–371.

Goyne, K.W., Chorover, J., Kubicki, J.D., Zimmerman, A.R., Brantley, S.L., 2005. Sorption of the antibiotic ofloxacin to mesoporous and nonporous alumina and silica. Journal of Colloid and Interface Science 283, 160–170.

Gregg, S.J., Sing, K.S.W., Salzberg, H.W., 1967. Adsorption Surface Area and Porosity. Journal of the Electrochemical Society 114, 279.

Guinea, E., Brillas, E., Centellas, F., Canizares, P., Rodrigo, M.O., Saez, C., 2009. Oxidation of enrofloxacin with conductive-diamond electrochemical oxidation, ozonation and Fenton oxidation. A comparison. Water Research 43, 2131–2138.

Guo, Z.B., Liu, J., Liu, F.L., 2015. Selective adsorption of p-CNB and o-CNB in silica-coating HZSM-5 zeolite. Microporous and Mesoporous Materials 213, 8–13.

Gupta, H., Gupta, B., 2015c. Adsorption of polycyclic aromatic hydrocarbons on banana peel activated carbon. Desalination and Water Treatment 57 (20), 9498–9509.

Gupta, H., Kumar, H., Kumar, M., Gehlaut, A.K., Gaur, A., Sachan, S., Park, J.W., 2020. Synthesis of biodegradable films obtained from rice husk and sugarcane bagasse to be used as food packaging material. Environmental Engineering Research 25, 506-514.

Gupta, V.K., Nayak, A., 2012. Cadmium removal and recovery from aqueous solu-tions by novel adsorbents prepared from orange peel and Fe_2O_3 nanoparticles. Chemical Engineering Journal 180, 81–90.

Gupta, V.K., Nayak, A., Agarwal, S., 2015a. Bioadsorbents for remediation of heavy metals: current status and their future prospects. Environmental Engineering Research 20 (1), 001–018.

Gupta, V.K., Saleh, T.A., Pathania, D., Rathore, B.S., Sharma, G., 2015b. A cellulose acetate based nano composite for photocatalytic degradation of methylene blue dye under solarlight. Ionics 21, 1787–1793.

Hameed, B.H., Mahmoud, D.K., Ahmad, A.L. 2008. Equilibrium modeling and kinetic studies on the adsorption of basic dye by a low-cost adsorbent: Coconut (Cocosnucifera) bunch waste**.** Journal of Hazardous Materials 158, 65–72.

Hapeshi, E., Fotiou, I., Fatta-Kassinos, D., 2013. Sonophotocatalytic treatment of ofloxacin in secondary treated effluent and elucidation of its transformation products. Chemical Engineering Journal 224, 96–105.

Hassan, S.A., Ali, F.J., 2014. Assessment of the Ofloxacin (Novecin) Adsorption from aqueous solutions by Two Agricultural Wastes. International Journal of Advanced Scientific and Technical Research 2, 950–965.

Hayyan, M., Looi, C.Y., Hayyan, A., Wong, W.F., Hashim, M.A., 2015. In vitro and in vivo toxicity profiling of ammonium-based deep eutectic solvents. PLoS One 10 (2), 1−18.

Ho, Y.S., McKay, G., 1999. Pseudo-second order model for adsorption processes. Process Biochemistry 34, 45−465.

Hu, D., Wang, L., 2016. Adsorption of amoxicillin onto quaternized cellulose from flax noil: Kinetic, equilibrium and thermodynamic study. Journal of the Taiwan Institute of Chemical Engineers 64, 227–234.

Huang, X., Sillanpää, M., Gjessing, E.T., Peräniemi, S., Vogt, R.D., 2010. Environmental impact of mining activities on the surface water quality in Tibet: Gyama valley. Science of the Total Environment 408, 4177–4184.

Ibrahim, S.C., Hanafiah, M.A.K.M., Yahya, M.Z.A., 2006. Removal of cadmium from aqueous solution by adsorption on sugarcane bagasse. Journal of Agricultural Environment Sciences 1, 179–184.

Ifelebuegu, A.O., Ukpebor, J.E., Obidiegwu, C.C., Kwofi, B.C., 2015. Comparative potential of black tea leaves waste to granular activated carbon in adsorption of endocrine disrupting compounds from aqueous solution. Global Journal of Environmental Science and Management 1, 205–214.

Ihsanullah, H.A., Asmaly, T.A., Saleh, T., Laoui, V.K., Gupta, M.A., 2015. Enhanced adsorption of phenols from liquids by aluminum oxide/carbon nanotubes: comprehensive study from synthesis to surface properties. Journal of Molecular Liquids 206, 176–182.

Imteaz, M.A., Ahsan, A., Shanableh, A., 2013. Reliability analysis of rainwater tanks using daily water balance model: Variations within a large city. Resources, Conservation and Recycling 77, 37–43.

Iveti, T.B., Dimitrievska, M.R., Fincur, N.L., Dacanin, L.R., Guth, I.O., Abramovi, B.F., 2014. Effect of annealing temperature on structural and optical properties of Mg-doped ZnO nanoparticles and their photocatalytic efficiency in alprazolam degradation. Ceramics International 40, 1545–1552.

Ji, L., Chen, W., Zheng, S., Xu, Z., Zhu, D., 2009. Adsorption of sulfonamide antibiotics to multiwalled carbon nanotubes. Langmuir 25, 11608–11613.

Jiang, L., Liu, Y., Zeng, G., Xiao, F., Hu, X., Hu, X., Wang, H., Li, T., Zhou, L., Tan, X., 2016. Removal of 17β-estradiol by few-layered graphene oxide nanosheets from aqueous solutions: External influence and adsorption mechanism. Chemical Engineering Journal 284, 93–102.

Jung, C., Park, J., Lim, K.H., Park, S., Heo, J., Her, N., Oh, J., Yun, S., Yoon, Y., 2013. Adsorption of selected endocrine disrupting compounds and pharmaceuticals on activated biochars. Journal of Hazardous Materials 263, 702–710.

Kaliannan, D., Palaninaicker, S., Palanivel, V., Mahadeo, M.A., Ravindra, B.N., Jae-Jin, S., 2019. A novel approach to preparation of nano-adsorbent from agricultural wastes (Saccharum officinarum leaves) and its environmental application. Environmental Science and Pollution Research 26(6), 5305–5314.

Kaur, G., Singh, N., Rajor, A., 2021a. Ofloxacin adsorptive interaction with rice husk ash: Parametric and exhausted adsorbent disposability study. Journal of Contaminant Hydrology 236, 103737.

Kaur, G., Singh, N., Rajor, A., 2021b. Efficient adsorption of doxycycline hydrochloride using deep eutectic solvent functionalized activated carbon derived from pumpkin seed shell. ChemistrySelect 6, 3139–3150.

Kaur, G., Singh, N., Rajor, A., 2021c. Adsorption of doxycycline hydrochloride onto powdered activated carbon synthesized from pumpkin seed shell by microwave-assisted pyrolysis. Environmental Technology and Innovation 23, 101601.

Kaur, G., Singh, N., Rajor, A., Kushwaha, J. P., 2021 d. Deep eutectic solvent functionalized rice husk ash for effective adsorption of ofloxacin from aqueous environment. Journal of Contaminant Hydrology 242, 103847.

Kaur, P., Rajani, N., Kumawat, P., Singh, N., Kushwaha, J.P., 2018. Performance and mechanism of dye extraction from aqueous solution using synthesized deep eutectic solvents. Colloids and Surfaces A 539, 85–91.

Kaur, P., Rajani, N., Kumawat, P., Singh, N., Kushwaha, J.P., 2018. Performance and mechanism of dye extraction from aqueous solution using synthesized deep eutectic solvents. Colloids and Surfaces A 539, 85–91.

Kavitha, D., Namasivayam, C., 2007. Experimental and kinetic studies on methylene blue adsorption by coir pith carbon. Bioresource Technology 98, 14–21.

Kezerle, A., Velic N., Hasenay, D., Kovacevic D., 2018. Lignocellulosic Materials as Dye Adsorbents: Adsorption of Methylene Blue and Congo Red on Brewers' Spent Grain. Croatica Chemica Acta 91 (1), 53–64.

Khan, F., Husain, T, Hejazi, R., 2004. An overview and analysis of site remediation technologies. Journal of Environmental Management 71, 95–122.

Kim, Y.H., Lee, B., Choo, K.H., Choi, S.J., 2014. Adsorption characteristics of phenolic and amino organic compounds on nano-structured silicas functionalized with phenyl groups. Microporous and Mesoporous Materials 185,121–129.

Kogbara, R.B., Al-Tabbaa, A., Yi, Y., Stegemann, J.A., 2013. Cement–fly ash stabilisation/solidification of contaminated soil: Performance properties and initiation of operating envelopes. Journal of Applied Geochemistry 33, 64–75.

Konicki, W., Pełech, I., Mijowska, E., Jasinska, I., 2012. Adsorption of anionic dye Direct Red 23 onto magnetic multi-walled carbon nanotubes-Fe_3C nanocomposite: kinetics, equilibrium and thermodynamics. Chemical Engineering Journal 210, 87–95.

Kosutic, K., Dolar, D., Asperger, D., Kunst, B., 2007. Removal of antibiotic from model wastewater by RO/NF membrane. Separation and Purification Technology 53, 244–249.

Kristiansson, E., Fick, J., Janzon, A., Grabic, R., Rutgersson, C., Weijdegard, B., Soderstrom, H., Larsson, D.J., 2011. Pyrosequencing of antibiotic-contaminated river sediments reveals high levels of resistance and gene transfer elements. PloS One 6 (2), 17038.

Kumar, M., Tamilarasan, R., 2017. Kinetics, equilibrium data and modeling studies for the sorption of chromium by Prosopis juliflora bark carbon. Arabian Journal of Chemistry 10, S1567– S1577.

Kumar, P., Wasewar, K.L., Chand, S., Padmini, B.N., Teng, T.T., 2010. Adsorption of Cadmium ions from Aqueous Solution using Granular Activated Carbon and Activated Clay. Journal of Clean soil air water 38 (7), 649-656.

Kumar, P.S., Ramalingam, S., Senthamarai, C., Niranjanaa, M., Vijayalakshmi, P., Sivanesan, S., 2010. Adsorption of dye from aqueous solution by cashew nut shell: Studies on equilibrium isotherm, kinetics and thermodynamics of interactions. Desalination 261, 52–60.

Kumar, S., Randhawa, J.K., 2015. Solid lipid nanoparticles of stearic acid for the drug delivery of paliperidone. Royal Society of Chemistry Advances 5, 68743–68750.

Kummerer, K., 2009. “Antibiotics in the aquatic environment – A review – part I”, Chemosphere 75 (4), 417–434.

Kummerer, K., 2010. Pharmaceuticals in the environment. Annual Review of Environment and Resources 35 (1), 57–75.

Kunquan, L., Zheng, Z., Ye, L., 2010. Characterization and lead adsorption properties of activated carbons prepared from cotton stalk by one-step of H_3PO_4 activation. Journal of Hazardous Materials 181, 440–447.

Kushwaha, J.P., Srivastava, V.C., Mall, I.D., 2010a. Organics removal from dairy wastewater by electrochemical treatment and residue disposal. Separation and Purification Technology 76, 198–295.

Kushwaha, J.P., Srivastava, V.C., Mall, I.D., 2010b. Treatment of dairy wastewater by commercial activated carbon and bagasse fly ash: Parametric, kinetic and equilibrium modelling, disposal studies. Bioresource Technology 101 (10), 3474–3483.

Kushwaha, J.P., Srivastava, V.C., Mall, I.D., 2011. Studies on electrochemical treatment of dairy wastewater using aluminium electrode. Environmental and Energy Engineering 57, 2589–2598.

Kyzas, G.Z., Fu, J., Lazaridis, N.K., Bikiaris, D.N., Matis, K.A., 2015a. New approaches on the removal of pharmaceuticals from wastewaters with adsorbent materials. Journal of Molecular Liquids 209, 87–93.

Kyzas, G.Z., Koltsakidou, A., Nanaki, S.G., Bikiaris, D.N., Lambropoulou, D.A., 2015b. Removal of beta-blockers from aqueous media by adsorption onto graphene oxide. Science of the Total Environment 537, 411–420.

Lakshmi, U.R., Srivastava, V.C., Mall, I.D., Lataye, D.H., 2009. Rice husk ash as an effective adsorbent: Evaluation of adsorptive characteristics for Indigo Carmine dye. Journal of Environmental Management 90, 710–720.

Langdon, K.A, Warne, M.S., Kookanaz, R.S., 2010. Aquatic Hazard Assessment for Pharmaceuticals, Personal Care Products and Endocrine-Disrupting Compounds from Biosolids-Amended Land. Integrated Environmental Assessment and Management 6, 663–676.

Langmuir, I., 1918. The adsorption of gases on plane surfaces of glass, mica and platinum. Journal of the American Chemical Society 40, 1361–1403.

Larsson, D.J., de Pedro, C., Paxeus, N., 2007. Effluent from drug manufactures contains extremely high levels of pharmaceuticals. Journal of Hazardous Materials 148 (3), 751–755.

Lataye, D.H., Mishra, I.M., Mall, I.D., 2009. Adsorption of α-picoline onto rice husk ash and granular activated carbon from aqueous solution: Equilibrium and thermodynamic study. Chemical Engineering Journal 147, 139–149.

Lawal, I.A., Lawal, M.M., Akpotu, S.O., Azeez, M.A., Ndungu, P., Moodley, B., 2018. Theoretical and experimental adsorption studies of sulfamethoxazole and ketoprofen on synthesized ionic liquids modified CNTs. Ecotoxicology and Environmental Safety 161, 542–552.

Lee, L.Y., Gan, S, Tan, M.S., Lim, S.S., Lee, X.J., Lam, Y.F., 2016. Effective removal of Acid Blue 113 dye using overripe Cucumis sativus peel as an eco-friendly biosorbent from agricultural residue. Journal of Cleaner Production 113, 194–203.

Liew, R.K., Nam, W.L., Chong, M.Y., Phang, X.Y., Su, M.H., Yek, P.N.Y., Ma, N.L., Cheng, C.K., Chong, C.T., Lam, S.S., 2018. Oil palm waste: An abundant and promising feedstock for microwave pyrolysis conversion into good quality biochar with potential multi-applications. Process Safety and Environmental Protection 115, 57–69.

Lin, Y., Xu, S., Jia, L., 2013. Fast and highly efficient tetracyclines removal from environmental waters by graphene oxide functionalized magnetic particles. Chemical Engineering Journal 225, 679–685.

Liu, H., Chen, W., Liu, C., Liu, Y., Dong, C., 2014. Magnetic mesoporous clay adsorbent: Preparation, characterization and adsorption capacity for atrazine. Microporous and Mesoporous Materials 194, 72–78.

Liu, M., Hou, L., Yu, S., Xi, B., Zhao, Y., Xia, X., 2013. MCM-41 impregnated with A zeolite precursor: Synthesis characterization and tetracycline antibiotics removal from aqueous solution. Chemical Engineering Journal 223, 678–687.

Liu, P., Liu, W., Jiang, H., Chen, J., Li, W., Yu, H., 2012. Modification of bio-char derived from fast pyrolysis of biomass and its application in removal of tetracycline from aqueous solution. Bioresource Technology 121, 235–240.

Liu, S., Xu, W., Liu, Y., Tan, X., Zeng, G., Li, X., Liang, J., Zhou, Z., Yan, Z., Cai, X., 2017. Facile synthesis of Cu(II) impregnated biochar with enhanced adsorption activity for the removal of doxycycline hydrochloride from water. Science of the Total Environment 592, 546–553.

Liu, Y., Liu, X., Lu, S., Zhao, B., Wang, Z., Xi, B., Guo, W., 2020. Adsorption and biodegradation of sulfamethoxazole and ofloxacin on zeolite: Influence of particle diameter and redox potential. Chemical Engineering Journal 384, 123346.

Liu, S.J., Liu, Y.G., Tan, X.F., Liu, S.B., Li, M.F., Liu, N., Yin, Z.H., Tian, S.R., 2019. Facile synthesis of MnO_x-loaded biochar for the removal of doxycycline hydrochloride: effects of ambient conditions and co-existing heavy metals. Journal of Chemical Technology and Biotechnology 94, 2187–2197.

Lombardo, A., Roncaglioni, A., Benfentati, E., Nendza, M., Segner, H., Fernandez, A., Kuehne, R., Franco, A., Patine, E., Schueuermann, G., 2014. Integrated testing strategy (ITS) for bioaccumulation assessment under REACH. Environment International 69, 40–50.

Lonappan, L., Rouissi, T., Brar, S.K., Verma, M., Rao, Y., 2018. An insight into the adsorption of diclofenac on different biochars: Mechanisms, surface chemistry, and thermodynamics. Bioresource Technology 249, 386–394.

Lu, M.C., Chen, Y.Y., Chiou, M.R., Chen, M.Y., Fan, H.J., 2016. Occurrence and treatment efficiency of pharmaceuticals in landfill leachates. Waste Management 55, 257–264.

Luyao, W., Sisi, Y., 2020. Factors Affecting the Solidification and Stabilization Effect of Hazardous Waste. IOP Conference Series: Earth and Environmental Science 512, 012040.

Mahapatra, K., Ramteke, D.S., Paliwal, L.J., 2012. Production of activated carbon from sludge of food processing industry under controlled pyrolysis and its application for methylene blue removal. Journal of Analytical and Applied Pyrolysis 95, 79–86.

Mahmood, T., Saddique, M.T., Naeem, A., Westerhoff, P., Mustafa, S., Alum, A., 2011. Comparison of different methods for the point of zero charge determination of NiO. Industrial and Engineering Chemistry Research 50 (17), 10017–10023.

Malik, P.K., 2003. Use of activated carbons prepared from sawdust and rice-husk for adsorption of acid dyes: a case study of Acid Yellow 36. Dyes and Pigments 56, 239–249.

Mall, I.D., Srivastava, V.C., Agarwal, N.K., Mishra, I.M., 2005. Removal of congo red from aqueous solution by bagasse fly ash and activated carbon: kinetic study and equilibrium isotherm analyses. Chemosphere 61, 492–501.

Martins, A.C., Pezoti, O., Cazetta, A.L., Bedin, K.C., Yamazaki, D.A.S., Bandoch, G.F.G., Asefa, T., Visentainer, J.V., Almeida, V.C., 2015. Removal of tetracycline by NaOH-activated carbon produced from macadamia nut shells: kinetic and equilibrium studies. Chemical Engineering Journal 260, 291–299.

Mashkoor, F., Nasar, A., Inamuddin, 2020. Carbon nanotube-based adsorbents for the removal of dyes from waters: a review. Environmental Chemistry Letters 18, 605–629.

Mestre, A.S., Pires, J., Nogueira, J.M.F., Carvalho, A.P., 2007. Activated carbons for the adsorption of ibuprofen. Carbon 45, 1979–1988.

Mestre, A.S., Pires, J., Nogueira, J.M.F., Parra, J.B., Carvalho, A.P., Ania, C.O., 2009. Waste-derived activated carbons for removal of ibuprofen from solution: Role of surface chemistry and pore structure. Bioresource Technology 100 (5), 1720–1726.

Michael, I., Hapeshi, E., Acena, J., Perez, S., Petrovic, M., Zapata, A., Barcelo, D., Malato, S., Fatta-Kassinos, D., 2013. Light-induced catalytic transformation of ofloxacin by solar Fenton in various water matrices at a pilot plant: Mineralization and characterization of major intermediate products. Science of the Total Environment 461–462, 39–48.

Mishra, S,B., Sachan, S., Mishra, P.K., Ramesh, M.R., 2014. Preparation and characterization of PPEES-TiO_2 composite micro-porous UF membrane for oily water treatment. Procedia Material Science 5, 123-129.

Mo, J., Yanga, Q., Zhang, N., Zhang, W., Zheng, Y., Zhang, Z., 2018. A review on agro-industrial waste (AIW) derived adsorbents for water and wastewater treatment. Journal of Environmental Management 227, 395–405.

Mohamed, R.M, Mkhalid, I.A., Barakat, M.A., 2015. Rice husk ash as a renewable source for the production of zeolite NaY and its characterization. Arabian Journal of Chemistry 8, 48–53.

Moussavi, G., Alahabadi, A., Yaghmaeian, K., Eskandari, M., 2013. Preparation, characterization and adsorption potential of the NH_4Cl-induced activated carbon for the removal of amoxicillin antibiotic from water. Chemical Engineering Journal 217, 119–128.

Mukoko, T., Mupa, M., Guyo, U., Dziike, F., 2015. Preparation of Rice Hull Activated Carbon for the Removal of Selected Pharmaceutical Waste Compounds in Hospital Effluent. Journal of Environmental & Analytical Toxicology S7, 2–9.

Munir, M., Xagoraraki, I., 2011. Levels of antibiotic resistance genes in manure, biosolids, and fertilized soil. Journal of environmental quality 40 (1), 248–255.

Nabi, S.A., Naushad, M., Khan, A.M., 2006. Sorption studies of metal ions on naphthol blue-black modified Amberlite IR-400 anion exchange resin: separation and determination of metal ion contents of pharmaceutical preparation. Colloids and Surfaces A: Physicochemical and Engineering Aspects 280, 66–70.

Nasuha, N., Hameed, B.H., 2011. Adsorption of methylene blue from aqueous solution onto NaOH-modified rejected tea. Chemical Engineering Journal 166, 783–786.

Navalon, S., Alvaro, M., Garcia, H., 2008. Reaction of chlorine dioxide with emergent water pollutants: products study of the reaction of three β-lactams antibiotics with ClO_2. Water Research 42, 1935–1942.

Nazari, G., Abolghasemi, H., Esmaieli, M., 2016. Batch adsorption of cephalexin antibiotic from aqueous solution by walnut shell-based activated carbon. Journal of the Taiwan Institute of Chemical Engineers 58, 357–365.

Nie, L.R., Lu, J., Zhang, W., He, A., Yao, S., 2015. Ionic liquid-modified silica gel as adsorbents for adsorption and separation of water-soluble phenolic acids from Salvia militiorrhiza Bunge. Separation and Purification Technology 155, 2–12.

Njoku, V.O., Foo, K.Y., Asif, M., Hameed, B.H., 2014. Preparation of activated carbons from rambutan (Nephelium lappaceum) peel by microwave-induced KOH activation for acid yellow 17 dye adsorption. Chemical Engineering Journal 250, 198–204.

Nooreini, M.G., Panahi, H.A., 2016. Fabrication of magnetite nanoparticles and modification with metal-organic framework of Zn^{2+} for sorption of doxycycline. International Journal of Pharmaceutics 512, 178–85.

Noroozifar, M., Khorasani-Motlagh, M., Fard, P.A., 2009. Cyanide uptake from wastewater by modified natrolite zeolite–iron oxyhydroxide system: application of isotherm and kinetic models. Journal of Hazardous Materials 166, 1060–1066.

Nurchi, V.M., Crespo-Alonso, M., Pilo, M.I., Spano, N., Sanna, G., Toniolo, R., 2015. Sorption of ofloxacin and chrysoidine by grape stalk. A representative case of biomass removal of emerging pollutants from wastewater. Arabian Journal of Chemistry 12, 1141–1147.

Omo-Okoro, P.N., Daso, A.P., Okonkwo, J.O., 2018. A review of the application of agricultural wastes as precursor materials for the adsorption of per and polyfluoroalkyl substances: A focus on current approaches and methodologies. Environmental Technology and Innovation 9, 100–114.

Ozacar, M., Sengil, I.A., 2005. Adsorption of metal complex dyes from aqueous solutions by pine sawdust. Bioresource Technology 96, 791–795.

Pal, P., 2018. Treatment and Disposal of Pharmaceutical Wastewater: Toward the Sustainable Strategy. Separation and Purification Reviews 47, 179–198.

Pam, A.A., 2019. Innovative Activated Carbon Based on Deep Eutectic Solvents (DES) and H_3PO_4. Journal of Carbon Research 5, 43.

Paria, S., Yuet, P.K., 2006. Solidification/Stabilization of Organic and Inorganic Contaminants using Portland cement: A Literature Review. Environment review 14, 217255.

Park, Y., Sun, Z., Ayoko, G.A., Frost, R.L., 2014. Bisphenol A sorption by organo-montmorillonite: Implications for the removal of organic contaminants from water. Chemosphere 107, 249–256.

Patel, S.K., Singh, D., Dev, R., 2020. Removal of Arsenic Contamination from Gomti River Water by using Activated Charcoal Absorbent Integrated with Solar Distillation Unit. Asian Journal of Chemistry DOI : https://doi.org/10.14233/ajchem.2020.22423

Pavithra, K.G., Kumar, S.P., Rajan, S.P., 2017. Sources and impacts of pharmaceutical components in wastewater and its treatment process: a review. The Korean Journal of Chemical Engineering 34, 2787–2805.

Peng, H., Li, H., Wang, C., Zhang, D., Pan, B., Xing, B., 2014. Sorption and solubility of ofloxacin and norfloxacin in water methanol cosolvent. Chemosphere 103, 322–328.

Peng, H., Pan, B., Wu, M., Liu, R., Zhang, D., Wu, D., Xing, B., 2012. Adsorption of ofloxacin on carbon nanotubes: Solubility, pH and cosolvent effects. Journal of Hazardous Materials 211–212, 342–348.

Peng, H., Pan, B., Wu, M., Liu, Y., Zhang, D., Xing, B., 2012. Adsorption of ofloxacin and norfloxacin on carbon nanotubes: Hydrophobicity and structure controlled process. Journal of Hazardous Materials 233–234, 89–96.

Peng, H., Guo, J., 2020. Removal of chromium from wastewater by membrane fltration, chemical precipitation, ion exchange, adsorption electrocoagulation, electrochemical

reduction, electrodialysis, electrodeionization, photocatalysis and nanotechnology: a review. Environmental Chemistry Letters 18, 2055–2068.

Petrovik, M., Hernando, M.D., Diaz-Cruz, M.S., Barcelo, D., 2005. Liquid chromatography-tandem mass spectrometry for the analysis of pharmaceutical residues in environmental samples: a review. Journal of Chromatography A 1067, 1–14.

Pezoti, O., Cazetta, A.L., Bedin, K.C., Souza, L.S., Martins, A.C., Silva, T.L., Junior, O.O.S., Visentainer, J.V., Almeida, V.C., 2016. NaOH-activated carbon of high surface area produced from guava seeds as a high efficiency adsorbent for amoxicillin removal: Kinetic, isotherm and thermodynamic studies. Chemical Engineering Journal 288, 778–788.

Pinheiro, A., Albano, R.M, Alves, T.C, Kaufmann, V., da Silva, M.R, 2013. Veterinary antibiotics and hormones in water from application of pig slurry to soil. Agricultural Water Management 129, 1–8.

Pirbazari, A.E., Saberikhah, E., Badrouh, M., Emami, M.S., 2014. Alkali treated foumanat tea waste as an efficient adsorbent for methylene blue adsorption from aqueous solution. Water Resources Industry 6, 64–8.

Pires, B.C., Dutra, F.V.A., Nascimento, T.A., Borges, K.B., 2017. Preparation of PPy/cellulose fibre as an effective potassium diclofenac adsorbent. Reactive and Functional Polymers 113, 40–49.

Pistorius, A.M.A., Degrip W.J., Egorova-zachernyuk T.A., 2009. Monitoring of Biomass Composition from Microbiological Sources by Means of FT-IR Spectroscopy. Biotechnology and Bioengineering 103 (1), 123–129.

Plecas, R., Pavlovic, S., 2004. Leaching behavior of ^{60}Co and ^{137}Cs from spent ion exchange resins in cement–bentonite clay matrix. Journal of Nuclear Materials 327, 171–174.

Polek, D., 2017. Solidification of hazardous waste as a part of the raw material recovery process. E3S Web of Conferences 18, 01026.

Poon, C.S., Qiao, X.C., Lin, Z.S., 2004. Effects of flue gas desulphurization sludge (FGD) on the pozzolanic reaction of reject fly ash blended cement pastes. Cement and Concrete Research 34, 1907–1918.23.

Portinho, R., Zanella, O., Feris, L.A., 2017. Grape stalk application for caffeine removal through adsorption. Journal of Environmental Management 202, 178–187.

Putra, E.K., Pranowo, R., Sunarso, J., Indraswati, N., Ismadji, S., 2009. Performance of activated carbon and bentonite for adsorption of amoxicillin from wastewater: mechanism, isotherms and kinetics. Water Research 43, 2419–2430.

Qi, Y.J., Liu, F., 2014. Analysis of antibiotics in groundwater: a review. Rock and Mineral Analysis 33 (1), 1.

Qureshi, T., Memona, N., Memonb, S.Q., Ashraf, M.A., 2015. Decontamination of Ofloxacin: optimization of removal process onto sawdust using response surface methodology. Desalination and Water Treatment 5, 1–9.

Rafati, L., Ehrampoush, M.H., Rafati, A.A., Mokhtari, M., Mahvi, A.H., 2016. Modeling of adsorption kinetic and equilibrium isotherms of naproxen onto functionalized nanoclay composite adsorbent. Journal of Molecular Liquids 224, 832–841.

Rameshraja, D., Srivastava, V.C., Kushwaha, J.P. Mall, I.D., 2012. Quinoline adsorption onto granular activated carbon and bagasse fly ash. Chemical Engineering Journal 181–182, 343–351.

Raoof, J., Hosseini, S.R., Rezaee, S., 2014. Preparation of Pt/poly(2-methoxyaniline)/multiwalled carbon nanotube nanocomposite and its application for electrocatalytic oxidation of methanol. Journal of Molecular Liquids 200, 196–204.

Rattanachueskul, N., Saning, A., Kaowphong, S., Chumha, N., Chuenchom, L., 2016. Magnetic carbon composites with a hierarchical structure for adsorption of tetracycline, prepared from sugarcane bagasse via hydrothermal carbonization coupled with simple heat treatment process. Bioresource Technology 226, 164–172.

Redlich, O., Peterson, D.L., 1959. A useful adsorption isotherm. Journal of Physical Chemistry 63, 1024–1026.

Rehman, M.S.U., Rashid, N., Ashfaq, M., Saif, A., Ahmad, N., Han, J.I., 2015. Global risk of pharmaceutical contamination from highly populated developing countries. Chemosphere 138, 1045–1055.

Reis, G.S.D., Sampaio, C.H., Lima, E.C., Wilhelm, M., 2016. Preparation of novel adsorbents based on combinations of polysiloxanes and sewage sludge to remove pharmaceuticals from aqueous solutions. Colloids and Surfaces A: Physicochemical and Engineering Aspects 497, 304–315.

Reynel-Avila, H.E., Mendoza-Castillo, D.I., Bonilla-Petriciolet, A., Silvestre-Albero, J., 2015. Assessment of naproxen adsorption on bone char in aqueous solutions using batch and fixed-bed processes. Journal of Molecular Liquids 209, 187–195.

Rodriguez-Diaz, J.M., Garcia, J.O.P., Sanchez, L.R.B., Silva, M.G.C.D., Silva, V.L.D., Luis, E. Arteaga-Perez, L.E., 2015. Comprehensive Characterization of Sugarcane Bagasse Ash for Its Use as an Adsorbent. Bioenergy Research 8, 1885–1895.

Rojas, R., Vanderlinden, E., Morillo, J., Usero, J., Bakouri, H., 2014. Characterization of sorption processes for the development of low-cost pesticide decontamination techniques. Science of the Total Environment 488–489, 124–135.

Rosales, E., Pazos, M., Sanromán. M.A., 2020. Prompt removal of antibiotic by adsorption/electro-Fenton degradation using an iron-doped perlite as heterogeneous catalyst. Process Safety and Environmental Protection 144, 100–110.

Rostamian, R., Behnejad, H., 2018. Insights into doxycycline adsorption onto graphene nanosheet: a combined quantum mechanics, thermodynamics, and kinetics study. Environmental Science and Pollution Research 25, 2528–2537.

Rozas, O., Contreras, D., Mondaca, M.A., Perez-Moya, M., Mansilla, H.D., 2010. Experimental design of Fenton and photo-Fenton reactions for the treatment of ampicillin solutions. Journal of Hazardous Materials 177, 1025–1030.

Safa, Y., 2016. Utilization of mustard and linseed oil cakes: novel biosorbents for removal of acid dyes. Desalination and Water Treatment 57 (13), 5914–5925.

Sahithya, K., Das, D., Das, N., 2015. Effective removal of dichlorvos from aqueous solution using biopolymer modified MMT–CuO composites: Equilibrium, kinetic and thermodynamic studies. Journal of Molecular Liquids 211, 821–830.

Salem, N.A., Yakoot, S.M., 2016. Non-steroidal Anti-inflammatory Drug, Ibuprofen Adsorption Using Rice Straw Based Biochar. International Journal of Pharmacology 12, 729–736.

Samarghandi, M.R., Al-Musawi, T.J., Mohseni-Bandpi, A., Zarrabi, M., 2015. Adsorption of cephalexin from aqueous solution using natural zeolite and zeolite coated with manganese oxide nanoparticles. Journal of Molecular Liquids 211, 431–441.

Sangal, V.K., Kumar, V., Mishra, I.M., 2013. Optimization of a divided wall column for the separation of C4-C6 normal paraffin mixture using Box-Behnken design. Chemical Industry and Chemical Engineering Quarterly 19 (1), 107–119.

Saucier, C., Adebayo, M.A., Lima, E.C., Cataluna, R., Thue, P.S., Prola, L.D.T., Puchana-Rosero, M.J., Machado, F.M., Pavan, F.A., Dotto, G., 2015. Microwave-assisted activated carbon from cocoa shell as adsorbent for removal of sodium diclofenac and nimesulide from aqueous effluents. Journal of Hazardous Materials 289, 18–27.

Saucier, C., Karthickeyan, P., Ranjithkumar, V., Lima, E.C., Reis, G.S.D., Irineu, A.S., Brum, D., 2017. Efficient removal of amoxicillin and paracetamol from aqueous solutions using magnetic activated carbon. Environmental Science and Pollution Research 24, 5918–5932.

Shang, Y., Zhang, J.H., Wang, X., Zhang, R.D., Xiao, W., Zhang, S.S., Han, R.P., 2015. Use of polyethyleneimine-modified wheat straw for adsorption of Congo red from solution in batch mode. Desalination and Water Treatment 57 (19), 8872–8883.

Sharma, B., Singh, N., Jain, T., Kushwaha, J.P., Singh, P., 2018. Acetonitrile Dehydration via Extractive Distillation Using Low Transition Temperature Mixtures as Entrainers. Journal of Chemical and Engineering Data 63, 2921−2930.

Sharma, B., Singh, N., Kushwaha, J.P., 2019. Ammonium-based deep eutectic solvent as entrainer for separation of acetonitrile–water mixture by extractive distillation. Journal of Molecular Liquids 285, 185–193.

Sharma, D., Chaudhari, P.K., Prajapati, A.K., 2019. Expulsion of Zn from the downstream of metal plating effluent onto modified agricultural adsorbent prepared from peanut shell. SSRN doi: 10.2139/ssrn.3368077.

Sharma, Y.C., 2011. Adsorption characteristics of a low cost activated carbon for the reclamation of colored effluents containing malachite green. Journal of Chemical and Engineering Data 56, 478–484.

Smith, E.L., Abbott, A.P., Ryder, K.S., 2014. Deep eutectic solvents (DESs) and their applications. Chemical Reviews 114, 11060–11082.

Sobsey, M.D., Bartram, S., 2002. Water quality and health in the new millennium: the role of the world Health organization guidelines for drinking-water Quality. Forum of Nutrition 56, 396–405.

Soltani, N., Bahrami, A., Pech-Canul, M.I., Gonzalez, L.A., 2015. Review on the physicochemical treatments of rice husk for production of advanced materials. Chemical Engineering Journal 264, 899–935.

Soltani, N., Soltani, S., Bahrami, A., Pech-Canul, M.I., Gonzalez, L.A., Moller, A., Tapp, J., Gurlo, A., 2017. Electrical and thermomechanical properties of CVI- Si_3N_4 porous rice husk ash infiltrated by Al-Mg-Si alloys**.** Journal of Alloys and Compounds 696, 856–868.

Soo, E.L., Salleh, A.B., Basri, M., Rahman, R.N.Z.A., Kamaruddin, K., 2004. Response surface methodological study on lipase-catalyzed synthesis of amino acid surfactants. Process Biochemistry 39, 1511–1518.

Srivastava, V.C., Mall, I.D., Mishra, I.M., 2006. Characterization of mesoporous rice husk ash (RHA) and adsorption kinetics of metal ions from aqueous solution onto RHA. Journal of Hazardous Materials 134, 257–267.

Stegemann, J.A., Zhou, Q., 2009. Screening tests for assessing treatability of inorganic industrial wastes by stabilization/solidification with cement. Journal of Hazardous Materials 161, 300–306.

Sturini, M., Speltini, A., Maraschi, F., Profumo, A., Pretali, L., Irastorza, E.A., Fasani, E., Albini, A., 2012. Photolytic and photocatalytic degradation of fluoroquinolones in untreated river water under natural sunlight. Applied Catalysis B 119–120, 32–39.

Sun, K., Shi, Y., Xu, W., Potter, N., Li, Z., Zhu, J., 2017. Modification of clays and zeolites by ionic liquids for the uptake of chloramphenicol from water. Chemical Engineering Journal 313, 336–344.

Tajernia, H., Ebadi, T., Nasernejad, B., Ghafori, M., 2014. Arsenic Removal from Water by Sugarcane Bagasse: An Application of Response Surface Methodology (RSM). Water air and soil pollution 225, 2-22.

Tambe, S.M., Sampath, L., Modak, S.M., 2001. In vitro evaluation of the risk of developing bacterial resistance to antiseptics and antibiotics used in medical devices. Journal of Antimicrobial Chemotherapy 47, 589–598.

Temkin, M.J., Pyzhev, V., 1940. Kinetics of ammonia synthesis on promoted iron catalysts. Acta Physiochimica URSS. 12, 217–222.

Tong, D.S., Zhou, C.H., Lu, Y., Yu, H., Zhang, G.F., Yu, W.H., 2010. Adsorption of acid red G dye on octadecyl trimethylammoniummontmorillonite. Applied Clay Sciences 50, 427–431.

Tonucci, M.C., Gurgel, L.V.A., Aquino, S.F.D., 2015. Activated carbons from agricultural byproducts (pine tree and coconut shell), coal, and carbon nanotubes as adsorbents for removal of sulfamethoxazole from spiked aqueous solutions: Kinetic and thermodynamic studies. Industrial Crops and Products 74, 111–121.

Treacy, M.M.J., Higgins, J.B. 2007. Collections of simulated XRD powdered patterns for zeolites. Commission of the international zeolite Association. Linde Type A dehydrated 250–251.

Umar, I.A., Giwa, A., Salisu, B., Sallahudeen, M., Mustapha, A., 2015. Kinetics, equilibrium and thermodynamics studies of C.I. Reactive blue 19 dye adsorption on coconut shell based activated carbon. International Biodeterioration and Biodegradation 102, 265–273.

Vansant, E.F., Voort, P.V.D., Vrancken, K.C., 1995. Characterization and Chemical Modification of the Silica Surface. Studies in Surface Science and Catalysis 93, 31–47.

Villaescusa, I., Fiol, N., Poch, J., Bianchi, A., Bazzicalupi, C., 2011. Mechanism of paracetamol removal by vegetable wastes: the contribution of π–π interactions, hydrogen bonding and hydrophobic effect. Desalination 270, 135–142.

Vinhal, J.O., Lage, M.R., Carneiro, J.W.M., Lima, C.F., Cassella, R.J., 2015. Modeling, kinetic, and equilibrium characterization of paraquat adsorption onto polyurethane foam using the ion-pairing technique. Journal of Environmental Management 156, 200–208.

Virkutyte, J., Sillanpää, M., 2006. Chemical evaluation of potable water in Eastern Qinghai Province, China: Human health aspects. Environment International 32, 80–86.

Vivek, V., Das, K., 2011. Removal of fluoride from drinking water using aluminium hydroxide coated rice husk ash. Journal of Hazardous Materials 185, 1287–1294.

Wang, F., Yang, B., Wang, H., Song, Q., Tan, F., Yanan, Cao, Y., 2016. Removal of ciprofloxacin from aqueous solution by a magnetic chitosan grafted graphene oxide composite. Journal of Molecular Liquids 222, 188–194.

Wang, L.G., Yan, G.B., 2011. Adsorptive removal of direct yellow 161dye from aqueous solution using bamboo charcoals activated with different chemicals. Desalination 274, 81–90.

Wang, Q., Zhang, J., Wang, A., 2013. Alkali activation of halloysite for adsorption and release of ofloxacin. Applied surface science 287, 54–61.

Wang, S.G., Gong, W.X., Liu, X.W., Yao, Y.W., Gao, B.Y., Yue, Q.Y., 2007. Removal of lead (II) from aqueous solution by adsorption onto manganese oxide-coated carbon nanotubes. Separation and Purification Technology 58, 17–23.

Wang, T., Pan, X., Ben, W., Wang, J., Hou, P., Qiang, Z., 2017. Adsorptive removal of antibiotics from water using magnetic ion exchange resin. Journal of Environmental Sciences 52, 111–117.

Weber, W.J., Morris, J.C., 1963. Kinetics of adsorption on carbon from solution. Journal of the Sanitary Engineering Division 89, 31–59.

Wieren, E.M.V., Seymour, M.D., Peterson, J.W., 2012. Interaction of the fluoroquinolone antibiotic, ofloxacin, with titanium oxide nanoparticles in water: Adsorption and breakdown. Science of the Total Environment 441, 1–9.

Witek-Krowiak, A., Chojnacka, K., Podstawczyk, D., Dawiec, A., Pokomeda, K., 2014. Application of response surface methodology and artificial neural network methods in modelling and optimization of biosorption process. Bioresource Technology 160, 150–160.

Wuana, R.A., Ato, R.S., Iorhen, S., 2015. Aqueous phase removal of Ofloxacin using adsorbents from Moringaoleifera pod husks. Advances in Environmental Research 4, 49–68.

Xu, J., Cao, Z., Zhang, Y., Yuan, Z., Lou, Z., Xu, X., Wang, X., 2018. A review of functionalized carbon nanotubes and graphene for heavy metal adsorption from water: Preparation, application, and mechanism. Chemosphere 195, 351–364.

Xu, W.H., Zhang, G., Zou, S.C., Li, X.D., Liu, Y.C., 2007. Determination of selected antibiotics in the Victoria Harbour and the Pearl River, South China using high performance liquid chromatography-electrospray ionization tandem mass spectrometry. Environmental Pollution 145, 672–679.

Yadav, D., Kapur, M., Kumar, P., Mondal, M.K., 2015. Adsorptive removal of phosphate from aqueous solution using rice husk and fruit juice residue. Journal of Process Safety and Environmental Protection 94, 402- 409.

Yang, M., 2011. A current global view of environmental and occupational cancers. Journal of Environmental Science and Health Part C 29, 223–249.

Yang, Y.C., Min, G.B., 2008. Solidification/Stabilization of soil contaminated with metal: a review. Journal - The Institution of Engineers, Malaysia 69, 37–43.

Ye, J., Cong, X., Zhang, P., Zeng, G., Hoffmann, E., Liu, Y., Wu, Y., Zhang, H., Fang, W., Hahn, H.H., 2016. Application of acid-activated Bauxsol for wastewater treatment with high phosphate concentration: characterization, adsorption optimization, and desorption behaviors. Journal of Environmental Management 167, 1–7.

Yu, L.J., Shukla, S.S., Dorris, K.L., Shukla, A., Margrave, J.L., 2003. Adsorption of chromium from aqueous solutions by maple sawdust. Journal of Hazardous Materials 100, 53–63.

Yuan, T.Q., He, J., Xu, F., Sun, R.C., 2009. Fractionation and Physico-chemical analysis of degraded lignins from the black liquor of Eucalyptus pellita KP-AQ pulping. Polymer Degradation and Stability 94, 1142–1150.

Zhang, B., Han, X., Gua, P., Fang, S., Bai, J., 2017. Response surface methodology approach for optimization of ciprofloxacin adsorption using activated carbon derived from the residue of desilicated rice husk. Journal of Molecular Liquids 238, 316–325.

Zhang, C.L., Qiao, G.L., Zhao, F., Wang, Y., 2011b. Thermodynamic and kinetic parameters of ciprofloxacin adsorption onto modified coal fly ash from aqueous solution. Journal of Molecular liquids 163, 53–56.

Zhang, D., Pan, B., Wu, M., Wang, B., Zhang, H., Peng, H., Wu, D., Ning, P., 2011a. Adsorption of sulfamethoxazole on functionalized carbon nanotubes as affected by cations and anions. Environmental Pollution 159, 2616–2621.

Zhang, L., Pan, F., Liu, X., Yang, L., Jiang, X., Yang, J., Shi, W., 2013. Multi-walled carbon nanotubes as sorbent for recovery of endocrine disrupting compound-bisphenol F from wastewater. Chemical Engineering Journal 218, 238–246.

Zhang, W., Li, H., Kan, X., Dong, L., Yan, H., Jiang, Z., Yang, H., Li, A., Cheng, R., 2012. Adsorption of anionic dyes from aqueous solutions using chemically modified straw. Bioresource Technology 117, 40–47.

Zhang, X., Bai, B., Wang, H., Suo, Y., 2016. Facile fabrication of sea buckthorn biocarbon (SB)@a Fe_2O_3 composite catalysts and their applications for adsorptive removal of doxycycline, wastewater through a cohesive heterogeneous Fenton-like regeneration. Royal Society of Chemistry Advances 6, 38159–38168.

Zhao, Y., Liu, F., Qin, X., 2017. Adsorption of Diclofenac onto Goethite: Adsorption Kinetics and Effects of pH. Chemosphere 180, 373–378.

Zhou, Y., Zhang, L., Cheng, Z.J., 2015. Removal of organic pollutants from aqueous solution using agricultural wastes: A review. Journal of Molecular Liquids 212, 739–762.

Zuccato, E., Castiglioni, S., Bagnati, R., Melis, M., Fanelli, R. 2016. Source, occurrence and fate of antibiotics in the Italian aquatic environment. Journal of Hazardous Material 179, 1042–1048.

RESEARCH PUBLICATIONS

SCI JOURNALS

1. Gurleenjot Kaur, Neetu Singh, Anita Rajor, Ofloxacin Adsorptive Interaction with Rice Husk Ash: Parametric and Exhausted Adsorbent Disposability Study. ***Journal of Contaminant Hydrology*** 236 (2021) 103737. (***Impact Factor: 3.188*****)**.

2. Gurleenjot Kaur, Neetu Singh, Anita Rajor, Adsorption of Doxycycline hydrochloride onto powdered activated carbon synthesized from pumpkin seed shell by microwave-assisted pyrolysis. ***Environmental Technology and innovation*** 23 (2021) 101601. (***Impact Factor: 5.263*****)**.

3. Gurleenjot Kaur, Neetu Singh, Anita Rajor, Jai Prakash Kushwaha, Deep eutectic solvent functionalized rice husk ash for effective adsorption of ofloxacin from aqueous environment. ***Journal of Contaminant Hydrology*** 242 (2021) 103847. (***Impact Factor: 3.188*****)**.

4. Gurleenjot Kaur, Neetu Singh, Anita Rajor, Efficient Adsorption of Doxycycline Hydrochloride Using Deep Eutectic Solvent Functionalized Activated Carbon Derived from Pumpkin Seed Shell. ***ChemistrySelec*****t** 6 (2021) 3139–3150. (***Impact Factor: 2.109*****)**.

UNDER REVIEW

1. Gurleenjot Kaur, Neetu Singh, Anita Rajor, Adsorptive decontamination of Doxycycline hydrochloride via Prosopis juliflora activated carbon: Parameter study, optimization using RSM-CCD and disposal study. ***Water Environment Research***. Manuscript No. WER-2021-10-0494. (Under Review).

2. Gurleenjot Kaur, Neetu Singh, Anita Rajor, RSM-CCD optimized Prosopis juliflora activated carbon for the Adsorptive uptake of Ofloxacin and disposal studies. ***Environmental Technology and innovation.*** Manuscript No. ETI-D-21-02393 R1 (Revision Submitted).
3. Gurleenjot Kaur, Neetu Singh, Anita Rajor, Raj Kumar Arya, Removal of doxycycline hydrochloride from wastewater by rice husk ash using response surface methodology and disposability study. ***Environmental Science and Pollution Research***. Manuscript No. ESPR-D-21-11747 R1 (Revision Submitted).

International Conference

1. Gurleenjot Kaur, Neetu Singh, Anita Rajor, Adsorption of pharmaceutical active compounds in wastewater using ash derived from agri-residue & its solidification, ***CHEMCON 2018*** *– Seamless Chemical Engineering in Service of Humanity: Innovations, Opportunities & Challenges* (December 27–30, 2018), Dr. B. R. Ambedkar National Institute of Technology, Jalandhar, India.

National Conference

1. Gurleenjot Kaur, Neetu Singh, Anita Rajor, Removal of Ofloxacin antibiotic from wastewater using agri-residue ashes & its solidification, *A Multi-track National Conference* **SLIETCON – 2019** (March 1–2, 2019) at NITTTR Chandigarh, India. **(WON SECOND PRIZE)**.

Reprints of published articles

Journal of Contaminant Hydrology 236 (2021) 103737

Contents lists available at ScienceDirect

Journal of Contaminant Hydrology

journal homepage: www.elsevier.com/locate/jconhyd

Ofloxacin adsorptive interaction with rice husk ash: Parametric and exhausted adsorbent disposability study

Gurleenjot Kaur [a], Neetu Singh [b,*], Anita Rajor [a]

[a] School of Energy and Environment, Thapar Institute of Engineering and Technology, Patiala 147004, India
[b] Department of Chemical Engineering, Thapar Institute of Engineering and Technology, Patiala 147004, India

ARTICLE INFO

Keywords:
Ofloxacin
Rice husk ash
Adsorption kinetics
Isotherms
Solidification and stabilization
Toxicity

ABSTRACT

The present study investigates the adsorptive interaction of rice husk ash (RHA) with Ofloxacin (OFL) antibiotic. The OFL loaded RHA was studied for its disposability by solidification to find its possible use as a building material. Further, toxicity analysis of leachate from the solidified RHA was also studied for probable leaching of OFL. The effects of adsorption parameters such as initial pH, the dosage of RHA (m), initial OFL concentration (C_0), and contact time (t) on the responses % OFL removal (X_1) and adsorption capacity (mg/g) (X_2) were evaluated using the central composite design (CCD) based on response surface method (RSM). Kinetic and thermodynamic studies were performed at optimized parameters, and adsorption equilibrium data were illustrated by using Langmuir, Redlich-Peterson (R-P), and Tempkin isotherm models. Optimum condition was found as $m = 7.94$ g/L, $t = 430$ min and $pH = 6$, and at this actual responses X_1 and X_2 were evaluated as 79.71% and 6.28 mg/g, respectively. Pseudo-first-order kinetic fitted best for the adsorption kinetic data. Toxicity analysis of leachate from solidified RHA indicated that most of the OFL was encapsulated inside the cement and the OFL present in leachate is not sufficient to eradicate the growth of *E.coli* and *Bacillus subtilis*.

1. Introduction

Antibiotics have been broadly used to treat the many bacterial infectious diseases in humans and animals. The primary role of these antibiotics is to abate the DNA replication in bacteria by hampering the usual activity of DNA topoisomerase (Lhiaubet-Vallet et al., 2009). An enormous quantity of antibiotics are being used and regularly discharged into the atmosphere from pharmaceutical industries, hospitals, domestic wastewater, and excretion from living beings (El-Ghenymy et al., 2013). During the rainy season, these antibiotics could be leached out and thus contaminate the groundwater. The major health risk due to the antibiotics available in the environment has attracted the interest of the scientific community. Out of all the antibiotics, the fluoroquinolones class of antibiotics has been observed everywhere in wastewater, surface, soil, and sediments due to its extensive use and the fact that it is not easily degradable (Zaidi et al., 2016). Ofloxacin (OFL), a fluoroquinolone (FQ) antibiotic finds its application against gram-positive and gram-negative bacteria. OFL is suggested to the patients with urinary tract infections, respiratory tract infections, prostatitis, and skin infection. The concentration of OFL in treated effluents was found in the range of 0.005–31.7 μg/L in different countries. The excessive use of this antibiotic causes side effects like tendon damage, peripheral neuropathy, and in serious cases; it can result in lifetime disabilities (Vasquez et al., 2013).

Due to the non-biodegradable nature of OFL, conventional treatment techniques can eliminate only a small fraction of it, remaining runs off to surface water (Paul et al., 2010). Fluoroquinolone antibiotics have been detected in different concentration ranges, in-hospital sewage ~60–120,000 ng/L, in surface waters ~5–1300 ng/L, and in wastewater treatment plant effluents ~2–580 ng/L all over the world (Wammer et al., 2013). About 20–90% of fluoroquinolones ingested are released in their pharmacologically active forms, foremost to considerable loads being discharged into domestic wastewater (Li et al., 2013). Currently, many treatment methods like adsorption (Hao et al., 2012), chemical oxidation (Mehrjouei et al., 2014), photocatalytic and photolytic treatment (Li et al., 2012), electro-oxidation (Kaur et al., 2018; Kaur et al., 2019) and biodegradation (Vasquez et al., 2013) are usually adapted for the elimination of toxic antibiotics from the aquatic system. Out of these available methods, adsorption is an efficient and favorable technique as it offers great effectiveness, little expenditure, and simple operation (Ahmed et al., 2015). Adsorption is one of the broadly utilized techniques for toxin elimination from the polluted system. Many materials

* Corresponding author.
E-mail address: neetu.singh1479@gmail.com (N. Singh).

https://doi.org/10.1016/j.jconhyd.2020.103737
Received 18 August 2020; Received in revised form 26 September 2020; Accepted 23 October 2020
Available online 31 October 2020

Environmental Technology & Innovation 23 (2021) 101601

Contents lists available at ScienceDirect

Environmental Technology & Innovation

journal homepage: www.elsevier.com/locate/eti

Adsorption of doxycycline hydrochloride onto powdered activated carbon synthesized from pumpkin seed shell by microwave-assisted pyrolysis

Gurleenjot Kaur [a], Neetu Singh [b,*], Anita Rajor [a]

[a] School of Energy and Environment, Thapar Institute of Engineering and Technology, Patiala 147004, India
[b] Department of Chemical Engineering, Thapar Institute of Engineering and Technology, Patiala 147004, India

ARTICLE INFO

Article history:
Received 11 February 2021
Received in revised form 2 May 2021
Accepted 3 May 2021
Available online 7 May 2021

Keywords:
Pumpkin seed shell
Bio-sorbent
Microwave-assisted pyrolysis
Doxycycline hydrochloride
Adsorption mechanism
Reusability

ABSTRACT

In the present study, pumpkin seed shell activated carbon (PSSAC) was efficiently synthesized via microwave-assisted pyrolysis technique, employing pumpkin seed shell as the precursor and H_3PO_4 activator. The adsorptive performance of PSSAC was quantified for decontamination of water from a doxycycline hydrochloride (DOX) antibiotic. Prepared PSSAC was characterized to determine its chemical and morphological characteristics employing FTIR, XRD, FESEM and zeta potential. Surface area and pore size distribution were evaluated with the help of BET and BJH characterization techniques respectively. The effect of relevant process parameters like solution pH, PSSAC dose, contact time and temperature were assessed to get the optimum experimental conditions. The kinetic and isotherm studies reveal that the adsorption process is performed via pseudo-second-order reaction and multilayer adsorption. The calculated thermodynamic parameters (ΔH^0, ΔS^0 and ΔG^0) represented that the adsorption of DOX onto PSSAC was endothermic, instinctive and practicable in the temperature extent of 288–318 K. Moreover, the investigation about adsorption mechanisms resulted that H-bonding and $\pi-\pi$ electron–donor–acceptor (EDA) interactions heavily affected DOX adsorption over PSSAC. The maximum identified adsorption capacity value was 23.6 mg/g at 318 K. Good regeneration capability and high adsorption capacity of PSSAC represents its excellent potential to alleviate emerging contaminants from wastewater.

1. Introduction

The global trend of industrialization, urbanization and the release of numerous toxic compounds have become the main cause of water pollution. Among the several noxious chemicals and organics, pharmaceutically active compounds (PACs) are of great concern (Gupta and Nayak, 2012; Gupta et al., 2015a). PACs are accredited as arising pollutants because of their bioactivity, broad application and probable health & environmental hazards (Gupta et al., 2015b). Antibiotics are a main type of PACs which are very often recommended to save the human being from diseases caused due to bacterial infections and animal growth improvement (Qi and Liu, 2014). The existence of these drugs in the H_2O cycle of the ecosystem are widely recognized throughout the world. While examining, these contaminants were also visible in the ground and drinking water samples at low concentrations (ng/L to mg/L).

* Corresponding author.
E-mail address: neetu.singh1479@gmail.com (N. Singh).

https://doi.org/10.1016/j.eti.2021.101601
2352-1864/

Journal of Contaminant Hydrology 242 (2021) 103847

Contents lists available at ScienceDirect

Journal of Contaminant Hydrology

journal homepage: www.elsevier.com/locate/jconhyd

Deep eutectic solvent functionalized rice husk ash for effective adsorption of ofloxacin from aqueous environment

Gurleenjot Kaur [a], Neetu Singh [b,*], Anita Rajor [a], Jai Prakash Kushwaha [b]

[a] School of Energy and Environment, Thapar Institute of Engineering and Technology, Patiala 147004, India
[b] Department of Chemical Engineering, Thapar Institute of Engineering and Technology, Patiala 147004, India

ARTICLE INFO

Keywords:
Rice husk ash
DES functionalized RHA
Ofloxacin
Adsorption isotherms
Kinetics

ABSTRACT

Deep eutectic solvents (DESs) have achieved the rising attention of the scientific community because of their distinctive physicochemical properties and variety of applications. Herein, DES composed of choline chloride as hydrogen bond acceptor (HBA) and glycolic acid as hydrogen bond donor (HBD) was synthesized. Next, the prepared DES was examined as a functionalization agent for rice husk ash (RHA) to form a novel adsorbent (DES–RHA). To ensure the formation of DES and to recognize the modifications occurred due to the functionalization process, a comprehensive characterization study was performed using ^{1}HNMR, FTIR spectroscopy, TGA, XRD, FESEM, HR-TEM and BET surface area. Potential of the prepared DES–RHA was investigated for the uptake of ofloxacin (OFL) from an aqueous environment. The impact of relevant process parameters was evaluated under optimum conditions, and the data were examined applying various kinetic and isotherm models. As per the regression findings, adsorption kinetics data were well described by pseudo-second-order model, and the isotherm data were in good agreement with Langmuir, Temkin, RP and Freundlich isotherm models. Further, the adsorption procedure was endothermic and spontaneous. The high regeneration and adsorption capacity of DES–RHA than untreated RHA adds a promising approach to eliminate emerging pollutants present in effluent sites.

1. Introduction

Antibiotics have been extensively used for the prevention and cure of human and animal diseases originated due to different pathogenic bacteria. Because body cannot metabolize these antibiotics, therefore direct discharge of these antibiotics take place into the environment. Presently, pollution with antibiotics has created pandemonium in the aquatic environment due to its large consumption and discharge (Hapeshi et al., 2013). According to the statistics, India gets the 3rd position worldwide in production of pharmaceutical compounds, afterwards Europe and North America, with an estimated turnover of USD 75 billion per year by 2020 (Kaur et al., 2021a). Among different categories of antibiotics, Fluoroquinolones are widely prescribed due to their broad-spectrum activity and remarkable tissue permeation. Ofloxacin (OFL) which is also a fluoroquinolones antibiotic, is prescribed generally because of its well-known effectiveness against many common bacterial infections. Due to the large consumption, OFL is generally found in wastewater, groundwater and surface water. Because of its non-biodegradable and genotoxic nature, conventional management methods can remove only small fractions of it. Residual concentrations always exist in the atmosphere for longer periods. Water pollution due to these antibiotics may lead to serious consequences like the development of antibiotic-resistant bacteria (Radjenovic et al., 2009; Kaur et al., 2021b). To avoid the adverse effects of these antibiotics, suitable methods are required for their removal from the environment.

Many physical, chemical, biological and advanced oxidation methods like filtration, coagulation, ion exchange, flocculation, reverse osmosis, UV/H_2O_2, ozonation etc. have been explored for separation/degradation of OFL from wastewater (Gadipelly et al., 2014; Pal, 2018; Kaur et al., 2018b). These techniques have proven to be energy-intensive and inexpedient (Lin et al., 2016; Kaur et al., 2019a). Moreover, the distinct COD removal competence of these methods for different nature and organic load of the wastewater hinders their practical applications. On the other hand, chemical oxidation and biodegradation processes exhibit limitations like; production of more stable intermediates and toxic by-products than their parent compound during treatment processes.

Adsorption is considered one of the most assured physical technique

* Corresponding author.
E-mail address: neetu.singh1479@gmail.com (N. Singh).

https://doi.org/10.1016/j.jconhyd.2021.103847
Received 3 March 2021; Received in revised form 20 May 2021; Accepted 6 June 2021
Available online 8 June 2021

Electro, Physical & Theoretical Chemistry

Efficient Adsorption of Doxycycline Hydrochloride Using Deep Eutectic Solvent Functionalized Activated Carbon Derived from Pumpkin Seed Shell

Gurleenjot Kaur,[a] Neetu Singh,*[b] and Anita Rajor[a]

The emerging deep eutectic solvents (DESs) are being utilized in different areas of science and engineering due to their exceptional physicochemical properties. In this study, choline chloride-based DES was prepared in conjugation with glycolic acid (GA) as a hydrogen bond donor (HBD). Activated carbon was derived from pumpkin seed shell (PSS) using microwave-assisted pyrolysis technique in an N_2 environment. The potential of synthesized DES was evaluated as a functionalization agent for PSSAC. DES functionalized PSSAC (DES-PSSAC) was characterized using FTIR, XRD, FESEM and BET surface area to confirm the functionalization and identify the physicochemical changes. This prepared DES-PSSAC was used as an adsorbent for the uptake of Doxycycline hydrochloride (DOX) from its aqueous solution. The influence of different process parameters was inspected in order to determine the optimal experimental conditions. At optimized parameters, the kinetics and thermodynamics studies were explored. Used DES was confirmed to be effectively grafted onto the PSSAC surface. The experimental data, best suited to the Pseudo second-order kinetic model, whereas adsorption isotherm data were best represented by Freundlich and R-P isotherm models. The recorded maximum adsorption capacity (q_{max}) was found to be 30.35 mg/g. High adsorption performance of DES-PSSAC towards DOX uptake and its reusability exhibited that this novel adsorbent can be applied to remove pharmaceutical pollutants.

1. Introduction

Undoubtedly, the advancement in the medical field has led to the longer lifespan of humans and animals. However, the exponential use of antibiotics affects our aqueous environments (drinking water, surface water, and groundwater) and its metabolized forms remain present in the effluents.[1] The antibiotic or xenobiotic compounds come under the emerging contaminants category due to their wide reactivity and consumption on a larger scale, which can cause chronic health hazards, and potential ecological risks.[2] The antibiotic contaminants are most commonly found in hospital effluents, drug industry effluents, and landfill sites.[3,4] Moreover, contaminants along with their metabolites (in a concentration range from ng/L to mg/L) eventually leads to the enlargement of drug-resistant genes generated by micro-organisms that has the great potential to develop a serious universal problem.[5,6]

Common drugs like erythromycin, chlortetracycline, norfloxacin, ofloxacin, doxycycline hydrochloride, atenolol, and sulfadimethoxine are found in surface and groundwater samples in the concentration of 381.5, 122.3, 134.2, 135.1, 77.3, 52.9, and 164 ng/L, respectively.[7] The high production and usage rate of antibiotics has led to their water reservoirs and accumulation in the aquatic environment. Consequently, it has become an emerging issue in environmental science to achieve effective antibiotic removal from the wastewaters before discharge into the environment. Thus, major efforts to examine this problem and palliate its effects are a priority.

The synthetic classes of antibiotics such as fluoroquinolones, sulfonamides, tetracyclines and trimethoprim are consumed broadly into the medicines of human beings and stock-feed. Among all these, tetracyclines (TCs) are a family of antibiotics invoked for the treatment of various infections and are also frequently effective in agricultural farming and aquaculture for their growth, development, and therapeutic importance.[8] Amongst 25 antibiotics, TCs were broadly detected that accounts for 80% in the effluents and sewage systems. Doxycycline hydrochloride (DOX) is a broad-spectrum antibiotic used against gram-positive and negative bacterial infections.[9,10] Due to the more complex physicochemical structural properties of DOX, it causes complicated behaviour in the atmosphere. That is why developing an effectual, economically reliable, and sustainable technique is required, like adsorption. It is an effective way for the eradication of antibiotics pollution contaminating various water bodies.[11–13]

Few researchers came out investigating the adsorption of TCs by using adsorbents such as montmorillonite, carbon nanotubes, graphene, mesoporous silica, Fe_3O_4, and sea buckthorn biocarbon.[14–16] However, challenges are associated with

[a] G. Kaur, Dr. A. Rajor
School of Energy and Environment,
Thapar Institute of Engineering and Technology,
Patiala-147004, India
[b] Dr. N. Singh
Department of Chemical Engineering,
Thapar Institute of Engineering and Technology,
Patiala-147004, India
Tel.: +91-9876019399
E-mail: neetu.singh1479@gmail.com

Supporting information for this article is available on the WWW under https://doi.org/10.1002/slct.202100182